Lancaster University

Uranium extraction from seawater using natural byproducts: Evaluation and Testing

Steven McGowan,
s.mcgowan@lancaster.ac.uk
Department of Engineering
Lancaster University
A thesis submitted for the degree of Doctor of Philosophy
February 2024

Abstract

Nuclear power has experienced a resurgence in recent years due to the valuable contribution it can make in countering global warming. The operation of these next generation reactors still rely on uranium from finite geological sources. The IAEA estimates that, in the event of a high usage scenario, the currently known geological resources would reach $300 per kg in the next 80 years. (NEA and IAEA, 2016)

This is considered the cap, because at that price amidoxime filtration from seawater would become economically viable. However, the mining and refinement of ores has other environmental effects, and it would be desirable to make this transition at a lower cost. One option for achieving this would be to use a low cost filtration medium, such as a naturally occuring byproduct of some other process, such as farming. This study aims to begin preliminary testing of these materials, and to attempt to model the properties of the capture reactions, in order to optimise the process, with a view to minimising the costs involved

Acknowledgements

I would like to thank Prof. Claude Deguelde, Dr. Farid Aiouache, Prof. Hao Zhang, Dr. Vesna Najdanovic, Prof. Martine Leermakers and Prof. Yue Gao for their contributions towards the modelling and practical work, Michelle Dalton for her assistance in editing, and generally keeping me grounded, and my family for their support.

Declaration

I declare that the work presented in this thesis is, to the best of my knowledge and belief, original and my own work. The material has not been submitted, either in whole or in part, for a degree at this, or any other university. This thesis does not exceed the maximum permitted word length of 80,000 words including appendices and footnotes, but excluding the bibliography.

A rough estimate of the word count is: 72590, of which 3387 are bibliography

Steven McGowan

Contents

Table of Tables

Table of Figures

1.0 Introduction

Nuclear power represents one of the cleanest energy vectors available to humans (Birol, 2019) partly due to the energy density of the fuel and partly due to the low mobility of the radioisotopes in their waste form and the engineered environment, due to their strong sorption [[i]]). (Degueldre, et al., 1996; Degueldre, et al., 1994) With careful management, it is possible to ensure that all significant risks are mitigated through engineering. In 1976, Pigford stated:

"The environmental acceptability of nuclear fission power plants rests upon the careful control of environmental effluents from each of the many diverse steps in the nuclear fuel cycle including uranium mining, fuel preparation, reactor operation, fuel reprocessing, and the storage and disposal of radioactive wastes."

This is still fundamentally true today, as it was at the time. While the fuel cycle itself is under constant review, economics have dictated that geological mining has continued to be the preferred route for sourcing the uranium (U) necessary for the operation of a nuclear system at the current time (Ewing, 2004). However, uranium geological sources are finite, with some high-usage scenarios limiting the supply of U to 80 years, with an estimated 7.6 Mt of U available at production costs of up to $260/kg of U extracted (NEA and IAEA, 2016).

A potential alternative exists, by extracting uranium from seawater.

TABLE 1 GEOLOGICAL RESERVES OF MINERALS OF ECONOMIC INTEREST, AND THE CORRESPONDING RESERVES IN SEAWATER DILUTION

Element	2022 terrestrial reserves ($\times 10^6$ tonnes)	2022 world production ($\times 10^6$ tonnes)	2022 reserve supply ratio (years)	seawater concentration (mg/L)	dissolved metals in seawater ($\times 10^6$ tonnes)	Aquatic reserve supply ratio at annual production (years)
Cu	0.89	0.026	34	0.0009	1170	45000
Ni	1000	3.3	303	0.0066	8580	2600
V	26	0.1	260	0.0019	2470	24700
Mo	12	0.25	48	0.01	13000	52000
Li	98	0.13	754	0.178	231400	1780000
Co	25	0.19	132	0.00039	507	2670
Nb	17	0.079	215	0.000015	1.3	16.5
Ag	0.052	0.0031	17	0.00028	364	117400
Au	0.55	0.026	21	0.000011	14.3	550
U	6.078	0.049	124	0.0033	4290	87550

2022 TERRESTRIAL DATA FROM NATIONAL MINERALS INFORMATION CENTER (2023) EXCEPT FOR URANIUM WHICH USED WORLD NUCLEAR ASSOCIATION (2023) SEAWATER CONCENTRATIONS AND RESERVES FROM TUREKIAN (1978), AND DIALLO, KOTTE, & CHO (2015)

Natural erosion of geological materials results in a flow of dissolved elements of interest from the land, into the sea, carried in rivers or other surface flows. These elements exist in equilibrium, balancing deposition in sea floor deposits with the influx from the geological sources (Zhang, et al., 2021). These would be functionally, a renewable resource, as our mineral requirements would be significantly lower than these geological fluxes (Degueldre, et al., 2019).

An advantage of this approach is that seawater contains a wide variety of potential elements of interest, such as those listed in **Table 1**.

Most approaches for extraction are based on selectively extracting a particular element of interest onto a media, which it can be recovered from, either directly from the seawater, or from brine, which is the concentrated by-product of desalinisation (Cipolletta, et al., 2021; Zhang, et al., 2021).

2.0 Background

Uranium is present at concentration of trace scale with an average of 3.3 parts per billion (ppb) in standard seawater conditions (i.e., 35% salinity and pH 8.0). An averaged reserve of 4500 Mt of uranium in seawater at any time is the result of the dynamic equilibrium of approximately 10^4 tonnes uranium between uranium gained from the rivers by geological erosion and lost by deep sea deposition of sediments as postulated by Schenk, et al. (1982). This uranium is present in multiple forms, including (in order of prevalence) tricarbonato-uranyl [$UO_2(CO_3)_3^{4-}$], dicarbonato-uranyl [$UO_2(CO_3)_2^{2-}$], uranyl $^{(VI)}$ tri-hydroxide [$UO_2(OH)_3^-$], uranyl [UO_2^{2-}], uranyl hydroxide [$UO_2(OH)^+$], and uranyl di-hydroxide [$UO_2(OH)_2$]. The dominant form (84.9%), the tricarbonato-uranyl, is most commonly assumed to be bound to calcium ions as reported by Djogic & Branica (1993; Djogic, et al. (1986); Aihara, et al. (1992); Zhang, et al. (2005); Yamashita, et al. (1980); and Sekiguchi, et al. (1994).

As $[UO_2]^{2+}$ has a specific, linear, shape, it is able to form coordination with four, five or six ligands, all around the equator, this species has a high feasibility of forming mixed ligand complexes. The prevalent (simple) ligands with strong affinities for uranyl in saline environments are Cl^-, OH^-, CO_3^{2-}, HO_2^- and SO_4^{2-} (Djogic & Branica, 1993). The relatively near-neutral-to-weakly-alkaline (pH 8) nature of seawater is the primary driver on selection, as these ligands are pH sensitive, and the relative concentrations in solution, and their relative log β, or cumulative partition co-efficients which exhibit a dense buffering effect, due to the median conditions being controlled by the dominance of seawater by volume, produces relatively fixed prevalences. Djogic & Branica (1993) calculated these log β, and were able to demonstrate the cumulative distributions in significant detail.

The strong affinity of these ligands are the driving reason that extracting the uranyl is so challenging: the dicalcium tricarbonato-uranyl structure which is so prevalent at these conditions is a neutral but soluable complex, which limits the ability to interact with sorbing media (Krestou & Panias, 2004). Other complexes are more accessible, but have lower prevalences. Other complexes, such as uranium phosphates are hydrophobic, which results in precipitation (Kim, et al., 2024).

The extraction of uranium from seawater does not induce the same pollution risks than those associated with solid ore geological mining.

Geological mining can be categorised as either direct ore extraction, followed by crushing and leaching, or by in situ leaching. These techniques have threes area of direct environmental challenges, specifically tailings, waste rock and contamination by wastewater (Atomic Energy Agency (IAEA), 2009) and the general environmental consideration of reduction of process energy consumption, in order to meet the mitigation strategies for sustainable processes, as reported by Carvalho (2017). However, most of the uranium concentration techniques that focused on natural seawater generate mixed

brines, including other elements, such as co-extracted metals from the seawater. It should be noted that these co-extracted metals are often valuable resources, which create opportunities for their recovery. The nature of co-extracted element depends on the methodology used but vanadium, exhibiting similar sorption properties to uranium, is a common co-extracted metal. Lithium extraction from seawater, as alternative option, is seen of sustainable commercial interest as well, see Loganathan, et al., (2017).

2.1 Previous Research

There have been some attempts to extract uranium resource on test scales. The most successful test was run by Sugo, et al. (2001) who placed braided chains of amidoxime-grafted polyethylene in deep-water conditions and estimated a recovery of U at \$300 kg^{-1}, assuming 20 reuses of the sorbing material. This is considered the "Best Possible Technology" existing so far for the application but remains uneconomic under current market conditions e.g. (NEA and IAEA, 2016; Schneider & Sachde, 2012).

Several issues were highlighted with this methodology by subsequent research, including the reusability being more limited than estimated, due to polymer swelling, affecting the capture rates, and limiting the working lifetime, see Wiechert, et al. (2018) and Xu, et al. (2019). The amidoxime-doped chains are a common sorbent material in the purification and concentration technologies, but they remain non-cost effective as the synthesis of one tonne of the material costs approximately \$8800, leading to 40% of the total cost for synthesis and capture, see Schneider & Sachde (2012). Another issue is that the maximum deployable time of the materials was found less than the optimum sorption time due to biofouling as noted by Ao, et al. (2019 and Park, et al. (2016). Drysdale & Buesseler (2020) carried out extensive work on attempting to control biofouling on fibres, demonstrating that conventional approaches to countering biofouling, the use of copper infused coatings, was itself an interferent, and reuse strategies developed for laboratory use are not successful in the more complex environments of natural coastal waters.

There have been other attempts to develop alternatives by using polymers, novel sorbents, or protective measures. Approaches include grafting amidoxime onto a variety of substances, including amidoximated polymer gel that was synthesized from radiation-polymerization and crosslinking of acrylonitrile and methacrylic acid monomer such as the one reported by Wongjaikham, et al. (2018) and palygorskite/amidoxime polyacrylonitrile composite, of which the work by Yu, et al. (2015) is a good example. Information on amidoximated electron-beam-grafted polypropylene membrane was reported by Das et al. (2008) and relevant applications of the functionalities to braided polymeric materials were reported by Lashley, et al. (2016).

The specific site structures of adsorbents (e.g. mono-, bi-, tri- dentate complexes) have been used to selectively sorb the elements of interest. These include polyamine and amidoxime groups modified bifunctional polyacrylonitrile-based ion exchange fibres as reported by Cheng *et al* (2019), hyper-branched topological swollen-layers of multi-active sites of polyacrylonitrile (PAN) adsorbent, as reported by Ju *et al* (2019) polyethyleneimine, polyacrylic acid hydrogel and Luffa cylindrical fibre, as used by Su *et al* (2018) have all been recently proposed. As covered in their respective sources, these sorbents demonstrate at least partial effectiveness but suffer from significant costs due energy requirements of the synthesis process.

A potential alternative to this approach would be the use of a natural material to sorb uranium which would not require specific absorbent synthesis. Many natural materials include structures that are anticipated to interact selectively with relevant elements in solution. These can be the functional, nutritional, or protective parts of the biological structure. However, the original purpose is actually irrelevant, if the relevant compounds can be straightforwardly extracted, as suggested by Matharu et al (2016).

Some bio-sourced resins, such as the chitosan phosphate, have been tested in controlled flow experiments as reported by Sakaguchi, et al (1979) & (1981). These tests were not pursued in detail as the yield of sorption was low under typical seawater conditions, due to the preferential sorption of uranyl compared with the carbonate-uranyl complexes, which predominate in these conditions. Additionally, this material has several issues, such as the production of phosphoric acid during the recovery process (Dotto, et al., 2013).

Microbial modulated capture has also been attempted, but the yield was found to be low compared with natural deposition, as reported by Nakajima, et al (1982). This is likely due to the uranium reduction by bioprocesses in solution being a preferred metabolic pathway, see Senko, et al. (2002). However, Bogolitsyn, et al. (2023) have demonstrated that the limiting factor in these capture processes are not due to the inherent capacity, but are instead due to the persistence of uranium in the biofilms, relative to other metals, having achieved 80-84% capture in batch system, but was only able to retain 40% of the net total, when exposed to desorbing conditions. The films demonstrate the ability to passively reject the complexes, which, as it describes, would be the primary purpose of the films would be to filter nutrients to their source cells and protect against toxic elements.

While biomaterials have not been subject to a full-scale attempt for the extraction of uranium from seawater specifically, some data is available from leach and tailing mining environments. In these environments, attempts have been made, to test their capacity to decontaminate ground or surface waters with a number of substances, or aimed at elements other than uranium, see Ramamoorthy, et

al (1969); El-Sheikh (2016) ; Tang, et al (2013) Diallo, et al. (2015) Gondhalekar & Shukla (2014) and Satari & Karimi (2018) . These investigations are generally based on testing the sorption isotherm of the material, most commonly in conjunction with a simulated liquid phase. The tested materials specifically with uranium included *Myricae Cortex* barks (Nakajima & Sakaguchi, (1989)), *Citrus Limetta* peels (Gondhalekar & Shukla, 2014) pyrolyzed tea and coffee wastes (Aly & Luca 2013) and *Citrus* reprocessing wastes (Satari & Karimi, (2018); Pathak *et al* (2015)).

The nature of these materials means they are often prone to degradation in seawater conditions under longer timeframes, limiting the deployment time, especially potential reuse, as this could introduce pollution risks. They are however selected for their lower costs, mitigating the costs associated with replacing them. Biofouling is still likely to be also a limiting factor in contact time, as algae growth is fuelled by the nutrients lost to solution from the material. This will prevent further contact with the seawater, capping the influx (Ao *et al* (2019) & Park *et al* (2016)), although this is known to be a capture process, see Nakajima *et al* (1982) and Senko *et al* (2002).

A secondary advantage to this approach is co-capture: for example grape peel (Zhang, et al., 2023) has been used in the recovery of other economic minerals from leachate, as has orange peel (Nalladiyil, et al., 2023; Satari & Karimi, 2018) and tree bark (Linde, et al., 2007). These materials not only absorb these elements, but have pre-existing mineral loads, which can augment the captured content. For example, in peanut shells (Ahmad, et al., 2012).

2.2 Chemical Concept

Sorption is traditionally described by reactions between specific groups and metal or complex ions (Degueldre, *et al.,* 1994; Van Loon, et al., 2013).

Considering a generic surface >*Su*, above a macromolecule, substrate, or colloid (◊), associated with one or more exposed 'hydroxyl' groups ◊>*Su*$(OH)_n$. They are in contact with an aqueous phase with which specific chemical exchanges may take place. Typically, for biomaterials, these groups could be phenolic or carboxylic.

A metal ion M^{n+} or their complexes ($M(OH)_i^{(n-i)+}$) may complex to the surface, by substitution with one or more of the protons.

$$\text{◊>}Su\text{OH} + M^{n+} \Leftrightarrow \text{◊>}Su\text{O}M^{(n-1)+} + H^+ \quad \{1\}$$

$$\text{◊>}Su(OH)_2 + M^{n+} \Leftrightarrow \text{◊>}Su\text{O}_2M^{(n-2)+} + 2H^+ \quad \{2\}$$

These reactions may result in a bond which may be of variable strength (Degueldre, *et al.,* 1994). There are three factors that control how strong surface complexation is and how likely that this reaction is to be reversible.

1) The species of **ions or complexes** in solution dictate the strength of surface complexation on a site. To estimate their surface complexation constant values correlations with the hydrolysis constants are used. These values which are readily available for a large body of ions and complexes and can be extended by correlation to others (Degueldre, *et al*., 1994; Degueldre, *et al*., 2001).
2) The **active groups at the surface** of the sorbing material have an effect on the surface complexation of the bond. These structures can be classified into groups of compounds with similar mechanisms, but different morphologies. The two common examples in bioorganic systems are carboxylic and phenolic groups.
3) The relative **concentration of these species** in solution and the **pH** plays a relevant role in the surface complexation process starting with the strongest (poly-dentate) to the weakest (mono-dentate).

The sorption is traditionally described on the basis of the concentration of metal sorbed on the solid $[M]_s$, and the dissolved metal in the fluid (water) phase $[M]_w$ or $[M]_l$ depending on the unit basis.

For dynamic systems, it is possible to quantify sorption using the sorbed fraction *F* (%) as defined in Eq. (1) below.

$$F = 100 \frac{[M]s}{([M]s + [M]l)} \quad (1)$$

Where $[M]_s$ and $[M]_l$ are in µg kg^{-1}. Note that this is primarily a "living" ratio and may be calculated even if the system is not at equilibrium. When this ratio is at equilibrium however, it is possible to calculate the sorption constant *Kd*, as defined by Eq. (2) for reactions {1} & {2} at equilibrium:

$$K_d = \frac{[M]_{sorb}}{[M]_{Sol}} \quad (2)$$

Where $[M]_{sorb}$ is the concentration of all metal species on the surface of the absorbent (g g^{-1}) and $[M]_{sol}$ the concentration of all metal species in solution (g mL^{-1}). The K_d values are then given in mL g^{-1} (or L kg^{-1}).

For redox sensitive species, in addition to the direct sorption process occurring for a given redox state, there are indirect redox effects, as different forms of complexes and ions (oxidative and reductive) have different hydrolysis constants, so have different sorption properties. The reactions at the surface and in the area of effect form a cycle that can be generalised to {3} - {6}:

$$\text{◊>}Su(OH)_2 + M^{o+} \Leftrightarrow \text{◊>}SuO_2M^{(o-2)+} + 2H^+ \quad \{3\}$$

$$\text{◊>}Su(OH)_2 + M^{r+} \Leftrightarrow \text{◊>}SuO_2M^{(r-2)+} + 2H^+ \quad \{4\}$$

These equations are related by redox equilibriums between both surface and soluable states by equations {5} and {6}.

$$M^{o+} + (o\text{-}r)e^- \Leftrightarrow M^{r+} \quad \{5\}$$

$$\text{◊>}SuO_2M^{(o-2)+} + (o\text{-}r)e^- \Leftrightarrow \text{◊>}SuO_2M^{(r-2)+} \quad \{6\}$$

This concept of K_d can be applied, and a net Eq. (2) can be adapted for all species at the surface and in solution. For example, if the direct effect of sorption described by reaction {4} produces stronger sorbed species than {3} then the reduction of the metal by {5} will control the sorption by {4} to a greater degree than {3}. The net result would be the sorption of the oxidative species may generate the reductive complexes at the surface, due to a reduction of the sorbed species after fixation.

For the specific example of U, as the focus of this study, the ion can exist under several oxidative states. In surface waters, U is normally hexavalent. Its sorption in neutral conditions is strong, but when reduced as tetravalent U, it exhibits even stronger sorption. This was proposed to be due to a Coulomb effect, as the binding for U^{4+} complexes by Langmuir (1978), as the binding to ores proved

to be stronger than that measured for the UO_2^{2+} complexes (McKee & Todd., 1993). MOHAGHEGHI, et al. (1985) proposed a two-step bio-geochemical process, involving accumulation of $U^{(VI)}$ onto bacterial cell walls and subsequent microbial reduction to $U^{(IV)}$ under suitable conditions. The micro-organisms known to carry this out are common (Strandberg, et al., 1981). Therefore, these act as a natural reducing agent, fuelled by their own biochemistry, and those of antioxidants from the biomass material, introduced into solution, will increase the proportion of U^{4+} present, and increase the effective K_d values for U.

These sorbed species still have an interactive potential for further reactions with species in solution, which means they have become a reactive surface. This is a factor for both free species, and other surfaces. For example, in these circumstances, colloidal materials can interact as per {7}:

$$\text{◊>}Su\text{O}_2M^{(r-2)+} + \text{◊>}Su(\text{OH})_2 \quad \Leftrightarrow \quad \text{◊>}Su\text{O}_2M^{(r-4)+}\text{O}_2Su\text{<◊} + 2\text{H}^+ \qquad \{7\}$$

Clearly in this case the ◊>$Su\text{O}_2M^{(r-4)+}\text{O}_2Su$<◊ structure will not allow the ions $M^{(r-4)+}$ (which may be a complex of the form $M(\text{OH})_i^{(r-i)+}$) to return to the aqueous phase. They are "quenched" in the macromolecular phase of the colloid aggregate and are fixed on it with only extremely low possibility of desorption. In this case, the sorption becomes effectively irreversible, and the K_d becomes a plain sorption ratio, leading to very high effective K_d values.

An additional factor to this model is, in practice, natural sorbents are not exclusively one sorbing site type, and exist on a sliding scale, between wholly polyphenolic, and wholly carboxylic polysaccharides. However, both materials are based on a similar sized replicating unit for lignin or hesperidin in polyphenolic compounds, and cellulose or demi-cellulose for polysaccharide, due to the mechanical processes in synthesis in biomaterials (Boudet, 2000). This has the consequence that it is only necessary to measure the proportion of the relevant structures to be able to estimate the material composition net (direct effect) K_d. Further to this, it is necessary to consider that certain compounds and classes of compounds are known to be high in antioxidants: for example, tannins are a class of compounds with antioxidant properties present in many plant species, due to their use in transport and defence mechanisms. As a polyphenolic compound, these also function as a sorption site, and some are known to actively co-chelate to form insoluble compounds with metal ions, permanently removing from solution (Zhang, et al., 2016).

For the purposes of maximising the effective surface area of sorbent, if it is finely dispersed, the processes would favour the aggregation, making sorption of U irreversible on specific biomaterial. Therefore, these materials are to be investigated to find the optimum performance for the extraction of U.

2.3 Model Concept

The sorption process of metal species is a consequence of a complex series of reactions. These include the formation, alteration, or deconstruction of complexes with ligand in solution or with active surface sites of "weak acid" nature (somewhat covalent bound). When occurring on surfaces, it is referred to a surface complexation, as a distinction from ion exchange processes with the "strong acid" active sites (ionic bound). It is best described by the distribution ratio (R_d), which yields a distribution coefficient (K_d) in mL g^{-1} at the sorption/desorption equilibrium given in (2).

In the context of low-density compounds, such as the organic materials, it is often difficult to measure the concentration $[M]_{sorb}$ at the surface of the particulate material at equilibrium, so it is necessary to modify Eq. 1 to include the particle concentration as an additional factor and adapt it to wet phase conditions. K_d becomes:

$$K_d = \frac{[M]'_{sorb}}{[M]'_{sol}} \frac{1}{[Part]} \qquad (3)$$

Where both (total) concentrations $[M]'_{sorb}$ and $[M]'_{sol}$ are given in mol mL^{-1} and [part] is the particle concentration in g mL^{-1}.

2.3.1 Site availability

For the purpose of this implementation in the model, the surface was considered to be a spherical particle of fixed average size, defined by radius *r* in nm. From this, the average surface area (S) can be calculated using Eq 4. With addition of the material specific mass ρ in g nm^{-3}, the average mass (m_a) can be calculated as per Eq 5.

$$S = 4 \pi r^2 \qquad (4)$$

$$m_a = (4/3) \pi r^3 \rho \qquad (5)$$

S is calculated in nm^2 and m_a is derived in g.

For the purposes of standardising the structure, the interaction region was considered to be a fixed plane, which was defined as rectangular, of dimensions *a* and *b* with *c* sites interacting with the ion or the available complex. This shape was selected to allow easy use of unit cell dimensions from crystallisation studies, for example as gained from Jones & Templeton (1958). Note that non-interactive materials, such as unsuitable molecule orientations, hydrating water molecules, or underlying mounting matrix would be included in the region of the plane, allowing an average the molecular site surface density *c/ab* in mol nm^{-2} which can be combined with S to estimate an average amount of site (mol) per particle.

In previous implementations of this model, such as (Degueldre & McGowan, 2020), the surface site density was taken directly from empirical (experimental) results. The modification to this derived value, calculated based on fixed physical characteristics, allowed this value to be intrinsically justified.

Consequently, the site molar density N_s (mol per average particle surface area) was estimated using the average surface area of the particle as calculated in Eq. 4, and the total surface, as displayed in Eq. 6:

$$N_s = c\ S\ N_{av}^{-1}\ (1\text{-}I)\ (a.b)^{-1} \qquad (6)$$

where *c* being active sites number at the surface ($a \cdot b$), *I* the inactive surface fraction and N_{av} being Avogadro's constant.

Total site concentration ($[>Su]_{tot}$) in mol mL^{-1} was then calculated from the site density, average mass, and the particle concentration [part]:

$$[>Su]_{tot} = \frac{N_s.[\text{part}]}{m_a} \qquad (7)$$

The $[>Su]_{tot}/[\text{part}]$ ratio may be estimated experimentally using the specific surface provided by BET measurements, which was used to verify the results. Note that the site can be formulated as >*Su*, >*Su*OH, >*Su*O^-, >(*Su*OH)$_c$, … according to conditions.

2.3.2 Effect of acidity on the sites

The most common protonated form of site is >(*Su*OH)$_c$. As the sites which are suitable to be receptive to the metal ion can be modified by protonation and deprotonation of the sites at different pH's. These acid-base reactions are usually written as:

$$>SuOH \Leftrightarrow\ >SuO^- + H^+ \qquad \{8\}$$

Where >*Su*OH, >*Su*O^- and >*Su* represents the active groups as protonated and deprotonated and their substrate respectively. The acid/base constant associated to these sites is defined by:

$$K_a = \frac{[>SuO^-]\,[H^+]}{[>SuOH]} \qquad (8)$$

The total site (non-complexed site) concentration equals:

$$[>SuOH]_{tot} = [>SuOH] + [>SuO^-] \qquad (9)$$

Consequently, the protonated site concentration is expressed by:

$$[> SuOH] = \frac{\frac{[>SuOH]_{tot}\,[H^+]}{K_a}}{\frac{1+[H^+]}{K_a}} \qquad (10)$$

Consequently, for a specific pH, and for a known K_a, it is possible to use Eq. 10 to calculate the concentration of sites suitable for complexation, from the total number of sites calculated using Eq. 7.

In the case where a second site is in the vicinity of a first one, it is possible that they participate in two acid-base reactions and may become coupled in the same fashion as in reaction {2}. This reaction would be quantified by a cumulative acid-base constant, $\beta_{a(2)}$, defined by:

$$\beta_{a(2)} = \frac{[>(SuO^-)_2]\,[H^+]^2}{[>(SuOH)_2]} \qquad (11)$$

In a general case, of multi-site reactions, reaction {1} becomes:

$$>(SuOH)_c \quad \Leftrightarrow \quad >(SuO^-)_c + c\,H^+ \qquad \{10\}$$

The cumulative multi-acid-base constant is given by:

$$\beta_{a(c)} = \frac{[>(SuO^-)_c]\,[H^+]^c}{[>(SuOH)_c]} \qquad (12)$$

2.3.3 Hydroxo complexes properties

The acid base properties of metal ions are described by their build-up of hydroxo complexes on metal ions and their successive hydroxo complexes reactions:

$$(HOH) + M^{m+} \Leftrightarrow (HO)M^{(m-1)+} + H^{+} \quad \{11\}$$

$$.c(HOH) + M^{m+} \Leftrightarrow (HO)_c M^{(m-c)+} + c\,H^{+} \quad \{12\}$$

When the equilibria are reached, the hydroxo complexation constants $K_{h(1)}$ and $\beta_{h(c)}$ associated to the reactions {11} and {12} are given as:

$$K_{h(1)} = = \frac{[(HO)\mathrm{M}^{(m-1)}]\,[\mathrm{H}^{+}]}{[\mathrm{M}^{m+}]} \quad (13)$$

and

$$\beta_{h(c)} = \frac{[(HO)\mathrm{cM}^{(m-c)}]\,[\mathrm{H}^{+}]c}{[\mathrm{M}^{m+}]} \quad (14)$$

with c = 2, 3, 4, 5 or 6. The cumulative hydrolysis constant, $\beta_{h(c)}$, as displayed in (15)

$$\beta_{h(c)} = \prod K_{\mathrm{h}(1)}.K_{\mathrm{h}(2)}).K_{h(3)}..K_{h(c)} \quad (15)$$

2.3.4 Formation of surface complexes

On the surface structure, *>Su*, associated with one or several groups (*c*) also called dentate which are available to form with active groups *>(Su*OH)$_c$ a surface complex with a metal ion or a complex containing such an ion. The simplest case (c = 1) is displayed in reaction {13}:

$$>SuOH + M^{m+} \Leftrightarrow >SuOM^{(m-1)+} + H^{+} \quad \{13\}$$

This reaction may be reversible under normal conditions and the constant of surface complexation may be written as:

$$K_{s(0)} = \frac{[(>(SuO)\mathrm{M}^{(m-1)+}]\,[\mathrm{H}^{+}]}{[>SuOH][\mathrm{M}^{m+}]} \quad (16)$$

for the sorption of the naked ion.

In general case, bonds to several sites may occur, as per reaction {14}.

$$>(SuOH)_c + M^{m+} \Leftrightarrow >(SuO)_c M^{(m-c)+} + cH^{+} \quad \{14\}$$

Where ***c*** denotes the dentate state. The cumulative constant of surface complexation may be written as:

$$\beta_{s(c)} = \beta_c\, K_{s(c)} = \frac{[(>(SuO)_c\mathrm{M}^{(m-c)+}]\,[\mathrm{H}^{+}]^c}{[(>(SuOH)c][\mathrm{M}^{m+}]} \quad (17)$$

It may also be that the metal or soluble complex may bind with additional sites after being bound to one or more initially as illustrated in {15}

$$>(SuO)_{c-1}(OH)M^{+} \Leftrightarrow (>SuO)_{c}M + H^{+} \qquad \{15\}$$

It is thus possible to adapt Eq. 17 to calculate a $K_{s(c)}$ for the concentration on the surface and in solution in mol g^{-1} and mol mL^{-1}, respectively. The equations (Eq 16 and 17) are related to the formation of mono- and multi-dentate complexes respectively. The multi-dentates are subdivided into bi- (2), tri- (3) and tetra- (4) dentates. However, it must be noted that not every complex can exist in every state. So, in some cases the surface may not act as a tetra-dentate ligand, or a tri-dentate ligand for example.

It should be noted that the organic molecules are notable as being more flexible than the inorganic ones described in the prior work, increasing the likelihood that multiple bonds (or "multidentate") could be made with a wider range of sizes of single ion or complexes than the rigid structures of the clay-like minerals, such as (Degueldre & McGowan, 2020).

2.3.5 Correlation for mono- and multi- dentate

In order for the metal or complex to form a surface complex, a consistent approach was suggested by Degueldre *et al* (1994) for prediction of stability constants of the surface complexes, $K_{s(0)}$, by correlating with the corresponding the hydrolysis constants $K_{h(1)}$ of the ions and complexes involved in the surface complexation states.

This analogy is ruled by the set of reactions {11} with {13}, and {12} with {14}.

The reaction couples that can be compared for the mono-dentate are:

$$>(SuOH) + M^{m+} \Leftrightarrow >(SuO)M^{(m-1)+} + H^{+} \qquad \{13\}$$

$$(HOH) + M^{m+} \Leftrightarrow (HO)M^{(m-1)+} + H^{+} \qquad \{11\}$$

With the equivalent couple for comparison with the multi-dentate would be:

$$>(SuOH)_c + M^{m+} \Leftrightarrow >(SuO)_cM^{(m-c)+} + c\,H^{+} \qquad \{14\}$$

$$c(HOH) + M^{m+} \Leftrightarrow (HO)_cM^{(m-c)+} + c\,H^{+} \qquad \{12\}$$

The analogy between reactions {13} and {11} was proposed and the following relation suggested:

$$\text{Log}\, K_{s(0)} = T_m + S_m \,\text{Log}\, K_{h(1)} \qquad (18)$$

where S_m and T_m are surface-specific constants.

In previous work, this relation was limited to mono-dentate such as in Degueldre *et al* (2001). Analysis of multi-dentate constants has shown however that successive multi-dentate can be described by the same relation form as Eq (18), with the successive hydrolysis constants of the element, but that these constants are specific to the dentate state: so an active site will have mono-, bi-, tri- and tetra- values of $S_{m(c)}$ and a mono-, bi-, tri- and tetra- values of $T_{m(c)}$, where the correlations are due to the analogy between reactions {14} and {12}. The correlation coefficients $S_{m(c)}$ and $T_{m(c)}$ are then unique surface-specific constants, in each state.

$$\text{Log}\, K_{s(c-1)} = T'_{m(c)} + S'_{m(c)}\ \text{Log}\ K_{h(c)} \qquad (19)$$

Where c is the dentate state for the individual surface complexation constant $K_{s(c+1)}$ and for the hydration constant for $K_{h(c)}$. In these correlation plots, $S_{m(c)}$ represents the impact of an increasing complexation binding strength with the hydroxide complexation and the values of $T_{m(c)}$ follows the initial threshold required to make initially the bond.

However, several authors have shown that multi-dentates are common e.g., (Carbonaro, et al., 2011; Loiseau, et al., 2014). In case of organic molecules >*Su*OH active groups are more flexible than the inorganic one, e.g., >SiOH, >FeOH and >AlOH leading to a binding with a larger degree of freedom for the considered ions or complexes. They are known to flex around complexes, leading to stronger S_m values. However, counter effects would also expect difficulties, such as the lack of suitable sites, which would be reflected in lower T_m values.

It should be noted that the logarithmic plots comparing the successive logarithm of the mono-hydroxide complexation constants with the logarithm of the mono-dentate surface complexation constants, as well as those of the logarithm of a given multi- hydroxide complexation constants with their corresponding multi-dentate surface complexation constants, allowed observation of linear relationships between these stability constants. These correlations are surface site specific.

2.3.6 Complexes formation in the redox range

The hydrolysis stability constants of both redox species ($K_{h(i,k)}$ for oxidising and $K_{h(j,l)}$ for reducing species) can be evaluated for the stepwise reactions {11} and {12}. It should be noted that this notation is generic and can be used for both oxocative and non-oxocative relations between species.

Further complications due to metal complexation by k-ligands (L^{-p}) or l-ligands (L^{-p}) such as carbonates, were also considered. The complexation reactions in solution for both redox species read as:

$$MO_x(\mathrm{OH})_{i-1}L_k^{\,z-2x-n-i+1-kp} + \mathrm{H_2O} \overset{K_{i,k}}{\Leftrightarrow} MO_x(\mathrm{OH})_i L_k^{\,z-2x-n-i-kp} + \mathrm{H^+} \quad \{16\}$$

$$MO_y(\mathrm{OH})_{j-1}L_l^{\,z-2y-n-j+1-lp} + \mathrm{H_2O} \overset{K_{j,l}}{\Leftrightarrow} MO_y(\mathrm{OH})_j L_l^{\,z-2y-n-j-lp} + \mathrm{H^+} \quad \{17\}$$

Therefore, it is possible to describe the generalised redox couple $MO_x^{(z-2x)+}/MO_y^{(z-n-2y)+}$ (where $MO_x^{(z-2x)+}$ is the oxidised species and $MO_y^{(z-n-2y)+}$ the reduced one), by reaction {18}.

$$MO_x^{\,(z-2x)+} + ne^- + (2x-2y)\mathrm{H^+} \overset{K_h}{\Leftrightarrow} MO_y^{\,(z-n-2y)+} + (x-y)\mathrm{H_2O} \quad \{18\}$$

The surface complexation for the hydrolysed (and complexed) species is described by reactions {13} and/or {14}, considering the generalised quasi-neutral site >*Su*OH. The surface complexation constants are Ks(i,k) for the oxidising species and Ks(j,l) for the reducing species. The indices k and l refer to the relevant co-ordination numbers of the metal ions, in the context of those selected ligands. Furthermore, effects of the redox potentials in solution and at the surface are taken into account by reactions {20} and {21} below.

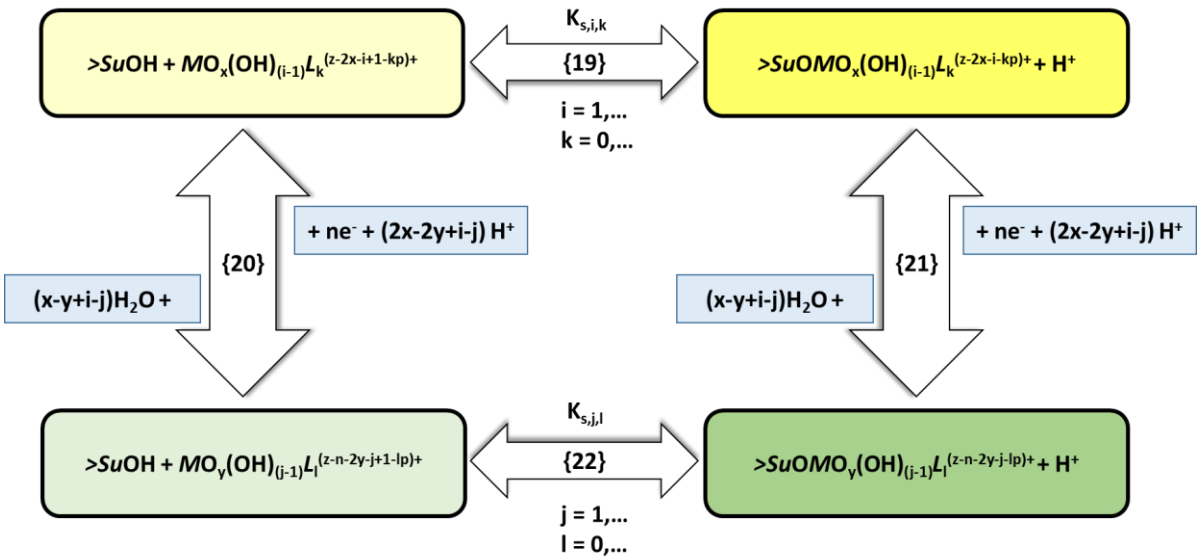

When the reactions are written in terms of free metal M^{z+}, the cumulative constants are β_i and β_j, respectively ($\beta_{i \text{ or } j} = \beta_{1..i \text{ or } j} = \prod K_i$ where i or j= 0, 1,..).

The ratio between the concentrations of both redox species is written as a function of the redox potential (E) by applying the Nernst equation (20):

$$E = E^{\circ} + (2x - 2y + i - j)\,\mathrm{RT}\,(n\mathrm{F})^{-1}\ln[\mathrm{H}^{+}] + \mathrm{RT}\,(n\mathrm{F})^{-1}\ln\{[MO_x{}^{(z-2x)+}]\,[MO_y{}^{(z-n-2y)+}]^{-1}\} \quad (20)$$

Where the apparent standard redox potential (E'°) is linked to the standard redox potential (E°) in water, according to eq (21):

$$E'^{\circ} = E^{\circ} + (2x - 2y + i - j)\mathrm{RT}\,(n\mathrm{F})^{-1}\,ln[\mathrm{H}^{+}] \quad (21)$$

Rearranging these equations by considering surface complexation for both redox forms and including concurrent complexation with ligands as formulated in the above-mentioned equations and reactions lead K_d (from Eq.3) to be written in terms of the redox potential and evaluated by Eq (22).

$$K_d = \frac{\{\sum_{i,k}\left[\frac{\mathrm{K}_{s,i,k}\cdot\beta_{i,k}\cdot[L_k]^k}{[\mathrm{H}^{+}]^i}\right] + \sum_{j,l}\left[\frac{K_{s,j,l}\cdot\beta_{j,l}\cdot[L_l]^l}{[\mathrm{H}^{+}]^j}\right]\exp(A)\}\,.\,\frac{[>Su\mathrm{OH}]}{[H^{+}]}}{\{\sum_{i,k}\left[\frac{\beta_{i,k}\cdot[L_k]^k}{[\mathrm{H}^{+}]^i}\right] + \sum_{j,l}\left[\frac{\beta_{j,l}\cdot[L_l]^l}{[\mathrm{H}^{+}]^j}\right]\,.\,\exp(\mathrm{A})\,\}.\,[\mathrm{part}]} \quad (22)$$

where $A = \frac{(E'^{\circ}-E)n\mathrm{F}}{\mathrm{R}T}$ and the sorbing particle concentration [part] is given in g.mL^{-1} (for a K_d in ml.g^{-1}). The free ligand concentration [L] can be written in terms of the total ligand concentration (mol L^{-1}).

The formulation of Eq (22) implies occurrence of linear adsorption isotherms (of Langmuir type, see Eq. 2) and no saturation effects. It should be noted that no electrostatic effects and no activity corrections were considered at this stage.

Equation (22) can be understood as a sum series of couplets, each consisting of the concentration sorbed and a concentration in solution, fractionated by the proportion of the specific ion at a given redox state. Each element of $\frac{\mathrm{K}_{s,i,k}\cdot\beta_{i,k}\cdot[L_k]^k}{[\mathrm{H}^{+}]^i}$ represents the concentration of the ion, of a specific coordination, reduced by the concentration of corresponding ligands, in the case of *i,k* specifically the ground state on the surface, whereas the equivalent element noted by its state *j,l* represents those in a reduced state, as mentioned, proportioned by exp(A).

These are corresponded in the denominator, to an element $\frac{\beta_{i,k}\cdot[L_k]^k}{[\mathrm{H}^{+}]^i}$, which correlates to the previously mentioned *i,k* or *j,l* appropriately, representing the concentration in solution.

Using this as the basis, any K_d calculated on this basis using Eq (22) can be evaluated for a given pH at any specific value of *E*.

Equation (22) can further be extended by considering sorption on different multi-dentate groups, utilising the appropriate cumulative constant. For these multidentate surface complexes the $K_{d(c)}$ becomes:

$$K_{d(c)} = \frac{\{ \sum_{m,n}[\frac{K_{S,m,n} \cdot \theta_{m,n} \cdot [L_n]^n}{[H^+]^m}] + \sum_{o,p}\left[\frac{K_{s,o,p} \cdot \theta_{o,p} \cdot [L_p]^p}{[H^+]^o}\right] \exp(A)\} \cdot \frac{[>(SuOH)c]}{[H^+]c}}{\{\sum_{m,n}[\frac{\theta_{m,n} \cdot [L_n]^n}{[H^+]^m}] + \sum_{o,p}[\frac{\theta_{o,p} \cdot [L_p]^p}{[H^+]^o}] \cdot \exp(A) \} . [part]} \quad (23)$$

For the multi-dentate complexes, the formulation is similar to that described for mono-dentate, however c protons are exchanged instead of 1. Since the same metal species are considered, m, o, n, and p will match those of i, j, k, and l, respectively, forming the same couplets, but now adjusted to account for the increased number of bindings (and underlying form of surface sites) required for the complexation. As stated earlier, these values are cumulative and represent a mixed species collective.

As independent processes, a total net K_d ($K_{d(net)}$) which represents every species in solution, and every form of multi-dentate surface complexes, is calculated by Eq (24).

$$K_{d(net)} = K_{d_{.}} + K_{d_{.}(2)} + K_{d_{.}(3)} + K_{d_{.}(4)} \quad (24)$$

3.0 Model implementation

3.1 General Characteristics of the Liquid Environment

As the model is intended to represent sorption of uranium in saline conditions, the concentration of uranium was taken as the average seawater value is $3x10^{-9}$ g L^{-1} (3 ppb) Millero (2013). The pH of seawater directly used for calculations is around 8.0. For example, as reported by Rérolle et al (2012), Irish Sea seawater has a pH between 7.995 and 8.210 and a redox potential of about +0.4 V in surface conditions.

For the carbonated seawater environment, the total carbonate concentration has been assumed to be $[CO_3]_{Tot} = 2.2 \times 10^{-3}$ mol L^{-1} and their first and second Log partition coefficients are 10.329 and 16.681 (Sharp et al (2017))

3.1.1 General Characteristics of Uranium Complexes

The molecular weight of uranium is assumed to be 238 g mol^{-1}. The pK_h for each of its hydroxide complexes and the E° for each of its redox couples are as listed in Table 2 and 3. These values are the input variables used in eq (23), for calculating the corresponding Exp(A) for each complex.

Table 2: Hydrolysis Constants & Standard Redox Potentials of Uranium (NEA (2004) & Grenthe et Al (2006)

Coordination (i or j)	pK_h $U^{(III)}$	E° (V)	pK_h $U^{(IV)}$	E'° (V)	pK_h $U^{(V)}$	E'° (V)	pK_h $U^{(VI)}$	E'° (V)
=1	6.80	0	0.54	-0.553	0.00	0.053	0.00	0.006
=2	7.30	0	0.70	-0.553	11.30	0.053	5.25	0.006
=3	11.60	0	3.60	-0.553	12.30	0.053	6.90	0.006
=4	14.35	0	5.30	-0.553			8.10	0.006
=5			13.10	-0.553			12.15	0.006

The pK_h for each of the hydrolysis constants and E° (V) are listed below in Table 3, ranked over an order that follows the number of carbonating- ligands.

Table 3: Hydroxide complex constants & standard redox potentials of uranium carbonated states data from NEA (2004) & Grenthe et al (2006))

i & l (for $K_{s,i,l}$)	pK_h $U^{(III)}$	E° (V)	j & l (for $K_{j,l}$)	pK_h $U^{(IV)}$	E° (V)
i=0, l=1/ 2/ 3	5.12 /1.80 / -1.90	0	j=0, l=1/ 2/ 3/ 4	6.5/ 5.3/ 1.6/ -3.4	-0.553
i= 1, l=0	-11.3	0	j= 1, l=0/1/2	-6.8 /-5.8 /-7.8	-0.553
i= 2, l=0	-12.3	0	j= 2, l=0/1	-7.3/ -7.9	-0.553
			j= 3, l=0	-11.6	-0.553
			j= 4, l=0	-14.35	-0.553
j & l (for $K_{j,l}$)	pK_h $U^{(V)}$	E° (V)	j & l (for $K_{j,l}$)	pK_h $U^{(VI)}$	E° (V)
j=0, l=1/ 2/ 3/ 4	13.7/ 10.6/ 7.6/ 3.3	0.053	j=0, l=1/ 2/ 3/ 4	9.94/6.67/ 5.23/7.6/ 3.3	0.006
j= 1, l=0	-0.54	0.053	j= 1, l=0	-5.25	0.006
j= 2, l=0	-0.7	0.053	j= 2, l=0	-6.9	0.006
j= 3, l=0	-3.6	0.053	j= 3, l=0	-8.1	0.006
j= 4, l=0	-5.3	0.053	j= 4, l=0	-12.15	0.006
j= 5, l=0	-13.1	0.053			

3.1.2 Speciation of uranium in water, effect of pH, E, and carbonate complexes

In aqueous environment uranium can form tetravalent, pentavalent, and hexavalent species, which stability domains can be recalculated as a function of pH and E for given ligand concentrations. The E vs pH diagrams for uranium were replotted, with the results are presented in **Figure 1**.

Uranium hexavalent in water exists primarily as ionic as well as carbonate and hydroxide complexes. In seawater uranium (oxidising), carbonate complexes are often found bound to calcium ions. In order of prevalence, these are tri-carbonate-uranyl [$UO_2(CO_3)_3^{4-}$] (as the dominant form, constitutes 84.9% of all free uranium), di-carbonate-uranyl [$UO_2(CO_3)_2^{2-}$], uranyl $^{(VI)}$ tri-hydroxide [$UO_2(OH)_3^-$], uranyl [UO_2^{2+}], uranyl hydroxide [$UO_2(OH)^+$], and uranyl di-hydroxide [$UO_2(OH)_2$] as reported by Djogic & Branica (1986), Zhang *et al* (2005), Sekiguchi *et al* (1994), Aihara *et al* (1992) and Yamashita *et al* (1980).

In reducing seawater conditions, uranium forms trivalent species which are at pH8 mainly uranium tetra-hydroxide [$U(OH)_4$], along with some uranium tri-hydroxide $U(OH)^{3-}$]. The carbonate complexes are absent under these pH – E conditions.

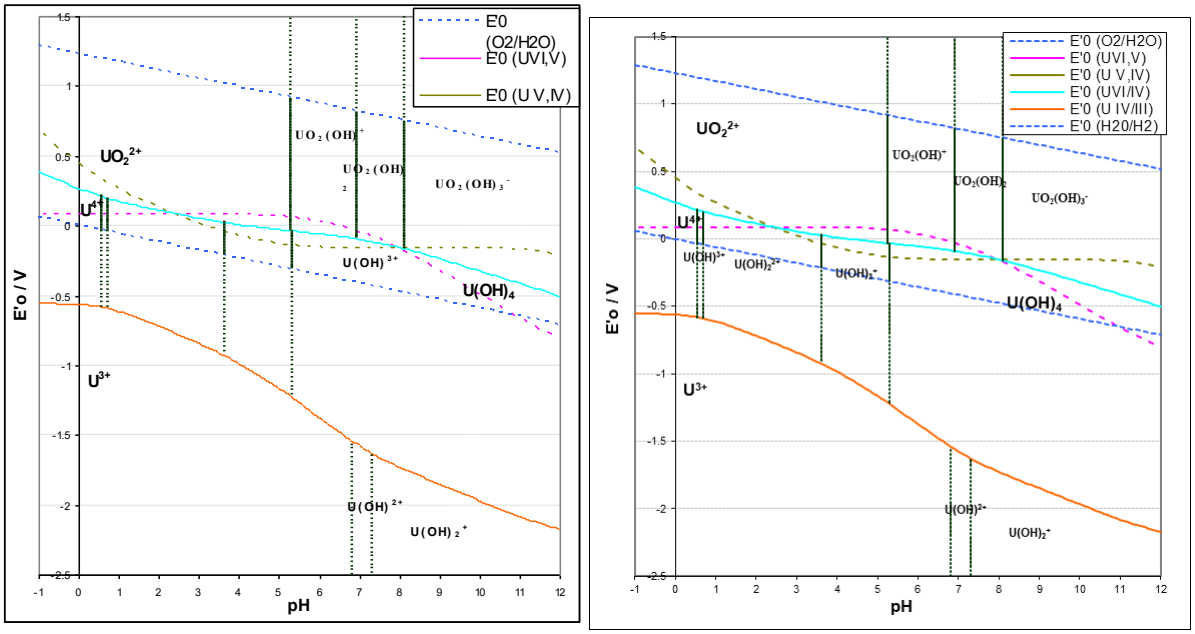

FIGURE 1 INDICATIVE URANIUM E'° – PH PLOTS FOR A. CARBON FREE AND B. CARBONATED SOLUTIONS ($[CO_3]_{TOT}$ = 2.2x10^{-3} M) SOLUTIONS

3.1.3 Sorbent environmental context: carboxylic phases

A review of stability constant data of transition metals, lanthanides, and actinides (d and f elements) complexes with carboxylic ligands has first been carried out. The carboxylic groups ranged from methanoic (formic**)**, to butanoic, and hexanoic, and the correlations between stability constant and respective hydroxide complexes are shown in **Figure 2**.

This data was collected from the literature; however, it was noted that in order that the data set was sufficiently large, it had to include sources with incontistent methodologies, leading occasionally to contradicting results. The data points were considered without independent validation. This can be attributed in part to minor variation in testing conditions, as reported by Smith & Martell (1990) in their introduction.

Most values reported for stability constants and hydrolysis constants have been tested at 25 °C, but some variations in operating temperature, between 18 °C and 32 °C, when reported, were included. This had generally minor impact.

More ranging variability can be identified to stem from the range of ionic strength of solutions reported by the sources, which would lead them to deviate from the reference used for the hydrolysis

constant. In cases where corresponding conditions were not available, values were computed by simple mathematical interpolation by using those that were available.

Furthermore, data on multi-dentate interactions were not fully distributed across the dataset, leading to more challenging extrapolation. These interactions have however limited the calculation of $T_{m(c)}$ and $S_{m(c)}$ to the mono and bidentate forms for all considered materials. The tri-dentate values were calculated, with similar characteristics, but the confidence intervals were found relatively large. The tetra-dentate relation was considered but was later discarded due to the very low availability of source of data.

The correlations between the Log stability constant for poly-dentate complexes of various metals on ethanoic acid surface groups, with the Log of the corresponding hydrolysis constant are shown in **Figure 3** for mono-dentate complexes of various metals, for bi-dentate complexes and for tri-dentate complexes. Here again data was primarily sourced from Smith & Martell (1990).

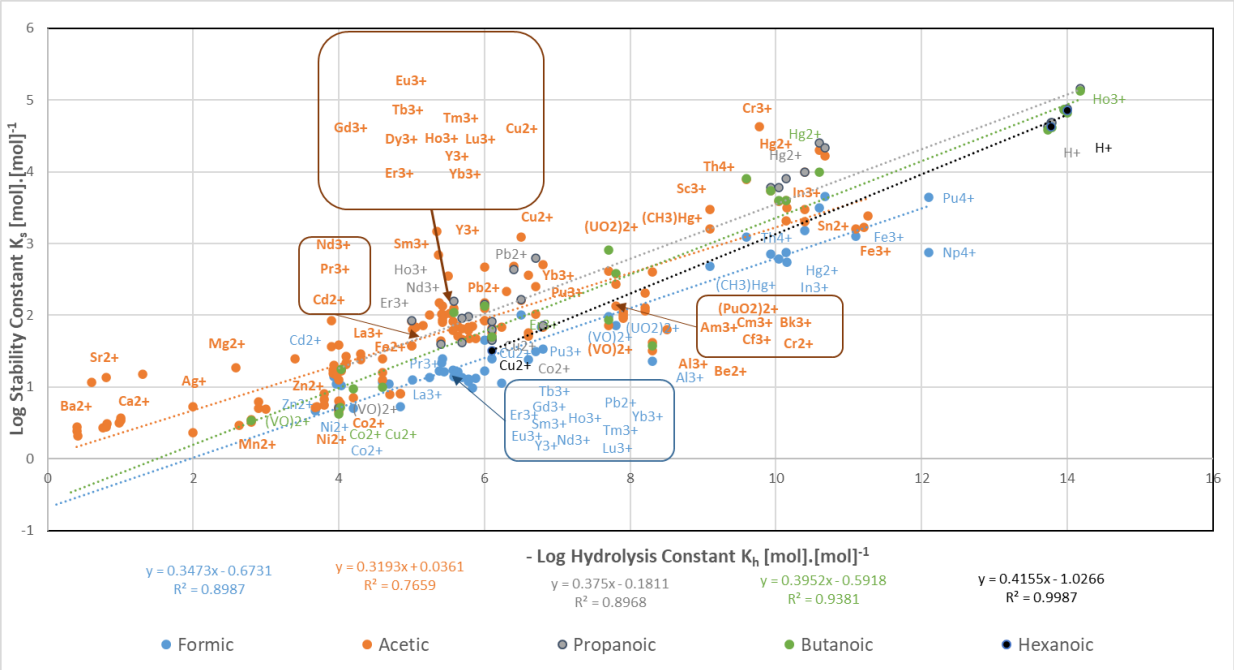

FIGURE 2 COMPARISON OF CORRELATION BETWEEN CARBOXYLIC MONO-DENTATE SURFACE COMPLEXATION CONSTANTS OF VARIOUS METALS AND THEIR RESPECTIVE HYDROXIDE COMPLEXATION CONSTANTS. CONDITIONS: DATA FROM SMITH & MARTELL (1990)

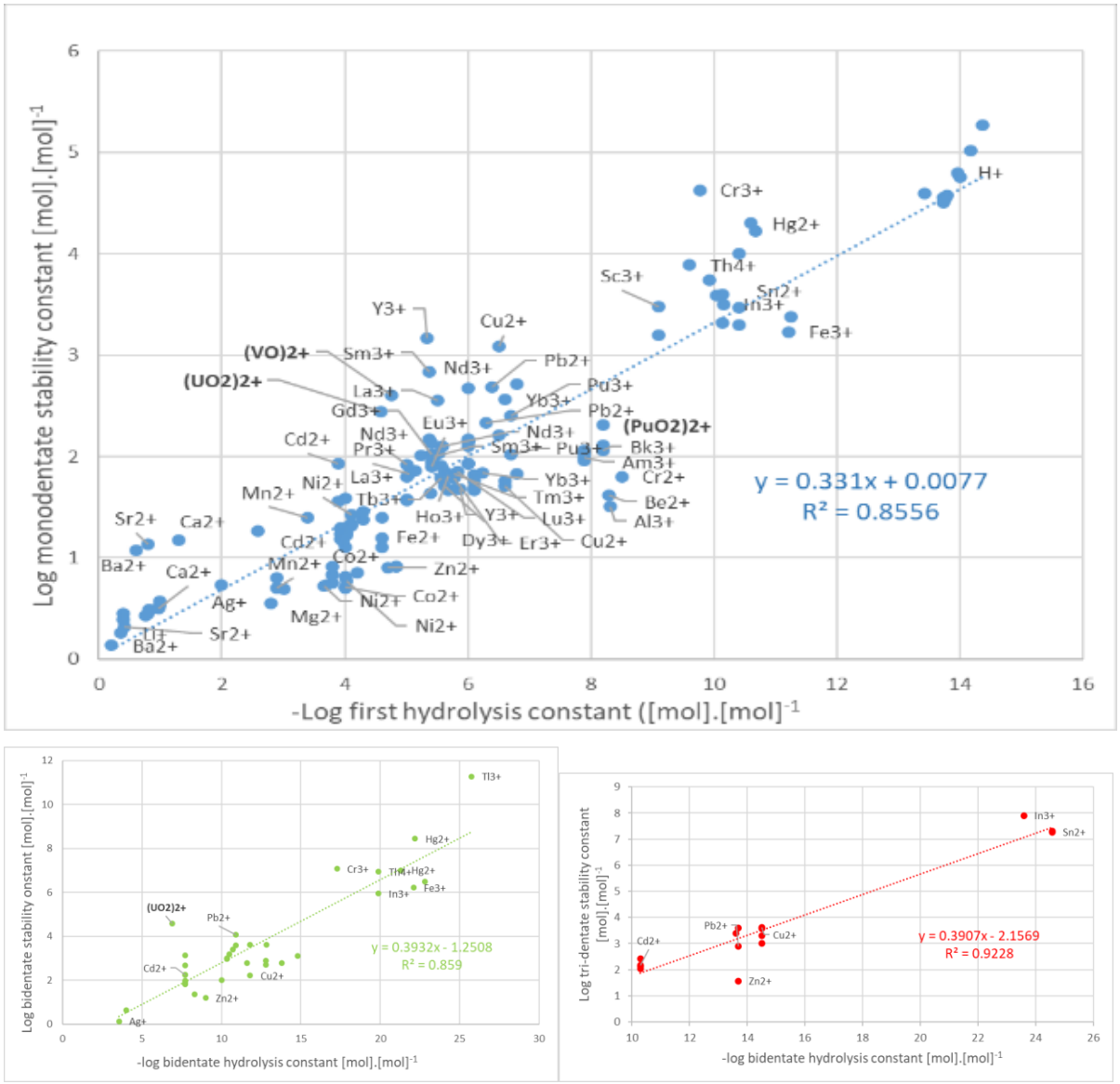

FIGURE 3 CORRELATION BETWEEN THE LOG STABILITY CONSTANT FOR POLY-DENTATE COMPLEXES OF VARIOUS METALS ON ETHANOIC ACID SURFACE GROUPS, WITH THE LOG OF THE CORRESPONDING HYDROLYSIS CONSTANT. CONDITIONS: DATA FROM SMITH & MARTELL (1990)

For the purposes of mapping the relationship, the Log of the hydrolysis constant was compared to the Log of the stability constant. It showed that the predicted relationship was linear (with the majority of trend line fits exhibiting an R^2 greater than 0.8 for first and second ligands on the five acids, with one exception), with the trend lines forming a regular series. Methanoic acid proved to be exceptional with regard to this relationship, but for longer chains, a S_m of between 0.3 and 0.4 was shown to be consistent across the series.

The reduced gradient exhibited by methanoic acid is most likely an exception, stemming from a result of water/acid component interactions with the reagents in solution, creating more complex environment at the microscale. As these effects are less relevant for the longer chains, they were

discounted from the model, as they would represent non negligible deviations for the purposes of calculating the stability of methanolates.

The minimum energy threshold T_m (see **Figure 2 and 3**) displayed a linear relationship with the chain for the first and second binding of ligands, with the exception to the second ligand of propanoate. The fit of this trend line was poor (R^2 of 0.72). These are displayed in **Table 4**. The slope S_m of these linear plots are given in **Table 5**.

TABLE 4. T_M OF VAR. CARBOXYLIC ACIDS FOR THE 1ST TO 4TH DENTATE BINDING COMPLEX CONDITIONS: DATA EXTRACTED FROM FIGURE 2 & FIGURE 3

T_m	Methanoic	Ethanoic	Propanoic	Butanoic		Hexanoic
1st	0.0453	0.0077	-0.527	-0.2516		-1.0266
2nd	-1.1295	-1.2508	-3.037	-1.3621		
3rd	-2.376	-5.0538				
4th	0.0191	-4.0819				

TABLE 5. S_M OF VAR. CARBOXYLIC ACIDS, FOR THE 1ST TO 4TH DENTATE BINDING COMPLEX. CONDITIONS: DATA EXTRACTED FROM FIGURE 2 & FIGURE 3

S_m	Methanoic	Ethanoic	Propanoic	Butanoic		Hexanoic
1st	0.2574	0.331	0.3981	0.3633		0.4155
2nd	0.298	0.3932	0.4668	0.3439		
3rd	0.3336	0.5967				
4th	0.1938	0.5599				

This pattern appears to be caused by the bond strength which is consistent with the forms and dictated by the carboxylic “head”, while the length of chain would affect the initial energy requirement: this is possibly due to restrictions on the angle of incidence that makes the initial contact, or the probability of correct orientation in the plane. This would also illustrate the relation as the binding increases, since the third and fourth bonds necessarily need to form from a different surface complex, which would significantly reduce the likelihood to have a simple mechanism for decoupling from the surface.

While the correlation coefficients for tri- and tetra- dentate were not available for propanoic and butanoic acid derived ligand, specific values were available for some metals at higher chain lengths. The calculated values for UO_2^{2+} is found to be below the known actual values but is within the R^2 values.

Based on this, it was decided that ethanoic acid would be sufficiently representative for the structural repeating unit for longer, more complex mono acids, or poly acids with short inter site chain lengths. While the predicted value for these larger structures have limited data availability, it is a reasonable that from the available data it could be possible to modify the relation.

The minimum energy threshold $Tm_{(c)}$ and the slope $Sm_{(c)}$ values for ethanoic acid used for the simulations are given in **Table 6**. The standard deviation on the minimum energy threshold is given by $\sigma = (1/N)\,[(y-\hat{y})^2]^{1/2}$ with N number of data, y: data value and $\hat{y}$ data obtained by regression.

Table 6. Tm(c) and Sm(c) values for ethanoic acid used for the simulation. Conditions: data from (Smith & Martell, 1990)

Dentate (c)	$T_{m(c)}$ ±SD	$S_{m(c)}$	N
Mono	0.0077±0.0541	0.331	110
Bi	-1.25±1.81	0.3932	32
Tri	-5.05±1.68	0.5967	13
Tetra	-4.08±nc	0.5599	NC

For the purposes of the model, the carboxylic content of the organics is assumed to be 70%, so *I* = 30%

3.1.4 Sorbent environmental context: various phenolic phases

As with the carboxylic molecules, a review of stability constant data for solid phase phenolic acids with d and f block metal ions has been carried out, considering hydroxy-benzene, the (1,2) and the (1,3) isomers of dihydroxy-benzene, and the (1,3) isomer of dihydroxy-naphthalene. The (1,4) isomer of dihydroxy-benzene was considered, but the data was insufficient to make a correlation. In practice, the (1,2) and (1,3) isomers of dihydroxy-benzene proved to be co-linear: and the data was combined to increase the dataset accuracy.

As with the carboxylics, due to the ranging of source data used to compute the relations, testing error was not considered, as the sources do not follow a consistent methodology. The reported values span a (narrow) range of testing conditions (Smith & Martell, 1990). Most values reported for stability

constants and hydrolysis constants were tested at 25 °C, but some variations which varied between 18°C and 32°C were included. More ranging variability stem from the range of ionic strength of solution, which would lead them to be distinct from the basis used for the hydrolysis constant. In cases where corresponding conditions were not available, an interpolated value was computed from those that were available, when possible or discounted otherwise. This variability was combined to produce a single variability characteristic, for the final T_m and S_m variance for simplicity.

Furthermore, data on multi-dentate interactions are limited, with data available for the mono- and bi-dentates of dihydroxy-benzene, and mono- only for the other two. This is likely not directly relevant in practice, as this effect results from the product compounds being too unstable to have detectable residence times in solution. This has limited the calculated T_m and S_m to the mono form, especially since dihydroxy-benzene was found to exhibit a collinear trend and the reported values would be indistinguishable at the reported precision.

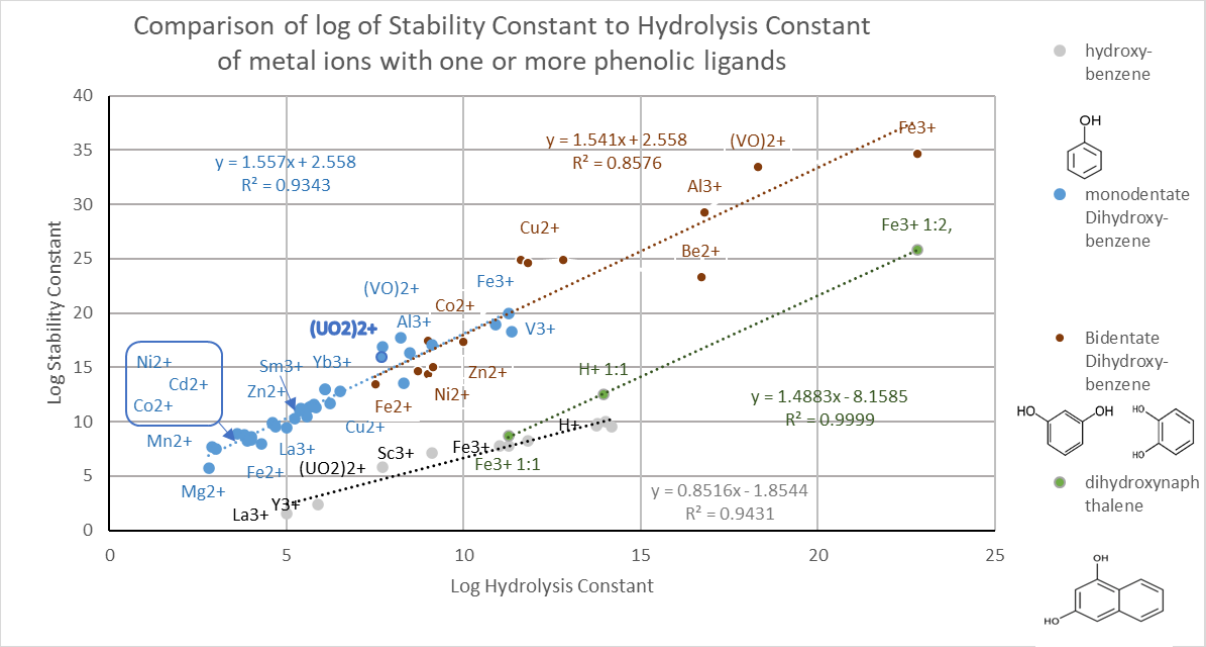

Figure 4. Comparison of various phenolic complexation constants & hydroxide complexation constants of various metal ions, in mono-dentate (1:1) & bi-dentate (1:2) binding, data from (Smith & Martell, 1990)

For the purposes of mapping the relationship, the -Log of the hydrolysis constant was compared to the -Log of the stability constant. It showed that the relationship is linear with all trend line fits, exhibiting an R^2 greater than 0.85. Relationships between the different forms are rather evident. The mono and the bidentate forms of dihydroxy-benzene are almost fully co linear with the small discrepancy likely due to measurement error. Although there is only very limited data available, dihydroxy-naphthalene also exhibits a very similar S_m. Additionally, the S_m of the mono- hydroxyl-benzene form is approximately half that of the di-hydroxy-aromatic form, suggesting a strongly fixed

relation. The minimum energy threshold T_m exhibits the primary difference between forms. These are displayed in **Table 7**.

Although not displayed due to lack of data, data for (1,4) dihydroxy-benzene had a similar T_m value to the displayed dihydroxy- form, but a value of S_m consistent with the mono-hydroxyl form, supporting the hypothesis suggested above. This relation therefore is assumed to hold for the other phenolics.

In order to make the work relevant to our ongoing experimental work, the sorbent materials were assumed to consist of spherical particles 0.2 mm in diameter, with a total concentration of 30 g L^{-1}. The characteristics of each of the three are listed in **Table 7** and the values are based on standard temperature (25°C) and pressure (1 atm) where appropriate.

Table 7 Material property of various hydroxy-benzene group complexes values used for the simulation.

	a (nm)	*b* (nm)	*c* (-)	Density (g cm^{-3})	Molar Mass (g)	pK_a
Hydroxy-benzene	0.43	0.57	1	1.07	94.11	9.99
(1,2) and (1,3) dihydroxy-benzene	0.55	1.01	2	1.34	154.21	9.45
(1,2) dihydroxy-naphthalene	1.1	1.0	2	1.3	160.17	9.04
	T_m (c:1/2)	S_m (c:1/2)	Error (±)	Site Density (nm^{-2})	$[>SuOH]_{Tot}$ ($Mol.g^{-1}$)	
Hydroxy-benzene	-1.85 /-1.85	0.85 /0.85	1.86	4.08	9.50E-08	
(1,2) and (1,3) dihydroxy-benzene	2.56 /2.56	1.54 /1.56	0.60 /2.00	3.61	3.35E-08	
(1,2) dihydroxy-naphthalene	-8.15 /-8.15	1.48 /1.48	5.19	1.80	1.73E-08	

Biomass typically has a phenolic content of 30%, so for the purposes of the model, *I* =70%.

3.2 Modelling Results: Carboxylic

Utilizing the data listed in the previous sections as inputs to equation 23, it is possible to calculate a β_d value for the form of particle specified. This β_d is the total partition coefficient at a given pH and redox, at equilibrium, for the four forms of uranium that were considered ($U^{(iii)}$ to $U^{(vi)}$). In general, at most points in the output, there is a dominant form: usually one form has a $K_{(d)}$ which several orders of magnitude greater than that of the other forms, usually $U^{(IV)}$ or $U^{(VI)}$, especially when considering the particle forms which were selected to correspond to those used in the practical work. However, these are not the only forms considered, and there are circumstances where these can produce dominant forms: for example, $U^{(III)}$ can be predicted to be the dominant form in conditions outside the range considered (pH 2.0, at E(h) < -0.8), corresponding to its very rare existence in nature (Wooles, et al., 2018). It is also possible to predict the Kd of $U^{(V)}$. While it is never the dominant form in the below results, it is possible for it to become such, especially in the context of high concentrations of ligands, or very fine particles, which have very high site availability result in it dominating one phase. These phases are visible as local points of inflection in the transitional zone, rarely larger than 0.05 V wide. In a wider context, the presence of $U^{(V)}$, even if it is never the dominant form, has influence on the transitional zone, in dictating the gradient, and hence the sensitivity to changes in E(h). The curves with the widest transition zones are the ones where $U^{(V)}$ exhibits the greatest K_d. Although these features are not present in the results reported, it is useful to consider these zones, as a demonstration of this influence.

3.2.1 Kd calculations, effect of pH and E for mono-, bi- and tri- carboxylic group complexes.

The K_d (mL g^{-1}) for uranium surface complexation by **individual carboxylic groups** on bioorganic particles in a carbonate free environment as a function of redox potential for various pH values was first calculated. The surfaces of the particles of 0.2 mm diameter are covered by ethanoic groups forming first mono-dentate complexes with $U^{(VI)}$ and at lower E values $U^{(IV)}$. In this case, the calculations were done using the correlations with T_m and S_m given listed in Table 6 for mono-dentates. The results are plotted in Figure 5.

At pH 4 and in oxidative conditions, the Log K_d values are found at **-1.59** for $U^{(VI)}$ (here from -0.1 to +0.96 V) and at the apparent redox potential (-0.26 V) Log K_d has increased to **-0.02** for $U^{(IV)}$.

Subsequently, at pH 6 and in oxidative conditions, Log K_d values are found at **+1.25** for $U^{(VI)}$ (from -0.36 to +0.84 V) and at the apparent redox potential of -0.48 V Log K_d increases up to **+1.58** for $U^{(IV)}$. The later reduction takes however place below the redox stability domain of water.

Later, at pH 8 and in oxidative conditions, Log K_d is found at **+2.53** for $U^{(VI)}$ (from -0.48 to 0.72 V), below the minimum apparent redox potential (-0.48 V) it decreases down to **+1.67** for $U^{(IV)}$ (from -0.48 to -0.62 V). This reduction starts however outside the redox stability domain of water.

Finally, at pH 10 and in oxidative conditions, Log K_d is found at **+2.77** for $U^{(VI)}$ (-0.60 to +0.60 V) and below the minimum apparent redox potential (-0.60 V) Log K_d decreases down at **+1.68** for $U^{(IV)}$ for -0.96 V.

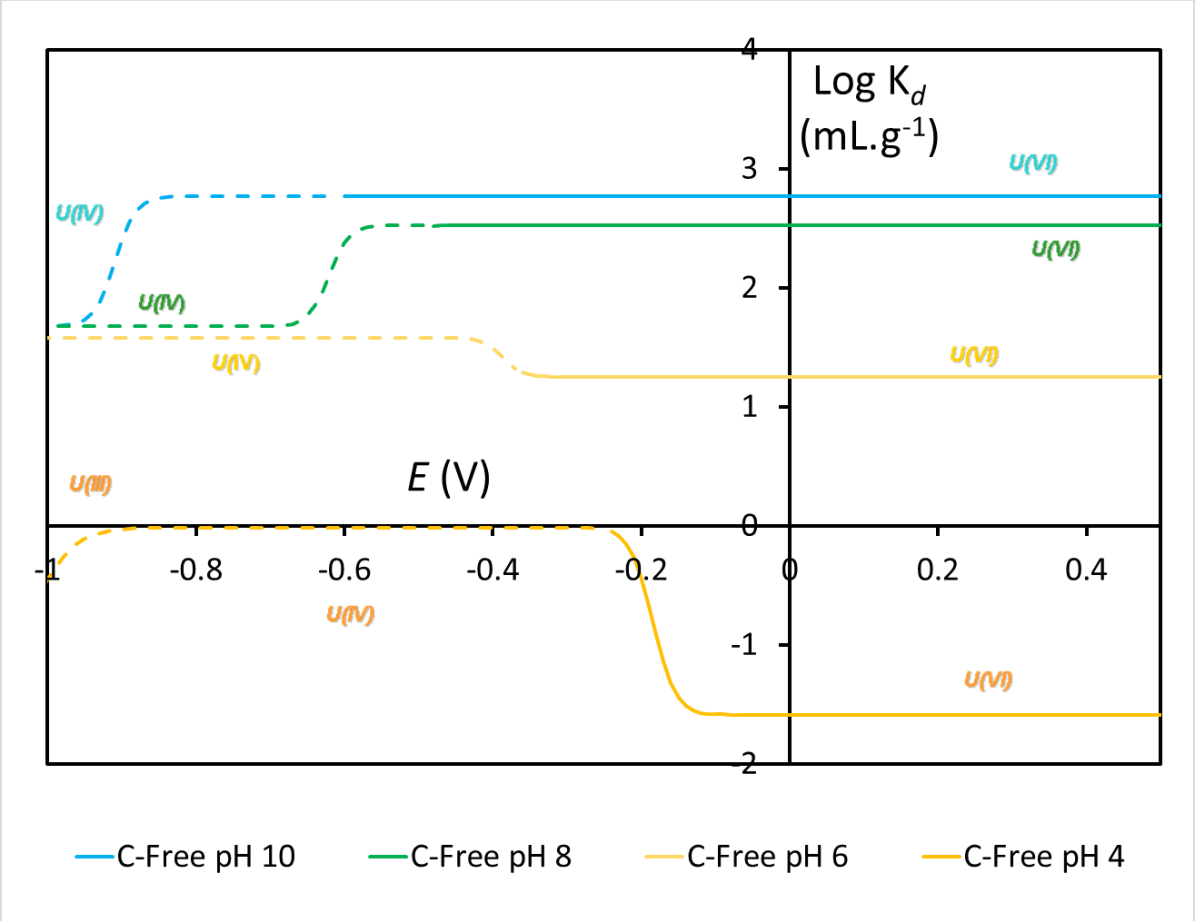

FIGURE 5 URANIUM SORPTION COEFFICIENT KD (ML G^{-1}) AS A FUNCTION OF POTENTIAL FOR VARIOUS PHS ON MONO-DENTATE CARBOXYLIC (ETHANOIC) GROUP LOADED PARTICLES. CONDITIONS: PARTICLES OF 0.2 MM DIAMETER, POTENTIAL VS NHE, SITE DENSITY: 2 NM^{-2}, CARBONATE FREE. SOLID LINES: IN THE WATER REDOX STABILITY DOMAIN, DASHED LINE: OUTSIDE THE WATER REDOX STABILITY DOMAIN.

The K_d (mL g^{-1}) for uranium surface complexation by **two carboxylic groups** on bioorganic particles was then calculated again in carbonate free environment as a function of redox potential for various pH's. The surfaces of the particles of 0.2 mm diameter were covered by ethanoic groups forming bi-dentate complexes with $U^{(VI)}$ and at lower E values with $U^{(IV)}$. Calculations were done using the correlations with T_m and S_m given in Table 6 for bi-dentates. The results are plotted in Figure 6.

At pH 4 and in oxidative conditions (-0.15 to +0.96 V), Log K_d values are found at **-4.06** for $U^{(VI)}$. Below the apparent redox potential Log K_d increases up to **-3.09** for $U^{(IV)}$ (from -0.15 to -0.23 V) just prior the water stability limit (-0.24 V).

Further, at pH 6 and in oxidative conditions, Log K_d values are found at **-0.43** for $U^{(VI)}$ in the redox range -0.3 to +0.84 V Log K_d decreases down to **-1.13** for $U^{(IV)}$ (at -0.43 V, i.e., below the stability limit of water (-0.36 V).

Follow then at pH 8, in oxidative conditions, Log K_d becomes **+0.45** for $U^{(VI)}$ in the domain -0.57 to +0.72 V and then it decreases down to **-1.01** for $U^{(IV)}$ at -0.66 V (i.e., below the water stability limit of -0.48 V) and below.

And finally, at pH 10 and in oxidative conditions, Log K_d is found at **+0.30** for $U^{(VI)}$ and below the apparent redox potential (-0.84 to +0.60 V) Log K_d decreases down to **-1.01** for $U^{(IV)}$ at -0.95 V (below -0.60 V the water limit) and below.

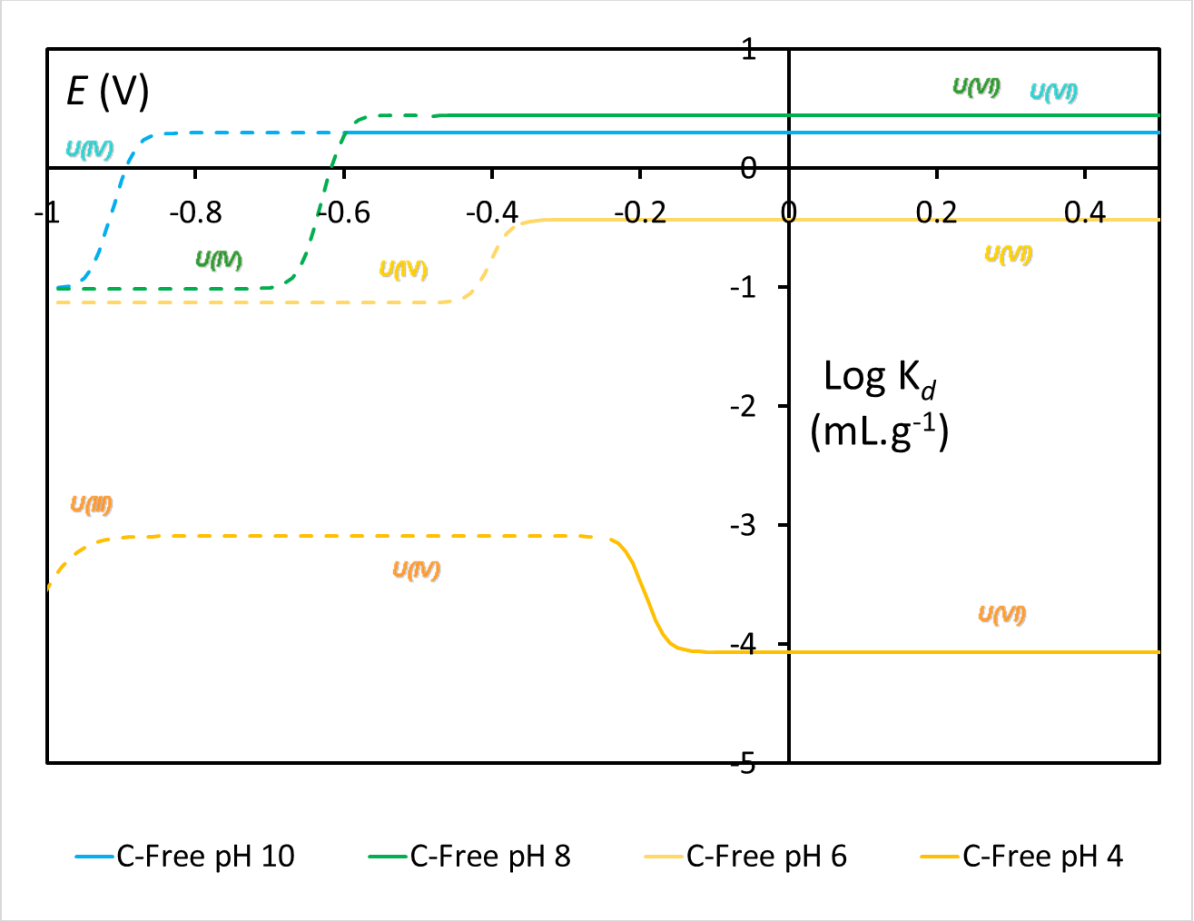

FIGURE 6 URANIUM SORPTION COEFFICIENT KD (ML G-1) AS A FUNCTION OF POTENTIAL FOR VARIOUS PHS ON BI-DENTATE CARBOXYLIC (ETHANOIC) GROUP LOADED PARTICLES. CONDITIONS: PARTICLES OF 0.2 MM DIAMETER, POTENTIAL VS NHE, SITE DENSITY: 2 NM^{-2}, CARBONATE FREE. SOLID LINES: IN THE WATER REDOX STABILITY DOMAIN, DASHED LINE: OUTSIDE THE WATER REDOX STABILITY DOMAIN.

The K_d (mL g^{-1}) for uranium surface complexation by **three carboxylic groups** on bioorganic particles was then calculated in carbonate free environment as a function of redox potential for various pH's. The surfaces of the particles of 0.2 mm diameter are covered by ethanoic groups, forming tri-dentate complexes with $U^{(VI)}$ and at lower E values with $U^{(IV)}$. Calculations were done using the correlations with Tm and Sm given in Table 6 for tri-dentates. The results are plotted in Figure 7.

At pH 4 and in oxidative conditions, Log K_d is found at -6.77 for $U^{(VI)}$ and for the apparent redox potential range: -0.16 to +0.96 V. It then increases up to -5.84 for $U^{(IV)}$ at -0.24 V, i.e., at the reduction limit of water.

Then at pH 6, in oxidative conditions, Log K_d is found at -2.33 for $U^{(VI)}$ in the potential range going from -0.35 to +0.84 V, and would decrease slightly down to +9.2 for $U^{(IV)}$ at -0.43 V, below the water redox limit -0.36 V.

At pH 8 and in oxidative conditions, Log K_d is found at -1.43 for $U^{(VI)}$ in the redox domain (-0.54 to +0.72 V) and then decreases to -5.89 for $U^{(IV)}$ at -0.68 V again below the water limit (-0.48 V).

At pH 10 and in oxidative conditions, Log K_d is found at -1.59 for $U^{(VI)}$ from the apparent redox potential +0.6 down to -0.85 V and should increases subsequently up to -5.95 for $U^{(IV)}$ at -0.95 V.

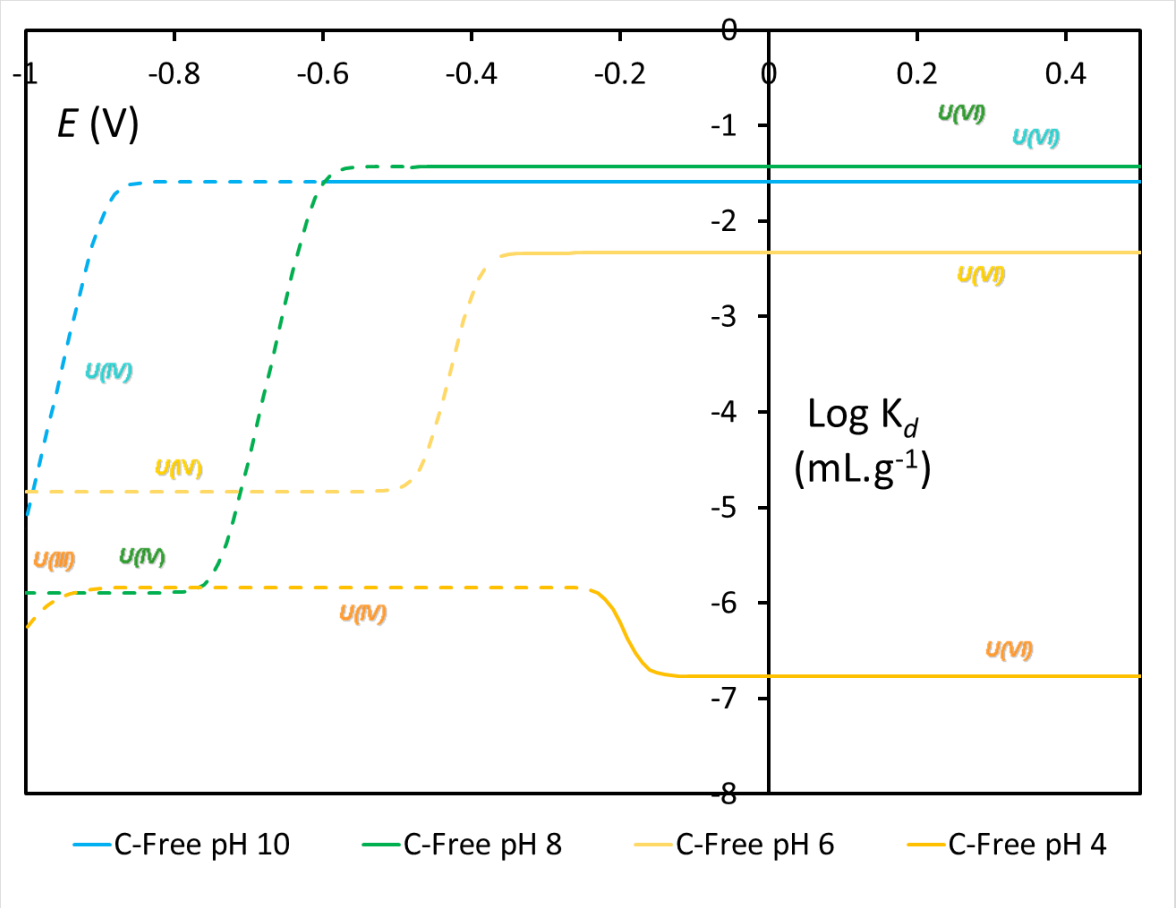

FIGURE 7 URANIUM SORPTION COEFFICIENT KD (ML G-1) AS A FUNCTION OF POTENTIAL FOR VARIOUS PHS ON TRI-DENTATE CARBOXYLIC (ETHANOIC) GROUP LOADED PARTICLES. CONDITIONS: PARTICLES OF 0.2 MM DIAMETER, POTENTIAL VS NHE, SITE DENSITY: 2 NM^{-2}, CARBONATE FREE. SOLID LINES: IN THE WATER REDOX STABILITY DOMAIN, DASHED LINE: OUTSIDE THE WATER REDOX STABILITY DOMAIN.

3.2.2 K_d calculations, effect of pH and E for mono-, bi- and tri- carboxylic group complexes, effect of carbonate

The K_d (mL g^{-1}) for uranium surface complexation by **single carboxylic groups** on bioorganic particles was first calculated in a $2x10^{-3}$ M carbonate suspension (i.e., seawater case at pH 8) as a function of redox potential for various pH's. The surfaces of the particles of 0.2 mm diameter are covered by ethanoic groups, forming mono-dentate complexes with $U^{(VI)}$ and at lower E values $U^{(IV)}$. Calculations were first done using the correlations with Tm and Sm given in Table 6 for mono-dentates. The results are plots are plotted in Figure 8.

At pH 4 and in carbonated conditions, Log K_d is found at -15.43 for $U^{(VI)}$ (from -0.06 to 0.96 V) and below the apparent redox potential of -0.06 V it transitions down to -17.35 for $U^{(IV)}$ (at -0.25 V).

For pH 6, in carbonated conditions, Log K_d is observed at -11.75 for $U^{(VI)}$ (from -0.34 to +0.84 V). It then increases up to -9.14 for $U^{(IV)}$. Below -0.48 V however, these values are below the reduction limit of water (-0.36 V).

Further at pH 8 and in carbonated conditions, Log K_d is found at -7.22 for $U^{(VI)}$ for the apparent redox potential ranging from -0.48 to +0.72 V. It would then transit up to -1.13 for $U^{(IV)}$, however this would be below the redox stability limit of water (-0.48V).

Finally, at pH 10, in carbonated conditions, Log K_d is found at -1.34 for $U^{(VI)}$ (from -0.6 to 0.60 V) in the apparent redox potential range (-0.60 to +0.60 V), it would increase up to +1.68 for $U^{(IV)}$ below -0.7 V.

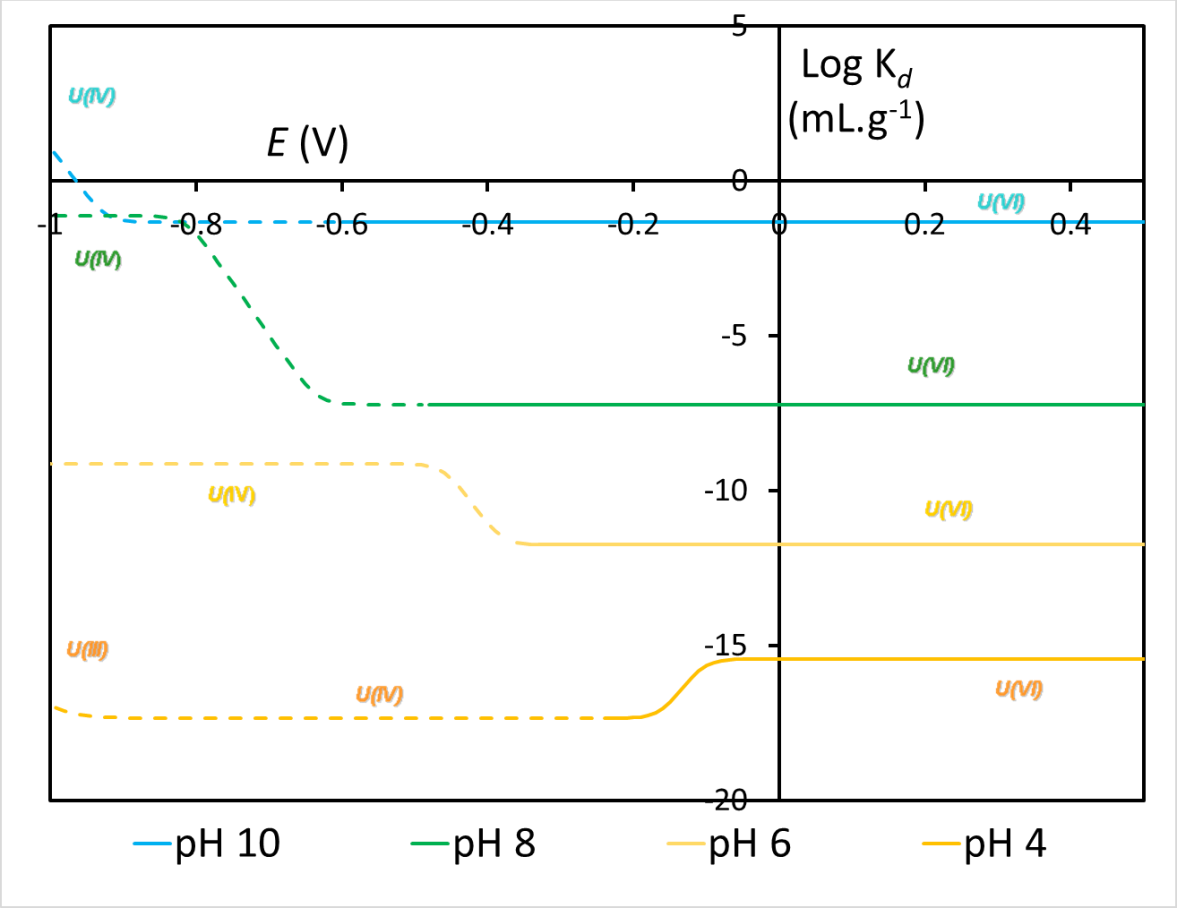

FIGURE 8 URANIUM SORPTION COEFFICIENT K_D (ML G^{-1}) AS A FUNCTION OF POTENTIAL FOR VARIOUS PHS ON MONO-DENTATE CARBOXYLIC (ETHANOIC) GROUP LOADED PARTICLES. CONDITIONS: PARTICLES OF 0.2 MM DIAMETER, POTENTIAL VS NHE, SITE DENSITY: 2 NM^{-2}, 2.2 X 10^{-3} M TOTAL CARBONATE CONCENTRATION. SOLID LINES: IN THE WATER REDOX STABILITY DOMAIN, DASHED LINE: OUTSIDE THE WATER REDOX STABILITY DOMAIN.

The K_d (mL g^{-1}) for uranium surface complexation by **double carboxylic groups** on bioorganic particles was first calculated in a 2x10^{-3} M carbonate suspension as a function of redox potential for various pH's. The surfaces of the particles of 0.2 mm diameter are covered by ethanoic groups, forming bi-dentate complexes with $U^{(VI)}$ and at lower E values $U^{(IV)}$. Calculations were first done using the correlations with T_m and S_m given in Table 6 for bi-dentates. The results are plots are plotted in Figure 9.

At pH 4, in carbonated conditions, Log K_d is found at **-17.91** for $U^{(VI)}$ for the apparent redox potential going from -0.10 to +0.96 V. It then transitions down to **-20.43** for $U^{(IV)}$ at -024 V (water stability limit).

Subsequently, at pH 6, in carbonated conditions, Log K_d is found at **-13.44** for $U^{(VI)}$ for the apparent redox potential range -0.36 to +0.84 V. It then increases up to **-11.85** for $U^{(IV)}$ at -0.50 V.

For pH 8, in carbonated conditions, Log K_d becomes **-9.30** for $U^{(VI)}$, for the apparent redox potential going from -0.59 to +0.72 V. It then increases up to **-3.81** for $U^{(IV)}$ (-0.84 V i.e., below the water stability limit).

Finally, at pH 10, in carbonated conditions, Log K_d reaches the value of **-3.81** for $U^{(VI)}$ for the apparent redox potential, going from -0.60 to +0.60 V and before the formation of $U^{(IV)}$ (below -0.90 V).

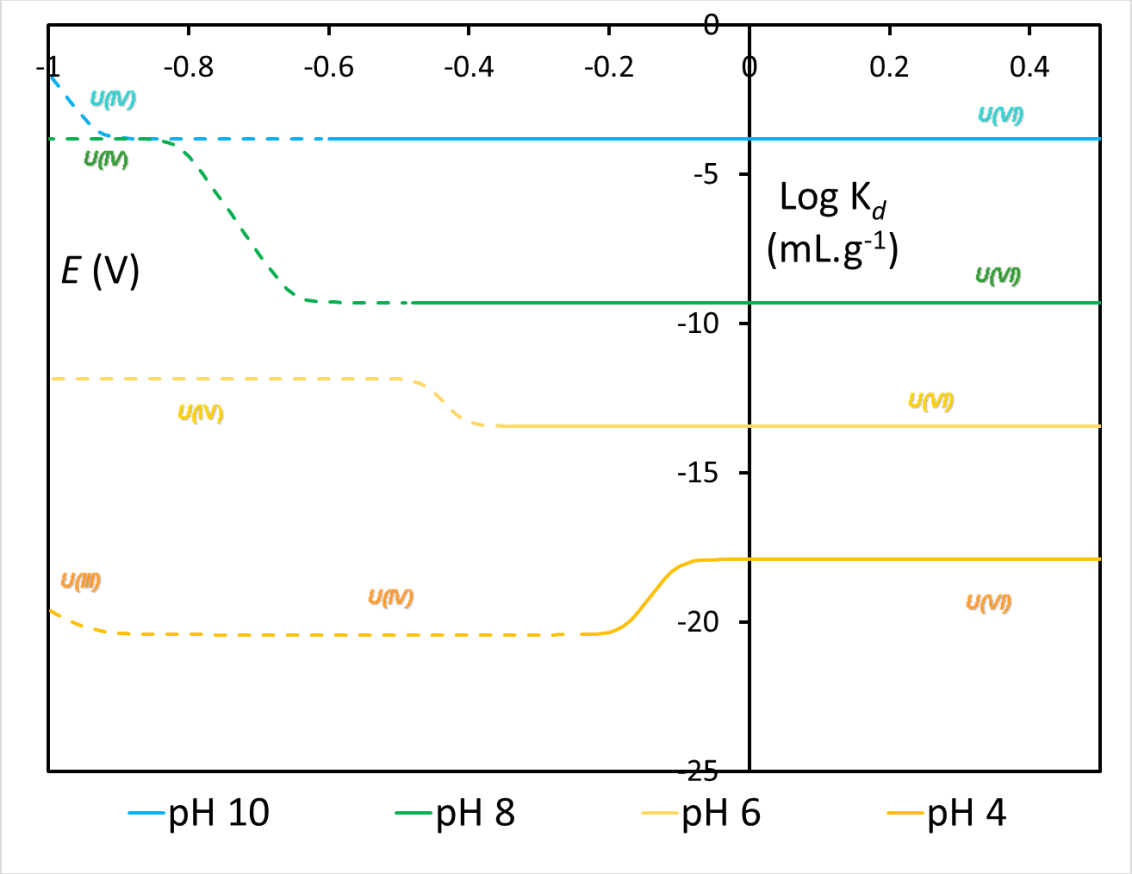

FIGURE 9 URANIUM SORPTION COEFFICIENT K_D (ML G^{-1}) AS A FUNCTION OF POTENTIAL FOR VARIOUS PHS ON BI-DENTATE CARBOXYLIC (ETHANOIC) GROUP LOADED PARTICLES. CONDITIONS: PARTICLES OF 0.2 MM DIAMETER, POTENTIAL VS NHE, SITE DENSITY: 2 NM^{-2}, 2.2 X 10^{-3} M TOTAL CARBONATE CONCENTRATION. SOLID LINES: IN THE WATER REDOX STABILITY DOMAIN, DASHED LINE: OUTSIDE THE WATER REDOX STABILITY DOMAIN.

The K_d (mL g^{-1}) for uranium surface complexation by **triple carboxylic groups** on bioorganic particles was first calculated in a $2x10^{-3}$ M carbonate suspension as a function of redox potential for various pH's. The surfaces of the particles of 0.2 mm diameter are covered by ethanoic groups forming tri-dentate complexes with $U^{(VI)}$ and at lower E values $U^{(IV)}$. Calculations were first done using the correlations with T_m and S_m given in Table 6 for tri-dentate. The results are plots are plotted in Figure 10.

At pH 4, in carbonated conditions, Log K_d is found at **-20.61** for $U^{(VI)}$ for the apparent redox potential of -0.06 to +0.96 V. It then transitions down to **-23.17** for $U^{(IV)}$ at -0.21 V just above the water limit (-0.24V).

Then, at pH 6, in carbonated conditions, Log K_d is found to be **-15.34** for $U^{(VI)}$ in the apparent redox potential ranging from -0.33 to +0.84 V. It then increases up to **-15.55** for $U^{(IV)}$ at -0.48V, below the water limit (-0.36V).

For pH 8, in carbonated conditions, Log K_d is to be found at **-11.18** for $U^{(VI)}$ above the apparent redox potential of -0.6 to +0.72 V. It would then increase up to **-8.69** for $U^{(IV)}$ at -0.86 V. This would be below the water limit of -0.48 V.

Finally, at pH 10, in carbonated conditions, Log K_d becomes **-5.70** for $U^{(VI)}$ for the apparent redox potential range: -0.88 to +0.60 V. It would increase up to **-5.95** for $U^{(IV)}$ at -1.06 V. This reduction would however take place below the stability of water (-0.60 V) at this pH.

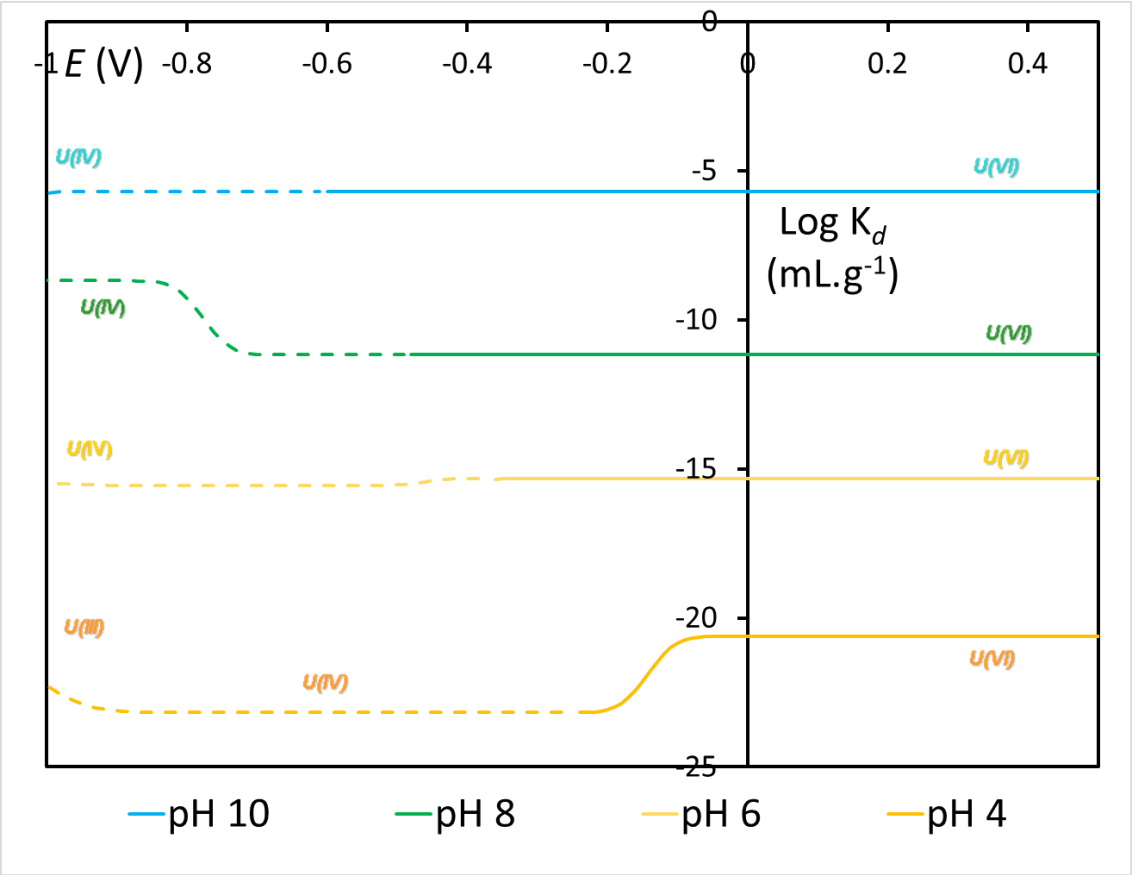

FIGURE 10 URANIUM SORPTION COEFFICIENT K_D (mL g^{-1}) AS A FUNCTION OF POTENTIAL FOR VARIOUS PHS ON TRI-DENTATE CARBOXYLIC (ETHANOIC) GROUP LOADED PARTICLES. CONDITIONS: PARTICLES OF 0.2 MM DIAMETER, POTENTIAL VS NHE, SITE DENSITY: 2 nm^{-2}, 2.2 x 10^{-3} M TOTAL CARBONATE CONCENTRATION. SOLID LINES: IN THE WATER REDOX STABILITY DOMAIN, DASHED LINE: OUTSIDE THE WATER REDOX STABILITY DOMAIN.

3.2.3 K_d calculations under varying carbonate concentrations

The K_d (mL g^{-1}) for uranium surface complexation by a **single carboxylic group** on bioorganic particles was calculated in a carbonate suspension, which can vary between 0, $2.2x10^{-6}$ and $2.2x10^{-0}$ or 2.2 M as a function of redox potential for pH 8.0. This range was selected as it provides reasonable values of surface carbonate concentrations and pH in the Irish Sea (e.g., Rérolle, *et al* (2012)) The surfaces of the particles of 0.2 mm diameter are covered by ethanoic groups, forming mono-dentate complexes with $U^{(VI)}$ and at lower E values with $U^{(IV)}$. Calculations were first done using the correlations with T_m and S_m given in **Table 6** for mono-dentates. The results are plotted in Figure 11, and summarised in Table 8.

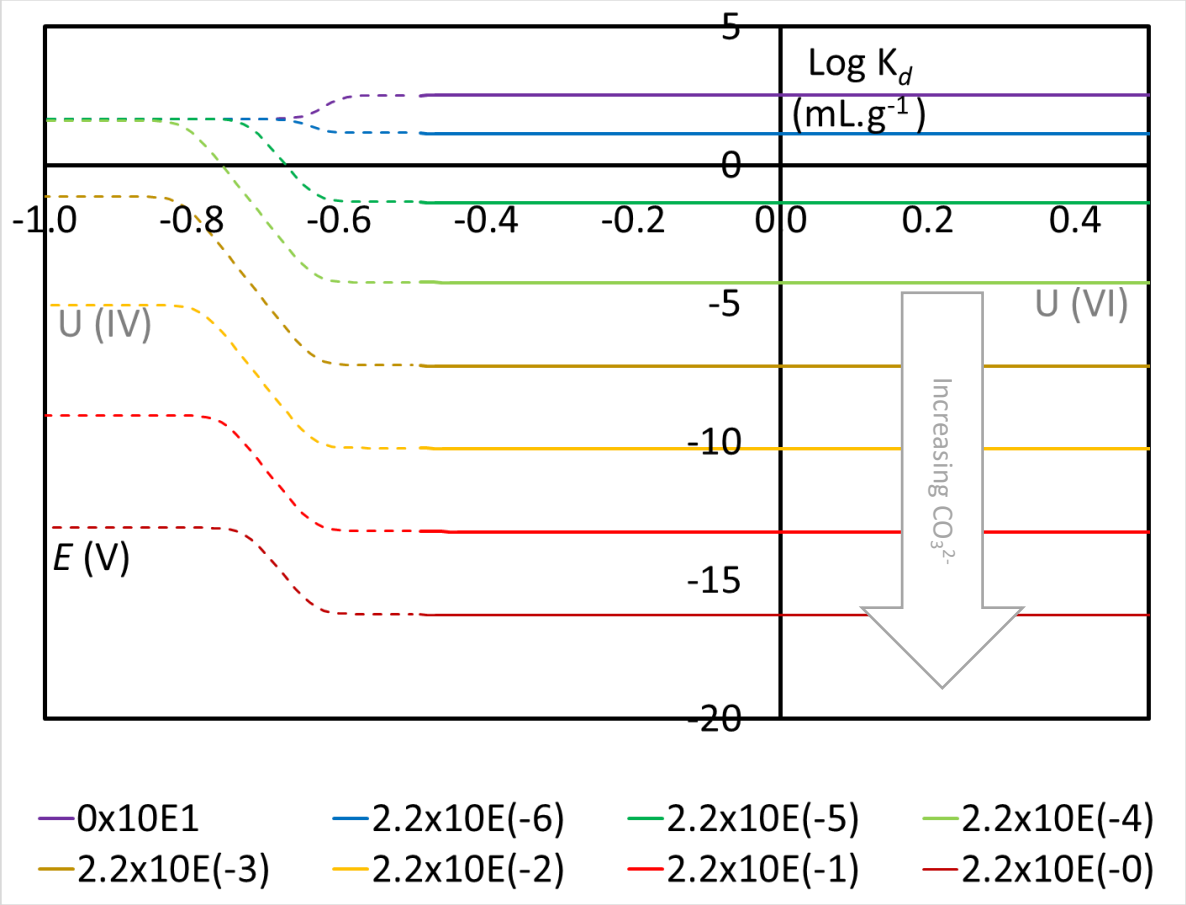

FIGURE 11 URANIUM SORPTION COEFFICIENT K_D (ML G^{-1}) AS A FUNCTION OF POTENTIAL FOR PH 8.0 AND OVER VARYING CARBONATE CONCENTRATIONS ON MONO-DENTATE CARBOXYLIC (ETHANOIC) GROUP LOADED PARTICLES. CONDITIONS: PARTICLES OF 0.2 MM DIAMETER, POTENTIAL VS NHE, SITE DENSITY: 2 NM^{-2}. SOLID LINES: IN THE WATER REDOX STABILITY DOMAIN DASHED LINE: OUTSIDE THE WATER REDOX STABILITY DOMAIN TOTAL CARBONATE CONCENTRATION: 0, $2.2x10^{-6}$, $2.2x10^{-5}$, $2.2x10^{-4}$, $2.2x10^{-3}$, $2.2x10^{-2}$, $2.2x10^{-1}$ AND $2.2x10^{-0}$ M FROM ABOVE TO BELOW.

For carbonate concentrations below $2.2x10^{-6}$ M, the Log K_d is consistent, at ~2.8. As the carbonate concentration rises, it increasingly interferes with the surface complex formation, reducing the K_d. This K_d change is observed for $U^{(IV)}$ and $U^{(VI)}$.

It then begins a transition to the $U^{(VI)}$ associated K_d, which is much more displaced by the presence of the carbonates. Each order of magnitude increase in carbonate concentration decreases the log K_d by about 3.

The $U^{(IV)}/U^{(VI)}$ point of transition, E'°, is consistent at around -0.60 V, but the inflexion point varies: the most negative point (-0.72 V) being found for a carbonate concentration of $2.2x10^{-3}$ M. This is due to the presence of the $U^{(VI)}$ carbonato complexes. At higher carbonate concentrations, $U^{(IV)}$ starts to form complexes increasing the apparent standard redox potential of the couple. It must be noted that all the redox domains, where $U^{(IV)}$ forms, are below the stability limits of water i.e., -0.48 V.

TABLE 8 TRANSITION POINT E'° AND LOG K_D'S (ML G^{-1}) FOR $U^{(VI)}$ AND $U^{(IV)}$ SORPTION ON MONO-DENTATE CARBOXYLIC GROUPS VARYING THE TOTAL CARBONATE CONCENTRATION AT PH 8.

CO_3 Conc.(M)	$U^{(VI)}$ Log K_d	$U^{(IV)}$ Log K_d	$U^{(IV)}/U^{(VI)}$ E'° (V)
0.00E+00	+2.53	+1.67	-0.60
2.20E-06	+1.17	+1.67	-0.60
2.20E-05	-1.32	+1.67	-0.66
2.20E-04	-4.23	+1.61	-0.71
2.20E-03	-7.22	-1.13	-0.71
2.20E-02	-10.2	-5.05	-0.70
2.20E-01	-13.2	-9.04	-0.69
2.20E+00	-16.2	-13.1	-0.68

The K_d mL g^{-1}) for uranium surface complexation by **two carboxylic groups** on bioorganic particles was calculated in a carbonate suspension which varies between 0, $2.2x10^{-6}$ and $2.2x10^{-0}$ (or 2.2) M as a function of redox potential for pH 8.0. Calculations were first done using the correlations with T_m and S_m given in **Table 6** for bi-dentates. The results are plotted in **Figure 12**, and summarized in **Table 9**.

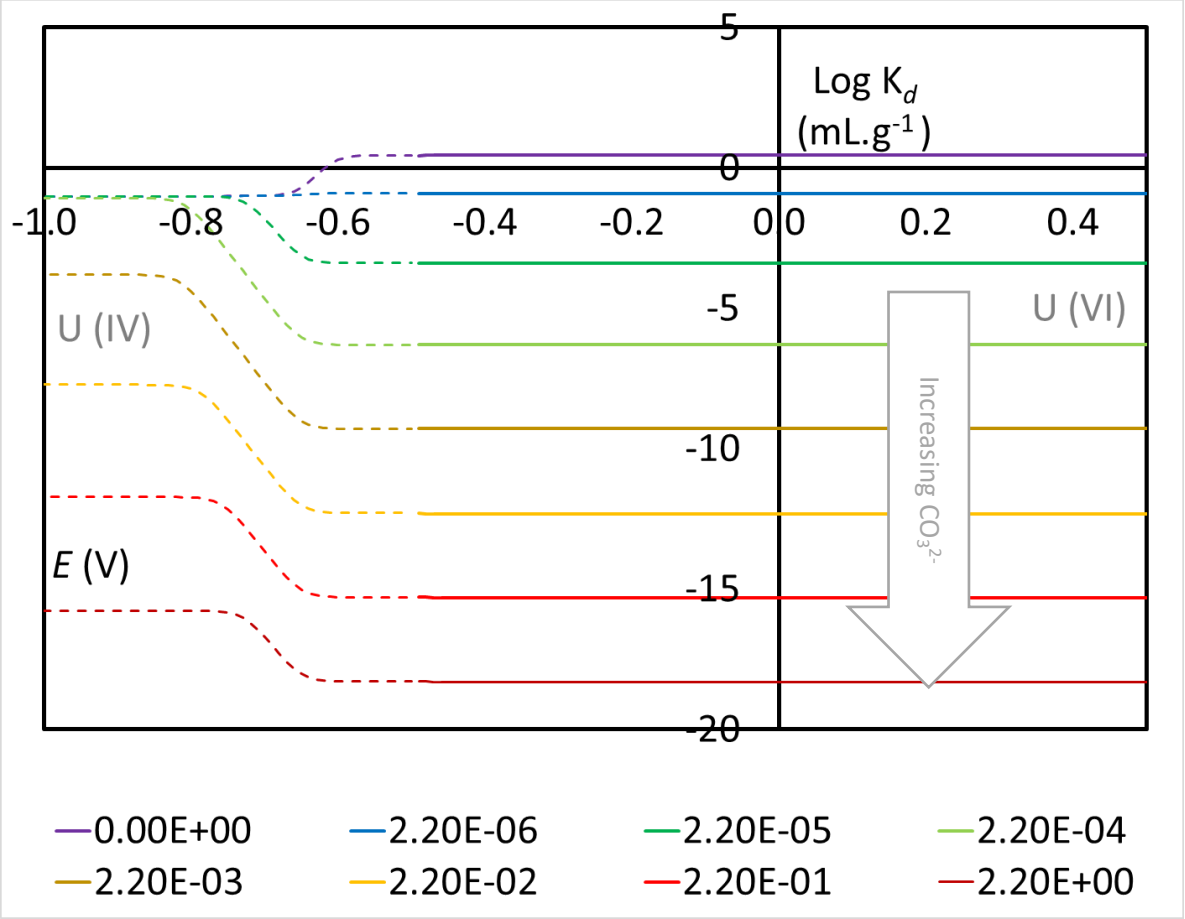

FIGURE 12 URANIUM SORPTION COEFFICIENT K_D (ML G^{-1}) AS A FUNCTION OF POTENTIAL FOR PH 8.0 & OVER VARYING CARBONATE CONCENTRATIONS ON BI-DENTATE CARBOXYLIC (ETHANOIC) GROUP LOADED PARTICLES. CONDITIONS: PARTICLES OF 0.2 MM DIAMETER, POTENTIAL VS NHE, SITE DENSITY: 2 NM^{-2}. SOLID LINES: IN THE WATER REDOX STABILITY DOMAIN, DASHED LINE: OUTSIDE THE WATER REDOX STABILITY DOMAIN. TOTAL CARBONATE CONCENTRATION: 0, $2.2x10^{-6}$, $2.2x10^{-5}$, $2.2x10^{-4}$, $2.2x10^{-3}$, $2.2x10^{-2}$, $2.2x10^{-1}$ AND $2.2x10^{-0}$ M FROM ABOVE TO BELOW.

For carbonate concentrations below $2.2x10^{-6}$, the Log K_d is consistent, at ~9.9. As the carbonate concentration rises, it increasingly interferes with the binding, reducing the K_d. This K_d would be associated with $U^{(IV)}$.

It then begins a transition to the $U^{(VI)}$ associated K_d, which is much more displaced by the presence of the carbonates. For each order of magnitude increase in concentration the log K_d decreases by about 3.

$U^{(IV)}/U^{(VI)}$ point of transition, E'°, is consistent at around -0.63 V, but the inflection point varies: the most negative point (-0.73 V) being found for a carbonate concentration of $2.2x10^{-3}$ M. This is due to the presence of the $U^{(VI)}$ carbonato complexes. At higher carbonate concentrations, $U^{(IV)}$ starts to form complexes increasing the apparent standard redox potential of the couple. Here again all the redox domains, where $U^{(IV)}$ forms are below the water stability limits i.e., -0.48 V.

TABLE 9 TRANSITION POINT E'° AND LOG K_D'S (ML G^{-1}) FOR $U^{(VI)}$ AND $U^{(IV)}$ SORPTION ON BI-DENTATE CARBOXYLIC GROUPS VARYING THE CARBONATE CONCENTRATION AT PH 8.

Carbonate Conc. (M)	$U^{(VI)}$ Log K_d	$U^{(IV)}$ Log K_d	$U^{(IV)}/U^{(VI)}$ E'° (V)
0.00E+00	+0.45	-1.01	-0.63
2.20E-06	-0.91	-1.01	-0.63
2.20E-05	-3.40	-1.01	-0.67
2.20E-04	-6.31	-1.08	-0.71
2.20E-03	-9.30	-3.81	-0.73
2.20E-02	-12.3	-7.73	-0.71
2.20E-01	-15.3	-11.7	-0.70
2.20E+00	-18.3	-15.8	-0.68

The K_d (mL g^{-1}) for uranium surface complexation by **three carboxylic groups** on bioorganic particles was calculated in a carbonate suspension which varies between 0, $2.2x10^{-6}$ and $2.2x10^{-0}$ M as a function of redox potential for pH 8.0. The surfaces of the particles of 0.2 mm diameter are covered by ethanoic groups, forming tri-dentate complexes with $U^{(VI)}$ and at lower E values $U^{(IV)}$. Calculations were first done using the correlations. The results are plots are plotted in **Figure 13** and are summarized in **Table 10**.

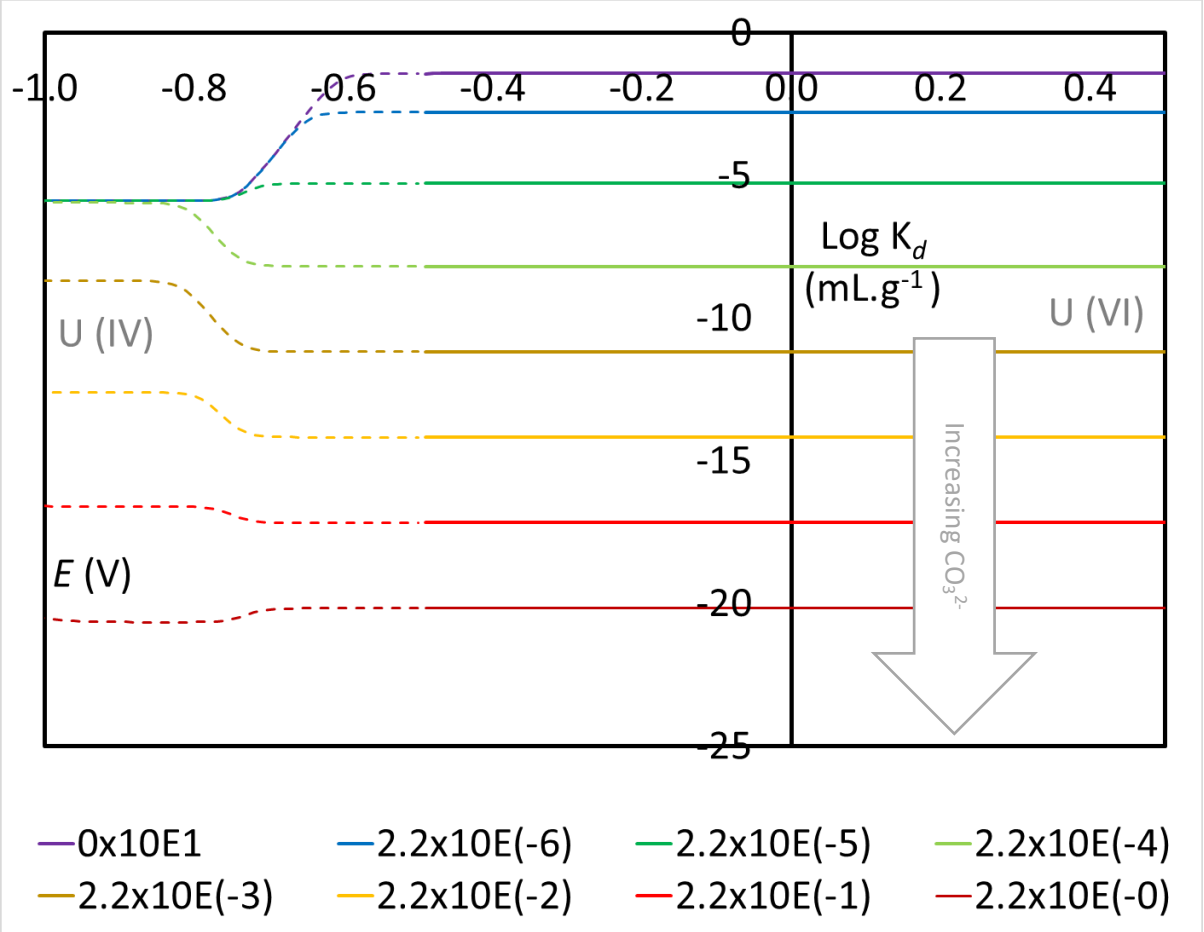

FIGURE 13 URANIUM SORPTION COEFFICIENT K_D ($mL\ g^{-1}$) AS A FUNCTION OF POTENTIAL FOR PH 8.0 AND OVER VARYING CARBONATE CONCENTRATIONS ON TRI-DENTATE CARBOXYLIC (ETHANOIC) GROUP LOADED PARTICLES. CONDITIONS: PARTICLES OF 0.2 MM DIAMETER, POTENTIAL VS NHE, SITE DENSITY: 2 NM^{-2} SOLID LINES: IN THE WATER REDOX STABILITY DOMAIN, DASHED LINE: OUTSIDE THE WATER REDOX STABILITY DOMAIN. TOTAL CARBONATE CONCENTRATION: 0, $2.2x10^{-6}$, $2.2x10^{-5}$, $2.2x10^{-4}$, $2.2x10^{-3}$, $2.2x10^{-2}$, $2.2x10^{-1}$ AND $2.2x10^{-0}$ M FROM ABOVE TO BELOW.

For concentrations below $2x10^{-6}$ M, the Log K_d is found at ~9.4 for $U^{(VI)}$. As the carbonate concentration rises, it increasingly interferes with the binding, reducing the K_d.

Each order of magnitude increase in carbonate concentration decreases the Log K_d by ~3.

For the $U^{(IV)}/U^{(VI)}$ couple the apparent redox potential, E'°, is found around -0.62 V, but its value varies: the most negative point (-0.72 V) being found for a carbonate concentration of $2.2x10^{-2}$ M. This is due to the presence of the $U^{(VI)}$ carbonato complexes. At higher carbonate concentrations $U^{(IV)}$ starts to form complexes, increasing the apparent standard redox potential of the couple. Again, all the redox domains where $U^{(IV)}$ forms are below the stability limits of water i.e., -0.48 V.

TABLE 10 TRANSITION POINT E'° AND LOG K_D'S (ML G^{-1}) FOR $U^{(VI)}$ AND $U^{(IV)}$ SORPTION ON TRI-DENTATE CARBOXYLIC GROUPS VARYING THE CARBONATE CONCENTRATION AT PH 8.

Carbonate Conc. (M)	$U^{(VI)}$ Log K_d	$U^{(IV)}$ Log K_d	$U^{(IV)}/U^{(VI)}$ E'° (V)
0.00E+00	-1.43	-5.89	-0.62
2.20E-06	-2.79	-5.89	-0.65
2.20E-05	-5.28	-5.89	-0.67
2.20E-04	-8.19	-5.96	-0.70
2.20E-03	-11.2	-8.69	-0.71
2.20E-02	-14.2	-12.6	-0.72
2.20E-01	-17.2	-16.6	-0.70
2.20E+00	-20.2	-20.7	-0.69

3.2.4a Effect of pH, E, and dentate state on K_d in carbonate free solution

As the simplest case, the carbonate free systems exhibited the clearest trends (**Figure 5**, **Figure 6** and **Figure 7**). The dominating factor under moderate to high pH (6-10) was the transition between conditions where $U^{(IV)}$ prevails, and those where $U^{(VI)}$ species are dominant. As expected, the $U^{(IV)}$ is generally more sorbing than $U^{(VI)}$, likely due to the stereochemistry effects, stronger hydrolysis of $U^{(IV)}$ than $U^{(VI)}$ or both. An increase in pH also increases the Log K_d. This is manifested by an increasing negative apparent redox potential E'°. Below pH 4, the possibility of U(III) became significant at low redox potentials, mitigating consequently the K_d.

Between the three forms considered (mono-, bi- and tri-), mono-dentate is slightly different than the multi-dentate forms. In mono- form, the effect of increasing pH slightly raising Log K_d, this is also observed for the bi-dentate and for the $U^{(VI)}$ in the tri-dentate case. In addition, increasing pH has an increasing effect on tri-dentate than on bi-dentate.

However, both are similar at pH 6-8 range, which exhibits values that are consistent with real world measurements in natural environments. At low pH, both are reduced, but the effect is more marked in tridentate systems. It is presumably to be due to the slopes in the correlations e.g. data see **Figure**

2 & **Figure 3**. The model applied here (see Section 2) is also applicable to other redox sensitive elements.

3.2.4b Effect of pH, E, and dentate state on Kd in carbonated solution

In presence of carbonate ligands, the competition effects between the carbonates complexes formation and the sorption by surface complexation are noticeable (See **Figure 8**, **Figure 9** and **Figure 10**). The dominating factor under moderate to high pH is still the hydrolysis, but this is herein between conditions where $U^{(V)}$ is locally/occasionally found, and those where $U^{(VI)}$ and $U^{(IV)}$ are dominant. The effect of this transition is significantly different, reducing the degree of step difference between the $U^{(V)}$ form and both $U^{(VI)}$ and $U^{(IV)}$ forms.

As expected, the $U^{(IV)}$ is more sorbing, likely due to the stereochemistry effects or actually due to a stronger hydrolysis of $U^{(IV)}$ than $U^{(VI)}$. An increasing pH mitigates this effect however, which is probably due to build-up of $U^{(IV)}$ and $U^{(VI)}$ hydroxo complexes, reducing the sorption of U. These effects also negatively shift the redox point of transition in the Log K_d - E plot. Below pH 4, the possibility of $U^{(III)}$ is becoming significant at low redox potentials.

3.2.4c Comparing the model calculation with the literature data

To test the results obtained by applying the sorption model developed in this study, one would use results gained for the sorption of uranium onto carboxylic coated latex (or model) colloids. If the carboxylic coated latex colloids exist and have been used for environmental studies, they were unfortunately not studied in great detail for the uranium sorption on these colloids.

Earlier, Van Loon & Kopajtic ((Part1) 1991, (Part2) 1991) presented their data on radionuclide adsorption on bitumen for strontium and nickel on an experimental basis and extended the data to americium and uranyl on a theoretical basis. In these studies, they assumed that the surface of the bitumen particles is covered by carboxylic groups. Since their work was carried out in low ionic strength solution (10^{-3}), the ionic exchange was taken into consideration together with surface complexation. The bitumen particles are broadly dispersed 0.1-30 µm, however, even if their study reported the effects of pH on sorption and models the adsorption on the carbonyl groups, at the surface, any attempt of comparison with the results reported in this study is difficult because of the differing units used for the sorption data (cm or L g^{-1}, respectively).

Zhang, et al. (2018) reported data on the adsorption and desorption of $U^{(VI)}$ onto humic acids derived from uranium-enriched lignite in fixed batch experiments. The results showed that the optimum pH level at which all the humic acids adsorbed $U^{(VI)}$ ranged from 5 to 8. The high uranium content of the humic acids was released into the solution at the pH values between 1 and 3. The uranium present in the humic acids may not affect the adsorption capacity of the $U^{(VI)}$, but the carboxylic groups in the

humic acids play a significant role in controlling the adsorption capacity. Bampaiti, et al. (2016) investigated the biosorption of uranium from aqueous solutions by *Dictyopteris polypodioides* brown algae. The effects of pH, uranium concentration, mass of the adsorbent, temperature and contact time on the removal efficiency were studied and the results were simulated by various isotherm models. This study concluded that sorption process could be described as a combination of several mechanisms, including physical sorption, ion exchange and complexation, which would be expected from prior works, like Nakajima *et al* (1982) and Senko *et al* (2002).

In seawater conditions the sorption on particles (inorganic, organic and bioorganic) has been investigated by Li (1981). In these conditions, at pH 8 and in oxidising conditions Log K_d was found to be around 4 for $U^{(VI)}$ and 8 for $Th^{(IV)}$, an analogous of $U^{(IV)}$, both in carbonated water ($2x10^{-3}$ M). These values are larger than the data calculated for $U^{(VI)}$ and $U^{(IV)}$, using the mono-dentate model developed in this study. This may be due to the size of the particles or the irreversibility of the sorption e.g., by coupling surface complexation and particle aggregation.

More recently, the work reported in 4.0 Practical Research was published in McGowan *et al* (2022) investigated the sorption of uranium from seawater on biomass material particles of 2 mm in size. It was observed that there was very strong sorption of uranium on these materials, that was consistent with the specific structure of the uranyl complexes as reported by Lucks *et al* (2012).

The quantification of the uranium sorption data in the terms described by the model is usually difficult, as authors frequently use differing basis, such as providing them as fraction of $U^{(VI)}$ sorbed in %.

Investigation of surface complexation of thorium by humic acid was carried out by Szabo *et al* (2006) using chemically immobilized humic acid on silica gel. Thorium($Th^{(IV)}$) may be considered as an analogue of $U^{(IV)}$. Here the silica material (20 nm) is first loaded with humic acid. While the $Th^{(IV)}$ sorption is consistent with a Freundlich isotherm, it is possible to evaluate to a K_d of 2×10^4 mL g^{-1} at pH 4 and 4×10^4 mL g^{-1} at pH 6 for a total concentration of Th in solution of 1×10^{-8} mol L^{-1}. In these conditions (nonlinear isotherm), the K_d data at pH 6 for a Langmuir isotherm (K_{dL}) could be estimated for $K_{dL} = \lim_{c \to 0} K_{dF} \approx 1 \times 10^5$ mL g^{-1}. These Kd values are somewhat higher than predicted because in addition to carboxylic groups, stronger surface groups are reported for humic materials.

3.3 Modelling Results: Various Phenolic Group Complexes

3.3.1a Calculation of Kd for hydroxy-benzene group complexes

The K_d (mL g^{-1}) for uranium surface complexation by hydroxy-benzene groups on bioorganic particles in a carbonate free environment, and a $[CO_3]_{Tot}$ = 2.2 x 10^{-3} mol L^{-1} carbonated environment as a function of redox potential for various pH values was first calculated. The surfaces of the particles of 0.2 mm size are covered by hydroxy-benzene groups forming multi dentate complexes with $U^{(VI)}$ and at lower E values $U^{(IV)}$. In this case, calculations were done using the correlations with T_m and S_m given in **Table 7**. The results are plotted in **Figure 14** and **Figure 15**.

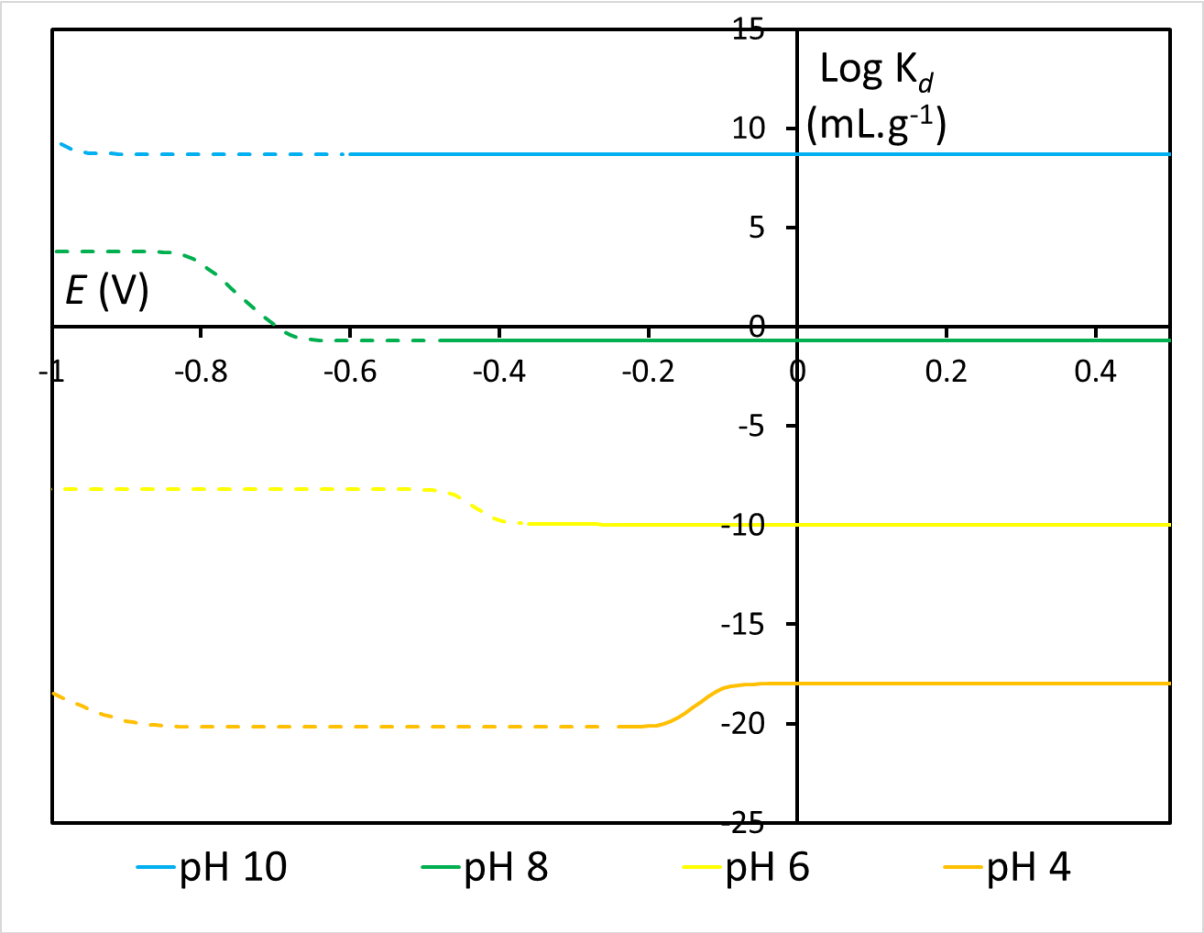

FIGURE 14 URANIUM SORPTION COEFFICIENT K_D (ML G^{-1}) AS A FUNCTION OF POTENTIAL FOR VARIOUS PHS ON MULTI-DENTATE (HYDROXYL-BENZENE) GROUP LOADED PARTICLES. CONDITIONS: PARTICLES OF 0.2 MM SIZE, POTENTIAL VS NHE, SITE DENSITY: 4.1 NM^{-2}, CARBONATED (2.2 X 10^{-3} MOL L^{-1})

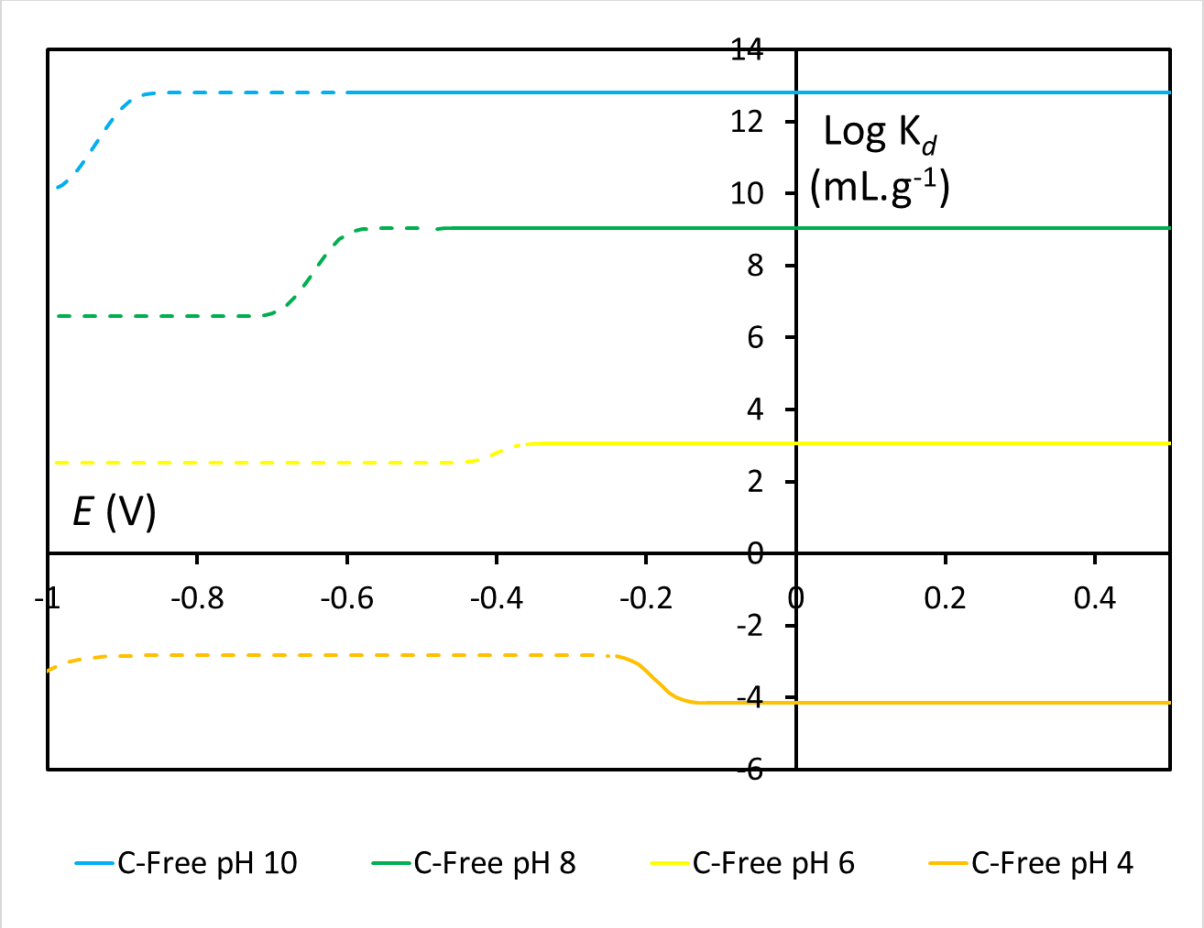

FIGURE 15 URANIUM SORPTION COEFFICIENT K_D (mL g^{-1}) AS A FUNCTION OF POTENTIAL FOR VARIOUS PHS ON MULTI-DENTATE (HYDROXYL-BENZENE) GROUP LOADED PARTICLES. CONDITIONS: PARTICLES OF 0.2 MM SIZE, POTENTIAL VS NHE, SITE DENSITY: 4.1 NM^{-2} CARBONATE FREE

The general form of the distribution is three distinct phases. Two of these are stable states, where the Log K_d is dominated by $U^{(iV)}$ and $U^{(VI)}$ complexes, respectively. In between the two phases there is a transition phase, which is characterised by a gradual change in dominant complex, from $U^{(IV)}$ to a hybrid $U^{(V)}/U^{(VI)}$ and $U^{(VI)}$ forms. The $U^{(V)}$ concentration does not become significant under these conditions. This transition phase is defined by the two *E* (V) where the stable Log K_d state starts to drift.

With hydroxy-benzene, the $U^{(IV)}$ form occurs outside the water stability zone, and therefore it is only theoretical value. In many cases, the transition phase is also outside this region. The exception is the pH 4 form. This curve also has a small phase, where the $U^{(III)}$ has a significant effect at very low *E*(V). However, this is also outside the water stability zone.

Without the presence of ligands, the trend is for the $U^{(VI)}$ phase to exhibit a greater log K_d than the $U^{(IV)}$ phase, except for at pH 4, but the balance is reversed, with the $U^{(VI)}$ form exhibiting higher K_d. The exception is again at pH 4, where the higher zone is the $U^{(IV)}$ phase.

With the carbonate acting as an interfering ligand, the trend is reversed.

These values are displayed in **Table 11**.

Table 11. Calculated characteristics of the K_d of hydroxy-benzene

pH	$U^{(IV)}$	$U^{(VI)}$	$U^{(IV)}$ limit (V)	$U^{(VI)}$ limit (V)	Water Stability zone (V)
4	-20.16	-18.00	-0.22	-0.02	-0.24
6	-8.20	-9.94	-0.52	-0.29	-0.36
8	3.79	-0.70	-0.88	-0.59	-0.48
10	9.99	8.71	-1.07	-0.89	-0.6
pH (Carbon Free)					
4	-2.83	-4.16	-0.26	-0.09	-0.24
6	2.52	3.07	-0.46	-0.31	-0.36
8	6.59	9.05	-0.74	-0.51	-0.48
10	9.99	12.82	-1.09	-0.8	-0.6

3.3.1b Effect of total carbonate concentration on the Kd of hydroxy-benzene group complexes

The K_d (mL g^{-1}) for uranium surface complexes by hydroxy-benzene groups on bioorganic particles was calculated in carbonate solutions which $[CO_3]_{Tot}$ ranges from 2.2 x 10^{-6} to 2.2 mol L^{-1}, as a function of the redox potential for pH 8.0. This range was selected as it reflects an order of magnitude on each side of the recorded concentration at depth in the Irish Sea (Rérolle, et al (2012). The surfaces of the particles of 0.2 mm size are covered by hydroxy-benzene groups, forming multi-dentate complexes with $U^{(VI)}$ and at lower E values $U^{(IV)}$. The Calculations were first completed using the correlations with T_m and S_m given in **Table 7**. The results are reported in **Fig. 16**.

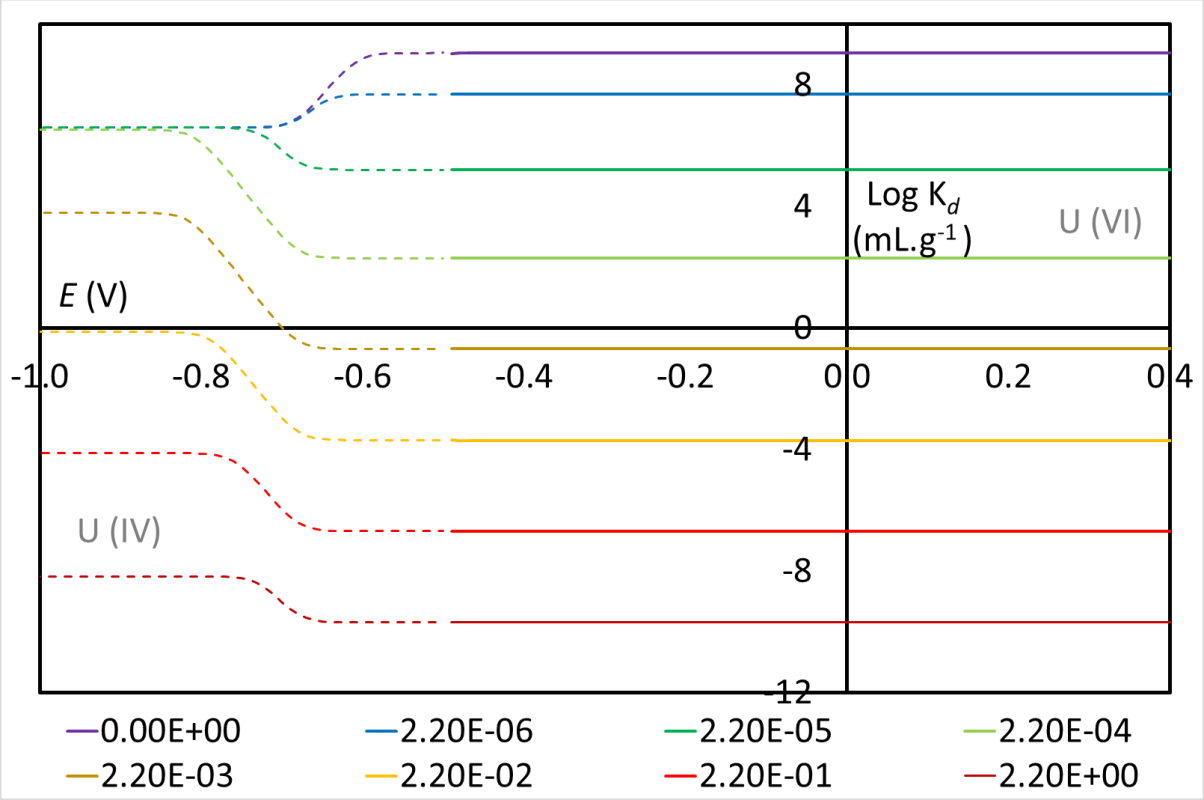

Fig. 16 Uranium sorption coefficient K_d (mL g^{-1}) as a function of potential for pH 8.0 on mono-hydroxy-benzene group loaded particles. Conditions: particles of 0.2 mm size, potential vs NHE, molecule characteristics per **Table 3**, over varying carbonate ($[CO_3]_{Tot}$) concentrations.

In general, increasing the CO_3^{2-} concentration decreases the sorption of U ions, which is to be expected, since carbonate acts as an interfering ligand. The interference effect on $U^{(IV)}$ is lower than the effect on the $U^{(VI)}$ complexes, so the transition step seen in Figure 5 is also in evidence. The exceptions are the carbon free curve and the concentration of 2.2 x 10^{-6} mol L^{-1} where the stronger bonding of the $U^{(VI)}$ can win out, without the presence of sufficient interfering ligand. The entry point for the transition varies but the exit point is always about -0.6, although at low concentrations, the pH effect on the solubility of the CO_3^{2-} causes a small degree of variation.

At pH 8, in practice, the transition is below the water stability region, so values for $U^{(IV)}$ follow theoretical ones.

Table 12. Calculated properties of the K_d of hydroxy-benzene in varying $[CO_3]_{Tot}$

CO3 Conc.(M)	U (IV) Kd	U(VI) Kd	U (IV) stability exit (V)	U (VI) stability exit (V)
$0x10^{1}$	5.33	7.79	-0.74	-0.50
$2.2x10^{(-6)}$	5.33	6.43	-0.73	-0.57
$2.2x10^{(-5)}$	5.33	3.94	-0.81	-0.63
$2.2x10^{(-4)}$	5.26	1.03	-0.87	-0.62
$2.2x10^{(-3)}$	2.53	-1.96	-0.89	-0.62
$2.2x10^{(-2)}$	-1.39	-4.96	-0.87	-0.62
$2.2x10^{(-1)}$	-5.39	-7.96	-0.82	-0.62
$2.2x10^{(0)}$	-9.44	-10.96	-0.79	-0.62

3.3.2a Calculation of Kd for dihydroxy-benzene group complexes

The K_d (mL g^{-1}) for uranium surface complexation by dihydroxy-benzene groups on bioorganic particles in a carbonate free environment and carbonated ($[CO_3]_{Tot}$ = 2.2 x 10^{-3} g L^{-1}) as a function of redox potential for various pH values was first calculated. The surfaces of the particles of 0.2 mm size are covered by phenolic groups forming multi-dentate complexes with $U^{(VI)}$ and at lower E values $U^{(IV)}$. In this case, the calculations were carried out using the correlations for T_m and S_m given in **Table 7**. The results are plotted in **Figure 17**.

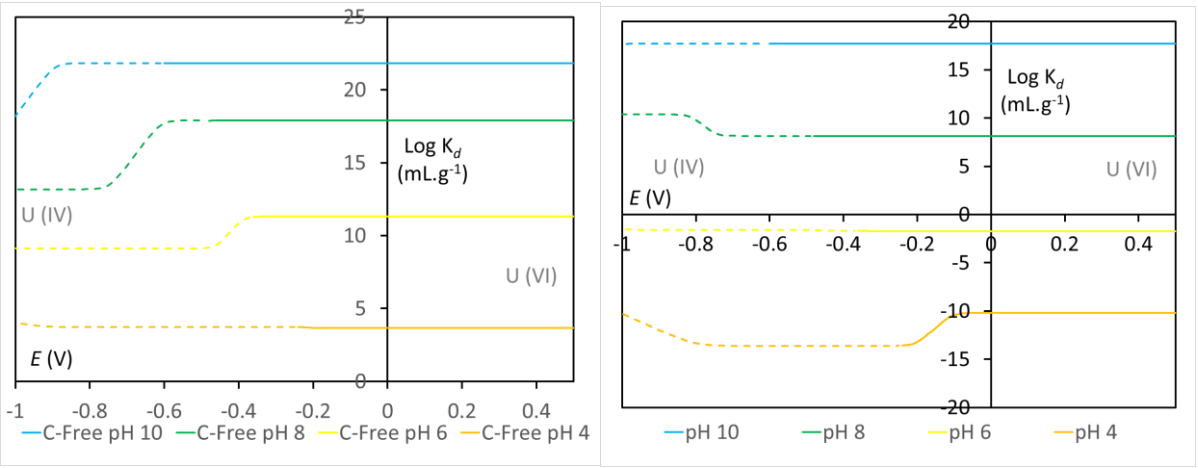

Figure 17 Uranium sorption coefficient K_d (mL g^{-1}) as a function of potential for various pHs on multi-dentate phenolic (dihydroxy-benzo-) group loaded particles. Conditions: particles of 0.2 mm size, potential vs NHE, site density: 3.6 nm^{-2}, a. carbonate free, and b. carbonated $[CO_3]_{Tot}$ = 2.2 x 10^{-3} M).

As with the mono-hydroxybenzene, the general form of the distribution shows three distinct phases. Two of these are stable states, where the Log K_d is dominated by $U^{(VI)}$ and $U^{(VI)}$ complexes, respectively. In between the two phases, there is a transition phase which is characterised by a gradual change in dominant complex, from $U^{(IV)}$, to $U^{(V)}/U^{(VI)}$, to $U^{(VI)}$ forms. The $U^{(V)}$ form does not become significant under these conditions, which means the transition follows a linear trend. This transition phase is defined by the two E (V) where the stable state starts to drift from the stable Log K_d.

For the ligand free results, the $U^{(VI)}$ zone has a higher K_d than the $U^{(IV)}$ zone, except for pH 4, where it has a slight fall. The carbonated environment is much more negative than the carbon free equivalents. The step is negative for pH 6 and 8, while the pH 4 and 10 are positive. In general, the transition zone is outside the stable water zone, so the values for the $U^{(IV)}$ are theoretical ones. The exception is at pH 4, where the transition zone is at a similar E (V) as the $U^{(IV)}$ transition point.

Table 13. Calculated characteristics of the K_d for dihydroxy-benzene complexes

pH	$U^{(IV)}$	$U^{(VI)}$	$U^{(IV)}$ limit (V)	$U^{(VI)}$ limit (V)	Water Stability zone (V)
4	-13.61	-10.19	-0.28	-0.02	-0.24
6	-1.61	-1.69	-0.5	-0.4	-0.36
8	10.38	8.15	-0.87	-0.65	-0.48
10	16.70	17.72	-1.11	-0.92	-0.6
pH (Carbon Free)	0	0	0	0	0
4	3.73	3.65	-0.25	-0.14	-0.24
6	9.11	11.32	-0.52	-0.27	-0.36
8	13.18	17.90	-0.81	-0.51	-0.48
10	16.70	21.83	-1.11	-0.8	-0.6

3.3.2b Effect of total carbonate concentration on dihydroxy-benzene complexes

The K_d (mL g^{-1}) for uranium surface complexation by dihydroxy-benzene groups on bioorganic particles was calculated in a carbonate suspension which $[CO_3]_{Tot}$ varies between 2.2 x 10^{-6} and 2.2 mol.L^{-1} as a function of redox potential for pH 8.0. This range was selected as it reflects an order of magnitude on each side of the recorded concentration at depth in the Irish sea (Rérolle, *et al* (2012)). The surfaces of the particles of 0.2 mm size are covered by dihydroxy-benzene groups forming multi-dentate complexes with $U^{(VI)}$ and at lower E values $U^{(IV)}$. The calculations were completed using the correlations with T_m and S_m given in Table 5. The results are plots are plotted in **Fig. 7**.

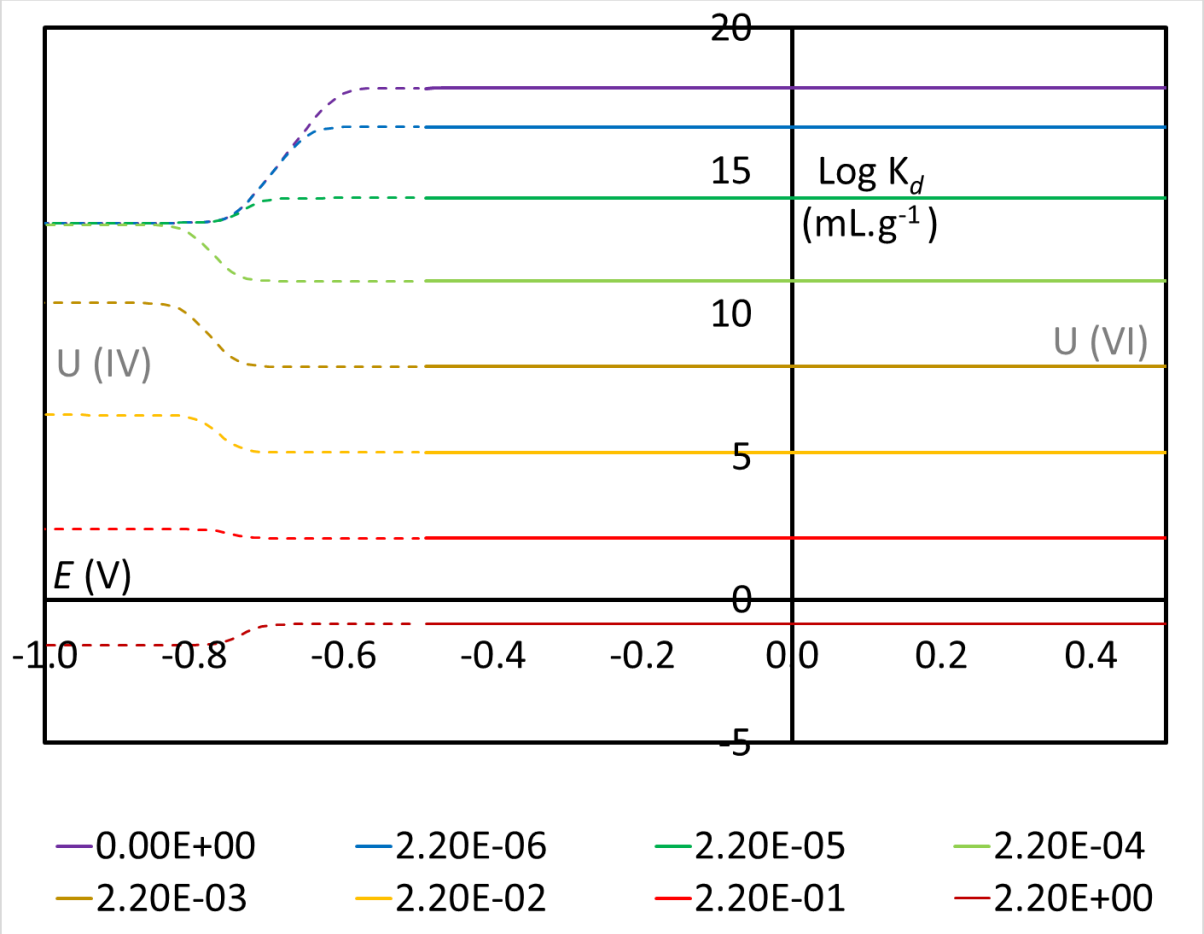

Figure 18 Uranium sorption coefficient K_d (mL g^{-1}) as a function of potential for pH 8.0 on multi-dentate group loaded particles. Conditions: particles of 0.2 mm size, potential vs NHE, characteristics per Table 3, over varying carbonate concentrations

In general, increasing the CO_3^{2-} decreases the sorption of U ions, which is to be expected, since it is an interfering ligand. The interference effect on $U^{(IV)}$ is lower than the effect on the $U^{(VI)}$ complexes, so the transition step seen in Fig. 5 is also in evidence. The exit point for $U^{(IV)}$ transition varies between -0.8 to -0.9 V, while the limit potential for $U^{(VI)}$ is -0.6 to -0.7 V. It is notable that in comparison to the mono-hydroxy-benzene, the 10^{-5} and below CO_3^{2-} concentrations, the interfering effect of the $U^{(VI)}$ form is insufficient to counteract the increased bonding potential of that form, compared with the $U^{(IV)}$ form, but at the highest concentration, these repeats, as the suppressive effect on the $U^{(IV)}$, form is higher. However, it should be noted that, as mentioned above, this concentration is an order of magnitude larger than peak real-world rates.

At pH 8, in practice, the transition is below the water stability region, so values for $U^{(IV)}$ are mostly theoretical, except some results close to the exit point.

Table 14. Calculated characteristics of the K_d for dihydroxy-benzene in varying $[CO_3]_{Tot}$

CO3 Conc.(M)	$U^{(IV)}$ Kd	$U^{(VI)}$ Kd	$U^{(IV)}$ limit (V)	$U^{(VI)}$ limit (V)
$0x10^{1}$	13.18	17.90	-0.81	-0.53
$2.2x10^{(-6)}$	13.18	16.54	-0.81	-0.58
$2.2x10^{(-5)}$	13.18	14.05	-0.81	-0.66
$2.2x10^{(-4)}$	13.11	11.14	-0.86	-0.68
$2.2x10^{(-3)}$	10.38	8.15	-0.87	-0.68
$2.2x10^{(-2)}$	6.46	5.15	-0.84	-0.68
$2.2x10^{(-1)}$	2.47	2.15	-0.87	-0.69
$2.2x10^{(0)}$	-1.58	-0.85	-0.80	-0.67

3.3.3a Calculation of Kd for dihydroxy-naphthalene group complexes

The K_d (mL g^{-1}) for uranium surface complexation by dihydroxy naphthalene groups on bioorganic particles in a carbonate free environment, and in a carbonated environment ($[CO_3]_{Tot}$ = 2.2 x 10^{-3} mol.L^{-1}) as a function of redox potential for various pH values was first calculated. The surfaces of the particles of 0.2 mm size are covered by phenolic groups, forming complexes with $U^{(VI)}$ and at lower E values $U^{(IV)}$. In this case calculations were done using the correlations with T_m and S_m given in Table 5. The results are plotted in Figure 8.

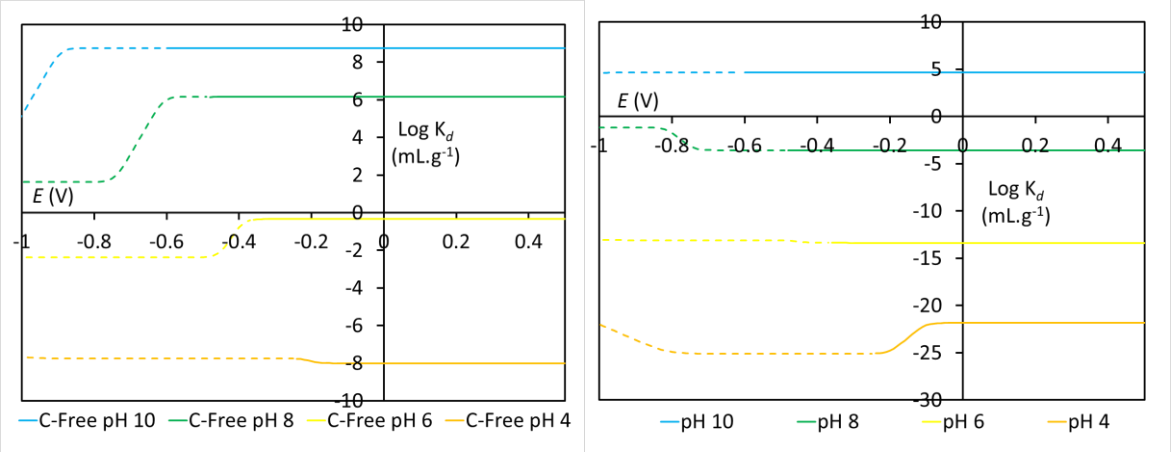

Figure 19 Uranium sorption coefficient K_d (mL g^{-1}) as a function of potential for variouds pHs on phenolic (dihydroxy-naphthalene) group loaded particles. Conditions: particles of 0.2 mm size, potential vs NHE, site density: 1.8 nm^{-2}

As with the previous forms, the general form of the distribution represents three distinct phases. Two of these are stable states, where the Log K_d is dominated by $U^{(IV)}$ and $U^{(VI)}$ complexes respectively. In between the two phases, there is a transition phase, which is characterised by a gradual change in dominant complex, from $U^{(IV)}$, to $U^{(V)}/U^{(VI)}$, to $U^{(VI)}$ forms. The $U^{(V)}$ form does not become significant under these conditions, which means the transition is of linear trend. This transition phase is defined by the two *E* (V) where the stable state starts to drift from the stable Log K_d. The transitions for this surface are of much softer changes than the other forms.

In the Carbon Free form, as discussed earlier, the $U^{(VI)}$ form is dominant, except in the case of pH 4. With the carbonated form, only the pH 4 and pH 10 curves have dominant $U^{(VI)}$ phases, with the other two having $U^{(IV)}$ dominant phases. In general, the transition zone is outside the stable water zone, so the values for the $U^{(IV)}$ are theoretical ones. The exception is at pH 6, where the transition zone is at a similar *E*(V) as the transition point, and pH 4, where it precedes it. The $U^{(IV)}$ exit point is consistent between the two, but the $U^{(VI)}$ exit point varies less consistently.

Table 15. Calculated characteristics of the K_d of dihydroxy-naphthalene

pH	U (IV)	U (VI)	U (IV) limit (V)	U (VI) limit (V)	Water Stability zone (V)
4	-20.16	-18.00	-0.22	-0.02	-0.24
6	-8.20	-9.94	-0.52	-0.29	-0.36
8	3.79	-0.70	-0.88	-0.59	-0.48
10	9.99	8.71	-1.07	-0.89	-0.6
pH (Carbon Free)					
4	-2.83	-4.16	-0.26	-0.09	-0.24
6	2.52	3.07	-0.46	-0.31	-0.36
8	6.59	9.05	-0.74	-0.51	-0.48
10	9.99	12.82	-1.09	-0.8	-0.6

3.3.3b Effect of total carbonate concentration on dihydroxy-naphthalene complexes

The K_d (ml g^{-1}) for uranium surface complexation by a dihydroxy-naphthalene group on bioorganic particles was calculated in carbonate solutions which $[CO_3]_{Tot}$ varies between 5 x 10^{-4} and 6 *x 10^{-3} as a function of redox potential for pH 8.0. This range was selected as a reasonable proximity for surface carbonate concentrations in the Irish sea (Rérolle, *et al* (2012)). The surfaces of the particles of 0.2 mm size are covered by dihydroxy-naphthalene groups forming multi-dentate complexes with $U^{(VI)}$ and at lower E values $U^{(IV)}$. The calculations were first done using the correlations with T_m and S_m given in **Table 5** for mono-dentate. The results are plotted in **Fig. 9**.

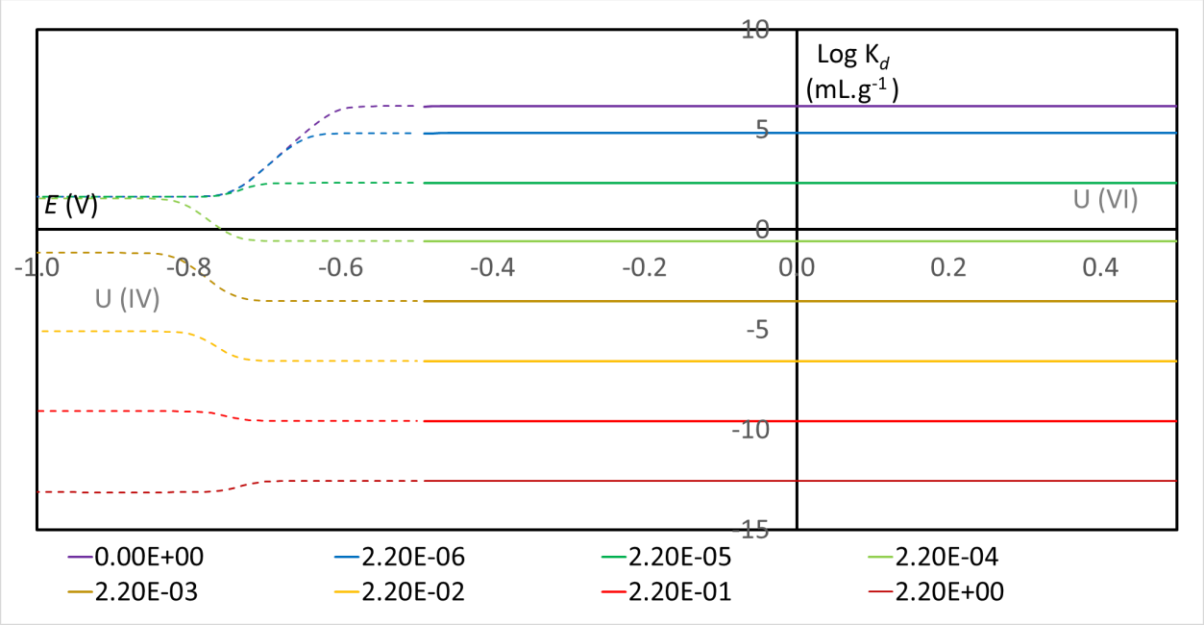

Figure 20 Uranium sorption coefficient K_d (mL g^{-1}) as a function of potential for pH 8.0 on dihydroxy-naphthalene group loaded particles. Conditions: particles of 0.2 mm size, potential vs NHE, , over varying carbonate concentrations

As the carbonate concentration increases, the interference effect in the complex formation proportionately increases. Below concentrations of $2.20*10^{-5}$ g.L^{-1}, the effect on the U $^{(IV)}$ Log K_d is negligible, with a value of 1.63. Above this concentration, the U $^{(IV)}$ Log K_d is reduced. The U $^{(VI)}$ phase would also be decreasing with increasing carbonate concentration, although the effect is not as significant as that during the $U^{(IV)}$ dominated phase. The dihydroxy-naphthalene response is notable as the log K_d is negative for all curves where the U $^{(VI)}$ phase is more affected by the presence of carbonate, than the U $^{(IV)}$ phase.

Table 16. Calculated characteristics of the K_d of dihydroxy-naphthalene in varying $[CO_3]_{Tot}$

CO3 Conc.(M)	U $^{(IV)}$ Kd	$U^{(VI)}$ Kd	U $^{(IV)}$ limit (V)	U $^{(VI)}$ limit (V)
$0x10^{1}$	1.63	6.17	-0.81	-0.55
$2.2x10^{(-6)}$	1.63	4.81	-0.81	-0.60
$2.2x10^{(-5)}$	1.63	2.33	-0.81	-0.63
$2.2x10^{(-4)}$	1.56	-0.58	-0.86	-0.69
$2.2x10^{(-3)}$	-1.17	-3.57	-0.87	-0.68
$2.2x10^{(-2)}$	-5.09	-6.57	-0.84	-0.68
$2.2x10^{(-1)}$	-9.08	-9.57	-0.84	-0.69
$2.2x10^{(0)}$	-13.13	-12.57	-0.79	-0.67

3.4 Review of Model Dynamics

The general case, over all the above modelled conditions, would be that the sorption (Log K_d) increases together with the pH, due to the deprotonation of the ligands. From the redox point of view, the reduction from $U^{(VI)}$ species in $U^{(IV)}$ species appears when decreasing *E*. This would be a fairly intuitive result, but the significance is the changes in thresholds for transition between the conditional variations.

3.4.1 Variation between phenolic systems.

In general, the three polyhydroxy-aromatic cases (

3.3 Modelling Results: Various Phenolic Group Complexes) follow the same pattern (Log K_d = f(E)) and have relatively narrow width of their transition phases between the $U^{(IV)}$ and the $U^{(VI)}$ forms (between 0.1 and 0.25 V), see Table 17. All the transition points are similar between the materials, varying only over the order of 0.05 V. Except for the pH 6 curve where the mono-hydroxy-benzene has a reduced $U^{(VI)}$ limit for the carbonated curves, compared to the other two, where this variation is ~0.1 V. This is due to relatively weak concentration of $U^{(V)}$ forms under these conditions, which leads to accelerated transition to the $U^{(VI)}$ dominated phase, while the other curves experience a longer transition.

TABLE 17 THE CALCULATED TRANSITION POINT CHARACTERISTICS OF VARIOUS PHENOLIC SURFACES REPORTED IN SECTION 3.3

	Height change			Transition phase width		
pH	hydroxy-benzene	di-hydroxy-benzene	dihydroxy-naphthalene	hydroxy-benzene	di-hydroxy-benzene	dihydroxy-naphthalene
4	2.16	3.42	3.24	0.19	0.21	0.24
6	-1.73	-0.08	-0.25	0.17	0.06	0.11
8	-4.49	-2.23	-2.40	0.28	0.19	0.18
10.00	-1.29	1.02	0.84	0.15	0.16	0.13
pH			(Carbon Free)			
4	-1.33	-0.16	-0.25	0.16	0.1	0.13
6	0.55	2.18	2.03	0.14	0.18	0.18
8	2.46	4.72	4.54	0.2	0.25	0.25
10	2.82	5.13	4.96	0.27	0.28	0.3

The transitions for the carbon free curves themselves are negative for pH 4 curve and positive for the pH 6-10 curves, while Log K_d = f(E) transitions for the carbonated case are negative for the pH 4 and 10 curves, and positive for the pH 6 and 8 curves.

The exceptions to this are mono-hydroxy-benzene, where the step changes are positive for pH 10. This is due to the interference effect of the site acidic form on the low pH curves and the reduced effect on sorption by the carbonate at high pH. The lower site density for the mono-hydroxy-benzene means it is not as suppressed by the carbonate as in the di-hydroxy forms.

Of the three simulated substrates, the mono- form displays exceptional differentiation in the transitions, whereas the bi-forms display broadly similar height changes at the same pH, the mono form follows a different pattern, with the effect of pH change on the separation between the $U^{(IV)}$ and

$U^{(VI)}$ stable states being maximised at low pH. Increasing the pH in the mono form increases the Kd in the carbon free system, but decreases it in the carbonated system, although the step change effect is maximised for the pH 8 curve, with the height change for pH 10 being reduced.

Considering the three under the curve closest to natural conditions mentioned previously (pH 8.0, a potential of 0.4), the mono- -benzene form would estimate it at -2.26, the di-hydroxy- forms are 6.74 and -4.66 respectively. To adjust these to allow IV dominance, these would require a shift of over -1 V for all three. This would require a two-electron redox shift to achieve (Lambert, et al., 2020). This is possible but unlikely to occur at the specified pH. However, in the context of a pH drop to 6.0, such as could occur during fermentation, as reported by Lambert et al (2020) shift of only -0.8 V (which would correspond to a single electron redox shift), would be possible.

3.4.2 Variation of carbonate concentration.

In the presence of carbonate ligands, the competition effects from the carbonates are noticeable. Below $[CO3]_{Tot}$ =2.2 x 10^{-5} M, the interfering effect on the $U^{(IV)}$ phase is insignificant, but rapidly increases until there is little difference between it and the $U^{(VI)}$, which experiences a continually increasing interfering effect at any concentration. This would most likely due to the stereochemistry effects limits return to solution of the $U^{(IV)}$, while the $U^{(VI)}$ complex is larger, and has more flexibility in internal structure, allowing rerelease if a carbonate complex interacted. In all three cases, the step change between the two phases decreases from the positive step at 0 mol L^{-1}, (the mono being just over half the step change of the bi forms, at 2.5 to 4.7), down to a maximum negative distance, then recedes to a lower value, becoming positive again at the highest concentration. The di forms mirror each other, but interestingly the peak separation occurs at real world surface conditions ($2.2x10^{-3}$ mol L^{-1}).

3.4.3 Comparison of results with experimental data

Comparing the values gained by applying the model with experimental data is challenging, as natural polyphenolics are often resonant and produced by under equilibriumic race conditions by dynamic systems, leading to picking out specific structures is next to impossible. This is why this model has been aimed towards representing a median structure, whose values can be used to direct by values to mirror the real-world comparisons.

For example, (Yu, et al., 2022) combined titanium oxide and bayberry tannins to form particles with capture rates peaking at base concentration corresponding to Log K_d of 4 at pH 6, although the surface ratio was signficiantly lower than those used for the model. Despite this, their structures were different, since they identified that the oxide was the primary capture mechanism at the lower pHs and the particle surface concentration of tannin was only half that of the value used in the model.

Their work with seawater was also quite different, since the seawater was spiked to concentrations 10^6-10^7 natural levels (e.g. 3‰). Despite all these changes, this work is one of the best for comparison, as they did identify the input conditions sufficiently that it could be simulated using this model, with pKa values equivalent to -1 at neutral conditions, and 4 at acidic: these correspond well with the values for dihydrox-benzene in these conditions.

(Zhang, et al., 2018) reported data on the adsorption and desorption of $U^{(VI)}$ onto humic acids derived from uranium-enriched lignites in batch experiments. These experiments showed optimum adsorption of $U^{(VI)}$ ranged from 5 to 8, although these highly saturated surfaces desorbed at pH values between 1 and 3, with values similar to those generated by the dihydroxnathalene the respective pH, if we assume it is at redox >0.2 (the paper did not report this aspect of the conditions). The uranium present in the humic acids may not affect the adsorption capacity for $U^{(VI)}$, but the phenolic groups in the humic acids play a significant role in controlling the adsorption capacity, approximately 20 to 30 percent (Ritchie & Perdue, 2003).

An investigation of surface complexation of thorium by humic acid was carried out by Szabo *et al* (2006) using chemically immobilized humic acid on silica gel. Thorium ($Th^{(IV)}$) is generally considered as reasonable analogue of $U^{(IV)}$. Like with Yu et al (2022), this means the surface has a second sorption site type, the ratios were not evaluated, the results have to be approximated, for example by combining with the data calculated with modelling carried out in Degueldre & McGowan (2020).

The $Th^{(IV)}$ sorption isotherm reported by Szabo is of the Freundlich variety and can tentatively evaluate K_d of 2 x 10^1 L g^{-1} at pH 4 and 4 x 10^1 L g^{-1} at pH 6 for a total concentration of Th in solution of 1 x 10^{-8} mol L^{-1}. In the context of this nonlinear isotherm, we can extrapolate the K_d data at pH 6 for a Langmuir isotherm to be (for $K_d = \lim_{c\to 0}$), K_d = 8 x 10^1 L g^{-1} ≈ 1 x 10^5 mL g^{-1} (with c the U concentration). Approximating a combined sorbance environment as suggested above, the silica sites generally dominate under these conditions, with the log of the averaged value being 2 higher than that calculated in the above extrapolation, but it is notable that the un-amalgamed values for the phenolic are more appropriate, suggesting that these are the dominant active site. This could be explained by site deactivation of the silica sites, through due to preferable capture of non-modelled interferent ions, which is an inherent limit of single element surface modelling: multi-element would be a significant extension of the project beyond the current scope.

Again, the sorption on particles (inorganic, organic and bioorganic) has been investigated by Li (1981) in seawater conditions. In these conditions at pH 8 and in oxidising conditions, Log K_d was found equal to 4 for $U^{(VI)}$ and 8 for $Th^{(IV)}$, which is generally accepted as an analogous of $U^{(IV)}$, both in carbonated water ($[CO_3]_{Tot}$ =2x10^{-3} M). These values fit reasonably with the data calculated for $U^{(VI)}$ and $U^{(IV)}$, using

the values calculated for the dihydroxy-naphthalene developed in this study. It was unusual in that it used similar particle sizes to those used in this model, which could explain the correspondence.

4.0 Practical Research

In order to calculate the sorption constant K_d, it is necessary to measure the concentration of the metal in solution and at the biomaterial surface, at equilibrium. The following section deals with the water sampling, selection and preparation of biomass materials, and the methodology of analysis.

4.1 Materials selected for sorption tests.

4.1.1 Water Samples

For the first batch of samples, 3 batches of 2.5 L seawater samples were collected from Trafalgar Point (54.075192 N, -2.878758 W), Stone Jetty, Morecambe, NW UK, on the Irish Sea (see Figure 21), at high tide, at 09:33am on the 19 of January 2019; at 10:38am on the 15 of June 2019 and at 07:32am on the 15 of August 2019. These water salinities (around 3.2%, per Jones (1991)) corresponding to 91% dilution and 1.023 g mL^{-1} density) are known to be slightly below the salinity the average seawater (3.5%) found on Earth because of some local mixing with estuary water. However, since these surface seawater samples were collected on non-rainy days over the Morecambe Bay area, these samples can be considered to be a good representative for the composition found in Irish seawaters.

The seawater used for the second and third batches, and the seawater used in the continuous flow experiment, were collected from the same point, were collected over 8 samplings but were pooled into a common tank, and allowed to equilibrate, which collectively reported a similar value on salinity and density (3.2% and 1.018 g mL^{-1}).

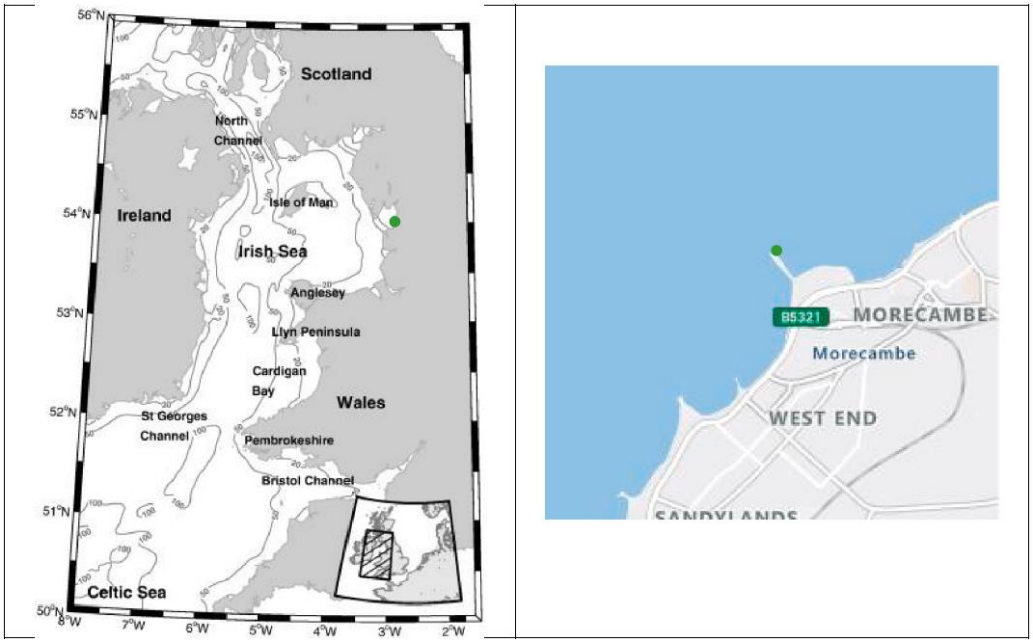

FIGURE 21 MAP OF THE IRISH SEA 50-56°N, 2-8°W, AND OF MORECAMBE 54°N, 3°W, SAMPLING POINT.

4.1.2 Biomass Samples

All biomass materials are vegetal and sourced through suppliers within Lancaster, except for the White Birch samples, which were donated by Forestry and Land Scotland, who supplied a sample from Carsewood Park (55°48'26.2"N 4°33'22.3"W) during routine felling.

To represent fruits, **orange skin** (*Citrus Sinensis*), **lemon skin** (*Citrus Limon*) and **nectarine skin** (*Prunus Persica*) were selected as readily available material which are commonly discarded. These have a large volume produced through industrial processing, mainly consisting of the skin, which is currently used for animal fodder, although some use for the production of flavourings are also common. These fruits are all known to have high polyphenolic compound concentrations for fruits, particularly in the skins, where they serve important biological functions. To prepare the samples, they were dried, and the pith on the oranges and lemons was removed, as far as practical. They were then diced so not to exceed 4 mm on any axis.

Grapes (*Vitis*) have extensive and specific regions dedicated to their harvest, for the purposes of wine production. These have a large volume of solid by-products, mainly consisting of the skin, which is currently mainly used for animal fodder. Grapes are associated with well-studied antioxidant chemicals e.g., tannin, and are known to be easily dried and powdered for the purposes of the present study. Given the range of species and cultivation purposes, two variants were selected as representatives.

A **red grape** (*Vitis Vitaceae*) was selected, as reasonable middle ground of grape varieties. One subsample was pulped whole, while a second had the skin separated, to measure its specific effect.

Furthermore, **sultanas grape** (*Vitis vinifera*), which are a variety of white grape that has been dried to raisin standards, were selected as an easily available grape material that had underwent commercial drying. As skinning was not practical, the samples were split into one subsample of whole sultanas, and one subsample minced through a 4 mm diameter grate, to compare exterior surface to internal bulk properties. This had limited effect, due to particle cohesion.

In subsequent tests, only the skins were tested. The previous red grape skin, and two other varieties were tested. A **table (or Vitis) grape (***Vitis vinifera Vital***)** and a **white grape (***Vitis vinifera Muscat***)** were tested for comparison.

Kale (*Brassica oleriaceae,* var. *Acephala*), **mange tout** (*Pisum sativum*, var. *macrocarpon)*, **garlic** (*Allium sativum*) **Spring Greens** (a mixed collation of various edible *Brassica)* and **Brussels sprouts** (*Brassica oleracea*) were selected to represent a number of useful species that are otherwise difficult to source as a by-product. Kale is known to be high in antioxidant properties, stemming from both polyphenolic compounds, and sulphur-rich compounds, and has a high surface area. Brussels sprouts are similar but have much higher proportion of sulphur-rich compounds compared to the polyphenolics present in kale. Spring Greens have reduced phenolic compounds, but high concentrations of iron rich compounds. Garlic contains several chelating acids known to precipitate heavy metals. Mange tout is high in a number of antioxidants, particularly retinoic acid, which have important scavenging effects in biological systems.

Ground vegetable tubers have been known to sorb heavy metals from their surrounding soil, during their normal life processes. These are filtered and concentrated utilizing their skin, so a **white potato** (*Solanum tuberosum*) and a **sweet potato** (*Ipomoea batatas*) variety were selected. As with the grapes, each were split into two subsamples, one where the skin was separated, and one where they were diced through a 4 mm diameter grate.

Another option is the common by-product of **Peanut** (*Arachis hypogaea*) products, where the shells are removed. These have a wide but weak use in a variety of industries, such as fibre production and in construction, but the most common disposal route is by incineration, either, for direct disposal or converted to smokeless fuel for domestic heating. These are known to have high site capacity, and fixed polyphenolic compounds suitable for heavy metal sorption, and have been used in remediation techniques, as a natural sorbent for some heavy metals. As with the previous materials, they were cut into 4 mm diameter squares.

Coffee Grounds (the insoluble components of a commercial blend of *Coffea arabica and Coffea Canephora*), **Red Tea** (*Aspalathus linearis*) and Blackberry (*Rubus fruticosus*) were identified due to their wide availability, and their antioxidant effects (Aguiar, Estevinho, & Santos, 2016; Monforte, et al., 2018; Crozier, Ashihara, & Tomas-Barberan, 2011).

As previously described, samples of the bio-materials were cleaned, chopped, and separated. For the first batch of samples that were not already sized were cut into 4 mm^2 segments. A small subsample of each (masses displayed in the appendix) was separated, weighed, and dried using an Aicok© Digital Dehydrator, at 50°C for 72 hours. It was then weighed (precision 1 mg), to establish the dry weight conversion factor. This was used to adjust the mass values in appendix 1 to dry basis.

FIGURE 22 VARIOUS SAMPLES BEING PREPARED FOR TESTING IN BATCH 1
SAMPLES ARE IN PRELIMINARY STATE, PRIOR TO SIZING

For the second batch and third batch, the entire sample was air dried, then ground using a mechanical grinder and the dried materials used as is, so no conversion was necessary.

Unlike the first batch, a sieve was used to partition the particle size, limiting the particle size to 0.2 mm, with oversized particles being returned to the grinder, until they meet the size requirement.

For the first batch, two replicates were used. For the second batch, this was increased to three plus one for pH monitoring, and for the third batch, this was increased to four plus one.

Additionally, for the third batch, instead of post contact filtering, the biomaterials were placed into a filter bag during the contact phase. The manufacturer (PPpanda Ltd) claimed these to be ash free nanocellulose membrane, with a reported pore diameter of 20 µm, which was equivalent to the filters used previously and was expected from literature to retain the materials (Varanasi, Low, & Batchelor, 2015). These claims are probably incorrect, as it produced a small quantity of residue in digestion that was not visible in the unbagged samples, and fine particle escape from the filter bags while they were in the centrifuge tubes. Both issues were accounted for in final results, by use of blanks, and through final weight adjustment respectively.

4.2 Experimental Methodologies

4.2.1 Batch methodology

Where mentioned, deionised water is Suprapure© Quality. A 100 mL and 500 mL volumetric flask is approximately half filled with deionised water and labelled appropriately. In a fume cupboard, 64 mL of concentrated nitric acid (Aldrich© 70% redistilled, ≥99.999% pure) is slowly pipetted into the 100 mL volumetric flask, shaking regularly to fully disperse the acid and heat. Volume is then slowly made up to the mark with deionised water and shaken to ensure full dispersal. The 100 mL flask is then slowly added to the 500 mL flask, rinsing repeatedly to ensure complete transfer, and is made up to the mark, and mixed. The final solution is transferred to a storage bottle.

Samples were prepared in Corning™ 50mL Plug seal cap polypropylene self-standing centrifuge tubes. These were labelled, and pre-weighed, to establish the zero weight of the sample.

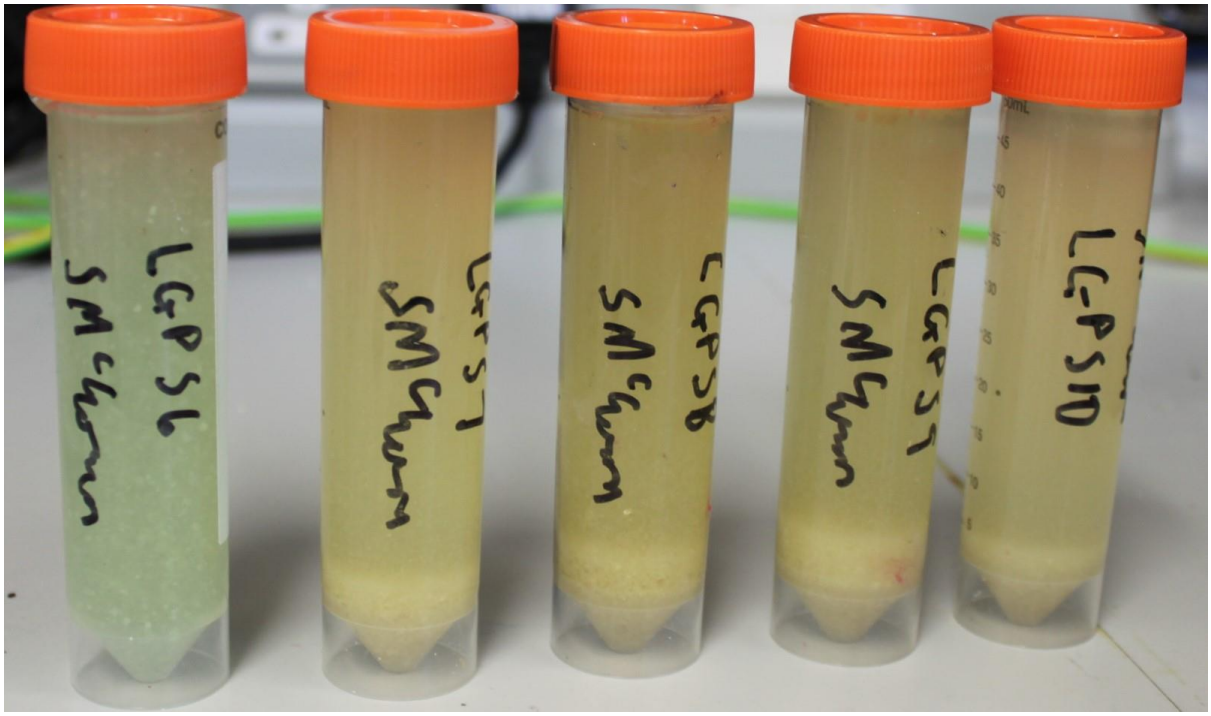

FIGURE 23 SAMPLES OF LIGHT GARLIC POWDER (LGP) IN SEAWATER AT MIXING
THE POWDER CAN BE SEEN TO BE PARTITIONED BY PARTICLE SIZE, WITH THE LEFTMOST FULLY DISPERSED, WHILE THERE IS A GRADUAL INCREASE IN SETTLED COMPONENTS BETWEEN SAMPLES, BUT THE GARLIC WAS NOTED AS IT'S SETTLING WAS NEVER TO FULL SEPARATION, UNLIKE OTHER HEAVIER MATERIALS

For the first batch, two replicated subsamples of each of the materials of was placed into the sample vials, and the weight recorded. Then the volume was made up to 40 mL, and the weight of water added is recorded. These samples were left undisturbed for at least one month to equilibrate.

For the second batch, this was increased to three replicates, with a fourth also being prepared for pH analysis.

For the third batch, a fourth replicate was also added, and each individual sample was placed into the filter bag before being placed into the tube. An extra step was added during the bagging process, to weigh the empty bag, before the sample was added to it.

One further sample of each of the biomaterials was separated and left without contact with the seawater, in order to establish ground state concentrations of the materials.

Further to this, samples of the seawater were placed into sample tubes, without any biomass present, to act as system controls, to establish if there were any losses in processing.

At the end of the leave time, the samples which had seawater present were partitioned.

A volume of 10 mL of the aqueous phase was extracted using a mechanical pipette and digested in 10 mL of heated 2 M HNO_3. This was then filtered using a Whatman™ 0.4 µm PTFE membrane filter, then

made up to 50 mL, using a clean volumetric flask. The solution was then transferred to a clean tube for storage.

A second volume of 10mL of the aqueous phase was extracted and filtered using a Whatman™ 0.4 µm PTFE membrane filter, before being digested in 10 mL of heated 2 M HNO_3. This was then filtered using a Whatman™ 0.4 µm PTFE membrane filter, then made up to 50 mL, using a clean volumetric flask. The solution was then transferred to a clean tube for storage.

In parallel to this, for the first two batches, the remainder was filtered using a Whatman™ 595 150 mm filter paper to capture the solids, then the filter paper and residues were digested in 20 mL of heated 2 M HNO_3.

For the third batch, the filter bag was carefully retrieved, and dried in the air dryer for 72 hours at 50®C, then was weighed to establish the new weight, before being digested in the same fashion.

The resultant digestate was then filtered through a Whatman™ 0.4 µm PTFE membrane filter then made up to 50 mL, using a clean volumetric flask. The solution was then transferred to a clean tube for storage. In addition to the samples themselves, the blank and control samples were also subjected to the same process.

All samples were then diluted by a factor of x16 with deionised water, to minimise the impact of salt precipitation on the ICP-MS instrumentation.

4.2.2 Continuous Flow experiment

Following on from the Batch testing, efforts were made to test the materials under a consistent flow of seawater.

This was achieved by attaching an a Jecod Marine Aquarium Fish Tank Auto Dosing Pumps (DP-5) to the storage tank, which is a computer controlled peristatic dispenser pump, intended for precision dispensing of micro doses on a regular schedule, via a small sediment trap.

This was attached initially to a single 4l tanks, which had been fitted with a level control overflow. This setup then continued into a smaller 500 ml tank, where a multimeter read temperature, pH, and conductivity. The system was set to dispense 10 ml an hour, for 28 days exactly (1200 28-01-22 until 1200 25-02-22). The multimeter successfully read the pH and temperature, which reported the pH dropped from 7.88 to 4.2, where it remained for the rest of the test, while the temperature remained at 21 ± 1.5 °C. The conductivity meter failed due to biofilm accumulation and did not register any change in reading.

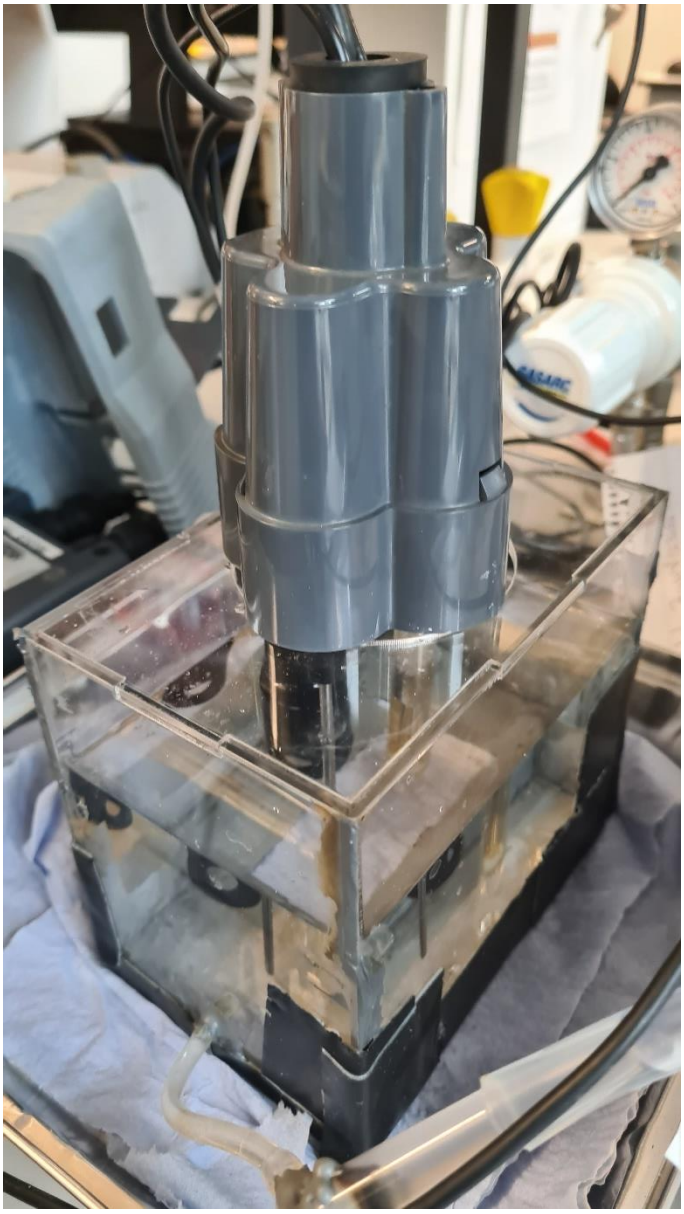

FIGURE 24 MULTIMETER SENSOR BOX

Inside the tank was a precise weight of biomass, which for the first run was orange peel, contained in the sample bags as the batch tests, which were further contained in a pair of cotton mesh bag, suspended from the top.

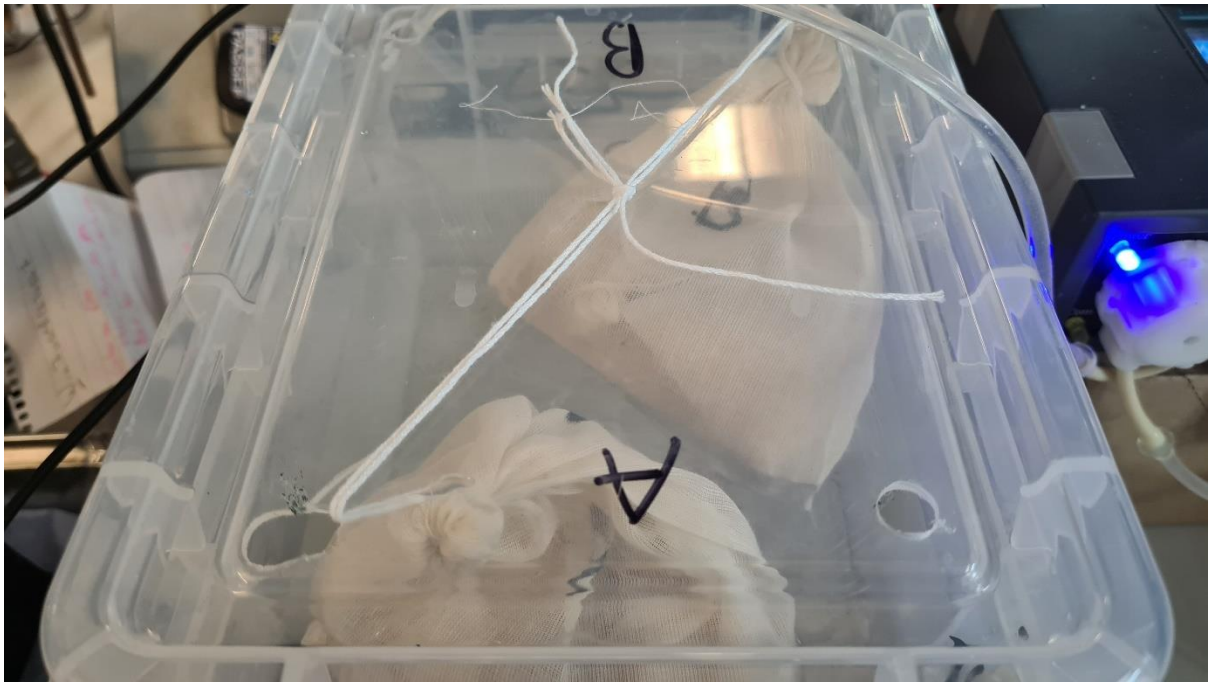

FIGURE 25 SAMPLE BOX 1, CONTINUOUS FLOW SAMPLES

This setup was then attached to 4 such tanks, but the multimeter was removed, as it could not read the four separate flows at the same time, but this was replaced by a filtration trap on each outflow, with Fisher brand™ Grade 113 Cellulose Medium Filtering Qualitative Filter Paper.

Each tank had a precise weight of one of four biomass as before, although they were reduced to a single cotton bag. These biomass were orange peel for the single run, and birch, garlic, peanut shell and potato skin for the parallel run.

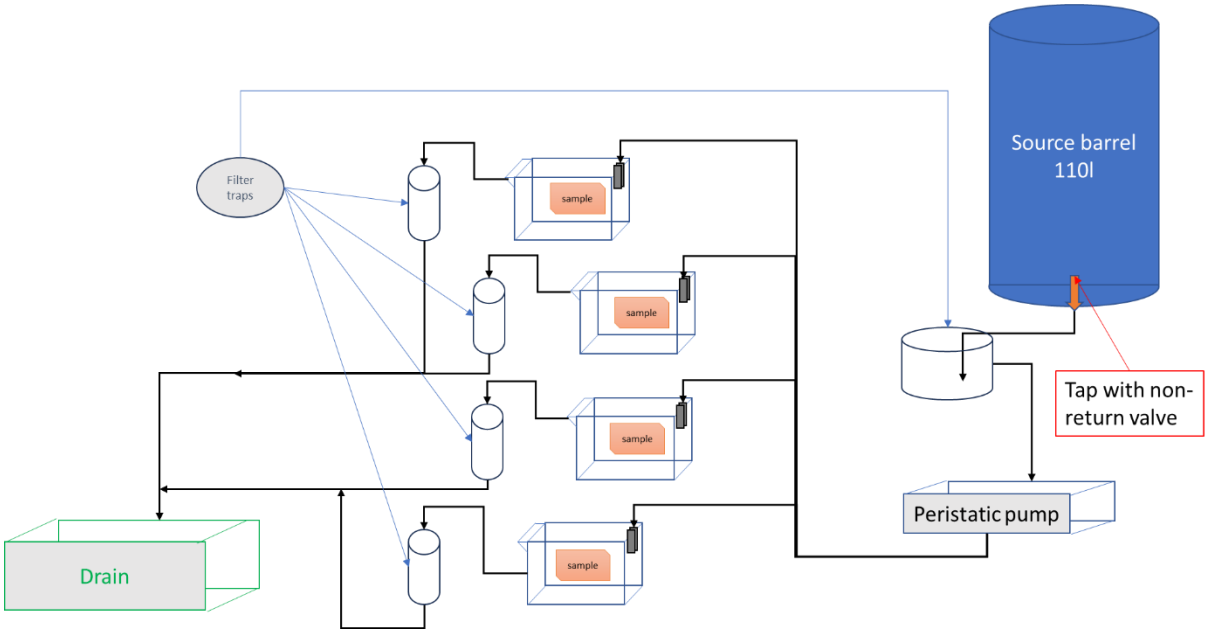

FIGURE 26 CONTINUOUS FLOW SCHEMATIC

Each tank was attached to a separate head of the pump, which were configured to dispense 50 ml an hour for one month, between 1200 01/08/23 and 1200 29/08/23. The system suffered a failure on the 08/08 at 1000 and had to be shut down from that date to 1200 16/08 (or 194 hours), so the final shutdown date and time was adjusted to 07/09/23 at 1400, to maintain the same run time. While it was shut down, the tanks remained filled, but there was no additional liquid added. There was visible evaporation from the tanks, estimated at approximately 300-500 ml depending on the tank. This failure was due to insufficient drainage, caused by the drain line being unable to maintain flow through gravity alone, and had become a reservoir. The shutdown was to engineer a system that could manage the output. When the system was restarted, a second replicate of the pump system was added to drain the outflow, which ensured that there was no overflow.

The reason for the increase of volume throughflow, and the addition of the filter traps was that the sample tanks displayed significant biofilm growth, with a mat covering the entire surface, which was presumed to be the reason for the sharp drop in pH, as the two features occurred at the same time. This proved to be successful from observations, in so far as it stopped the drop in pH, with the samples remaining at the same pH for most samples, and the film did not occur, except during the shutdown phase, where it had limited coverage, and dispersed when the pumping was restored.

Post contact, the pump was shut off, and the samples were left to equilibrate for 24 hours. Two subsamples of the supernatant were taken from each tank, one for ICP-Analysis, following the sample methodology as during Batch process, and one for pH measurement.

After contact, the solid samples where air dried per the preparation method and weighed. The filters were also air dried in the same manner and treated the same as the solid samples.

These were ashed in an acid washed crucible, using an electric oven, which used a slow temperature curve (+1 C per minute for 12 hours, with a 2 hour hold at 200 C followed by a 4 hour hold at 650 C, followed by a -5 C per minute for 2 hours), to reduce the carbon burden, then the ash was digested per the process for the Batch samples. This did require approximately 10x the acid listed due to the volume of the sample. One of the two sample bags from the initial run was attempted to be digested directly, but this proved unfeasible, as the initial attempt suggested that the quantity of acid required was too high to be performed safely without subdividing the sample, which would have potentially lost material. Instead, the resulting sample pulp was dried on a hotplate, then this dried pulp was ashed, and combined with the other sample for digestion.

4.3 ICP-MS analysis

Samples for the first and third batch of samples were analysed by ICP-MS at Lancaster Environmental Centre Trace Metals laboratory using a Thermo-Fisher Scientific Series X7. The ICP-MS spectrometer is installed in a dust free laboratory equipped to avoid contamination.

The second batch was analysed by Prof. Martine Leermakers and Prof. Yue Gao in AMGC Group, Vrije Universiteit Brussel (VUB), Belgium.

Because of interference with the salt, which is typically 35 g kg^{-1}, a dilution by a factor of 16 is required to record artefact free readings, as otherwise there is a potential for interference due to crystallisation on the cone. The injection rate was 0.3 mL per time unit (10 seconds). The dwell time for uranium was 10 ms.

For the first batch, the difference between an experimental and average value is referred to as the absolute error, which for paired samples would be equivalent to the Standard Deviation (SD). Otherwise, where the sampling involved multiple results, the formal definition of Standard Deviation was applied. When the absolute error is divided by the mean value it becomes the relative error, or the relative standard deviation, as appropriate. Percent error is relative standard deviation (RSD) multiplied by 100%.

4.4 Biomass sample characterisation

From the results of the first batch ICP-MS analysis, a subset of samples was identified as of particular interest and were selected for analysis by Fourier Transform Infrared (FTIR) spectroscopy. These were the dried kale sample, garlic powder, grape skin, orange peel, peanut shell, and potato skin. Spectra were also recorded on the dried sorbed samples after contact with seawater taken from the pH control samples and phase drying as described above for each sample which was dried using the same protocol as for the initial samples. Together with a control sample of each, they were analysed by a Shimadzu IRTracer-100 with attenuated total reflection (ATR) stage, in the UTGARD facility at the Engineering Department, Lancaster University.

Analysis was by absorbance of the total reflection using Happ-Genzel apodization. The spectral resolution was 1 cm^{-1}, over the range 600 – 4000 cm^{-1} and for 45 scans. Samples were analysed on the basis of a consistent volume, as they are intended for only comparative review to assess alteration.

4.5 Practical Research Results

4.5.1 FTIR Biomass sample analysis

Samples were analysed by FTIR on the basis of a consistent volume, as they are intended for only comparative review to assess alteration and compare the density of active groups from one sample to others. It was observed that the control samples were more homogeneous in size, as the contact samples had partially clumped, forming during the redrying process loosely cemented conglomerations of finer particles. This was mostly visible in orange peel, peanut shell, and grape skin, while the others were more consistent.

In most cases, the two samples have no variation in location of the peaks, only intensity, with the post contact samples generally being less intense than the pre contact samples. This can be attributed to a shielding effect from salt crystals, and the larger particle size (and hence lower surface area). This is illustrated by two samples which do not follow this pattern (garlic and kale) which experienced the highest fragmentation of the samples, and so the variation in intensity can be attributed to increased surface area through the contact period.

As would be expected, given the material's organic nature, the signals are dominated by those associated with cellulose. Peaks at ~ 3300 cm^{-1} (O-H), 1200 cm^{-1} ($C-H_2$) and 1050 cm^{-1} (C-O and C-C) are all clearly visible and are broadly similar between samples. Of interest as potential sites for sorption, in most cases, at least a single (merged) peak, or a double peak associated with carboxylic groups are visible at 1720-1620 cm^{-1} are clearly present in all samples, and a region of activity which would correspond with a double peak associated with polyphenolic groups is visible at 1400-1200 cm^{-1}. The IR spectra recorded for the prior and post contacted samples with natural seawater are given in Figure 27.

Post contacted grape skin has the notable exceptional feature of the carboxylic double peak at 1720-1620 cm^{-1} being more intense than pre contact, which can be attributed to either an increase in sorbance sites through specific processes, or the sorbance effects leaving them more exposed to be sensed by the FTIR.

Although kale exhibits much greater activity due to dispersal, one feature of a double peak at -2900-2800 cm^{-1} stands out as quite distinct: a C-H bond under stretched and aldehydic conditions respectively. This is probably a fermentation effect.

Garlic would be the normal response of the dispersing material. The increased response on each of the peaks is fairly consistent in proportion between the peaks.

Orange peel, peanut shell and potato skin are the three samples which exhibit consistent but reduced peak pattern between the samples. The notable exceptional features are potato skin having a higher carboxylic double peak, and peanut shell exhibiting a reduced carboxylic peak, compared to their pre-contact baseline.

Figure 27 (A-F) IR spectra of the samples prior and post contact with natural seawater. Samples: A grape skin, B kale, C garlic, D peanut shell, E potato skin, F orange peel

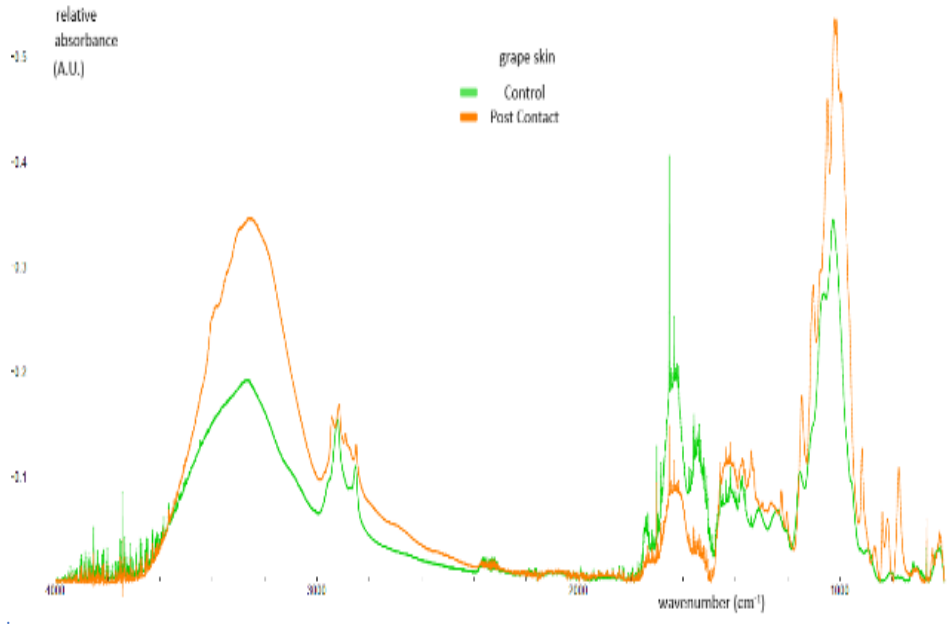

(A)

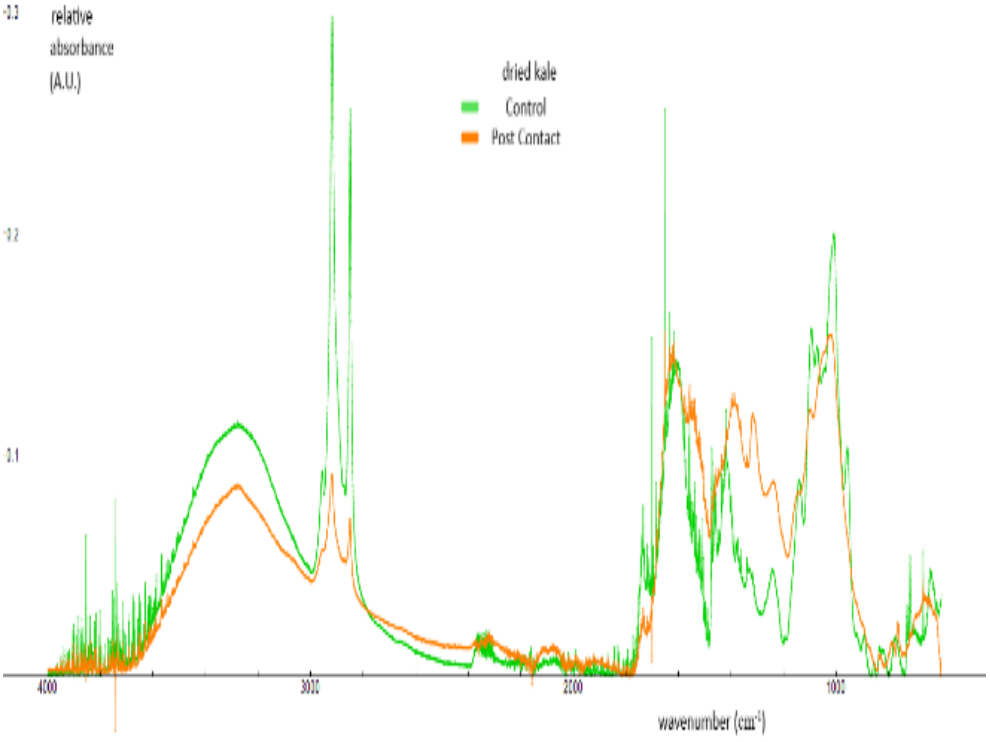

(B)

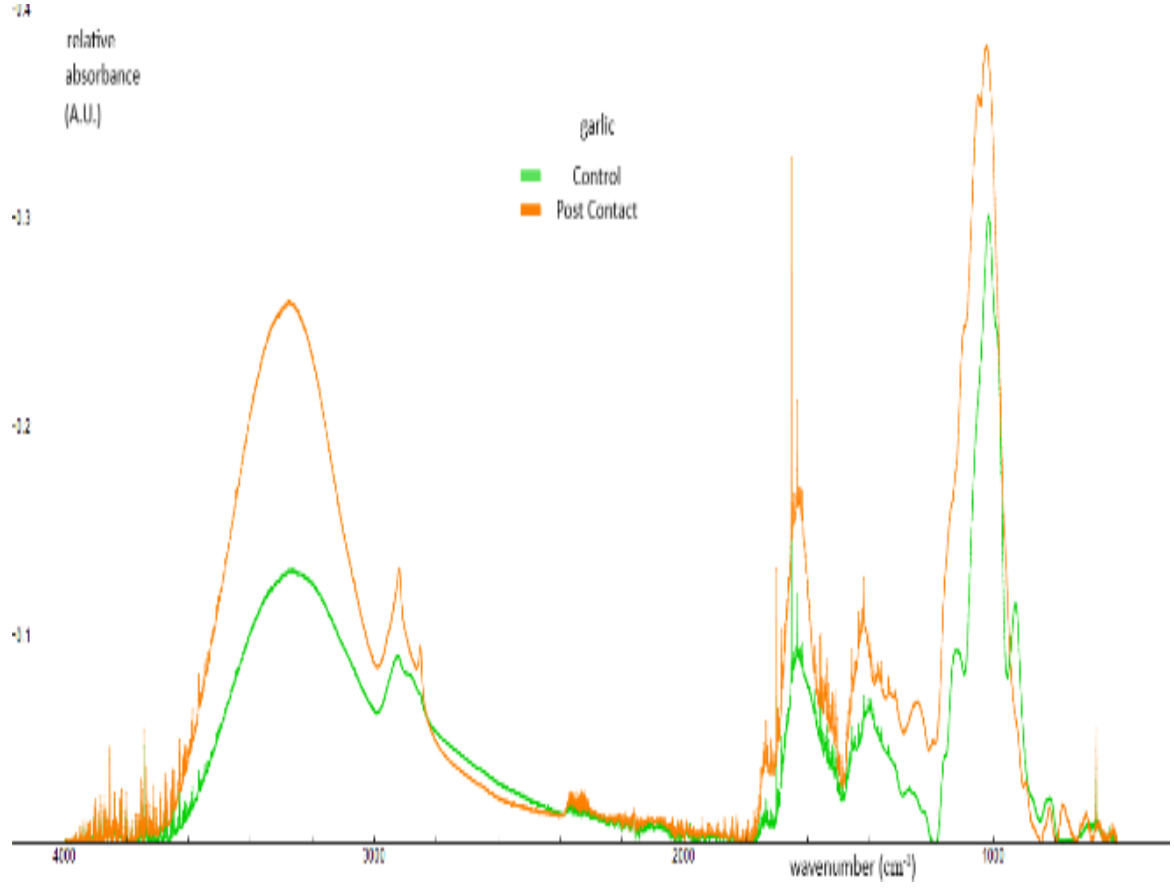
relative
absorbance
(A.U.)
garlic
Control
Post Contact
wavenumber (cm-1)

(C)

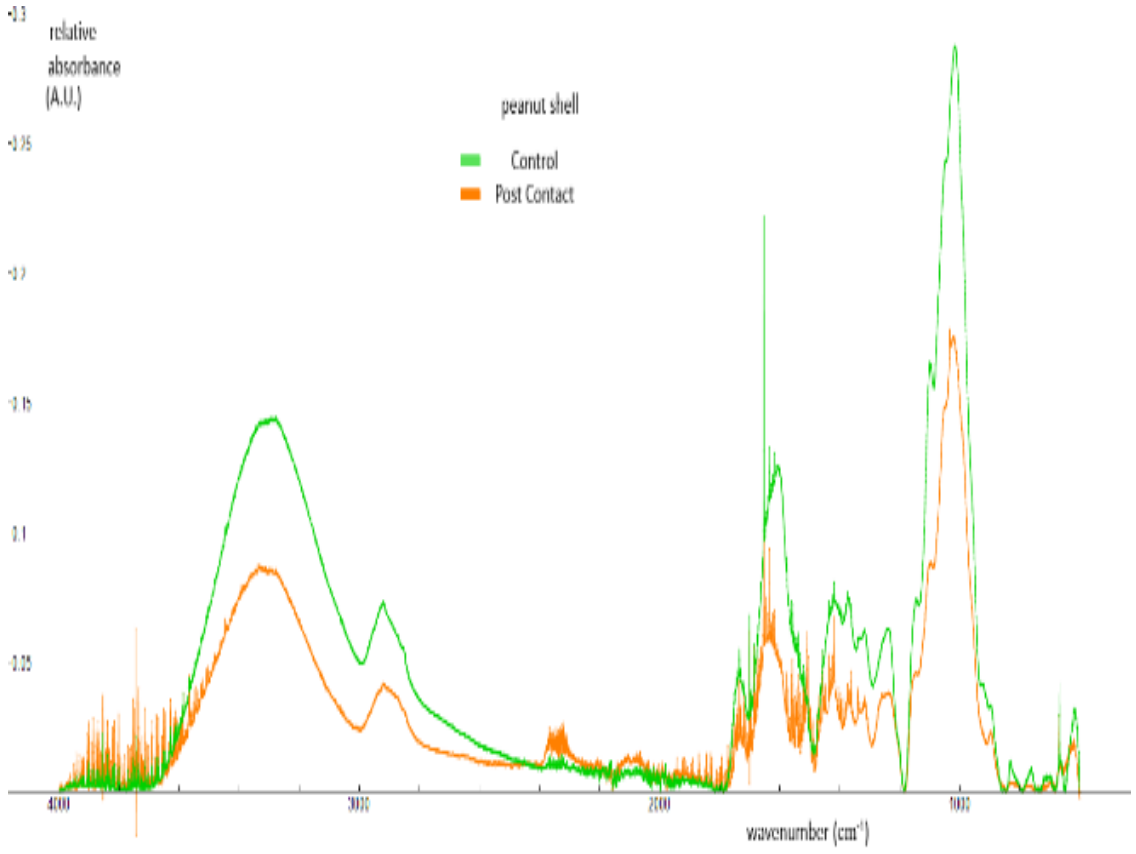
relative
absorbance
(A.U.)
peanut shell
Control
Post Contact
wavenumber (cm-1)

(D)

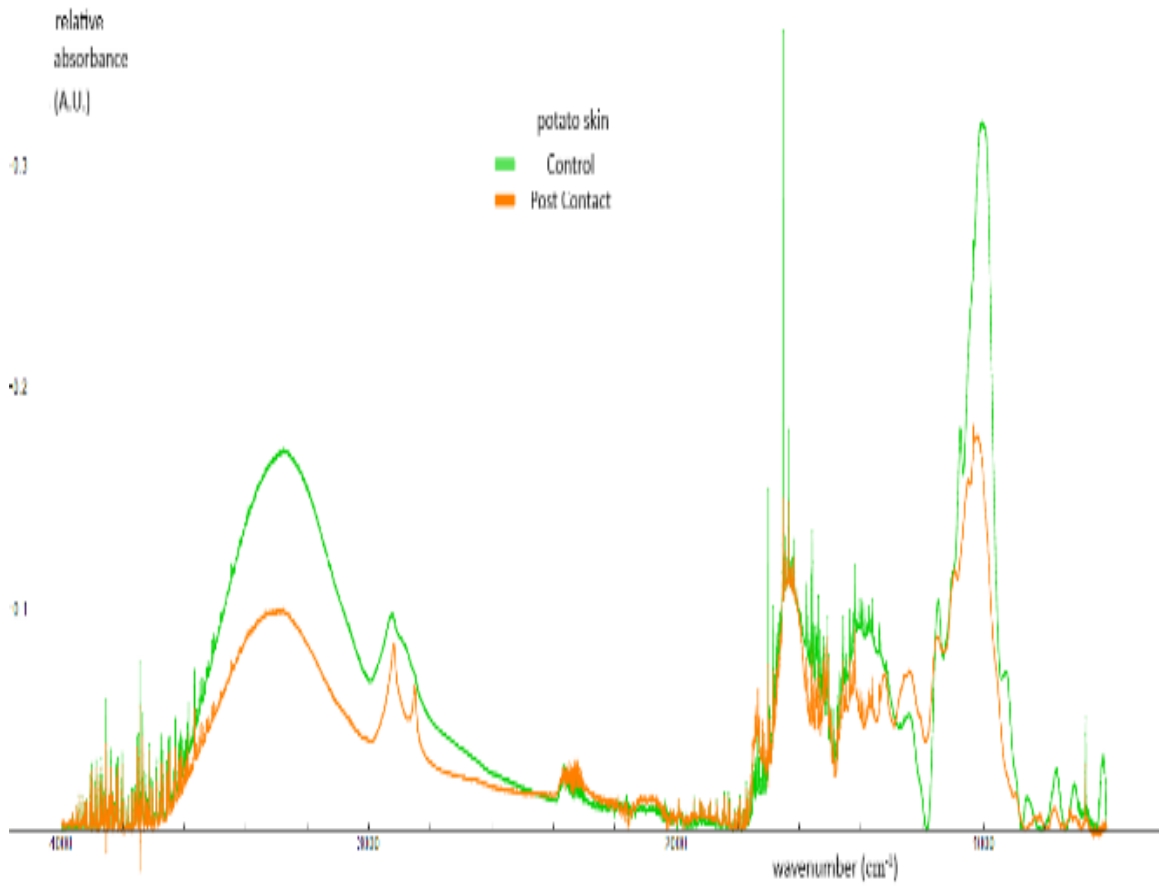
relative
absorbance
(A.U.)
potato skin
Control
Post Contact
wavenumber (cm-1)

(E)

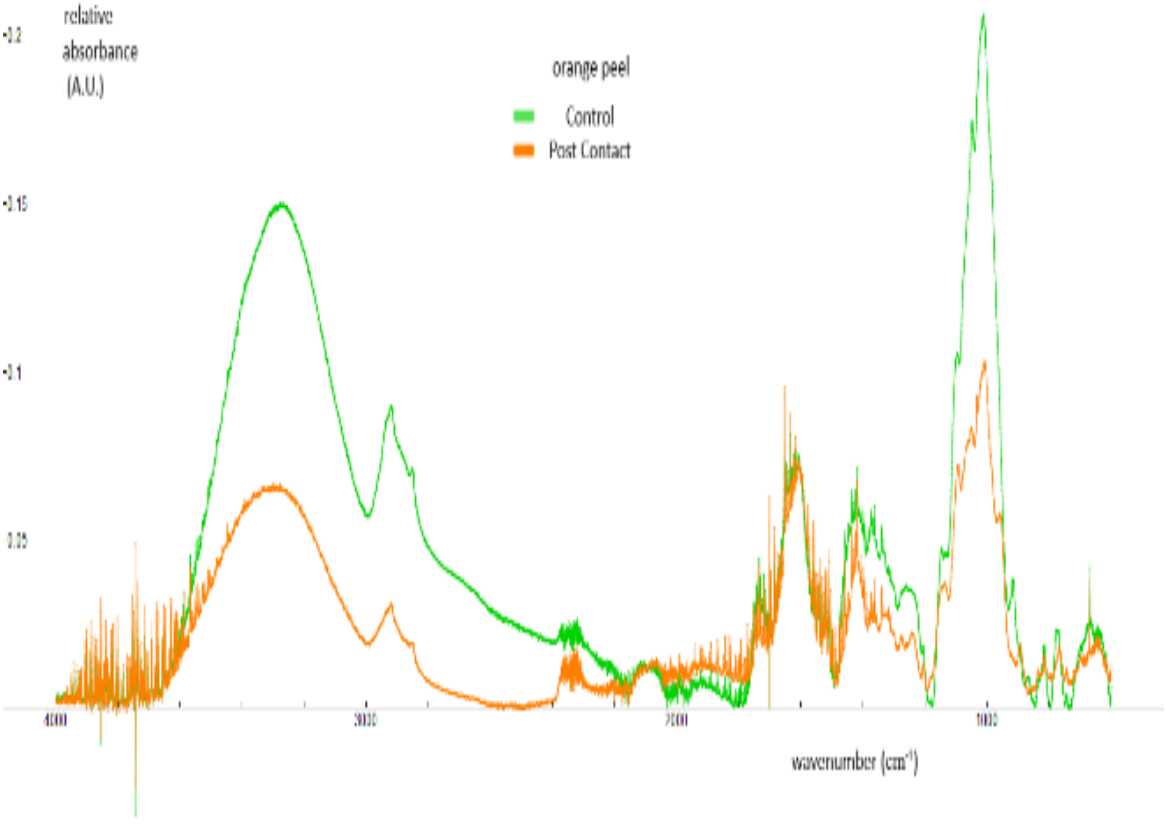
relative
absorbance
(A.U.)
orange peel
Control
Post Contact
wavenumber (cm-1)

(F)

4.5.2 ICP-MS multi element standard

For the first batch the mass scan range was first set for standardisation. It ranged from 45 (scandium), 103 (rhodium), 208 (lead) or 209 (bismuth) and 238 (uranium). For the second, third and continuous flow experiments, the mass scan range was set for standardisation on a range from 45 (scandium), 51(vanadium), 55 (manganese),59 (cobalt), 60 (nickel), 65 (copper), 95 (molybdenum), 103 (rhodium), 107 (silver), 197 (gold), or 209 (bismuth) and 238 (uranium).

4.5.2a Uranium analysis in standard

For the first batch, the uranium calibration used uranium solutions of 0.1, 0.3, 0.6 and 1.0 µg L^{-1} which were prepared from a reference standard uranium solution (sourced from VWR, Lutterworth, Lecestershire, England), together with a zero standard of ultrapure water were analysed for a calibration curve. In addition, a broadband reference standard was added for traceability. The calibration curve proved to be linear (see Figure 28) over this range (R^2 = 0.9948), with an increasing variance from 1.0 - 4.6%. Most of this variance is instrumental in nature: samples experience a small dilution effect between the first sampling and the following ones. The noise factor of the system was measured from the 0 standards, resulting in a zero variance of 8.62 counts, corresponding to a concentration of 0.000127 µg L^{-1}. Therefore, the 3-σ value for as the limit of detection is 0.0004 µg L^{-1} (ppb) or 0.4 ppt.

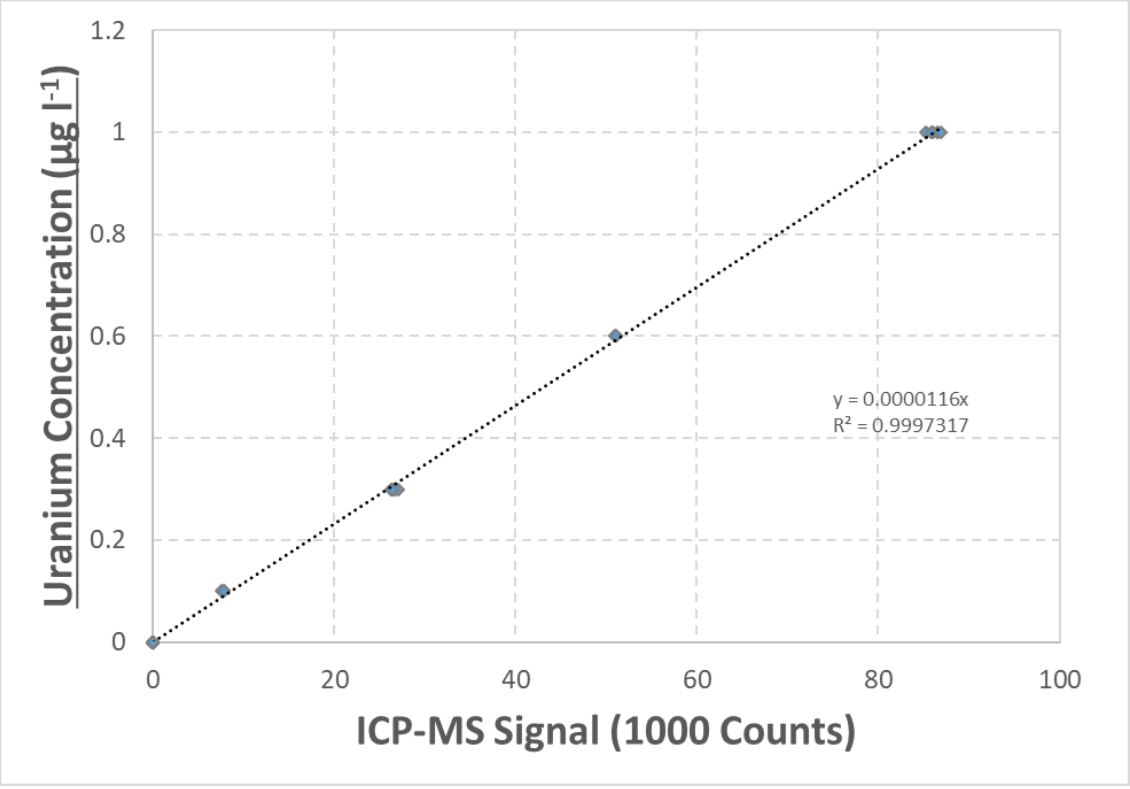

FIGURE 28 ICP-MS CALIBRATION CURVE FOR URANIUM. CONDITIONS: INJECTION RATE: 0.03 ML S^{-1}; DWELL TIME 10 MS

4.5.2b Vanadium analysis in standard

For the second and third batches, the reference standard which were prepared from a set of reference standard solutions (sourced from VWR), together with a zero standard of ultrapure water were analysed for a calibration curve from 0, 1, 2, 5, 10, and 20 µg l^{-1}. This standard covered all listed elements, and also included a broadband reference standard, for traceability.

As with the first batch, these proved to be linear (see Figure 29**)**, with an R^2 of 0.9997. Variance is 0.17-2.95%, with the majority of the variability is instrumental, due to a dilution to saturation effect.

The noise factor of the system was measured from the 0 standards, resulting in a zero variance of 756 counts, corresponding to a concentration of ~0.06 µg L^{-1}. Therefore, the 3-σ value for as the limit of detection is ~0.16 µg L^{-1} (ppb).

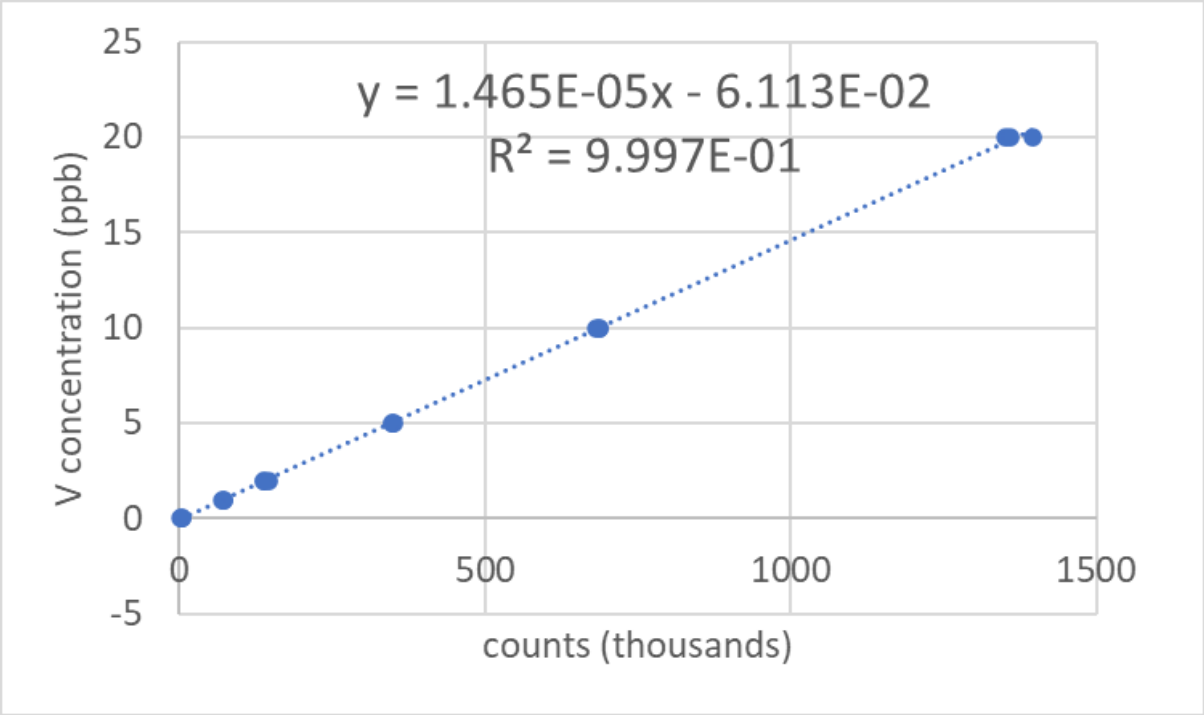

FIGURE 29 ICP-MS CALIBRATION CURVE FOR VANADIUM. CONCENTRATIONS MEASURED VS.. PREDICTED CONDITIONS: INJECTION RATE: 0.03 ML S^{-1}; DWELL TIME 10 MS.

4.5.2c Manganese analysis in standard

For the second and third batches, the reference standard which were prepared from a set of reference standard solutions (sourced from VWR), together with a zero standard of ultrapure water were analysed for a calibration curve from 0, 1, 2, 5, 10, and 20 µg l^{-1}. This standard covered all listed elements, and also included a broadband reference standard, for traceability.

As with the first batch, these proved to be linear (see **Figure 30**), with an R2 of 0.9997. Variance is 0.326-2.25%, with the majority of the variability is instrumental, due to a dilution to saturation effect.

The noise factor of the system was measured from the 0 standards, resulting in a zero variance of 6193 counts, corresponding to a concentration of ~0.12 µg L^{-1}. Therefore, the 3-σ value for as the limit of detection is ~0.37 µg L^{-1} (ppb).

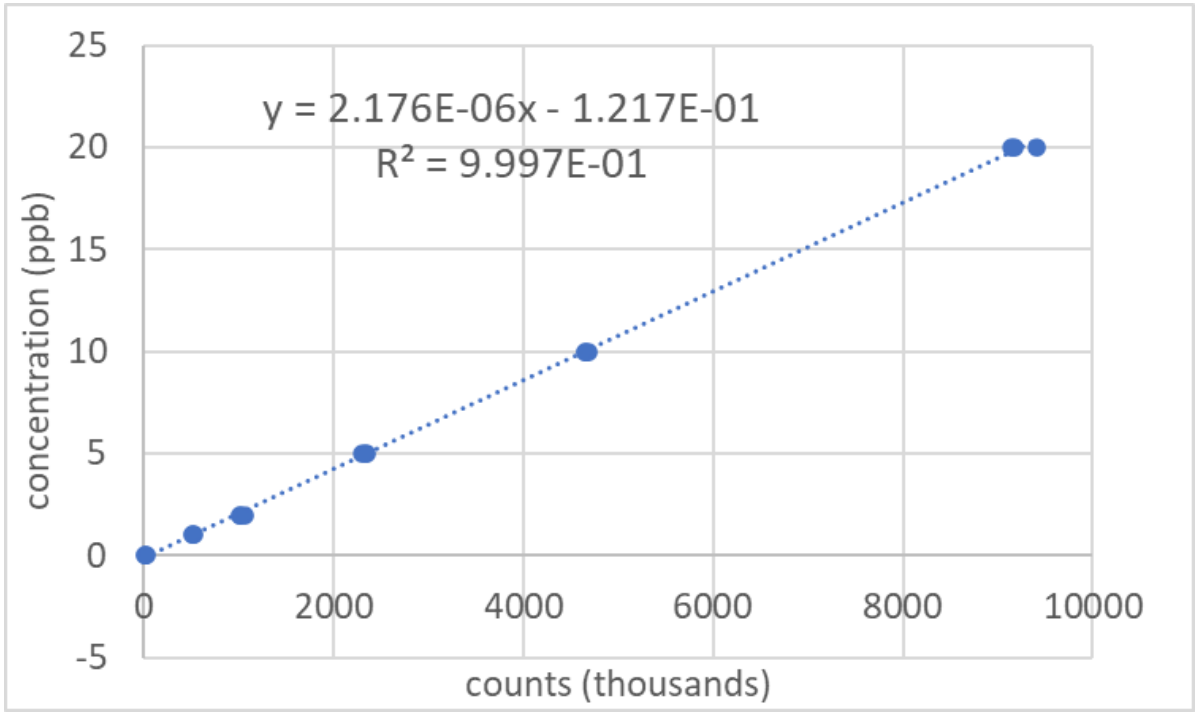

FIGURE 30 ICP-MS CALIBRATION CURVE FOR MANGANESE CONCENTRATIONS MEASURED VS.. PREDICTED CONDITIONS: INJECTION RATE: 0.03 ML S^{-1}; DWELL TIME 10 MS.

4.5.2d Nickel analysis in standard

For the second and third batches, the reference standard which were prepared from a set of reference standard solutions (sourced from VWR), together with a zero standard of ultrapure water were analysed for a calibration curve from 0, 1, 2, 5, 10, and 20 µg l^{-1}. This standard covered all listed elements, and also included a broadband reference standard, for traceability.

As with the first batch, these proved to be linear (see **Figure 31**), with an R2 of 0.9997. Variance is 0.8-2.5%, with the majority of the variability is instrumental, due to a dilution to saturation effect.

The noise factor of the system was measured from the 0 standards, resulting in a zero variance of 463 counts, corresponding to a concentration of 0.047 µg L^{-1}. Therefore, the 3-σ value for as the limit of detection is 0.14 µg L^{-1} (ppb).

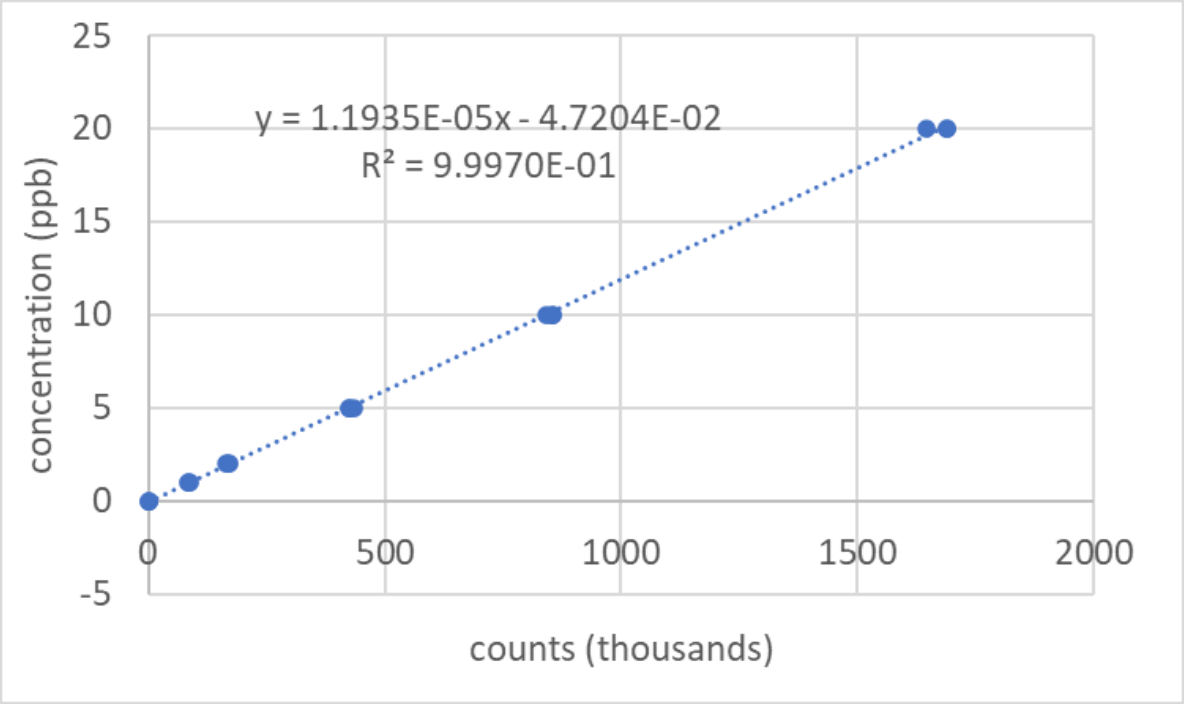

FIGURE 31 ICP-MS CALIBRATION CURVE FOR NICKEL CONCENTRATIONS MEASURED VS.. PREDICTED CONDITIONS: INJECTION RATE: 0.03 ML S^{-1}; DWELL TIME 10 MS.

4.5.2e Molybdenum analysis in standard

For the second and third batches, the reference standard which were prepared from a set of reference standard solutions (sourced from VWR), together with a zero standard of ultrapure water were analysed for a calibration curve from 0, 1, 2, 5, 10, and 20 µg l^{-1}. This standard covered all listed elements, and also included a broadband reference standard, for traceability.

As with the first batch, these proved to be linear (see **Figure 32**), with an R2 of 0.98683. Variance is 1.4-14%, with most of the readings at 1-2%. The 14% variability was generated by one rogue value in readings, discounting it adjusts the 2ppb value into line with this variability, with the majority of the variability is instrumental, due to a dilution to saturation effect.

The noise factor of the system was measured from the 0 standards, resulting in a zero variance of 216 counts, corresponding to a concentration of 0.00026 µg L^{-1}. Therefore, the 3-σ value for as the limit of detection is 0.000079 µg L^{-1} (ppb).

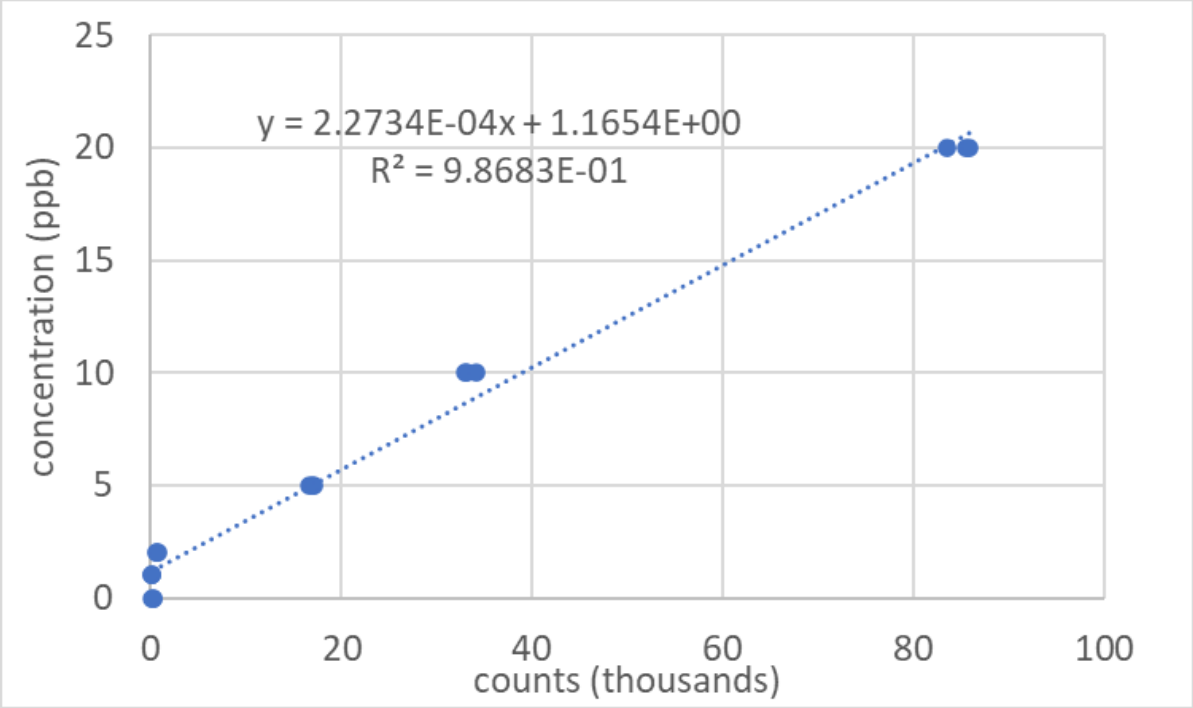

FIGURE 32 ICP-MS CALIBRATION CURVE FOR MOLYBDENUM CONCENTRATIONS MEASURED VS.. PREDICTED CONDITIONS: INJECTION RATE: 0.03 ML S^{-1}; DWELL TIME 10 MS.

4.5.2f Gold analysis in standard

For the second and third batches, the reference standard which were prepared from a set of reference standard solutions (sourced from VWR), together with a zero standard of ultrapure water were analysed for a calibration curve from 0, 1, 2, 5, 10, and 20 µg l^{-1}. This standard covered all listed elements, and also included a broadband reference standard, for traceability.

As with the first batch, these proved to be linear (see Figure 33), with an R2 of 0.9997. Variance is 0.3-2.3% with the majority of the variability is instrumental, due to a dilution to saturation effect.

The noise factor of the system was measured from the 0 standards, resulting in a zero variance of 94 counts, corresponding to a concentration of 0.0000212 µg L^{-1}. Therefore, the 3-σ value for as the limit of detection is 0.000064 µg L^{-1} (ppb).

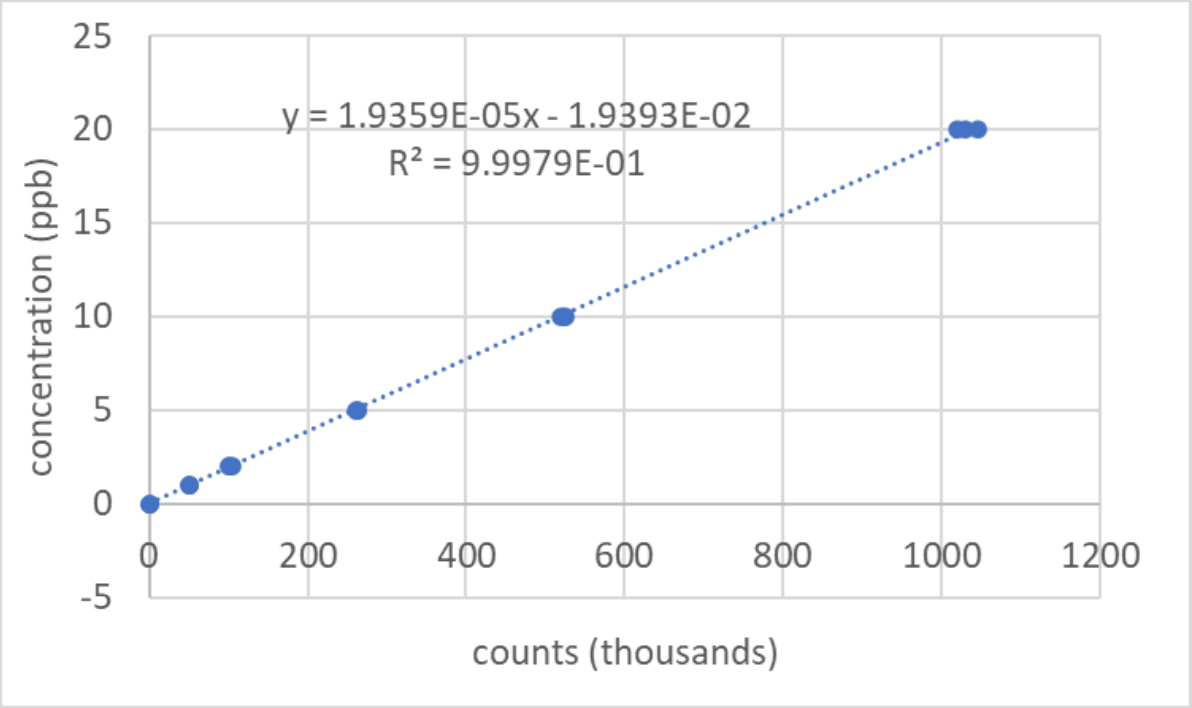

FIGURE 33 ICP-MS CALIBRATION CURVE FOR GOLD CONCENTRATIONS MEASURED VS.. PREDICTED CONDITIONS: INJECTION RATE: 0.03 ML S^{-1}; DWELL TIME 10 MS.

4.5.2g Silver analysis in standard

For the second and third batches, the reference standard which were prepared from a set of reference standard solutions (sourced from VWR), together with a zero standard of ultrapure water were analysed for a calibration curve from 0, 1, 2, 5, 10, and 20 µg l^{-1}. This standard covered all listed elements, and also included a broadband reference standard, for traceability.

As with the first batch, these proved to be linear (see **Figure 34**), with an R2 of 0.992. Variance is 1.8-11.5%. The very high variability was a single reading very first reading on the 0 standard, suggesting some persistent contamination. Discounting this value, the majority of the variability is instrumental, due to a dilution to saturation effect.

The noise factor of the system was measured from the 0 standards, resulting in a zero variance of 5 counts (after discounting), corresponding to a concentration of 0.00006 µg L^{-1}. Therefore, the 3-σ value for as the limit of detection is 0.00019 µg L^{-1} or 1.85 ppt. Including the flawed value decreases these to 0.00004 ppb, and 0.00014 ppb respectively.

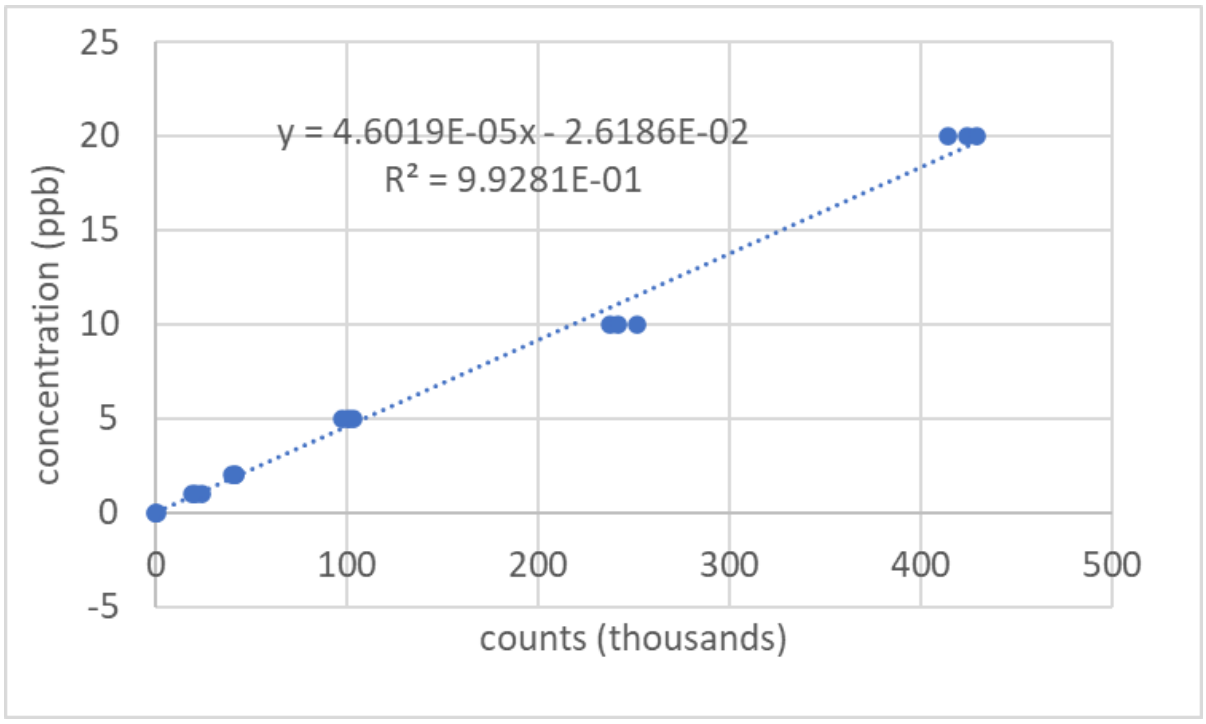

FIGURE 34 ICP-MS CALIBRATION CURVE FOR SILVER CONCENTRATIONS MEASURED VS.. PREDICTED CONDITIONS: INJECTION RATE: 0.03 ML S^{-1}; DWELL TIME 10 MS.

4.5.2h Uranium (2nd Batch) in standard

For the second and third batches, the reference standard which were prepared from a set of reference standard solutions (sourced from VWR), together with a zero standard of ultrapure water were analysed for a calibration curve from 0, 1, 2, 5, 10, and 20 µg l^{-1}. This standard covered all listed elements, and also included a broadband reference standard, for traceability.

As with the first batch, these proved to be linear (see **Figure 35**) up to concentration of 10ppb. The 20-ppb standard was non-linear, but since no sample tested outside this curve, this was deemed acceptable to discount. The revised curve had an R^2 of 0.9992. Variance is 0.6-4.3% with the majority of the variability is instrumental, due to a dilution to saturation effect.

The noise factor of the system was measured from the 0 standards, resulting in a zero variance of 502 counts, corresponding to a concentration of 0.000009 µg L^{-1}. Therefore, the 3-σ value for as the limit of detection is 0.000029 µg L^{-1} (ppb).

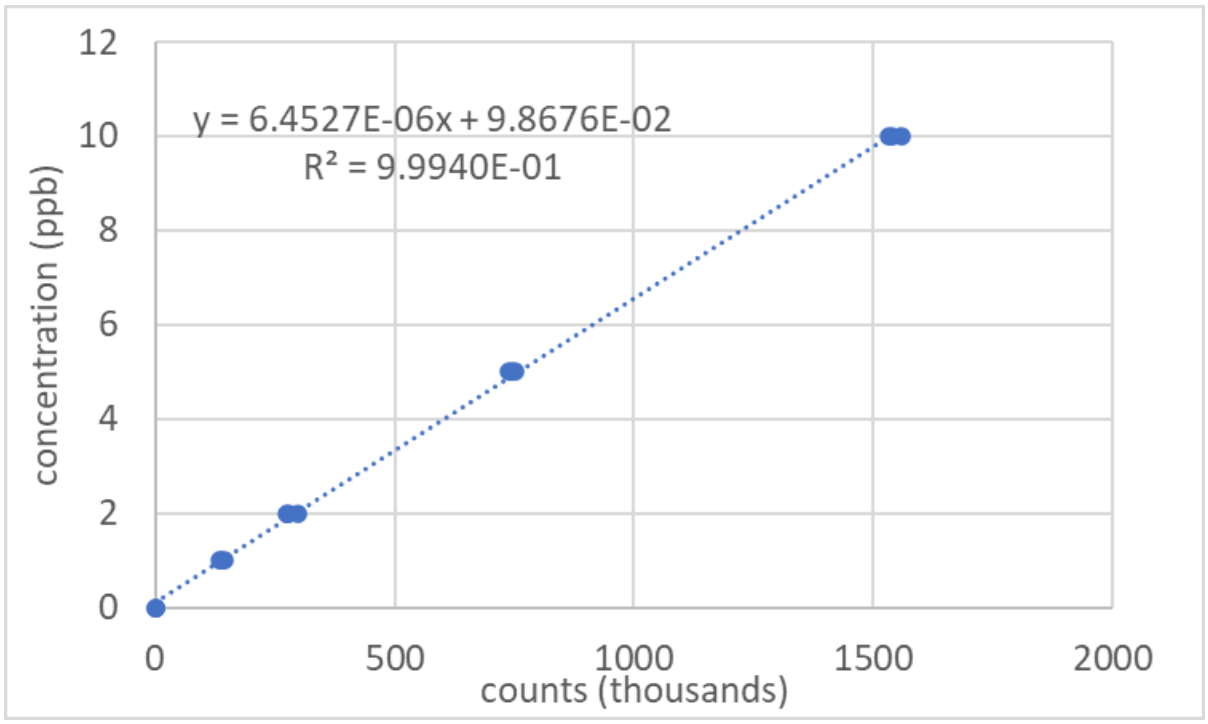

FIGURE 35 ICP-MS CALIBRATION CURVE FOR URANIUM CONCENTRATIONS MEASURED VS.. PREDICTED CONDITIONS: INJECTION RATE: 0.03 ML S^{-1}; DWELL TIME 10 MS.

4.5.2I Copper analysis in standard

For the second and third batches, the reference standard which were prepared from a set of reference standard solutions (sourced from VWR), together with a zero standard of ultrapure water were analysed for a calibration curve from 0, 1, 2, 5, 10, and 20 µg l^{-1}. This standard covered all listed elements, and also included a broadband reference standard, for traceability.

These proved to be linear (see **Figure 36**) up to concentrations of 20ppb. The revised curve had an R^2 of 0.9998. Variance is 0.68-3.1% with the majority of the variability is instrumental, due to a dilution to saturation effect.

The noise factor of the system was measured from the 0 standards, resulting in a zero variance of 907 counts, corresponding to a concentration of 0.00002 µg L^{-1}. Therefore, the 3-σ value for as the limit of detection is 0.000058 µg L^{-1} or 0.05 ppt.

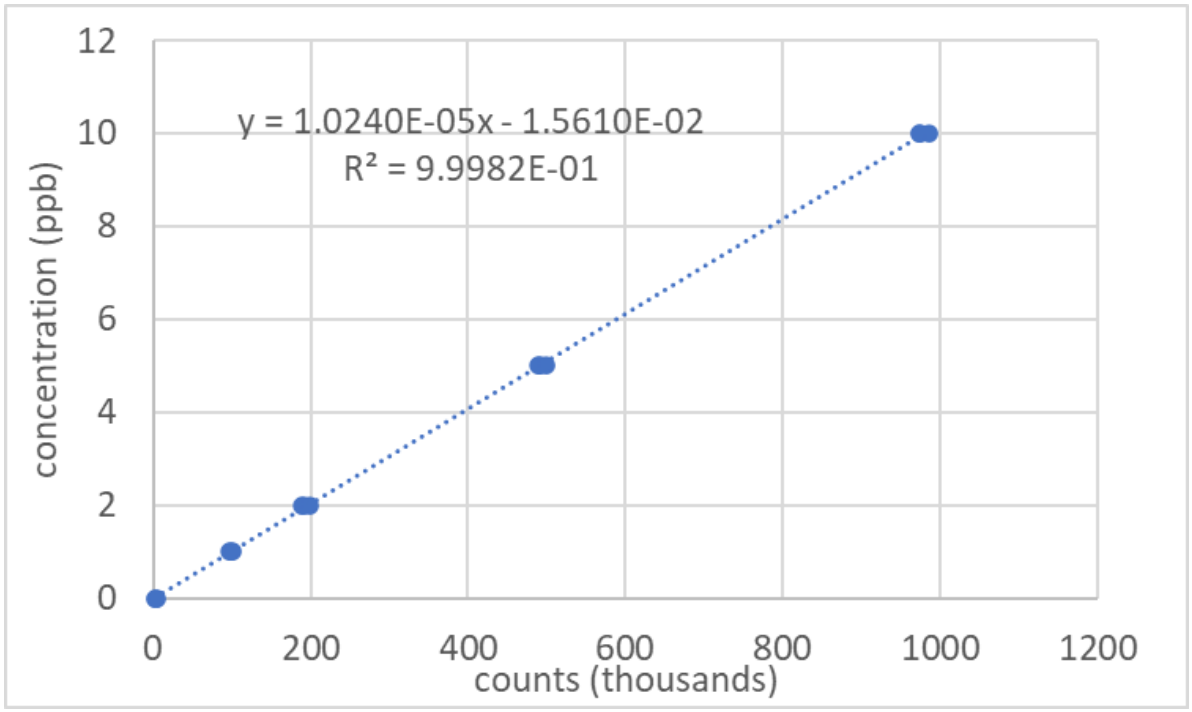

FIGURE 36 ICP-MS CALIBRATION CURVE FOR COPPER CONCENTRATIONS MEASURED VS.. PREDICTED CONDITIONS: INJECTION RATE: 0.03 ML S^{-1}; DWELL TIME 10 MS.

4.5.2J Cobalt analysis in standard

Attempting to calibrate on the cobalt standard proved ineffective, with no linearity identifiable (the best R^2 value was only 88%, for a best fit straight line as the predicted concentrations were not in sequence)

It was judged that the cobalt was not possible to be read at these concentrations.

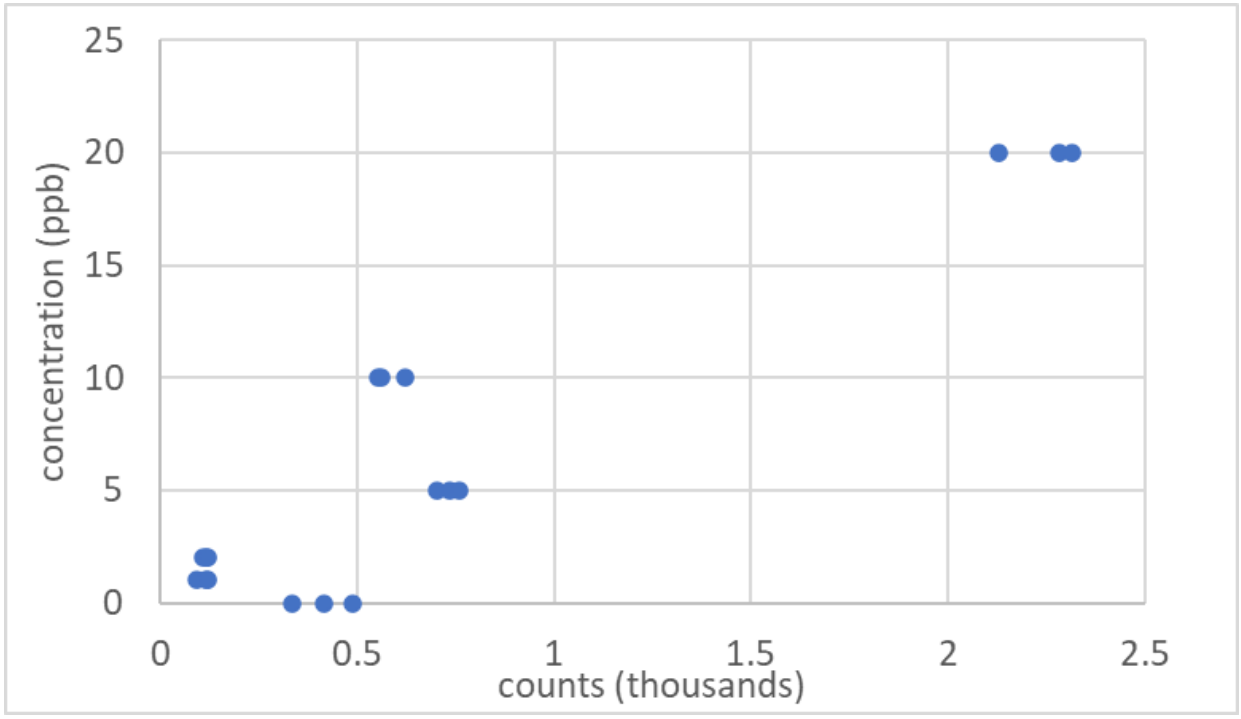

FIGURE 37 FAILED ATTEMPT FOR ICP-MS CALIBRATION CURVE FOR COBALT CONCENTRATIONS MEASURED VS.. PREDICTED CONDITIONS: INJECTION RATE: 0.03 ML S^{-1}; DWELL TIME 10 MS.

4.5.3 Analysis of uranium in seawater samples

The seawater samples for the first batch were gathered on 3 separate campaigns. These were analysed and were considered similar enough between the sampling times as to not have an appreciable effect on the results (see **Table 18**). The average value for the first batch was recorded of 2.69±0.41 µg L^{-1} is below (82%) that conventionally ascribed to the sea (3.3 µg L^{-1}, 100%) (Diallo, *et al*., 2015 [28]). However, this is likely due to sampling being near-shore, which is due to a small dilution factor (e.g. 91% see Section 3.1.1) due to freshwater runoff (Laane, et al., 1996), and a weak scavenging effect from phosphates, which are known precipitants for uranium (Beazley, et al., 2007).

TABLE 18 URANIUM CONCENTRATION IN SEAWATER AS SAMPLED FOR THIS STUDY.

Uranium concentration (µg L^{-1})	Sample 1 09:33 am, 19-01-19	Sample 2 10:38 am, 15-06-19	Sample 3 07:32 am, 15/08/19	Average
	2.27 ±0.07	2.29 ±0.02	2.48 ±0.00	
	2.89 ±0.16	2.66 ±0.29	3.53 ±0.17	
		2.92 ±0.03	3.21 ±0.03	
		2.32 ±0.31	2.35 ±0.38	
Average	2.58	2.55	2.89	2.69
RSD	12.10%	10.21%	17.00%	15.33%

For the second and third batch, as well as the continuous flow experiment, as previously mentioned, the water was gathered over 8 campaigns between March and June 2022, but were stored in a collective water tank, and allowed to mix and equilibrate. This was sampled at each batch, with an average of 2.81±0.15 µg L^{-1}, and 2.96±0.16 µg L^{-1}. Although below the median seawater concentration, this is higher than the first batch, which would likely confirm that the dilution effect was due to seasonal variability, as the weather was drier for a longer time period than during the first 3 campaigns.

TABLE 19 URANIUM CONCENTRATION IN SEAWATER, SAMPLING

Uranium concentration (µg L^{-1})	Tank Sampling 1 (Batch 2)	Tank Sampling 2 (Batch 3)	Tank Sampling (Continuous Flow)
	2.86 ±0.048	3.22 ±0.00	
	2.69 ±0.048	2.78 ±0.00	
	3.07 ±0.0	2.88 ±0.00	
	2.68 ±0.0	2.98 ±0.00	
	2.74 ±0.0		
Average RSD	2.81 ±0.15	2.96 ±0.16	

4.5.4 Interferences

There are several isobaric interferences that can be anticipated to impact on the accuracy of the ICP-MS measurements of uranium ^{238}U in seawater.

The only single isotope interference would be due to $^{238}Pu^{+}$. However, plutonium is nearly absent in seawater today (<<fg L^{-1}).

There are several cluster ions which could potentially impact readings. Heavy metal cluster ions where there is an attachment with O, C, Ar, Cl and H isotopes, which would all be present at significant concentrations. The most likely are the following cluster ions, which are given below, alone with their elemental concentration in seawater. From these, we can conclude that none of these cluster ions would significantly interfere with ^{238}U because the concentrations of their heavy element cluster ions are several order of magnitude below that of uranium in seawater.

- $[^{222}Rn^{16}O]^{+}$, with a maximum potential concentration of $6x10^{-19}$ g L^{-1} Rn (Gregorič, et al., 2008)
- $[^{226}Ra^{12}C]^{+}$, with a maximum potential concentration of ~9.8×10^{-14} g L^{-1} Ra (Walker & Rose, 1989)
- $[^{198}Hg\ ^{40}Ar]^{+}$ with a maximum potential concentration of 9.97% of 5×10^{-9} g L^{-1} Hg (Gardner., 1973)
- $[^{202}Hg^{36}Ar]^{+}$ with a maximum potential concentration of 29.86% of 5×10^{-9} g L^{-1} Hg and 0.337% Ar (Gardner., 1973)
- $[^{237}Np^{1}H]^{+}$ with a maximum potential concentration of $<10^{-12}$ g L^{-1} Np (Assinder, 1999)

• $[^{198}Pt\ ^{40}Ar]^{+}$ with a maximum potential concentration of 7.2% of $<10^{-12}$ g L^{-1} Pt (Turetta, et al., 2003) & (Goldberg, et al., 1989)

• $[^{201}Hg^{37}Cl]^{+}$ with a maximum potential concentration of 13.18 % of $<5 \times 10^{-9}$ g L^{-1} Hg, and 24.23% Cl (Gardner., 1973)

However, none of these cluster ions interfere with ^{238}U because the concentration their heavy element cluster ions is several order of magnitude below that of uranium in seawater.

4.5.5 Interferences of other elements analysed.

Reviewing the standards, and the high degree of variability with the response (and consequential loss of sensitivity) in regard to the standard concentration, it is not hard to spot those elements where known issues of interference are present (Tomoko, 2019).

For example, 51-vanadium, there are two potential interferences: $[^{35}Cl^{16}O]^{+}$ and $[^{34}S^{16}OH]^{+}$. 55-manganese has a known interferent in the form of $^{32}S^{23}Na^{+}$ (Tomoko, 2019). These result in low degrees of sensitivity exhibited in the relevant results.

Considering known interferants for Cobalt include NaCl, and NiH^{+}, it is not a surprise that it was not possible to produce a response curve at relevant concentrations (BLOXHAM, 1994). Bloxham also lists Nickel also has a known interference due to NaCl, but it is due to an isotope pairing but of lower frequency, as both isotopes are <10% of the element by weight, so has a cumulative frequency of less than 1%.

Outside these, the co-elements are mostly radioactive with short half-lives, very scarce to non-existent in seawater, or of poor electron stability (for example, $[Br0]^{-}$).

These would factor together to produce the sensitivities recorded.

4.6 batch analysis of supernatants after sorption test

Samples were analysed using ICP-MS, as described, and the results are reported in the sections below. Additionally, the +1 sample were analysed for pH, using a HANNA edge pH meter. The results of that analysis are displayed in Table 20. Samples were generally acidified relative to the seawater, following a broad trend following that of the relative fast calorific value, with high free sugar type materials being more acidified than lower samples. This would be consistent with the impact of mild fermentation in sample. Interbatch controls are similar, indicative that this system is close to an equilibrium.

TABLE 20 SAMPLE PH AFTER CONTACT OF BATCH 2 AND 3

Sample	pH
Batch 2	
Dried Kale	5.8
Garlic Powder	5.2
Orange Peel	4.9
Peanut shell	6.1
Potato Skin	6.1
Red Grape	4.8
Vitira Grape	4.3
White Grape	6.1
Batch 3	
Blackberry	4.3
Coffee Grounds	5.8
Garlic Powder	5.6
Dried Kale	5.9
Peanut Shell	5.9
Spring Greens	5.0
Red Tea Leaf	5.4
White Birch	6.2

4.6.1 First batch (uranium only) analysis

The replicate supernatant samples were subsequently analysed, and the results displayed in **Table 21**. The variances here are the difference between the average data (2 values) and the difference with the highest value. The variances ranges from 1 to 90% which is not unknown in biologically active systems. The supernatants concentration in uranium is well below that of uranium in the seawater which suggests a strong sorption.

The attempt to partition the supernatant by removing the particles with a 0.4 µm filter was unsuccessful for the first batch as these samples proved vulnerable to microbial biofilm growth, as the acidification was insufficient.

TABLE 21 RESULTS OF URANIUM CONC. FROM ANALYSIS OF SUPERNATANTS POSTCONTACT W. BIOMASS FOR MIN OF 1 MONTH

Biomaterial	Test 1 [U] (µg L^{-1})	Test 2 [U] (µg L^{-1})	Mean [U] (µg L^{-1})	RSD ±(%)
Orange skin	0.038 ±0.002	0.010 ±0.002	0.024	57.5
Lemon skin	0.033 ±0.002	0.040 ±0.003	0.037	10.4
Nectarine skin	0.153 ±0.007	0.207 ±0.007	0.180	15.0
Grape skin	0.032 ±0.001	0.018 ±0.001	0.025	27.5
Grape pulp	0.019 ±0.002	0.019 ±0.001	0.019	1.2
Sultana whole	0.094 ±0.003	0.006 ±0.001	0.050	87.7
Sultana diced	0.032 ±0.002	0.004 ±0.001	0.018	75.5
Brussels sprouts	0.016 ±0.001	0.016 ±0.001	0.016	1.3
Kale diced	-	0.062 ±0.002	0.062	-
Mange tout	0.091 ±0.001	0.070 ±0.003	0.080	13.5
Garlic diced	0.010 ±0.001	0.001 ±0.000	0.005	87.2
Peanut shell	0.017 ±0.002	0.020 ±0.002	0.019	7.3
Potato skin	0.017 ±0.002	0.018 ±0.001	0.018	3.0
Potato whole	0.009 ±0.001	0.015 ±0.000	0.012	22.3
Sweet potato whole	0.019 ±0.001	0.023 ±0.001	0.021	10.0

4.6.2 Second and third batch analysis

For the second and third batches, the post-processing biofilm issues with the supernatant were not significant, as the acidity of samples was increased compared to the first batch, but it should be noted that many of the samples tested below the limit of detection for the element, particularly for the particulate + wet phase samples. In these cases, the samples were assumed to be at the limit of detection for the element. The mean readings, and the variance, is reported in the tables below, with full data in the appendix. Furthermore, some of the elements exhibited lower values for the unfiltered samples than the prefiltered ones. This is presumed to be due to either release of masking elements, or deposition due to interactions with these elements, as this behaviour was not visible in the controls.

4.6.2.a Uranium supernatant analysis

The uranium concentrations in the supernatant were measured and reported in

Reviewing the data, the variances, it appears to follow the pH of the solutions (see Table 20), as the materials which tested as less acidic have greater variance as a %. Although both sets of samples were acidic, it appears that the consistent lower pH producted in the digestion step had influenced better transfer in the final filtration.

Table 22 for batch 2, and **Table 23** for batch 3. Samples were all above the limit of detection, and in most cases the variance was not significant, although some exceptions exist, particularly in batch 2, which was a reason for the increase in replicates in batch 3. These tend to be driven by one outlier in the triplets being slightly lower than the other pair.

In general, samples were lower than the free solution samples, indicating sorption, although it was mild in some cases. In most cases, as would be expected, the filtered U concentrations are either below the unfiltered, or are statistically indistinguishable from the filtered: high variance amongst the filtered seems to indicate that the microfilters, although hydrophobic, had an inconsistent effect on the final concentrations.

Reviewing the data, the variances, it appears to follow the pH of the solutions (see Table 20), as the materials which tested as less acidic have greater variance as a %. Although both sets of samples were acidic, it appears that the consistent lower pH producted in the digestion step had influenced better transfer in the final filtration.

TABLE 22 URANIUM CONCENTRATIONS IN SUPERNATANT IN BATCH 2

	U filtered concentration $\mu g\ L^{-1}$	U filtered variance ±	U unfiltered concentration $\mu g\ L^{-1}$	U unfiltered variance ±
Dried Kale	0.07	0.02	0.15	0.03
Garlic Powder	0.12	0.01	0.16	0.03
Orange Peel	0.10	0.01	0.09	0.05
Peanut shell	0.3	0.26	0.12	0.01
Potato Skin	0.1	0.04	0.05	0.01
Red Grape	0.04	0.02	0.12	0.06
Vitira Grape	0.15	0.08	0.04	0.02
White Grape	0.06	0.01	0.02	0.00

Table 23 Uranium concentrations in supernatant in Batch 3

	U filtered concentration $\mu g\ L^{-1}$	U filtered variance ±	U unfiltered concentration $\mu g\ L^{-1}$	U unfiltered variance ±
Blackberry	0.96	0.04	0.93	0.01
Coffee Grounds	0.91	0.01	0.92	0.02
Garlic Powder	1.18	0.06	1.40	0.16
Dried Kale	0.94	0.03	1.05	0.02
Peanut Shell	1.14	0.18	1.23	0.20
Spring Greens	0.98	0.06	0.91	0.02
Red Tea Leaf	0.93	0.01	0.97	0.04
White Birch	1.64	0.89	0.98	0.03

4.6.2b Vanadium supernatant analysis

For the second batch, the vanadium supernatant was unfortunately below the 3-σ value (of 2.4999, rounded to 2.50) in every case. Most of the samples actually tested between the 3-σ and the zero-variance. It is possible to estimate values for the concentration by extrapolating the calibration curve to 0, and using the count reading to calculate an estimated concentration: these are reported in **Table 24** below (dilution and background adjusted. It would appear that this approach will underestimate the actual K_d for vanadium by approximately one order of magnitude. More of a concern, the background reading for vanadium was consistently near those recorded, suggesting poor sorption.

TABLE 24 VANADIUM CONCENTRATIONS IN SUPERNATANT IN BATCH 2

	V filtered concentration (calculated/ estimated) $\mu g\ L^{-1}$	V filtered variance (calculated/ estimated) ±	V unfiltered concentration (calculated/ estimated) $\mu g\ L^{-1}$	V unfiltered variance (calculated/ estimated) ±
Dried Kale	3.9 /3.9	0 /0.07	2.5 /0.46	0 /0.12
Garlic Powder	0.07 /0.07	0 /0.02	2.5 /0.44	0 /0.06
Orange Peel	1.88 /1.88	0 /0.03	2.5 /0.9	0 /0.49
Peanut shell	1.45 /1.45	0.01 /0.89	2.5 /0.79	0 /0.33
Potato Skin	0.44 /0.44	0 /0.09	2.5 /0.7	0 /0.34
Red Grape	0.36 /0.36	0 /0.03	2.5 /0.46	0 /0.12
Vitira Grape	0.25 /0.25	0 /0.07	2.5 /0.19	0 /0.05
White Grape	0.34 /0.34	0 /0.03	2.5 /0.19	0 /0.06

For the third batch, which are reported in **Table 25** the filtered concentrations were within readable limits, but the unfiltered was not. Unlike the second batch, these were mostly not within the tolerance with the zero variance. These have been included for reference, and the values suggest that these readings also follow the approximation above, but this is unverified. The blackberry, white birch and spring green readings were so low, they were not possible to approximate. Given the approximation, no comparison between the filtered and unfiltered was practical.

TABLE 25 VANADIUM CONCENTRATIONS IN SUPERNATANT IN BATCH 3

	V filtered concentration (calculated/ estimated) µg L-1	V filtered variance (calculated/ estimated) ±	V unfiltered concentration (calculated/ estimated) µg L-1	V unfiltered variance (calculated/ estimated) ±
Blackberry	13.88 /13.88	0.72 /0.72	2.5 /0	0 /0.47
Coffee Grounds	14.5 /14.5	1.51 /1.51	2.5 /0.14	0 /1.02
Garlic Powder	12.87 /12.87	1.71 /1.71	2.85 /1.46	0.6 /1.45
Dried Kale	17.33 /17.33	0.39 /0.39	2.5 /0.23	0 /0.52
Peanut Shell	14.41 /14.41	4.11 /4.11	5.22 /5.02	1.7 /2.03
Spring Greens	14.41 /14.41	2.4 /2.4	2.5 /0	0 /0.37
Red Tea Leaf	16.9 /16.9	1.38 /1.38	2.5 /0.58	0 /0.78
White Birch	17.74 /17.74	1.58 /1.58	2.5 /0	0 /0.53

4.6.2c Manganese supernatant analysis

The concentration of the manganese in the second (**Table 26**) and third (

Table 27) batches were generally within the calibration region, except for two samples in the second batch, the blackberry, and the Red Tea Leaf, who were approximately 2x and 20x the measured concentration range respectively. These do not exhibit unreasonable variations across replicates, so these are assumed to be reasonably representative concentrations.

Most of the samples tested higher in manganese concentrations than the seawater controls, suggesting that the majority of Mn in solution is due to losses from the solids, although this is not verified on the digestate side.

There is little variance between the filtered and unfiltered, indicating the element was not particularly affected by particle transportation.

TABLE 26 MANGANESE CONCENTRATIONS IN SUPERNATANT IN BATCH 2

	Mn filtered concentration. $\mu g\ L^{-1}$	Mn filtered variance ±	Mn unfiltered concentration $\mu g\ L^{-1}$	Mn unfiltered variance ±
Dried Kale	11.83	3.89	19.64	4.66
Garlic Powder	55.07	3.67	65.06	5.48
Orange Peel	22.05	6.31	27.38	13.83
Peanut shell	76.8	33.39	75.38	26.41
Potato Skin	26.2	5.37	13.57	9.60
Red Grape	18.19	7.82	19.89	6.15
Vitira Grape	15.16	2.12	9.15	4.68
White Grape	32.29	1.86	21.13	7.37

Table 27 Manganese concentrations in supernatant in Batch 3

	Mn filtered concentration $\mu g\ L^{-1}$	Mn filtered variance ±	Mn unfiltered concentration $\mu g\ L^{-1}$	Mn unfiltered variance ±
Blackberry	182.30	20.38	216.72	32.01
Coffee Grounds	170.91	62.87	166.25	87.03
Garlic Powder	17.99	6.90	42.95	15.86
Dried Kale	99.70	4.96	123.72	16.94
Peanut Shell	58.66	32.95	40.70	14.23
Spring Greens	48.99	20.89	33.26	18.17
Red Tea Leaf	3231.60	188.97	3847.60	289.09
White Birch	621.76	64.55	387.74	378.67

4.6.2d Nickel supernatant analysis

The concentrations of nickel in the supernatant are displayed in **Table 28** for batch 2 and **Table 29** for Batch 3. Batch 2 was generally within the calibration curve. Batch 3 displayed values that tested between the 3-σ (2.27) and the zero valence, with reasonable correlation of results, so these are included for reference. Generally, these seem comparable to the values of the 3-σ, so can be assumed to be sufficient approximations, and the K_d can be assumed to be accurate, except for the White Birch sample, which had one reading close to the LoD, and three very low readings for the unfiltered sample.

TABLE 28 NICKEL CONCENTRATIONS IN SUPERNATANT IN BATCH 2

	Ni filtered concentration (calculated/ estimated) µg L-1	Ni filtered Variance (calculated/ estimated) ±	Ni unfiltered concentration (calculated/ estimated) µg L-1	Ni unfiltered Variance (calculated/ estimated) ±
Dried Kale	0 /0.6	0 /2.98	0 /18.92	0 /10.62
Garlic Powder	14.13 /0.64	2.98 /12.42	18.92 /60.53	10.62 /51.36
Orange Peel	13.73 /47.58	12.42 /2.79	60.53 /83.76	51.36 /8.28
Peanut shell	8.76 /12.19	2.79 /1.43	83.76 /34.27	8.28 /10.59
Potato Skin	12.7 /0.4	1.43 /2.27	34.27 /16.24	10.59 /5.88
Red Grape	8.45 /0.32	2.27 /0.5	16.24 /7.69	5.88 /0.74
Vitira Grape	6.37 /4.05	0.5 /0.39	7.69 /4.84	0.74 /1.78
White Grape	4.01 /0.7	0.39 /1.03	4.84 /4.49	1.78 /1.15

TABLE 29 NICKEL CONCENTRATIONS IN SUPERNATANT IN BATCH 3

	Ni filtered concentration (calculated/ estimated) µg L-1	Ni filtered Variance (calculated/ estimated) ±	Ni unfiltered concentration (calculated/ estimated) µg L-1	Ni unfiltered Variance (calculated/ estimated) ±
Blackberry	4.28 /4.28	0.28 /0.28	4.74 /4.74	0.97 /0.97
Coffee Grounds	2.27 /0.74	0 /0.23	137.04 /137.04	96.17 /96.17
Garlic Powder	2.85 /2.66	1.01 /1.15	141.76 /141.76	97.43 /97.43
Dried Kale	6.41 /6.16	6.07 /6.25	17.87 /17.62	26.95 /27.09
Peanut Shell	2.54 /2.36	0.44 /0.59	3.65 /3.39	1.86 /2.06
Spring Greens	2.42 /1.8	0.26 /0.65	2.27 /1.06	0 /0.59
Red Tea Leaf	2.27 /1.34	0 /0.46	46.5 /46.34	44.32 /44.48
White Birch	3.89 /3.19	2.81 /3.26	2.27 /0.56	0 /0.98

Given the large differences between the filtered and unfiltered, it is clear that much of the nickel in solution is in a surface complexation, or in particulate form.

4.6.2e Molybdenum supernatant analysis

The concentrations of Molybdenum (Mo) detected in the supernatant are displayed in **Table 30** for batch 2 and **Table 31** for batch 3. All results are within the calibration curve. The results for Mo are fairly consistent, except for one very high value recorded for White Birch, which would appear highly abnormal, suggesting a temporary contamination. The average concentration and variance are noted in the table, if this one result is discounted. The filtered and unfiltered results are all statistically indistinguishable.

TABLE 30 MOLYBDENUM CONCENTRATIONS IN SUPERNATANT IN BATCH 2

	Mo filtered concentration. µg L^{-1}	Mo filtered variance ±	Mo unfiltered concentration µg L^{-1}	Mo unfiltered variance ±
Dried Kale	1.46	0.07	2.34	0.81
Garlic Powder	2.04	0.20	2.49	0.32
Orange Peel	0.77	0.10	0.90	0.12
Peanut shell	0.5	0.15	0.71	0.14
Potato Skin	1.2	0.31	3.57	1.00
Red Grape	0.69	0.31	1.14	0.19
Vitira Grape	1.08	0.42	1.00	0.17
White Grape	0.73	0.09	0.29	0.04

TABLE 31 MOLYBDENUM CONCENTRATIONS IN SUPERNATANT IN BATCH 3

	Mo filtered concentration µg L-1	Mo filtered variance ±	Mo unfiltered concentration µg L-1	Mo unfiltered variance ±
Blackberry	2.59	2.31	0.38	0.09
Coffee Grounds	0.52	0.48	0.83	0.85
Garlic Powder	2.87	0.89	4.06	0.90
Dried Kale	2.45	0.76	6.65	2.07
Peanut Shell	0.98	0.54	2.13	0.55
Spring Greens	10.07	6.20	10.50	5.16
Red Tea Leaf	3.89	1.82	1.88	1.04
White Birch	15.39	23.55	1.72	0.69

4.6.2f Gold supernatant analysis

The concentrations of Gold (Au) detected in the supernatant are displayed in **Table 32** for batch 2 and Table 33 for batch 3. Many of the samples display results that exhibit results significantly outside the limit of detection, with results significantly below that of the zero valence. These values have been reported as 0.00, with the LoD being used for calculating the K_d. The filtered and unfiltered are mostly statistically indistinguishable, except for orange peel, which exhibited much higher concentrations in the filtered sample. This is unexplained, but the concentration is very low, and could be instrumental.

TABLE 32 GOLD CONCENTRATIONS IN SUPERNATANT IN BATCH 2

	Au filtered concentration µg L^{-1}	Au filtered variance ±	Au unfiltered concentration µg L^{-1}	Au unfiltered variance ±
Dried Kale	0.28	0.12	1.15	1.00
Garlic Powder	0.10	0.01	0.20	0.11
Orange Peel	0.27	0.04	0.06	0.01
Peanut shell	0.3	0.12	0.07	0.02
Potato Skin	0.2	0.03	0.05	0.01
Red Grape	0.28	0.07	0.38	0.17
Vitira Grape	0.14	0.03	0.09	0.03
White Grape	0.21	0.09	0.05	0.02

TABLE 33 GOLD CONCENTRATIONS IN SUPERNATANT IN BATCH 3

	Au filtered concentration µg L^{-1}	Au filtered variance ±	Au unfiltered concentration µg L^{-1}	Au unfiltered variance ±
Blackberry	0.12	0.20	0.00	0.00
Coffee Grounds	0.00	0.00	0.00	0.00
Garlic Powder	0.00	0.00	0.00	0.00
Dried Kale	0.00	0.00	0.00	0.00
Peanut Shell	3.11	3.09	5.68	3.70
Spring Greens	0.00	0.00	0.00	0.00
Red Tea Leaf	9.67	9.60	7.57	7.94
White Birch	0.30	0.51	0.00	0.00

4.6.2g Silver supernatant analysis

The concentrations of Silver (Ag) detected in the supernatant are displayed in **Table 34** for batch 2 and **Table 35** for batch 3. Although silver proved easily detected in solution, very few of the samples exhibited results that were significantly different than the background seawater, so there is not a great likelihood of capture being significant. Batch 2 was statistically insignificant, but Batch 3 had much higher concentrations in the filtered than the unfiltered: however, with the exception of the fraction that was in contact with silver birch, these are largely indistinguishable from each other and the seawater control and are probably instrumentation in nature.

TABLE 34 SILVER CONCENTRATIONS IN SUPERNATANT IN BATCH 2

	Ag filtered concentration $\mu g\ L^{-1}$	Ag filtered variance ±	Ag unfiltered concentration $\mu g\ L^{-1}$	Ag unfiltered variance ±
Dried Kale	0.19	0.08	0.04	0.01
Garlic Powder	0.09	0.04	0.07	0.01
Orange Peel	0.09	0.03	0.05	0.02
Peanut shell	0.1	0.01	0.07	0.01
Potato Skin	0.1	0.03	0.06	0.02
Red Grape	0.11	0.02	0.07	0.02
Vitira Grape	0.06	0.01	0.04	0.01
White Grape	0.05	0.01	0.04	0.01

TABLE 35 SILVER CONCENTRATIONS IN SUPERNATANT IN BATCH 3

	Ag filtered concentration $\mu g\ L^{-1}$	Ag filtered variance ±	Ag unfiltered concentration $\mu g\ L^{-1}$	Ag unfiltered variance ±
Blackberry	3.27	0.03	0.00	0.00
Coffee Grounds	3.31	0.04	0.00	0.00
Garlic Powder	3.61	0.20	0.00	0.00
Dried Kale	4.04	0.26	0.00	0.00
Peanut Shell	3.46	0.14	5.68	3.70
Spring Greens	3.42	0.06	0.00	0.00
Red Tea Leaf	3.53	0.11	7.57	7.94
White Birch	11.68	9.70	0.00	0.00

4.6.2h Copper supernatant analysis

The concentrations of Copper (Cu) detected in the supernatant are displayed in **Table 36** for batch 2 and **Table 37** for batch 3. Copper samples all test within the calibration curve, and other than a very high variance that is distributed widely over the dataset, the only specific point of note is the supernatant exhibit greater concentrations than the seawater controls, indicating the Cu ions are being lost to the liquid phase from the biomass.

TABLE 36 COPPER CONCENTRATIONS IN SUPERNATANT IN BATCH 2

	Cu filtered concentration $\mu g\ L^{-1}$	Cu filtered variance ±	Cu unfiltered concentration $\mu g\ L^{-1}$	Cu unfiltered variance ±
Dried Kale	65.13	7.74	79.97	3.91
Garlic Powder	77.65	21.25	73.29	12.66
Orange Peel	26.66	3.80	23.59	4.43
Peanut shell	60.7	10.24	79.41	4.47
Potato Skin	29.1	2.38	30.89	2.77
Red Grape	50.87	4.71	129.02	88.63
Vitira Grape	26.89	8.24	19.23	3.70
White Grape	37.15	20.46	25.29	12.14

TABLE 37 COPPER CONCENTRATIONS IN SUPERNATANT IN BATCH 3

	Cu filtered concentration $\mu g\ L^{-1}$	Cu filtered variance ±	Cu unfiltered concentration $\mu g\ L^{-1}$	Cu unfiltered variance ±
Blackberry	8.78	4.43	11.81	2.68
Coffee Grounds	4.24	1.13	12.16	6.22
Garlic Powder	10.09	5.65	22.24	9.31
Dried Kale	12.85	14.22	10.82	2.80
Peanut Shell	7.91	2.37	28.03	25.86
Spring Greens	12.13	5.97	5.84	2.72
Red Tea Leaf	5.60	1.93	15.52	6.72
White Birch	12.58	11.05	7.15	3.91

4.6.2J pH and ICP analysis of continuous flow supernatant

To measure the concentrations in the wet phase of the continuous flow experiment, pairs of subsamples were taken from the outlet at 2 weeks and at completion, except for the orange peel pretest, where it was planned to be subjected to continuous monitoring, so it was only taken at completion. One of these two subsamples was measured for pH, while the other was subjected to the same process as the batch samples liquid phase tests. These samples from the tank were analysed by ICP-MS, and the results reported below. The pH values did not change between the 2 and 4 weeks. In regard to ICP-MS, most samples were statistically indistinguishable from both each other, and the control, although in most cases this was because they were very close to the limit of detection. All concentrations are dilution adjusted.

The copper 4 week reading on the orange peel stands out as very anomalous, being an order of magnitude greater than any other reading. This is probably related to the failure of the multimeter probe: it failed between the two timepoints and it is likely it introduced contamination into the sampling tap loop, which was open to the sensor box. This value is therefore flawed and included only for reference.

TABLE 38 CONCENTRATIONS OF ELEMENTS OF INTEREST AND PH OF THE SUPERNATANT IN THE CONTINUOUS FLOW EXPERIMENT, DILUTION ADJUSTED. * MEASURED BY CONTINUOUS MONITORING

Concentration of element µg L^{-1}	pH	V	Mn	Ni	Cu	Mo	Ag	Au	U
					Birch				
2 week	6.19	1.75 ±2.02	23.98 ±26.08	2.06 ±2.64	26.05 ±2.45	24.03 ±1.17	4.03 ±1.2	25.59 ±24.38	0.38 ±0.58
4 week	6.20	1.43 ±2.03	20.61 ±26.03	1.33 ±2.62	47.2 ±2.33	19.07 ±1.79	11.13 ±1.74	24.79 ±24.16	0.26 ±0.59
					Garlic				
2 week	8.00	0.2 ±2.01	17.4 ±25.84	0.12 ±2.6	28.99 ±2.36	16.53 ±1.54	20.89 ±1.69	25.73 ±24.21	0.28 ±0.57
4 week	7.90	0.45 ±1.97	18.77 ±26.01	0.66 ±2.63	42.41 ±2.17	13.85 ±1.77	10.44 ±1.62	25.03 ±24.2	0.52 ±0.57
					Peanut shell				
2 week	7.90	1.66 ±2.03	21.73 ±26.05	0.45 ±2.59	61.84 ±1.99	6.55 ±1.65	8.49 ±1.92	24.29 ±24.12	0.47 ±0.59
4 week	7.90	1.49 ±2.03	22.88 ±26.11	1.03 ±2.65	28.28 ±2.24	8.25 ±1.55	5.14 ±1.92	24.5 ±24.13	0.24 ±0.59
					Potato Skin				
2 week	7.90	1.54 ±2.02	22.71 ±25.99	0.79 ±2.65	19.09 ±2.45	6.85 ±1.76	7.77 ±0.19	24.66 ±24.26	0.19 ±0.57
4 week	7.90	1.72 ±2.03	24.42 ±26.11	1.9 ±2.63	38.62 ±2.31	5.64 ±1.79	3.67 ±1.63	24.47 ±24.16	0.17 ±0.59
					Orange Peel				
2 week	4.2*	1.64 ±2.02	21.83 ±26.1	1.7 ±2.64	31.41 ±2.41	6.04 ±1.8	0.45 ±1.95	25.54 ±24.27	0.48 ±0.59
4 week		1.59 ±1.99	17.74 ±25.91	1.89 ±2.63	548.27 ±30.34	5.12 ±1.77	8.64 ±0.78	25.95 ±24.39	0.45 ±0.57
					Control				
2 week	7.90	1.77 ±2.01	11.65 ±26.09	1.88 ±2.64	18.16 ±1.48	3.86 ±1.79	2.24 ±1.68	25.25 ±24.16	0.54 ±0.59
4 week	7.90	1.56 ±2.01	15.55 ±26.07	1.65 ±2.61	2.77 ±2.17	4.64 ±1.78	0.82 ±1.88	26.51 ±24.4	0.46 ±0.59

4.7 ICP-MS analysis of the solid material fraction

4.7.1 Batch analysis of solid phase material of Batch 1 for uranium

The uranium content in the digested solid samples were quantified using the established calibration curve in Figure 28, and in the majority of cases, with readings Relative Standard Deviation (RSD) below 2% except for certain no-contact controls, which had readings below 5% of the lowest standard, or 0.0050±0.0005 µg L^{-1}. This is over 10 times the 3-σ, so can be considered to be noisy, but usable (Zhang & Davison, 1995)). The digested solid sample data are reported in

Table 39. Variance was also noted. The range is 2%-61%. There was no correlation displayed between pair variances (R^2=0.01).

Table 39 Uranium content from digested solid sample analysis without (control) and with (increase) contact with seawater

Assay Sample	No contact control. ($\mu g\ kg^{-1}$)	Test 1 Increase from control ($\mu g\ kg^{-1}$)	Test 2 Increase from control ($\mu g\ kg^{-1}$)	Average test 1&2 ($\mu g\ kg^{-1}$)	RSD (%)
Orange skin	0.2	336.7	131.2	234.0	43.9
Lemon skin	6.5	134.6	169.5	152.1	11.5
Nectarine skin	1.0	317.6	132.8	225.2	41.0
Grape skin	5.5	127.6	137.9	132.8	3.9
Grape pulp	5.5	42.6	10.4	26.5	60.9
Sultana whole	1.6	12.2	16.8	14.5	16.0
Sultana diced	1.6	12.2	16.8	18.2	3.7
Brussels sprouts	0.0	15.6	13.4	14.5	7.4
Kale diced	6.5	-	205.6	205.6	-
Mange tout	2.3	43.8	40.8	42.3	3.7
Garlic diced	1.1	81.4	20.8	51.1	59.3
Peanut shell	57.8	68.2	153.9	111.0	38.6
Potato skin	54.3	199.4	419.5	309.4	35.6
Potato whole	0.3	10.3	11.2	10.8	4.0
Sweet potato whole	1.5	18.6	18.0	18.3	1.6

The sweet potato skin samples, and the Brussels sprout controls suffered a fungal attack, and could not be analysed by ICP-MS. Kale 1 was lost during an accident during digestion, so could not be completed.

The loading of U on the biomass samples was then analysed. Data recorded either after 2 months (week beginning 23 Jan 19 - week beginning 11 March 19) contact time or 1 month (week 17 June 19 – week beginning 22 July 19) re-plotted in **Figure 38** as average fractions of U absorbed per mass unit of biomass.

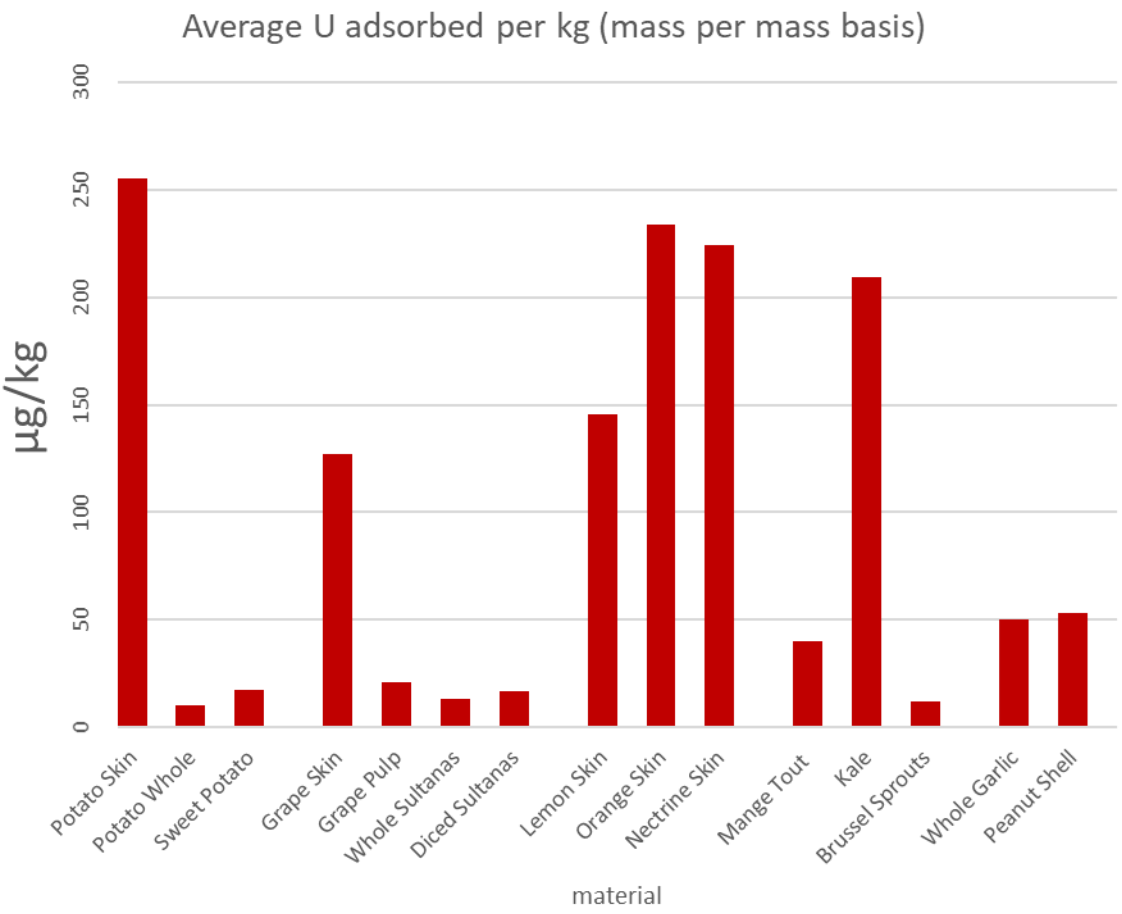

FIGURE 38 AVERAGE AMOUNT OF U ABSORBED PER DRY MASS UNIT OF BIOMASS.

The highest sorption by weight was by the potato skin (255 µg kg^{-1}), then by orange peel (233 µg kg^{-1}) and by nectarine peel (224 µg kg^{-1}). In addition, kale performed significantly better in this metric than the others (209 µg kg^{-1}).

Peanut shells get a special mention as they had the third highest actual U content measured of any of the samples, but the material efficiency was low, due to high background U concentration in the control, and high density of the material. In contrast, potato skin actual U was not significantly different from other materials in measured concentration, but its low density made it appears the greatest. Further testing was therefore required to establish if the high capture concentration represents an efficient surface, or an artefact of the high surface to mass ratio of the material.

Considering the U fraction between the solid phase and its total amount (consisting of the U sorbed onto suspended solids and the U in the aqueous phase) it is clear that the fractionation by the grapes (97%, except pulped sultanas, which had a wide RSD) are most effective in retaining the U, followed by garlic (96%), Brussels sprouts (94%), then the orange peel (93%). Kale and Peanut shells also had good capture rates (90%). Full data are presented in **Figure 39**.

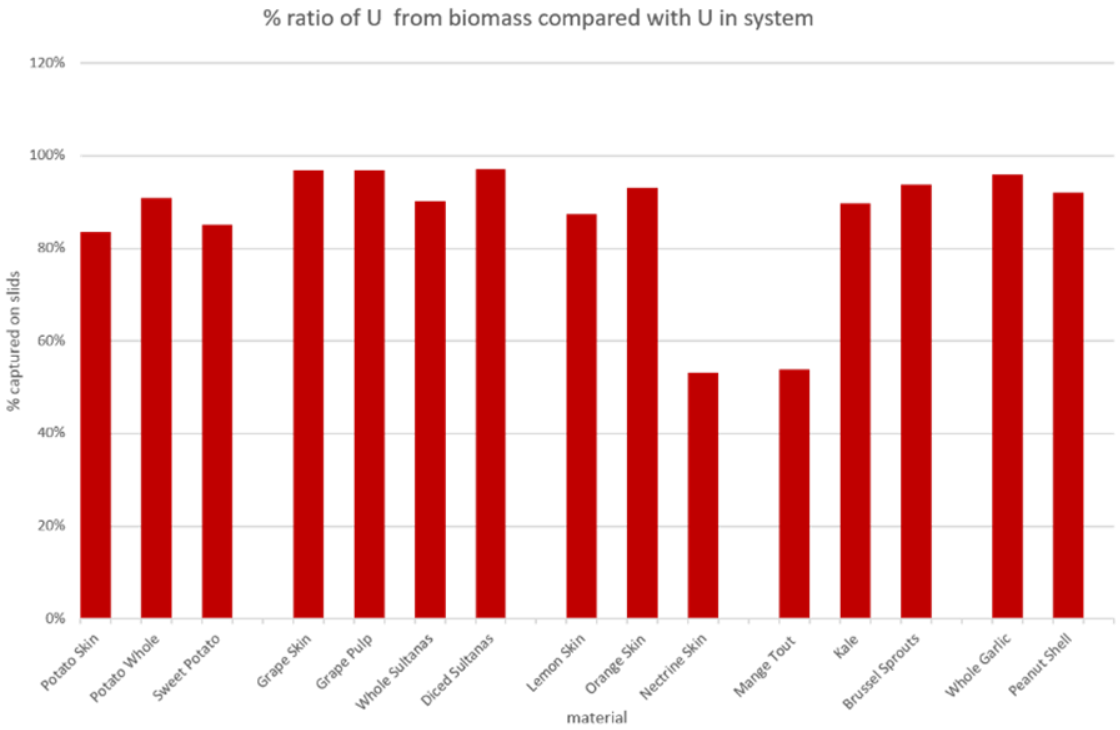

FIGURE 39 AVERAGE MASS FRACTIONS (EQ. 1) OF U ABSORBED ON THE BIO-SOLIDS

However, the general level of capture indicated that the surfaces were strongly depleting the U from the liquid phase, and that this net capture is therefore unlikely to represent saturation of the surfaces, which altered later testing, as much higher volume to solid ratios were possible.

The fraction ratio does indicate that the mange tout was not effective. This is a likely indicator that the antioxidants, such as retinoic acid was not providing an effective agent in reduction, despite it being known to function as such in other contexts, likely due to conditions in the sample vials.

Despite the high concentration on the surface of the potato skin and nectarine peel by weight, the net captures for these materials are weaker against the majority. Further testing is needed to establish if the capture % was impacted due to saturation, or if this is indicative of low retention due to decay.

The sorption coefficients K_d were calculated using (2) . Details are given in **Table 21**, and summarised in **Table 40**, which show that the K_d values are ranging from 52 to 1866 mL g^{-1}. As displayed in **Figure 39**, it is unlikely that these are a true equilibrium value, so should be considered indicative rather than a formal measurement. The highest indicative K_d was by the garlic (1886 L kg^{-1}), then by orange peel (1669.5 L kg^{-1}) and by nectarine peel (1401 L kg^{-1}). With the high degree of variability that is common in biologically active systems, it was appropriate to report each replicate as a distinct element, and report the mean average. **Table 40** shows the individual K_d of each replicate, as well as that of that of the averages.

Stronger sorption's are presumed to be due to uranyl reduction in tetravalent uranium by the antioxidants associated to these biomaterials. It was also suggested that the chemical sorption reactions may be coupled with colloidal aggregation, suggesting irreversible sorption hence increasing K_d values.

TABLE 40 SORPTION COEFFICIENTS (KD) OF SAMPLES

Sample	S1. K_d (mL g^{-1})	S2. K_d (mL g^{-1})	Average K_d (mL g^{-1})	SD (mL g^{-1})	RSD (%)
Orange Skin	1370.8	1968.2	1669.5	298.7	17.9
Lemon Skin	630.0	649.9	640.0	9.9	1.6
Nectarine Skin	311.7	99.6	205.6	106.1	51.6
Grape Skin	607.0	1142.7	874.8	267.9	30.6
Grape Pulp	348.7	85.3	217.0	131.7	60.7
Sultanas Diced	20.0	418.4	219.2	199.2	90.9
Sultanas Pulped	84.1	644.6	364.4	280.2	76.9
Brussels Sprouts Diced	148.6	131.8	140.2	8.4	6.0
Kale Diced	-	524.0	524.0	-	-
Mange Tout	46.1	58.7	52.4	6.3	12.0
Garlic Diced	772.8	2960.6	1866.7	1093.9	58.6
Peanuts Shell	349.9	653.0	501.5	151.5	30.2
Potato Skin	1023.4	1779.6	1401.5	378.1	27.0
Potato Diced	133.8	85.5	109.6	24.2	22.0

4.7.2 Batch analysis of solid phase material for Batch 2 and Batch 3

Samples were digested and analysed, and the net change results against the controls are reported in **Table 41** for Batch 2, and **Table 42** for Batch 3. Full results are tabulated in the appendix, including background, and individual replicates.

TABLE 41 NET CHANGE IN SOLID PHASE CONCENTRATIONS FOR VARIOUS ELEMENTS ON BIOMASS SOLID PHASE MATERIAL IN BATCH 2

	V Surface Conc $\mu g.g^{-1}$	V variance $\pm\mu g.g^{-1}$	Mn Surface Conc $\mu g.g^{-1}$	Mn variance $\pm\mu g.g^{-1}$	Ni Surface Conc $\mu g.g^{-1}$	Ni variance $\pm \mu g.g^{-1}$
Dried Kale	3.90	0.06	3.65	2.76	0.60	0.08
Garlic Powder	0.07	0.01	0.17	0.02	0.64	0.42
Orange Peel	1.88	1.79	6.32	6.05	47.58	41.37
Peanut shell	1.45	0.42	16.5	3.19	12.19	4.34
Potato Skin	0.44	0.06	9.7	0.77	0.40	0.06
Red Grape	0.36	0.10	0.83	0.24	0.32	0.09
Vitira Grape	0.25	0.06	0.50	0.21	4.05	2.76
White Grape	0.34	0.21	1.04	0.43	0.70	0.48
	Cu Surface Conc $\mu g.g^{-1}$	Cu variance $\pm \mu g.g^{-1}$	Mo Surface Conc $\mu g.g^{-1}$	Mo variance $\pm \mu g.g^{-1}$	Ag Surface Conc $\mu g.g^{-1}$	Ag variance $\pm \mu g.g^{-1}$
Dried Kale	15.11	5.19	2.39	0.66	1.13	0.45
Garlic Powder	0.94	0.71	0.10	0.03	0.02	0.01
Orange Peel	5.28	1.40	0.80	0.17	1.23	1.72
Peanut shell	26.79	5.45	0.88	0.10	0.01	0.00
Potato Skin	64.04	16.57	2.07	0.17	5.77	5.63
Red Grape	12.35	4.09	0.23	0.32	0.03	0.05
Vitira Grape	3.37	1.23	0.56	0.16	0.00	0.00
White Grape	4.69	3.35	0.89	0.88	0.12	0.05
	Au Surface Conc $\mu g.g^{-1}$	Au variance $\pm \mu g.g^{-1}$	U Surface Conc $\mu g.g^{-1}$	U variance $\pm \mu g.g^{-1}$		
Dried Kale	0.00	0.00	0.57	0.17		
Garlic Powder	0.00	0.00	0.03	0.01		
Orange Peel	0.01	0.00	0.47	0.07		
Peanut shell	0.01	0.00	0.17	0.06		
Potato Skin	0.01	0.00	0.36	0.07		
Red Grape	0.00	0.00	0.16	0.15		
Vitira Grape	0.00	0.00	0.18	0.07		
White Grape	0.00	0.00	0.28	0.26		

Most sample materials appear to, on average, net gained the relevant elements of interest against the controls, except for gold.

.

TABLE 42 NET CHANGE IN SOLID PHASE CONCENTRATIONS FOR VARIOUS ELEMENTS ON BIOMASS SOLID PHASE MATERIAL IN BATCH 3

	V Surface Conc $\mu g.g^{-1}$	V variance $\pm \mu g.g^{-1}$	Mn Surface Conc $\mu g.g^{-1}$	Mn variance $\pm \mu g.g^{-1}$	Ni Surface Conc $\mu g.g^{-1}$	Ni variance $\pm \mu g.g^{-1}$
Blackberry	1.33	0.06	28.9	2.76	0.61	0.08
Coffee Grounds	0.10	0.01	5.05	0.02	0.47	0.42
Garlic Powder	1.11	1.79	2.09	6.05	0.30	41.37
Dried Kale	0.89	0.42	7.51	3.19	0.21	4.34
Peanut Shell	2.46	0.06	4.94	0.77	0.69	0.06
Spring Greens	0.22	0.10	2.34	0.24	0.30	0.09
Red Tea Leaf	0.32	0.06	123	0.21	1.03	2.76
White Birch	0.85	0.21	51.2	0.43	1.22	0.48
	Cu Surface Conc $\mu g.g^{-1}$	Cu variance $\pm \mu g.g^{-1}$	Mo Surface Conc $\mu g.g^{-1}$	Mo variance $\pm \mu g.g^{-1}$	Ag Surface Conc $\mu g.g^{-1}$	Ag variance $\pm \mu g.g^{-1}$
Blackberry	0.09	5.19	0.35	0.66	0.01	0.45
Coffee Grounds	1.74	0.71	0.25	0.03	0.00	0.01
Garlic Powder	0.56	1.40	0.07	0.17	0.00	1.72
Dried Kale	0.36	5.45	0.03	0.10	0.00	0.00
Peanut Shell	4.54	16.57	0.88	0.17	2.34	5.63
Spring Greens	2.31	4.09	1.11	0.32	0.00	0.05
Red Tea Leaf	2.69	1.23	0.05	0.16	0.18	0.00
White Birch	1.56	3.35	0.42	0.88	0.05	0.05
	Au Surface Conc $\mu g.g^{-1}$	Au variance $\pm \mu g.g^{-1}$	U Surface Conc $\mu g.g^{-1}$	U variance $\pm \mu g.g^{-1}$		
Blackberry	0.14	0.00	0.11	0.17		
Coffee Grounds	0.10	0.00	0.07	0.01		
Garlic Powder	0.16	0.00	0.09	0.07		
Dried Kale	0.21	0.00	0.04	0.06		
Peanut Shell	0.19	0.00	0.21	0.07		
Spring Greens	0.28	0.00	0.17	0.15		
Red Tea Leaf	0.06	0.00	0.02	0.07		
White Birch	0.16	0.00	0.12	0.26		

The minimum standard necessary to achieve significant capture is for the process to adjust the materials to concentrations greater than parts per million, based on the ore grading standards for uranium, as detailed in NEA and IAEA (2016). Since most elements in seawater are in the parts per billion range, as detailed in **Table 1.** Since any recovery process would be begin with ashing the biomass, which could be tuned to discount a minimum of 90% of the mass post capture, it is assumed that the recovery concentration is 10x the capture rate. This definition of significant capture would result in the materials having concentrations corresponding to those present in Low Grade Ores.

Generally, there has been at least weak capture of materials, with exceptions of interest, but there is a mismatch between the cross samples where they are both in bags, and those that were freely in contact, with generally lower rates. This would indicate the specific bags were an interferent. Nickel, copper, and manganese exhibited the strongest captured of the target elements generally, which as these elements are biologically significant (Whitehead, 2000), would be expected. The inherent biological molecules will bind them by evolutionary design.

Considering across all elements of interest, on the basis of final concentration, the most successful material from the specific results is the potato skin, which exhibits relatively strong concentrations on all elements, compared to the others in the study, appearing in the top 3 concentrations for every element, except manganese, where it is the fifth highest surface concentration (which is an order of magnitude greater than the median of those samples tested) and the corresponding partition coefficient is the second highest, and gold, where the concentrations amongst all materials are so minor there is little variation. It did achieve the second highest ratio of captured to background for gold, and the highest partition ratio of any material tested. It must be noted that this high performance can be attributed to high background rates, in the cases of vanadium and nickel.

One of the advantages of using these materials is that the biomass often includes some concentration of an element of interest, prior to the use for capture. None of the materials exhibited measurable loss of the elements of interest. In order to display the breakdown of the materials pre and post capture, **Figure 40** to **Figure 47** are displayed below.

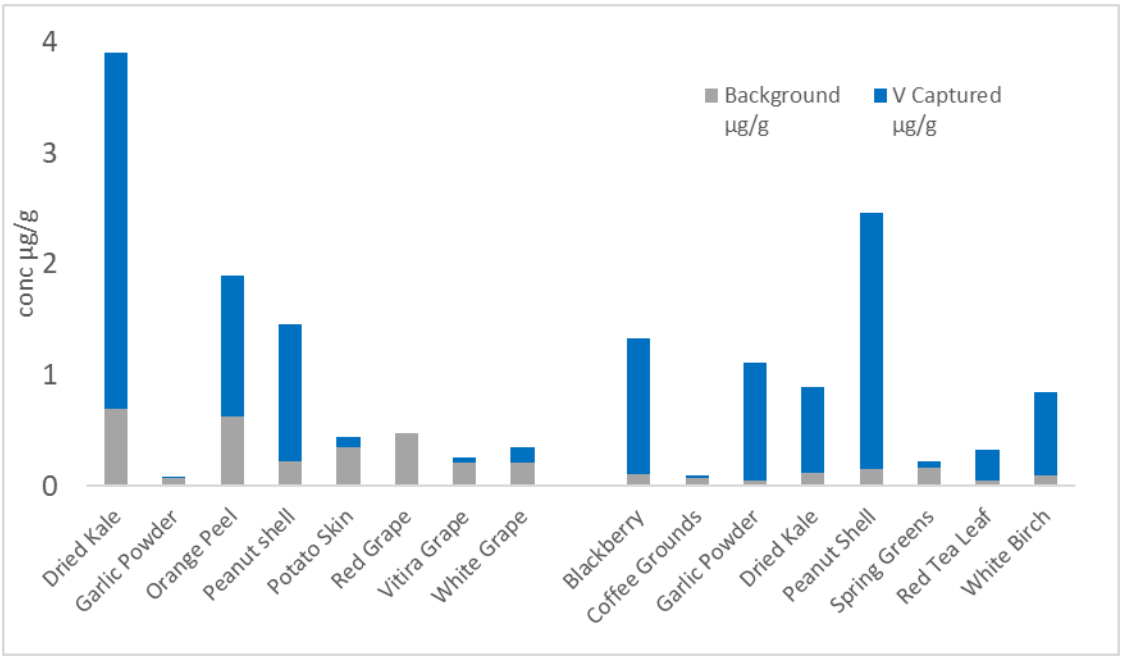

FIGURE 40 VANADIUM CONCENTRATION IN SOLID PHASE, BACKGROUND, AND INCREASE (µG.G^{-1})

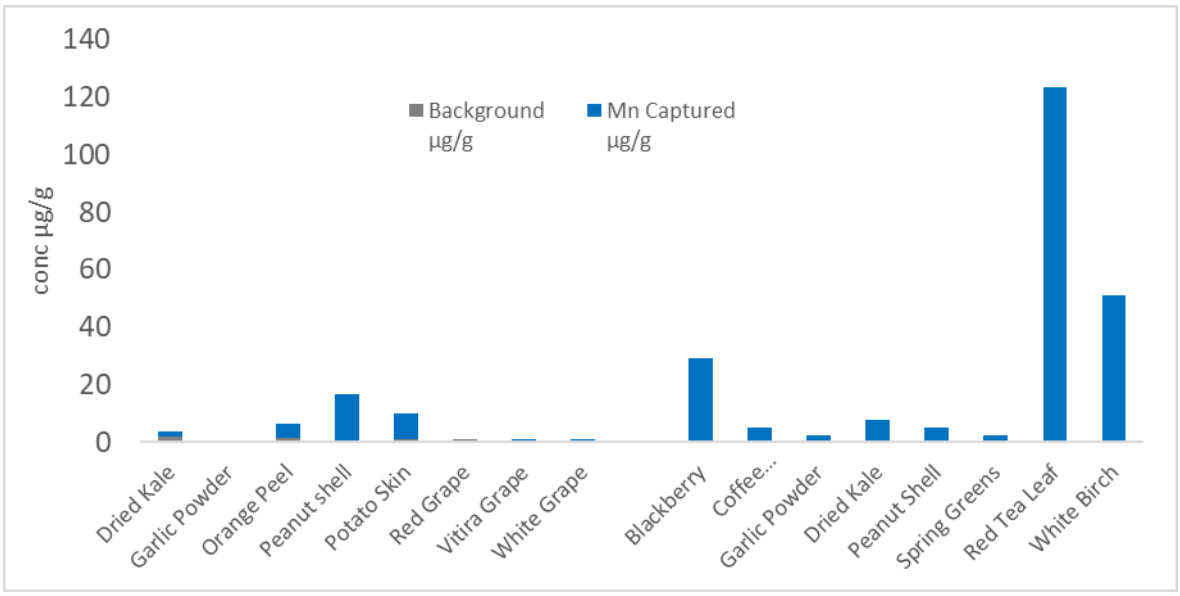

FIGURE 41 MANGANESE CONCENTRATION IN SOLID PHASE, BACKGROUND, AND INCREASE ($\mu G.G^{-1}$)

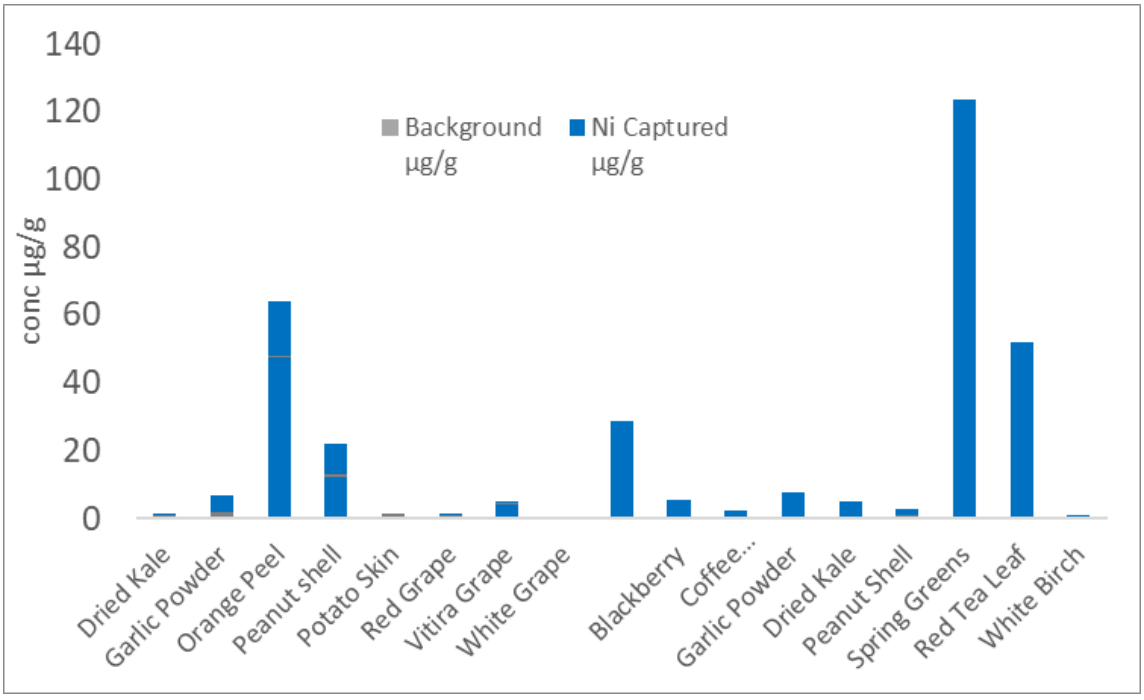

FIGURE 42 NICKEL VANADIUM CONCENTRATION IN SOLID PHASE, BACKGROUND, AND INCREASE ($\mu G.G^{-1}$)

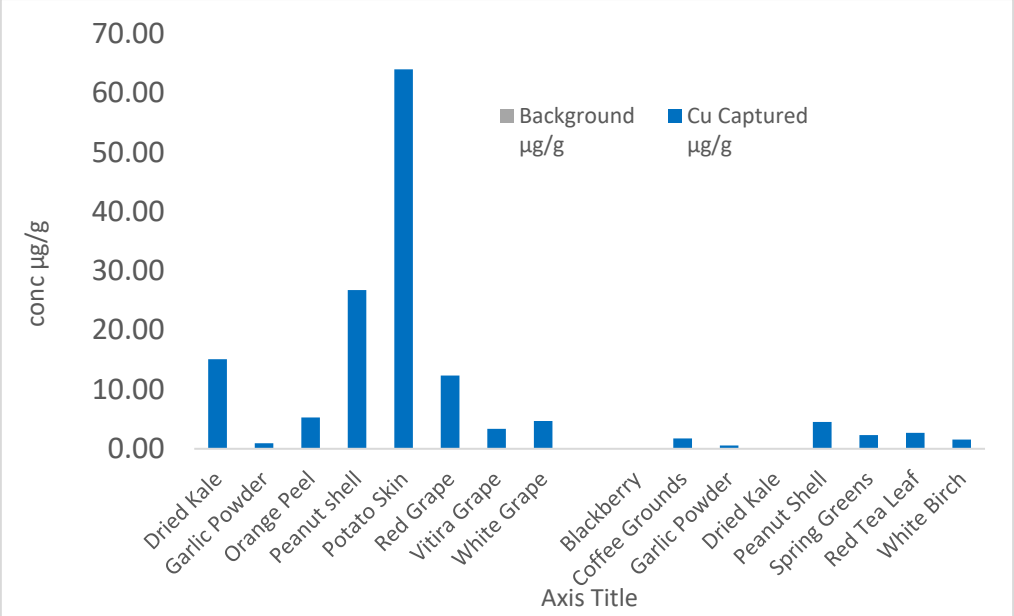

FIGURE 43 COPPER CONCENTRATION IN SOLID PHASE, BACKGROUND, AND INCREASE ($\mu G.G^{-1}$)

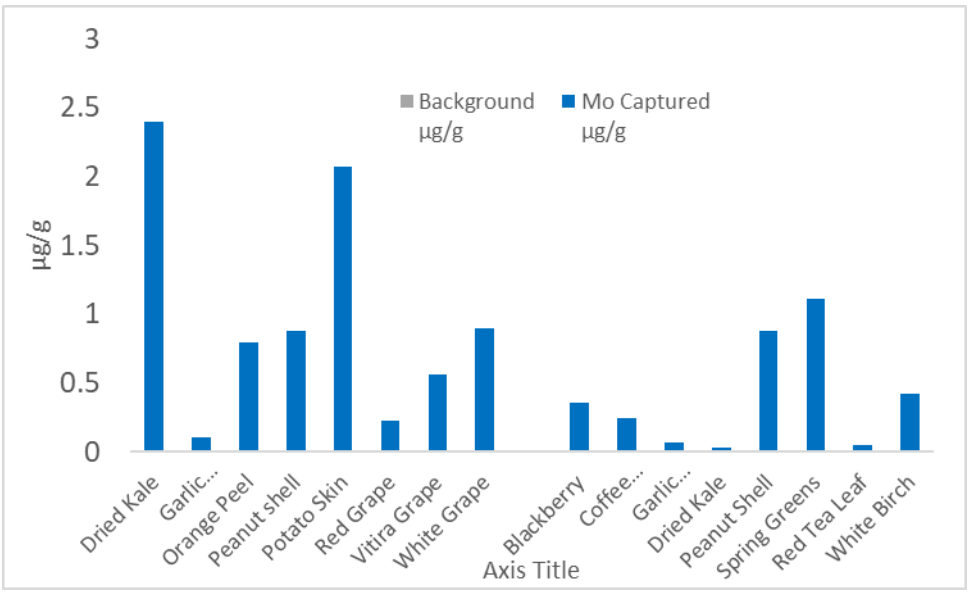

FIGURE 44 MOLYBDENUM CONCENTRATION IN SOLID PHASE, BACKGROUND, AND INCREASE ($\mu G.G^{-1}$)

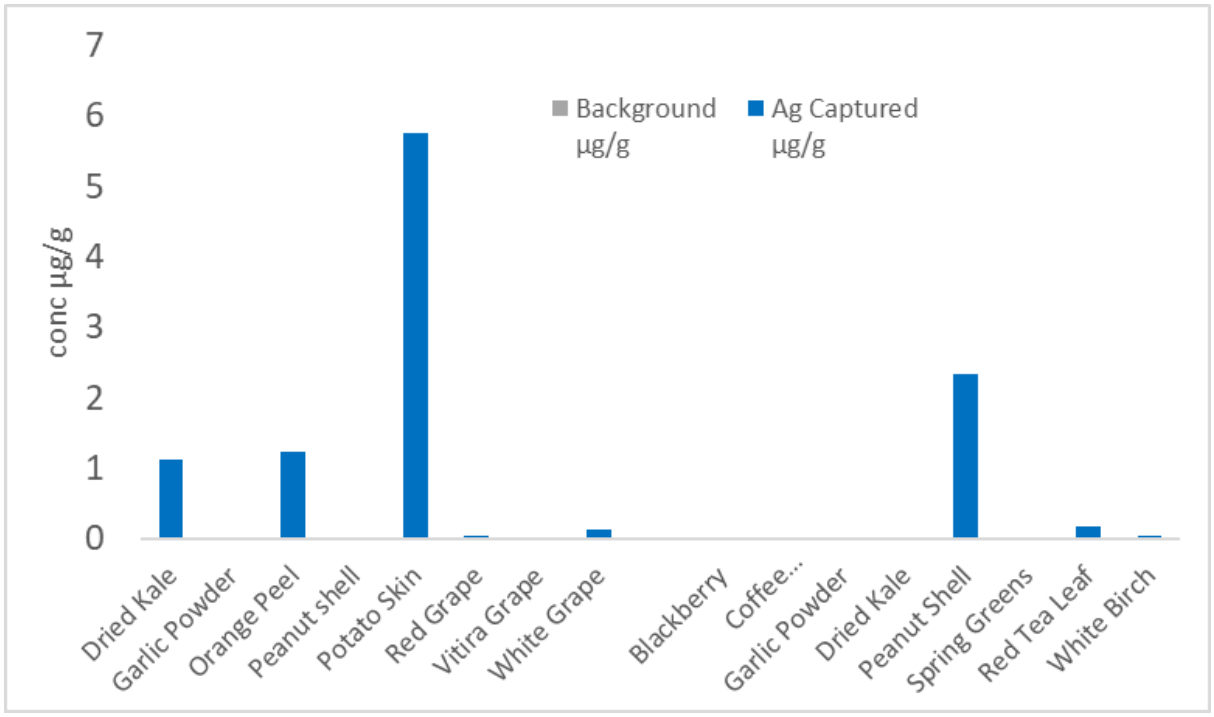

FIGURE 45 SILVER CONCENTRATION IN SOLID PHASE, BACKGROUND, AND INCREASE ($\mu G.G^{-1}$)

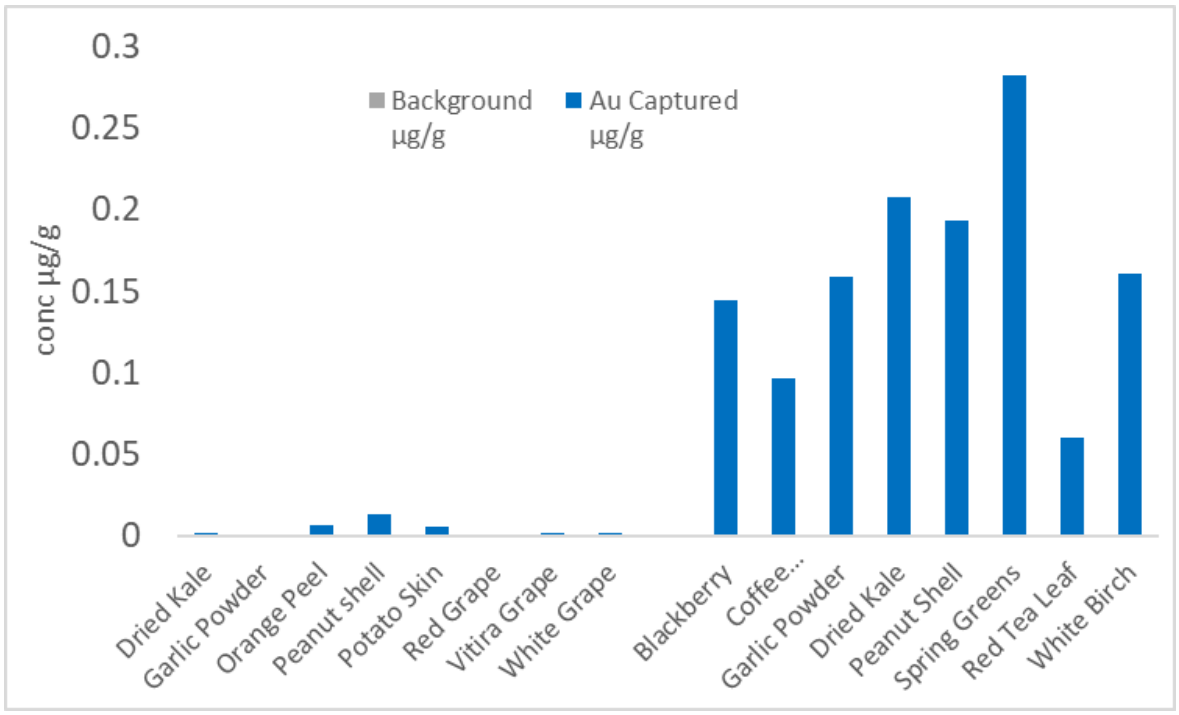

FIGURE 46 GOLD CONCENTRATION IN SOLID PHASE, BACKGROUND, AND INCREASE ($\mu G.G^{-1}$)

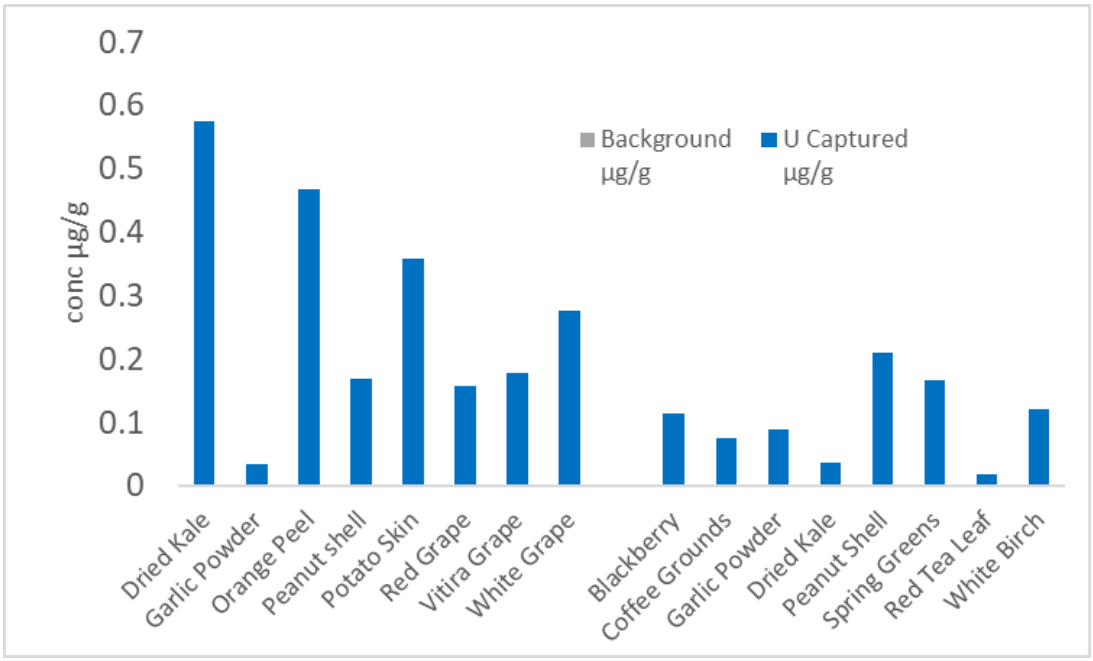

FIGURE 47 URANIUM CONCENTRATION IN SOLID PHASE, BACKGROUND, AND INCREASE ($\mu G.G^{-1}$)

4.7.3 Partition Coefficient (Kd) of Batch 2 and 3 on the basis of prefiltered samples

Using the data reported above, the Kd for the samples were calculated, per (3), using the prefiltered values. This partitioning is intended to represent the scenario where the sample has been successfully contained within filtered environment, using a barrier material of greater impermeability than those used in Batch 3.

Since nickel and vanadium both had a large number of samples with concentrations outside the calibration curve, both the adjusted and the approximated values are reported, which can be used as indicative of the range in which the true value should be. These values are generally reasonable but have very large variances due to these being very sensitive measurements, due to the levels of interference.

TABLE 43 PARTITION COEFFICIENT (KD) OF BATCH 2 BIOMASS USING PREFILTERED SUPERNATANT

	V Kd adjusted /approx g/ml	V Error adjusted /approx (+/- %)	Mn Kd g/ml	Mn Error (+/- %)	Mo Kd g/ml	Mo Error (+/- %)	Cu Kd g/ml	Cu Error (+/-)
Dried Kale	1561 /14306	2% /24%	442	101%	1661	32%	230	33%
Garlic Powder	30 /238	11% /15%	3	8%	51	35%	11	56%
Orange Peel	754 /7024	95% /84%	237	73%	1031	12%	209	37%
Peanut shell	581 /1969	29% /59%	276	54%	2157	44%	451	22%
Potato Skin	176 /1321	14% /34%	391	25%	1903	22%	2198	23%
Red Grape	143 /1906	29% /39%	59	50%	571	141%	250	38%
Vitira Grape	101 /1439	24% /57%	35	56%	656	62%	143	55%
White Grape	135 /1443	64% /60%	33	45%	1377	101%	134	88%
	Ni Kd adjusted /approx g/ml	Ni Error adjusted /approx (+/-)	Ag Kd g/ml	Ag Error (+/- %)	Au Kd g/ml	Au Error (+/- %)	U Kd g/ml	U Error (+/- %)
Dried Kale	46 /46	40% /40%	4518	51%	5	48%	8435	23%
Garlic Powder	80 /80	107% /107%	193	45%	13	68%	286	38%
Orange Peel	5905 /5905	101% /101%	4044	140%	73	43%	4996	25%
Peanut shell	985 /985	41% /41%	58	38%	143	22%	1668	91%
Potato Skin	52 /52	37% /37%	32373	100%	52	62%	4798	50%
Red Grape	52 /52	34% /34%	115	141%	4	38%	8775	115%
Vitira Grape	1012 /1012	68% /68%	1	56%	4	22%	2314	101%
White Grape	127 /127	53% /53%	579	20%	8	71%	4668	87%

TABLE 44 PARTITION COEFFICIENT (KD) OF BATCH 3 BIOMASS USING PREFILTERED SUPERNATANT

	V Kd adjusted /approx g/ml	V Error adjusted /approx (+/- %)	Mn Kd g/ml	Mn Error (+/- %)	Mo Kd g/ml	Mo Error (+/- %)	Cu Kd g/ml	Cu Error (+/-)
Blackberry	96 /96	22% /22%	162	137%	231	52%	13	173%
Coffee Grounds	7 /7	34% /34%	31	16%	830	65%	502	108%
Garlic Powder	88 /88	135% /135%	138	45%	34	90%	70	36%
Dried Kale	51 /51	102% /102%	74	44%	13	168%	66	173%
Peanut Shell	185 /185	28% /28%	121	56%	1403	69%	692	90%
Spring Greens	15 /15	63% /63%	51	49%	185	73%	171	114%
Red Tea Leaf	19 /19	26% /26%	38	13%	14	81%	558	43%
White Birch	50 /50	47% /47%	81	48%	233	76%	293	94%

	Ni Kd adjusted /approx g/ml	Ni Error adjusted /approx (+/-)	Ag Kd g/ml	Ag Error (+/- %)	Au Kd g/ml	Au Error (+/- %)	U Kd g/ml	U Error (+/- %)
Blackberry	147 /147	146% /146%	7460	173%	44	5%	118	2%
Coffee Grounds	207 /698	49% /60%	179	139%	29	39%	82	38%
Garlic Powder	120 /131	47% /43%	50	11%	44	15%	76	23%
Dried Kale	45 /59	41% /68%	60	12%	52	15%	39	13%
Peanut Shell	278 /315	21% /35%	1975	104%	55	41%	195	54%
Spring Greens	120 /177	47% /60%	87	63%	83	66%	167	56%
Red Tea Leaf	454 /848	11% /28%	213	159%	17	3%	18	59%
White Birch	532 /1238	57% /90%	46815	139%	22	50%	96	46%

4.7.4 Partition Coefficient (Kd) of Batch 2 and 3 on the basis of unfiltered samples

Using the data reported above, the Kd for the samples were calculated, per (3), using the Unfiltered values. This represents the scenario where the sample can't be contained by a barrier material of greater impermeability than those used in Batch 3.

Since nickel and vanadium both had a large number of samples with concentrations outside the calibration curve, both the adjusted and the approximated values are reported, which can be used as indicative of the range in which the true value should be. These values are generally reasonable but have very large variances due to these being very sensitive measurements.

TABLE 45 PARTITION COEFFICIENT OF BATCH 2 BIOMASS

	V Kd (adjusted /approx) g/ml	V Error (adjusted /approx) (+/- %)	Mn Kd g/ml	Mn Error (+/-%)	Mo Kd g/ml	Mo Error (+/- %)	Cu Kd g/ml	Cu Error (+/-)
Dried Kale	1561 /8885	2% /21%	240	97%	1051	12%	192	38%
Garlic Powder	30 /171	11% /10%	3	19%	40	15%	12	59%
Orange Peel	754 /3213	95% /109%	257	60%	910	29%	235	38%
Peanut shell	582 /2210	29% /58%	279	63%	1291	26%	342	26%
Potato Skin	176 /780	14% /48%	1052	46%	629	30%	2042	18%
Red Grape	143 /811	29% /40%	49	46%	264	141%	156	58%
Vitira Grape	101 /1622	24% /59%	75	63%	609	48%	192	53%
White Grape	135 /1700	64% /41%	67	78%	2895	89%	283	72%

	Ni Kd (adjusted /approx) g/ml	Ni Error (adjusted /approx) (+/-)	Ag Kd g/ml	Ag Error (+/- %)	Au Kd g/ml	Au Error (+/- %)	U Kd g/ml	U Error (+/- %)
Dried Kale	42 /42	48% /48%	13195	135%	19	15%	3819	13%
Garlic Powder	12 /12	50% /50%	174	78%	11	22%	220	27%
Orange Peel	583 /583	84% /84%	15353	140%	114	41%	7020	48%
Peanut shell	351 /351	4% /4%	193	31%	182	19%	1354	31%
Potato Skin	27 /27	22% /22%	123335	94%	85	64%	7673	10%
Red Grape	42 /42	30% /30%	188	141%	6	41%	1708	72%
Vitira Grape	866 /866	77% /77%	1	59%	6	30%	7805	84%
White Grape	159 /159	55% /55%	3095	67%	12	73%	17307	96%

TABLE 46 PARTITION COEFFICIENTS OF BATCH 3 BIOMASS

	V Kd (adjusted /approx) g/ml	V Error (adjusted /approx) (+/- %)	Mn Kd g/ml	Mn Error (+/-%)	Mo Kd g/ml	Mo Error (+/- %)	Cu Kd g/ml	Cu Error (+/-)
Blackberry	530 /2886	20% /107%	130	134%	1006	40%	7	173%
Coffee Grounds	40 /95	35% /280%	43	64%	1716	138%	108	91%
Garlic Powder	438 /2190	139% /131%	55	33%	20	60%	30	42%
Dried Kale	357 /767	102% /437%	59	38%	3	165%	25	173%
Peanut Shell	552 /667	46% /67%	134	26%	441	27%	375	84%
Spring Greens	87 /1025	63% /209%	89	67%	152	66%	688	100%
Red Tea Leaf	129 /416	27% /224%	32	5%	22	49%	203	36%
White Birch	339 /414	36% /566%	280	81%	306	64%	254	33%

	Ni Kd (adjusted /approx) g/ml	Ni Error (adjusted /approx) (+/-)	Ag Kd g/ml	Ag Error (+/- %)	Au Kd g/ml	Au Error (+/- %)	U Kd g/ml	U Error (+/- %)
Blackberry	115 /115	138% /138%	7471	172%	48809	6%	123	6%
Coffee Grounds	4 /4	21% /21%	179	139%	32519	39%	81	39%
Garlic Powder	3 /3	62% /62%	50	11%	53440	11%	66	30%
Dried Kale	48 /58	52% /62%	60	12%	70008	11%	35	12%
Peanut Shell	236 /285	44% /53%	384	62%	43	34%	185	57%
Spring Greens	132 /1021	53% /131%	87	63%	95410	65%	181	60%
Red Tea Leaf	132 /176	133% /143%	65	119%	31	96%	18	59%
White Birch	540 /1712	54% /331%	46825	139%	54097	15%	125	24%

4.7.5 Capture rate as percentage of system

The capture rates reported represent the mass sorbance in the solid phase, but it is important to realise that the small volumes of the batches do not necessarily represent the total capacity of the material, only that of the centrifuge tube.

By reporting the partition as a % of the total system, we can estimate whether the system has the potential to capture further elements of interest, in a larger scale, or indicate if more fundamental limits exist in the system.

The percentage of system is calculated as the ratio of the mass of the element present in the supernatant plus the mass of element in the solid phase, compared with the mass present in the solid phase.

For example, for uranium, the typical batch element total mass is, this would be approximately 0.15±0.02 µg for the Batch 2 replicates, and 0.3 ± 0.05 µg for the Batch 3 replicates.

TABLE 47 PERCENTAGE CAPTURED ON SOLID PHASE (%) FOR BATCH 2 AND 3

	V Sorbed adjusted /approx (%)	Mn Sorbed (%)	Ni Sorbed adjusted /approx (%)	Cu Sorbed (%)	Mo Sorbed (%)	Ag Sorbed (%)	Au Sorbed (%)	U Sorbed (%)
Dried Kale	54% /86%	14%	3% /3%	12%	44%	53%	1%	74%
Garlic Powder	17% /54%	2%	2% /7%	7%	21%	46%	7%	59%
Orange Peel	35% /56%	21%	21% /32%	19%	47%	41%	10%	84%
Peanut shell	54% /69%	31%	31% /43%	42%	72%	11%	24%	56%
Potato Skin	17% /45%	51%	51% /3%	70%	41%	98%	8%	90%
Red Grape	17% /53%	6%	6% /6%	16%	16%	13%	1%	54%
Vitira Grape	21% /77%	13%	13% /53%	30%	58%	0%	1%	92%
White Grape	17% /73%	8%	8% /21%	27%	57%	72%	2%	65%
Blackberry	30% /30%	25%	25% /22%	3%	47%	33%	16%	34%
Coffee Grounds	4% /4%	17%	17% /3%	37%	61%	34%	16%	34%
Garlic Powder	18% /18%	17%	17% /1%	10%	7%	17%	15%	20%
Dried Kale	13% /13%	17%	17% /13%	7%	1%	17%	15%	11%
Peanut Shell	39% /39%	24%	24% /44%	45%	59%	45%	11%	35%
Spring Greens	2% /2%	9%	9% /22%	17%	18%	13%	12%	22%
Red Tea Leaf	17% /17%	25%	25% /38%	66%	12%	23%	11%	15%
White Birch	18% /18%	23%	23% /63%	36%	37%	74%	8%	28%

4.8 Analysis of solid phase material used in continuous flow conditions.

The samples that were used as sorbants in the continuous flow experiments were dried and weighed per the pre-experiment conditions. The pre and post conditions are noted in the table below.

TABLE 48 MASS OF SAMPLES IN CONTINUOUS FLOW, PRE AND POST EXPERIMENT (G)

	Sample (g)	Control (g)	Post Experiment (air dry room temp) (g)	Post experiment (Air Dry 50 °C) (g)
Potato Skin	55.68	51.20	43.99	42.89
Peanut Shell	25.55	20.11	28.29	27.21
Garlic Powder	58.87	69.30	8.12	6.99
Birch	35.54	29.18	39.79	38.71
Orange Peel	86.04	32.75	157.82	80.21

As was seen in the batch experiment, the garlic powder proved to be unrestricted by the filter material, and a high percentage of the material was able to escape the sample. However, other than the orange peel, there was net mass gain in the samples.

The samples were then ashed, digested and analysed by ICP-MS.

4.8.1a Vanadium concentrations in solid phase

The vanadium concentrations in the solid phase were measured and reported in **Table 49**. Samples were all above the limit of detection. Only the garlic achieved significant capture, with the K_d halving between the two week and the four-week interval. This is probably due to the continuing loss of mass from the sample, as it suffered the worst mass loss. This would be a surprise, as vanadium is conventionally ascribed to follow similar reaction paths as uranium, the selecting element. (Cheng, et al., 2019) This is unexplained, but is probably partly due to the poor sensitivity, but would also might indicate that vanadium may not be a suitable proxy for uranium in the context of organics, and the option of co-mining, as was attempted by Sugo, et al. (2001), would not be as viable with these materials. However, if the negative impact factor exhibited by the filter bags in the batch experiment were applied to this data, which corresponds between a 3x to 10x reduction, an effective filtration would be sufficient to raise all values sufficiently meet the criteria for significant capture.

TABLE 49 VANADIUM CONCENTRATION IN DIGESTATE, WITH CORRESPONDING PER UNIT MASS, FOR THE SAMPLE AND CONTROL, AND CALCULATED CHANGE AND PARTITION CO-EFFICIENT IN SOLID PHASE OF THE CONTINUOUS FLOW TEST

V	Digestate Concentration ($\mu g.l^{-1}$)	Control Concentration ($\mu g.l^{-1}$)	Surface Concentration $\mu g.g^{-1}$	Control Concentration $\mu g.g^{-1}$	Surface Concentration increase $\mu g.g^{-1}$	Partition Co-efficient (Kd 2 week / 4 week) $ml.g^{-1}$
Birch	550.20	448.86	0.71	0.77	-0.06	407 / 498
Garlic	441.64	32.57	3.16	0.02	3.13	15663 / 7014
Peanut shell	151.56	94.58	0.28	0.24	0.04	168 / 187
Potato Skin	246.47	169.98	0.29	0.17	0.12	173 / 193
Orange Peel	49.00	58.26	0.03	0.09	-0.06	20 / 18

4.8.1b Manganese concentrations in solid phase

The manganese concentrations in the solid phase were measured and reported in **Table 50**. Samples were all above the limit of detection. All samples exhibited a drop in concentration between the sample and the control, with corresponding drops in the K_d, although it notable that the concentrations of element recovered from the solid phase are consistently the highest of any element.

Therefore, these materials would not be suitable for a precipitation method, although the potential of production as a byproduct of capture of a different element would be possible.

TABLE 50 MANGANESE CONCENTRATION IN DIGESTATE, WITH CORRESPONDING PER UNIT MASS, FOR THE SAMPLE AND CONTROL, AND CALCULATED CHANGE AND PARTITION CO-EFFICIENT IN SOLID PHASE OF THE CONTINUOUS FLOW **TEST**

Mn	Digestate Concentration ($\mu g.l^{-1}$)	Control Concentration ($\mu g.l^{-1}$)	Surface Concentration $\mu g.g^{-1}$	Control Concentration $\mu g.g^{-1}$	Surface Concentration increase $\mu g.g^{-1}$	Partition Co-efficient (Kd 2 week / 4 week) $ml.g^{-1}$
Birch	643.03	1213.07	0.83	2.08	-1.25	35 / 40
Garlic	1039.21	17621.55	7.43	12.71	-5.28	427 / 396
Peanut shell	285.45	1353.39	0.52	3.37	-2.84	24 / 23
Potato Skin	335.00	902.76	0.39	0.88	-0.49	17 / 16
Orange Peel	183.00	154.19	0.11	0.24	-0.12	5 / 6

4.8.1c Nickel concentration in solid phase

The nickel concentrations in the solid phase were measured and reported in **Table 51**. Samples were all above the limit of detection. Only the garlic exhibited a rise in concentration, but it was very

significant. The measurement for the 2 week is probably an anomaly, as the wet phase concentration was measured as an order of magnitude below the limit of detection, but any effect from this would be countered by the effect from the loss in mass to suspension.

Therefore, only the garlic would be suitable for capture purposes.

TABLE 51 NICKEL CONCENTRATION IN DIGESTATE, WITH CORRESPONDING PER UNIT MASS, FOR THE SAMPLE AND CONTROL, AND CALCULATED CHANGE AND PARTITION CO-EFFICIENT IN SOLID PHASE OF THE CONTINUOUS FLOW TEST

Ni	Digestate Concentration ($\mu g.l^{-1}$)	Control Concentration ($\mu g.l^{-1}$)	Surface Concentration $\mu g.g^{-1}$	Control Concentration $\mu g.g^{-1}$	Surface Concentration increase $\mu g.g^{-1}$	Partition Co-efficient (Kd 2 week / 4 week) $ml.g^{-1}$
Birch	57.90	78.39	0.07	0.13	-0.06	36 / 56
Garlic	199.25	326.32	1.42	0.24	1.19	11928 / 2162
Peanut shell	18.58	50.72	0.03	0.13	-0.09	75 / 33
Potato Skin	30.91	56.13	0.04	0.05	-0.02	46 / 19
Orange Peel	48.03	36.07	0.03	0.06	-0.03	18 / 16

4.8.1d Copper concentration in solid phase

The copper concentrations in the solid phase were measured and reported in **Table 52**. Samples were all above the limit of detection. The concentration increase was limited, but this is primarily due to the high background.

Although the Kd are not significant, the concentrations in background concentrations are high, making this a potential by-product option.

TABLE 52 COPPER CONCENTRATION IN DIGESTATE, WITH CORRESPONDING PER UNIT MASS, FOR THE SAMPLE AND CONTROL, AND CALCULATED CHANGE AND PARTITION CO-EFFICIENT IN SOLID PHASE OF THE CONTINUOUS FLOW TEST

Cu	Digestate Concentration ($\mu g.l^{-1}$)	Control Concentration ($\mu g.l^{-1}$)	Surface Concentration $\mu g.g^{-1}$	Control Concentration $\mu g.g^{-1}$	Surface Concentration increase $\mu g.g^{-1}$	Partition Co-efficient (Kd 2 week / 4 week) $ml.g^{-1}$
Birch	534.70	257.49	0.69	0.44	0.25	27 / 15
Garlic	359.02	447.51	2.57	0.32	2.24	89 / 61
Peanut shell	225.40	317.86	0.41	0.79	-0.38	7 / 15
Potato Skin	488.69	581.92	0.57	0.57	0.00	30 / 15
Orange Peel	182.26	277.97	0.11	0.42	-0.31	4 / NA

4.8.1e Molybdenum concentration in solid phase

The molybdenum concentrations in the solid phase were measured and reported in **Table 53**. Samples were all above the limit of detection. The garlic was again a very effective sorbant, despite the mass loss.

None of the samples achieved significant capture rates, but the digestate concentrations are high, meaning this element is a potential byproduct.

TABLE 53 MOLYBDENUM CONCENTRATION IN DIGESTATE, WITH CORRESPONDING PER UNIT MASS, FOR THE SAMPLE AND CONTROL, AND CALCULATED CHANGE AND PARTITION CO-EFFICIENT IN SOLID PHASE OF THE CONTINUOUS FLOW **TEST**

Mo	Digestate Concentration ($\mu g.l^{-1}$)	Control Concentration ($\mu g.l^{-1}$)	Surface Concentration $\mu g.g^{-1}$	Control Concentration $\mu g.g^{-1}$	Surface Concentration increase $\mu g.g^{-1}$	Partition Co-efficient (Kd 2 week / 4 week) $ml.g^{-1}$
Birch	603.46	259.13	0.78	0.44	0.34	32 / 41
Garlic	1698.78	47.75	12.15	0.03	12.11	735 / 877
Peanut shell	789.41	854.17	1.45	2.12	-0.67	222 / 176
Potato Skin	889.40	121.16	1.04	0.12	0.92	151 / 184
Orange Peel	389.54	130.72	0.24	0.20	0.04	40 / 47

4.8.1f Silver concentration in solid phase

The silver concentrations in the solid phase were measured and reported in **Table 54**. Samples were all above the limit of detection. Only the garlic exhibited a rise in concentration, but it wasn't very significant.

Overall, there was no significant capture, and the background concentrations are mostly insignificant. It is unlikely that it would present a useful capture or by-product option.

TABLE 54 SILVER CONCENTRATION IN DIGESTATE, WITH CORRESPONDING PER UNIT MASS, FOR THE SAMPLE AND CONTROL, AND CALCULATED CHANGE AND PARTITION CO-EFFICIENT IN SOLID PHASE OF THE CONTINUOUS FLOW TEST

Au	Digestate Concentration ($\mu g.l^{-1}$)	Control Concentration ($\mu g.l^{-1}$)	Surface Concentration $\mu g.g^{-1}$	Control Concentration $\mu g.g^{-1}$	Surface Concentration increase $\mu g.g^{-1}$	Partition Co-efficient (Kd 2 week / 4 week) $ml.g^{-1}$
Birch	143.54	170.75	0.19	0.29	-0.11	7 / 7
Garlic	35.35	60.78	0.25	0.04	0.21	10 / 10
Peanut shell	54.76	27.99	0.10	0.07	0.03	4 / 4
Potato Skin	238.14	97.80	0.28	0.10	0.18	11 / 11
Orange Peel	131.93	63.78	0.08	0.10	-0.02	3 / 3

4.8.1g Gold concentration in solid phase

The gold concentrations in the solid phase were measured and reported in **Table 55**. Samples were all above the limit of detection. The potato skin exhibited surprisingly high levels of capture, and would be economically viable, if the results reflect true capture, but it is possible that it may in fact be an artifact of its low density, but both the digestate and per mass concentration is very significantly greater than the control.

TABLE 55 GOLD CONCENTRATION IN DIGESTATE, WITH CORRESPONDING PER UNIT MASS, FOR THE SAMPLE AND CONTROL, AND CALCULATED CHANGE AND PARTITION CO-EFFICIENT IN SOLID PHASE OF THE CONTINUOUS FLOW TEST

Ag	Digestate Concentration ($\mu g.l^{-1}$)	Control Concentration ($\mu g.l^{-1}$)	Surface Concentration $\mu g.g^{-1}$	Control Concentration $\mu g.g^{-1}$	Surface Concentration increase $\mu g.g^{-1}$	Partition Co-efficient (Kd 2 week / 4 week) $ml.g^{-1}$
Birch	276.66	323.56	0.36	0.55	-0.20	89 / 32
Garlic	122.76	240.96	0.88	0.17	0.70	42 / 84
Peanut shell	309.65	113.66	0.57	0.28	0.29	67 / 111
Potato Skin	5657.74	341.15	6.59	0.33	6.26	849 / 1798
Orange Peel	308.08	228.87	0.19	0.35	-0.16	424 / 22

4.8.1h Uranium concentration in solid phase

The uranium concentrations in the solid phase were measured and reported in **Table 56**. Samples were all above the limit of detection. Unsurprisingly, since the selection criteria was based on previously.

The measured partition coefficients, were, with the exception of the garlic at 2 weeks, and the peanut shell at 4, under the criteria for significant capture, but barely, excluding the orange peel, which does not seem to have achieved any capture.

TABLE 56 URANIUM CONCENTRATION IN DIGESTATE, WITH CORRESPONDING PER UNIT MASS, FOR THE SAMPLE AND CONTROL, AND CALCULATED CHANGE AND PARTITION CO-EFFICIENT IN SOLID PHASE OF THE CONTINUOUS FLOW TEST

U	Digestate Concentration ($\mu g.l^{-1}$)	Control Concentration ($\mu g.l^{-1}$)	Surface Concentration $\mu g.g^{-1}$	Control Concentration $\mu g.g^{-1}$	Surface Concentration increase $\mu g.g^{-1}$	Partition Co-efficient (Kd 2 week / 4 week) $ml.g^{-1}$
Birch	187.57	23.83	0.24	0.04	0.20	631 / 949
Garlic	60.25	1.56	0.43	0.00	0.43	1526 / 827
Peanut shell	190.62	13.87	0.35	0.03	0.32	738 / 1437
Potato Skin	147.93	4.28	0.17	0.00	0.17	910 / 988
Orange Peel	51.43	29.16	0.03	0.04	-0.01	66 / 72

4.8.2 Summary

Overall, the first point of note is the ineffectiveness of the orange peel, which was completely different to the results from the batch tests. Given the differences in readings, the conclusion was that there was an interferent effect, which blocked capture for at least some, if not all of the run.

Reviewing the methodology, this could be one of two things: the spike in copper from the failure of the probe, or the microbial growth in the soluble phase.

A competitive sorption effect from the copper and other elements from the probe could have blocked the sorbance sites and saturated the surface (Groenenberg, et al., 2012).

Alternatively, the increased surface area of the box resulted in much greater mould growth than with the small batch container, as the mould was primarily on the surface: if either the mat itself, or fragments of the biofilm fragmenting into the supernatant, where it partially binding the elements, they may not be available to the sorbance site (Araújo & Oliveira, 2020). Aside from directly interfering, the biofilm could be altering the redox or pH environment in ways that prevented binding, although this seems less likely. This can't be confirmed from this data, since the batch samples were filtered post contact, and if the metals were integrated into the biofilm, it would not have been differentiable from the material biomass. In fact, this would likely aggravate the effect, as biofilm bound metals would have remained in suspension in the supernatant, with the larger particles prevented from adhering to the biomass by the filtrant.

This effect was avoided with the later flow boxes, due to the design changes intended to prevent biofilm growth, mentioned in the methodology section. That said, the metal per mass rate of the continuous flow system all displays greater concentration per gram than the equivalent batch experiment, even the orange peel, which was a factor of x20 on the batch concentrations. This raises the question of whether the partition coefficient in batch an effective measure of performance is. The limitation may not be the equilibrium rates.

Conventional modelling uses this factor, because it can be an effective way to predict situations once they become steady state when long term equilibriums dominate as time tends to the long term, but fast state effects in dynamic systems, such as biologically active systems, or very liquid environments (such as open sea), can result in strongly altering effects which curtail swiftly, or very slow mechanisms with cascading dynamics, creating run-away mechanisms (Groenenberg, et al., 2012)

Since the supernatant for the four which did not experience the biofilm, either remained at levels comparable to those of the seawater controls, or rose due to dissolutions, this indication the slower sorbance mechanisms are being overwhelmed by the influx, and creates either a Langmuir surface

saturation limit, albeit limited by the degradation mechanisms in play (Möser, et al., 2012), or an unlimited complexation layer, which would probably correspond to an expanding biofilm in practice (Bampaiti, et al., 2016), since known interactable mechanisms of binding between ions and complexes of interest are of limited rates (Gardner., 1973).

4.9 IR analysis of solid material prior and after sorption

As would be expected, given the material's organic nature, the signal is dominated by those associated with cellulose. Peaks at ~ 3300 (O-H), 1200 (C-H2) and 1050 (C-O and C-C) are all clearly visible and are broadly similar between samples.

Of interest as potential sites of sorbance, in most cases, at least a single (merged) peak, or a double peak associated with the C=O in carboxylic groups is visible at 1720/1620 are clearly present in all samples, and a region of activity which would correspond with a double peak associated with aromatic ring features such as polyphenolic grouping is visible at 1400/1200 .

However, it was hoped that it would be possible to correlate the peak intensity of the samples to the uranium concentration increase. This was not demonstrated, with the results displaying no significant correlation ($p > 0.05$) to the net change in peak intensity: this is probably a scoping issue, as the later testing shows, the uranium was not the only element interacting with the material surfaces, and doesn't properly take into account any other alterations to the surface from the liquid contact.

4.10 Discussion

4.10.1 Review of Batch 1

Based on the sorption results presented in Section 4.7 ICP-MS analysis of the solid material fraction the overall impression is of significant variability. This can be primarily attributed to the bio-variability of the samples which yield composition changes of the biomass samples. These samples are the fruits of plants which exist in variable stages of growth and decomposition, due to soil/plant interaction, watering conditions, plant/fruit orientation, maturity grade (leave, fruit, tuber …). There are further factors such as sample preparation, including sample cutting, size of biomass phases and biofouling. These factors may affect element uptake or the resultant K_d.

However, it is possible to draw some broad conclusions. It is noticeable that the samples with the highest retention all are associated with materials known to release free aromatic chemicals into solution. Grape fermentation is known, driven by their high sugar content, but garlic, Brussels sprouts and kale all release various organo-sulphur compounds such as allicin from garlic, glucosinolate from Brussels sprouts and kale, while peanut shells release compounds such as luteolin quickly under mildly anaerobic conditions e.g. (Eksi, et al., 2019). While samples were not sealed airtight, it suggests these localised low oxygen conditions within the samples are promoting depositions, which was detectable while working with the samples. These processes are commonly supposed to be microbe-associated; it will consequently be important to test their effects, and ensure controls are adequate to prevent leakage to environment.

However, the greatest proportion of polyphenols and antioxidants are currently bound with insoluble polymers and some of them (dry weighted, dw) sorb strongly uranyl ion, their polyphenols (PP) content is high.

Grapes are found with 40 to 400 mg PP per 100 g dw (Nile, et al., 2013) (Pastrana-Bonilla, et al., 2003)). Garlic is found with 40 to 50 mg PP per 100 g dw (Chekki, et al., 2014)). Brussels sprouts may contain about 100 mg PP per 100 g dw (Cieslik, et al., 2006). Kale samples have 500 to 600 mg PP per 100 g dw (Sikora & Bodziarczyk, 2012) Peanut shells are found with 300 to 450 mg PP per 100 g dw (Rosales-Martínez, et al., 2014) (Qiu, et al., 2012) Orange skins have 300 to 450 mg PP per 100 g dw (El-aal & Halaweish, 2010). Lime skins are found with about 60 mg PP per 100 g dw (Safdar, et al., 2017) Potato skins have 10 to 35 mg PP per 100 g dw (Akyol, et al., 2016). Nectarine skins are found with 20 to 60 mg PP per 100 g dw (Gil, et al., 2002) and mange tout samples are found with about 10 mg PP per 100 g dw (Lanzmann-Petithory, 2002) These polyphenols are expected to increase sorption. A plot of K_d versus the PP concentration displays little to no correlation (see **Figure 48**). There are several reasons

why this dispersion of data could be observed. Some of the compounds which are included in the PP fraction, are soluble while others remain on the surface or integrated into the biomaterial. This may also be due to the size or the fractal aspect of the biomass phases.

Alternatively, their reported PP concentrations are not fully reflective of the natural variability between specimens: the PP content of the samples may be significantly different due to variety, temperature, pH, and nutritional supply to the crop while growing. Another explanation would be if there are other forms of binding site within the materials. Most critically, we must also consider if part of the sorption is irreversible, which will disproportionately impact the ratio. This would be a valuable improvement to future methods.

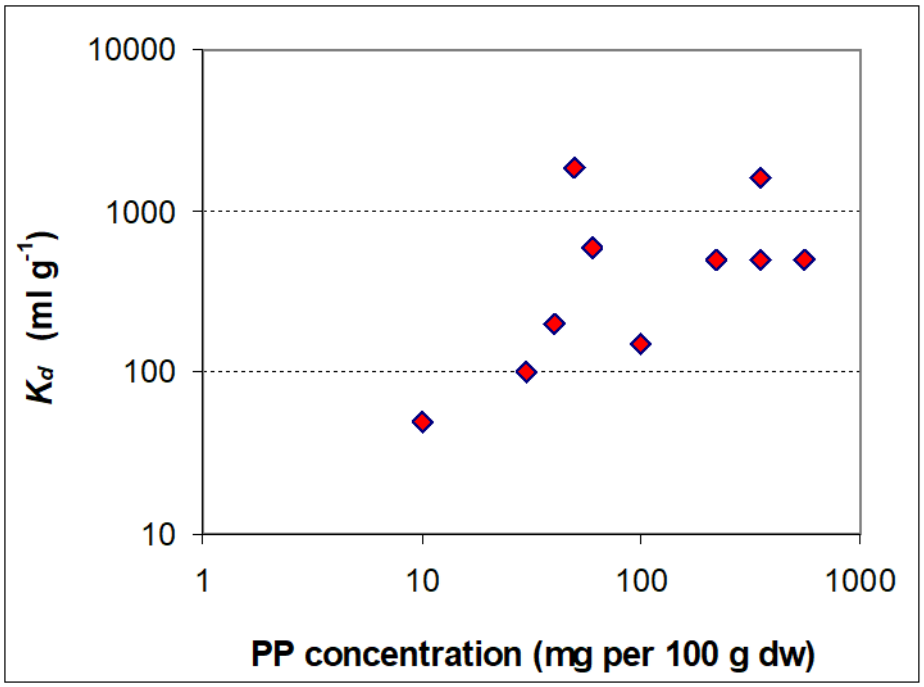

FIGURE 48 PLOT OF K_D WITH POLYPHENOL (PP) CONCENTRATION (BIOMASS DRY WEIGHT: DW).

The data also suggests two potential scenarios: materials with sacrificial antioxidants are more effective in retention, compared with more locational-specific antioxidants, or these materials are emitting chemicals which are stimulating the microcosm, which encourages deposition. These are not mutually exclusive hypotheses, but it is likely that one will have greater influence, and some elements of system design to test these would be valuable. In addition, it will dictate some of the practicalities of interaction. If the process requires release to solution, a contact space over the materials is required, while a surface micro-organism paradigm can be more enclosed.

The failure of the supernatant partitioning, and the loss of several of the samples through post experiment biofilm growth shows how biologically active these samples can be, even downstream

from the sample itself, and that the controls in place were insufficient. These lessons were incorporated in the updated experimental design for batch 2 and 3, through post extraction controls, and with the inclusion of containing structures, specifically filter bags.

In terms of feasibility, the work demonstrated that while using biomass, capture of U from seawater is possible, further work is needed to increase the usability of the methodology. The small sample batches are limited in capacity, and which has acted as a threshold on the quantities sorbed over time, as the low total system capacity is only of the order of 0.1-0.2 µg, and with most of the samples were in the 80-95% capture range suggesting this actually represented a systemic limit rather than a true equilibrium. Therefore, reducing the solid to seawater ratios was important, which can be achieved with smaller solid sample and larger seawater volumes, and larger vessels, to increase the water fraction.

In saline surface water, uranium is conventionally considered to be hexavalent, which, under neutral conditions, undergoes strong but reversible sorption. When reduced, for example by the antioxidant-functional groups on the biomass materials, to tetravalent uranium which exhibits stronger sorption. This is commonly supposed to be due to a Coulomb effect making the binding of U^{4+} complexes stronger than for the UO_2^{2+} complexes. Therefore, a reducing agent such as antioxidants from the biomass material, introduced into solution, increase the proportion of U^{4+} present, and higher K_d values for uranium. Finally, presence of fine biomass material facilitates condensation of the colloids via aggregation, masking metal ions and complexes in the biomaterial. This behaviour makes the sorption irreversible with the embedding of the metal in the colloidal structure.

This effect was modelled, but the redox potential necessary to map these together was not taken, but it is a notable observation that the samples associated with fermentation have similar K_d to those predicted for $U^{(IV)}$, which would be require a two electron redox transition.

Additionally, these materials had undergone no modification, beyond the sizing process: for example, to establish the synthetic materials, they are pre-treated with acid to prepare sorption sites for exchange. This process could also benefit the materials. Another avenue that would be valuable to address is whether materials currently being evaluated could be used in conjunction. For example, combining the kale's retention chemicals with the potato skin's surface area has the potential to be a path to improved net performance. These possibilities indicate that while there are significant improvements necessary to increase the method to practicality, there are pathways to explore for improved efficiency.

4.10.2 Review of Batch 2 and 3

4.10.2a comparison of intrabatch controls

Between Batch 2 and 3, there were three materials intended for intrabatch control, to test the changes made to the experimental procedure. These are displayed in **Table 57**. There is clearly a strong mismatch between those contained within the material, and those which are not.

Based on the results, it would appear generally that the nano-cellulose, although the manufacturer claimed it to be porous enough that the elements of interest could transition across it while restricting the biomaterials, with a pore diameter 20 µm, was an interferent in the capture.

However, this effect cannot be full ascribed simply to the migration through the filter material itself. Considering the three materials, using the surface concentrations, as displayed in **Figure 49** to **Figure 56**, V, Mo, Ag Au and U, the garlic powder and the dried kale exhibited lower concentrations when contained, while the peanut shell did not. However, in the case of Ni and Cu this did not happen, and all three were lower, while in the case of the Mn this is reversed, although this is probably because for these three, the gradient is from the surface to the solution, while in the other cases the likely explanation is the transmissibility of the samples across the barrier provided by the filter.

In the case of the garlic, the entire particle can transmit through the filter, while the only the kale's soluble fragments transition, and very little of the peanut shell transits. Elements which tend to be associated with the soluble complexes, like uranium, silver, molybdenum, and manganese will be trapped outside the filter, while free elements like copper (Wang, et al., 2013) , gold and vanadium will transit more freely.

TABLE 57 INTERBATCH CONTROLS TESTING NANOCELLULOSE CONTAINER.

	V Kd (measured /estimated) g/ml	Mn Kd g/ml	Mo Kd g/ml	Cu Kd g/ml	Ni Kd (measured /estimated) g/ml	Ag Kd g/ml	Au Kd g/ml	U Kd g/ml
Dried Kale Unfiltered	1561 /8885	239.62	1050.89	192.16	42 /42	13195.34	18.71	3818.83
Dried Kale Filtered	357 /767	58.73	2.91	24.86	48 /58	59.59	70008.28	35.35
Garlic Powder Unfiltered	30 /171	2.71	40.20	11.65	3 /3	50.02	53439.81	65.67
Garlic Powder Filtered	438 /2190	55.04	19.61	30.44	12 /12	173.62	11.17	219.89
Peanut Shell Unfiltered	582 /2210	279.05	1291.42	341.71	351 /351	193.23	181.71	1353.96
Peanut Shell Filtered	552 /667	133.51	441.20	375.47	236 /285	384.47	43.07	184.61

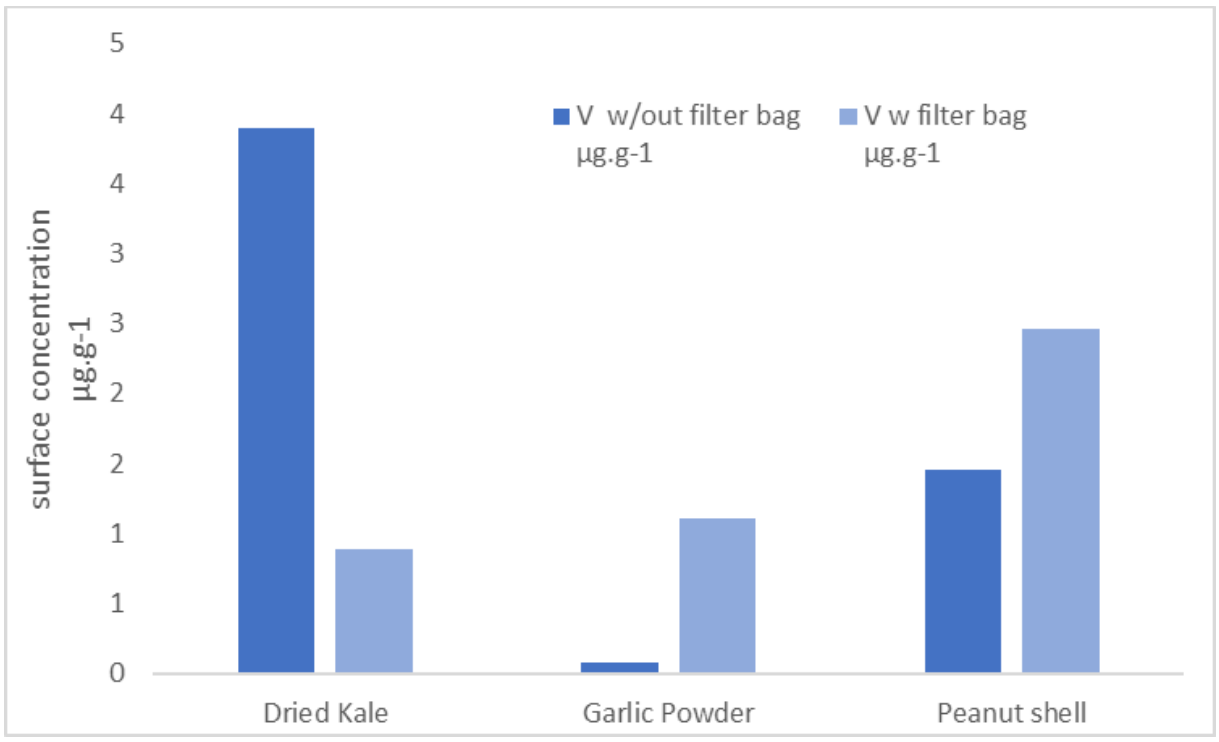

FIGURE 49 SURFACE CONCENTRATION OF VANADIUM IN INTRABATCH CONTROLS.

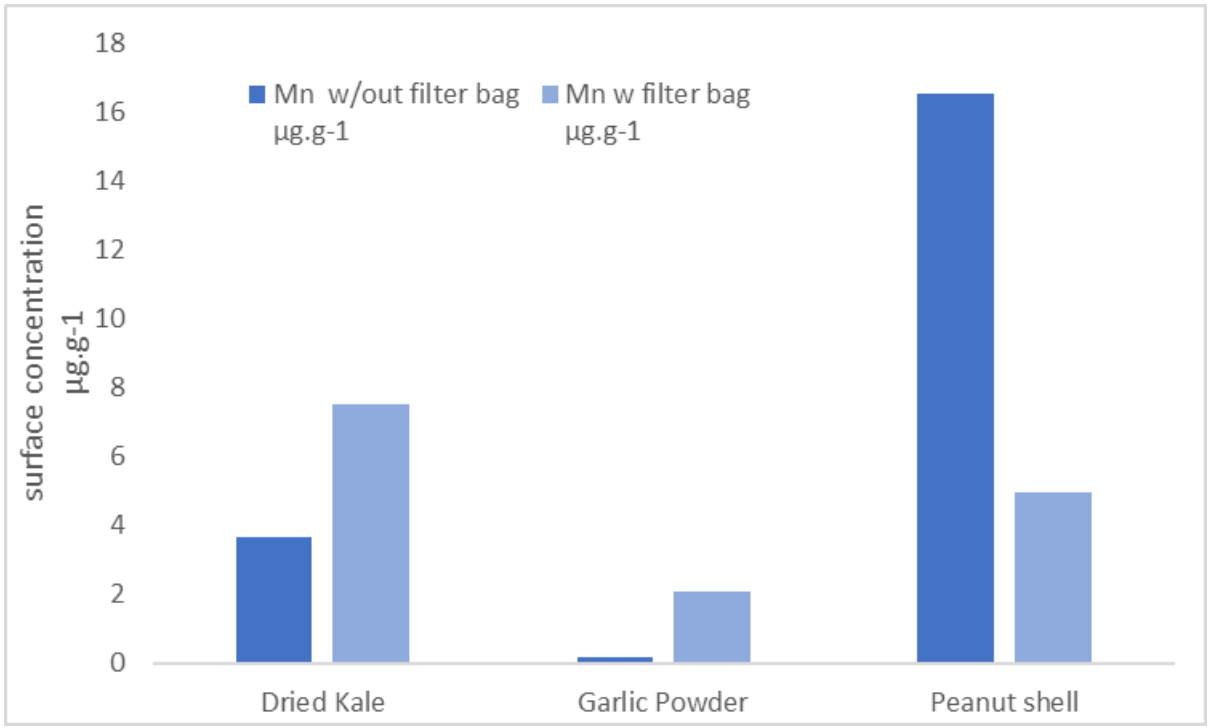

FIGURE 50 SURFACE CONCENTRATION OF MANGANESE IN INTRABATCH CONTROLS

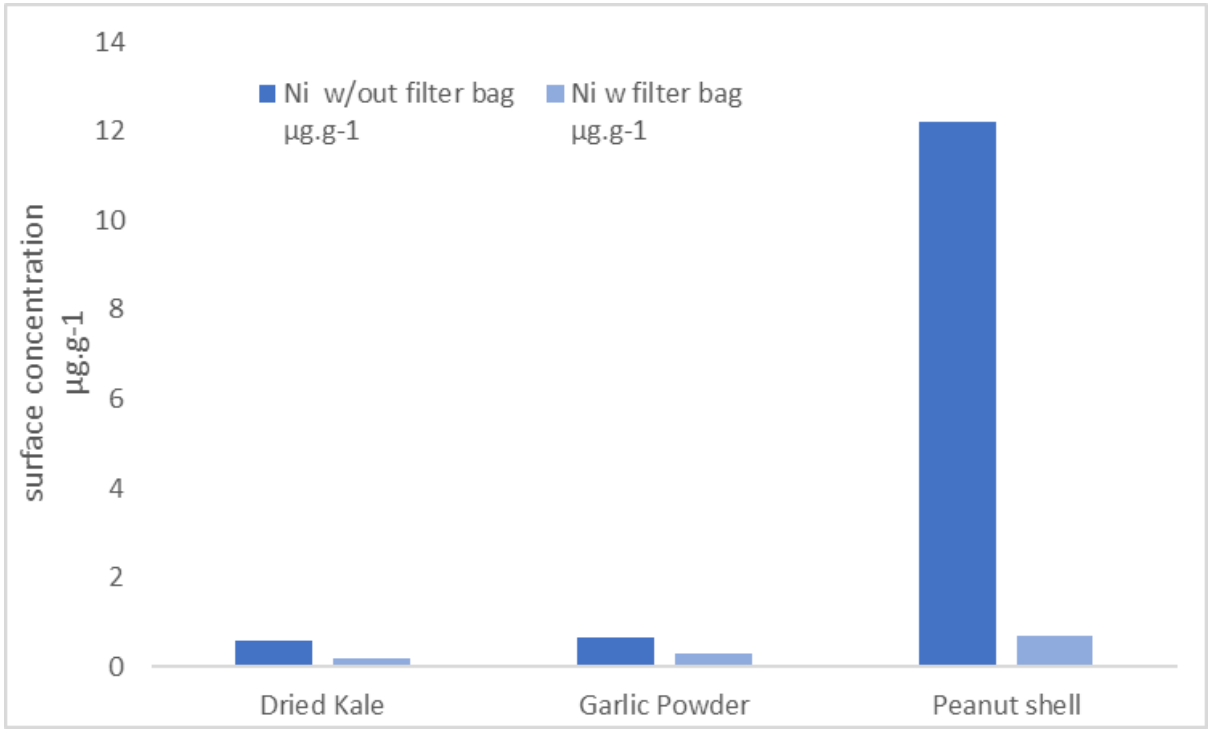

FIGURE 51 SURFACE CONCENTRATION OF NICKEL IN INTRABATCH CONTROLS

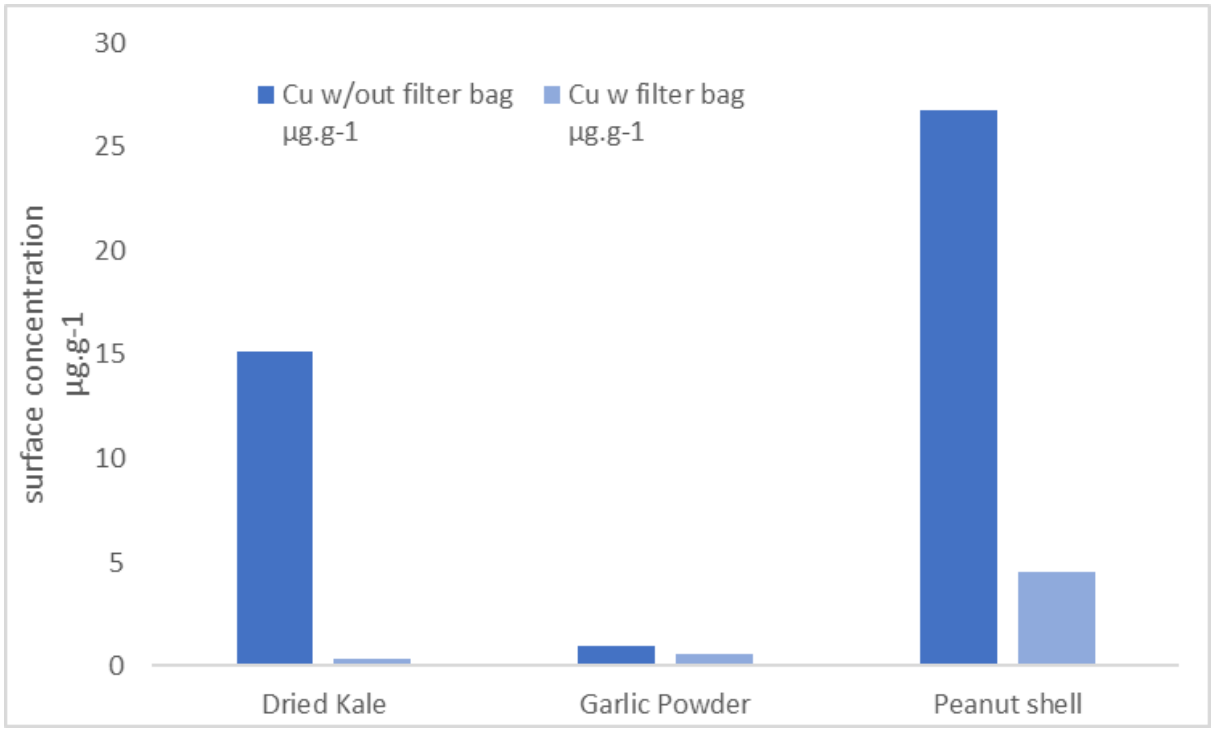

FIGURE 52 SURFACE CONCENTRATION OF COPPER IN INTERBATCH CONTROLS

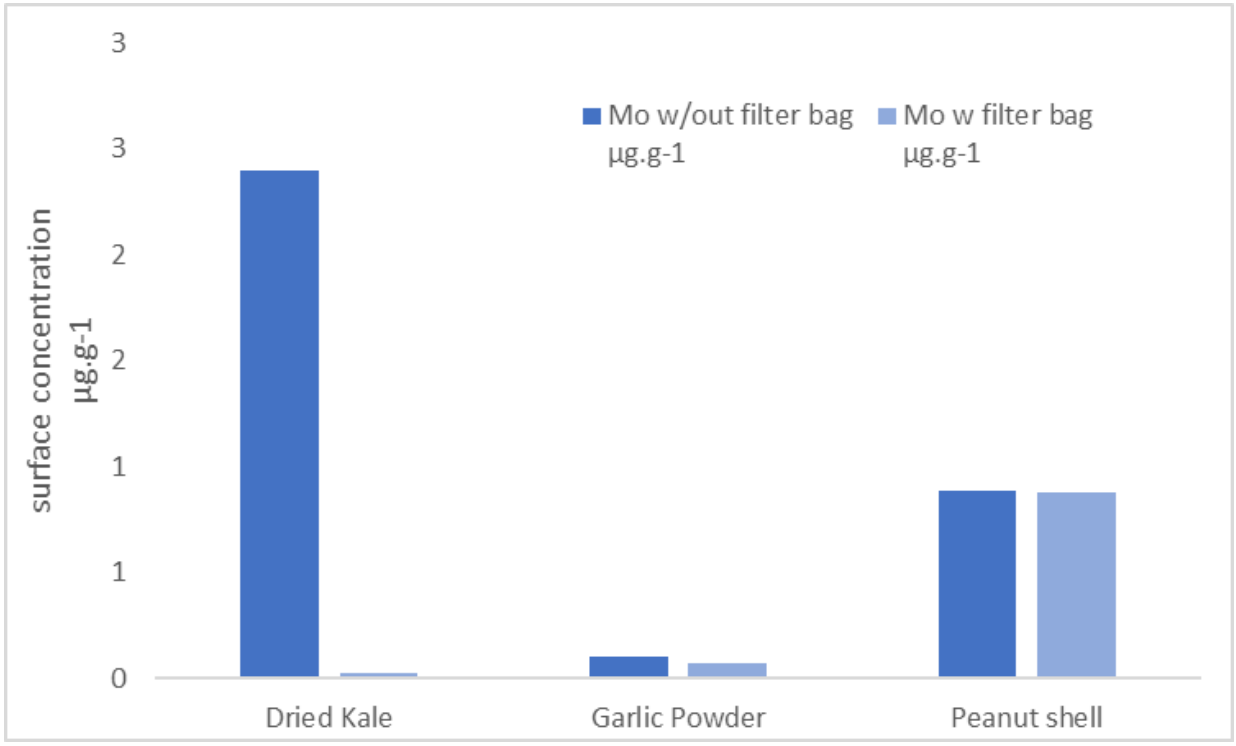

FIGURE 53 SURFACE CONCENTRATION OF MOLYBDENUM IN INTERBATCH CONTROLS

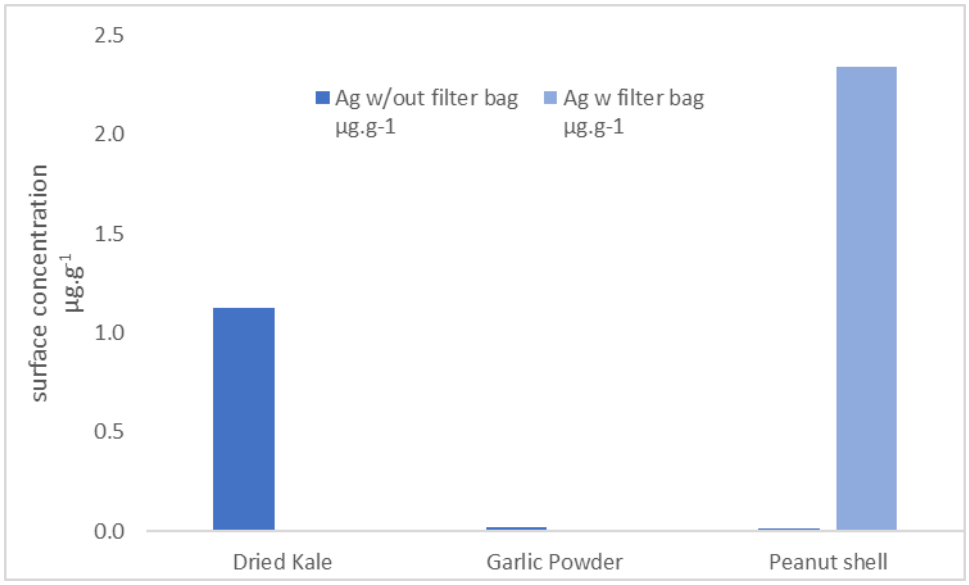

FIGURE 54 SURFACE CONCENTRATION OF SILVER IN INTERBATCH CONTROLS

FIGURE 55 SURFACE CONCENTRATION OF GOLD IN INTERBATCH CONTROLS

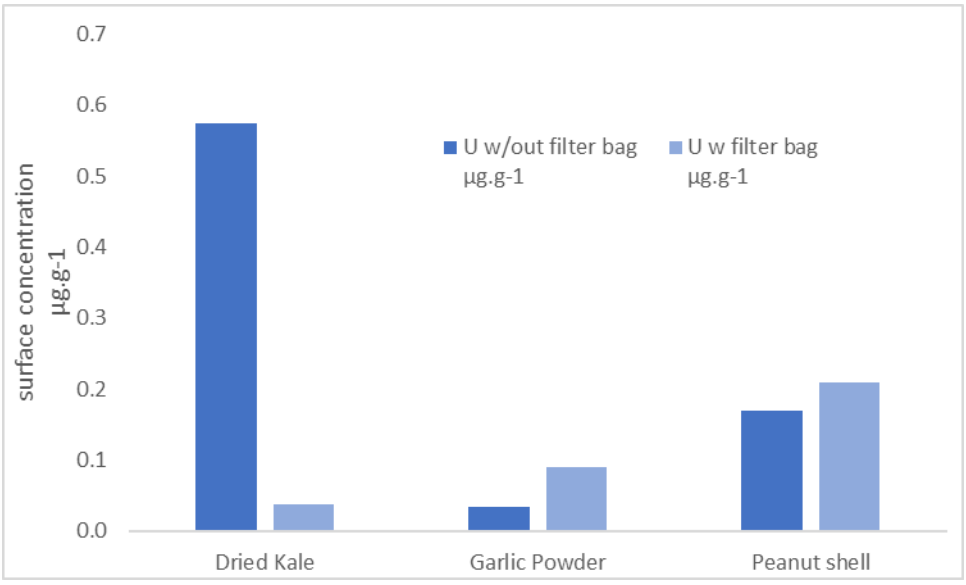

FIGURE 56 SURFACE CONCENTRATION OF URANIUM IN INTERBATCH CONTROL

Of the three samples themselves, only the gold in kale, and the Vanadium in garlic would meet the criteria of significance, using the filtered samples. The Au/kale value is due the wet phase exhibiting values below the limit of detection and can be discounted as an artifact.

Unfortunately, there does not appear to be any significant relationship ($p<5\%$) between the filtered and unfiltered samples in these tests, although that might be attributable to the number of factors involved: the variability of the surfaces, the starting concentrations both in solution and on the surface, the number of elements and the directionality of migration through the barrier, all appear to have contributed, and the interaction with the residue, resulting in a complex pattern of modification, leaving low confidence in the predictability of the samples. The conclusion is that, although the mesh bags did have potential for particle control, it does not appear that it contained these light organics effectively and did act to be a barrier to the complexes. As a general interpretation, considering only the uranium as the primary focus of the study, the bags reduced the concentrations absorbed by a factor of x10.

4.10.2b Continuous flow concentrations compared with batch 3 samples

The four samples used in the continuous flow experiment were selected on their performance in the batch phase, aiming to cover the spread of mechanisms that were posited to exist in literature.

These tests were conducted with the mesh bags, as the comparison testing was done in parallel, but in practice the larger containers used in the testing dictated that these were required for sample deployment: while post interaction filtration was considered, it would have required several modifications that would have made the assessment rig have more points of failure.

This means that only the batch 3 samples are directly comparable.

4.10.3 Comparison of modelling to the experimental results

Considering the modelling was limited to only the uranium data, the comparison between the two is the primary focus on the accuracy of the assumptions in the model. The direct limitation between the two is a consequence that it was not practical to test either the redox potential, nor the materials of the samples at batch level: to sample the redox potential in situ, which would be affected by changes in oxygen concentration, limited the ability to test, as moving a probe between samples would introduce complications in testing. The attempt to have the continuous flow measured was unsuccessful, as the probe failed.

However, we can make some interpretations, comparing the readings. The values obtained during batch 2 were the most directly relevant. Attempting to work back from measured values, which are summarised in **Table 58,** allows us to make a best guess, based on the model criteria, which site and which uranium complex was dominant in those conditions.

TABLE 58 BATCH 2 PARTITION CO-EFFICIENT (KD) FOR URANIUM AND PH

Sample	pH	Kd (U)	Log Kd
Dried Kale	5.80	3819	3.58
Garlic Powder	5.20	220	2.34
Orange Peel	4.90	7020	3.85
Peanut shell	6.10	1354	3.13
Potato Skin	6.10	7673	3.88
Red Grape	4.80	1708	3.23
Vitira Grape	4.30	7805	3.89
White Grape	6.10	17307	4.24

Most of the samples had pH of between 4 and 6, and K_d between 3 and 4. Of the materials modelled, none of the samples corresponded to these values at this pH: the model estimated these values to be quasi-zero at seawater conditions, and generally drop at lower potentials: this is not what is reported by the testing.

One potential explanation is that the redox potential shift action occurs at a higher pH, then there is not redissolution: this explanation could be due to linked-production of carbonate, a known step in oxidic respiration in soils: the bio reductive step of UO_2^{2+} to U^{4+} frees oxygen atoms to interact with the carbonyl released by the organism's incomplete digestion: the resulting (immobile) urano-

carbonates would be either a mono (pKa 5.5) or bi (pKa 7) form, while the tri form would not be present, as the pKa of that form is 9. These forms are insoluble in acidic conditions such as during digestion and would deposit in close proximity to the source. This process is known in biologically mediated uraninite weathering (Langmuir, 1978), and would fall outside the criteria placed upon the model in section 2.3.6, since it is a deposition mechanism, but would appear in the experimental results.

If this assumption holds, it would mean the interactive phase would occur between pH 8 and 7, then were precipitated as the pH fell. Of the elements measured, the carboxylic would not be active at this low a pH. The mono-hydroxybenzene would fit these measured values and would require a 2-electron shift (which is consistent with the redox change associated with fermentation (Lambert, et al., 2020)). The other phenolic surfaces would require a start point of pH greater than 8-10, which means that this explanation would only be feasible with the mono-hydroxybenzene surface. This theory would be consistent with the peak ratios obtained through FTIR in Section 4.9 but would be difficult to confirm in the context of the very low uranium complex concentrations, against that of other binding cations. For example, Ca^{2+} ions are present in concentrations three or four orders of magnitude greater than those of uranium (see **Table 1**), and would bind these carbonate anions as well, masking the impact of uranyl-minerals (Ao, et al., 2019). While selective extraction would remove the calcium, the process would shift the ratio interacting with the uranium.

In addition to this proposed mechanism, it can also be confirmed that less common insoluble compounds which may have captured uranium complexes being formed through the decay of the materials: For example, condensed tannins form through polymerisation of the products of oxic decay of polyphenolic molecules around metallic ion “cores” (Das, et al., 2020), which could include any uranyl atoms, especially if they were partly quenched by an organic complex, such as an alcohol group. This would also not be considered directly by the model.

Overall, testing the matrix for these trace molecules would be outside the scope of this work, but would likely contribute, at least partially.

A second possible explanation would be for an unmodelled site to be present, with very high affinity: however, such a site would need to have a log Kd greater than 3 higher than any modelled: not only would it need to overcome the difference in affinity, it would also be at a scale disadvantage, as the two sites modelled are found to account for an average of 90% of the surface area of biomass (Boudet, 2000): the maximum surface effectiveness is a maximum of 10% (with median concentrations of 2.5%), which translates to 25% of peak phenolic availability, and 14% peak carboxylic availability, per

Boudet. This would mean that it is unlikely to be the dominant case, but this hypothetical scarce but strong site type could have some limited effect in the discrepancy.

A third possibility is surface topography. As described in Section 2.3.1, the model assumes a spherical surface. If the biomass is porous, it is possible that the inner dimensions of the structure was active surface, not just the external sphere.

This possibility was considered and was attempted to be investigated through combining a more complex surface model with detailed Brunauer, Emmett and Teller (BET) theory specific surface area testing study to produce target measurements. The attempt to carry out the BET tests on the samples was unsuccessful, as it was unable to produce useful results with the samples used in the batch tests: the materials proved impossible to dry to standards sufficient for available equipment to test, without undergoing significant degradation. Attempts with less dried than those specified in the BET procedures produced very inconsistent results, and the possibility of implementing this was proved to be impractical with currently available equipment.

The literature does document some instances where this data is available. While data is not available for all materials, the surface area of garlic powder is between 0.68 and 0.71 $m^2 \cdot g^{-1}$ (Tavares, et al., 2021) and for orange peel it is reported as 1.03 $m^2 g^{-1}$ (Pathak, et al., 2017)). However, a value of 0.0067 $m^2 \cdot g^{-1}$ was used for the phenolic, and 0.0085 $m^2 \cdot g^{-1}$ for the carboxylic models. Even allowing that both site units would exist in the same particle, the surface areas therefore was significantly underestimated by the model: this would be consistent with the difference observed.

There is a significant variation between total surface area and active surface area: particularly with internalised spaces on organics, which can be anywhere on a spectrum from an actively participating, or completely inert, so a direct relation is difficult to establish. However, it is probably a reasonable to hypothesis at least part of the discrepancy is due to this variation.

Overall, it is likely that all three mechanisms are a contributing factor to the discrepancy between the model and the experimental results. The model, while more developed as a result of this research, proved to require further refinement to develop more accurate results.

5.0 Conclusions

Reviewing the results collated through **Section 4**, it is clear that capture of uranium using biomass is possible: the capture of other elements is possible is a small selection of cases but are more likely when considering the trace background rates that exists in the materials.

The more complex question is whether it is practical, and economic. The reduced performance due to the filter bags illustrate that there are substantial challenges in getting the materials into contact with the water flow in a way that does not interfere with the materials, while the increase of the flow test against the small batch tests highlights that the small batch tests have limited indicative value against that of the larger experiment. These are both key obstacles in any future research, which would need to be overcome to make the approach practical.

The difference in performance between the batch and the continuous flow results, which indicates a much more complex picture of conditions in the contact process, raises a fundamental question of whether the batch experiments can be indicative. There were clearly substantial and rapid changes in the conditions in potential and pH, which may have either been rate limiting, or a driver of precipitation as mechanism of interference, a point which the modelling is not immediately informing of. For example, the impact of carbonisation, which the modelling demonstrates to be an "interference" in the context of K_d of the sorbance site, may not be such in the context of the actual batches, where the resulting precipitate in fact is implied to contribute to the sorbance totals, since it mitigates the migration from the organics (Langmuir, 1978). The need to expand the model to overcome this knowledge gap would be important.

The question whether the materials are of economic advantage is broader, partly because of uncertainties in pricing at both ends of the process, but also because much of the system would be novel in some degree. One strong performer (peanut shell) is used as biofuel extensively (Perea-Moreno, et al., 2018) and there is only minor technical barriers to introducing its use in element capture pre-incineration, then the recovery of the elements of interest from the digestion waste of a biofuel generator, or ash from a biomass generator. Many of the other strong performers are under investigation for use in biomass, both for the energy potential, and as a landfill reduction measure (Ganguly, et al., 2020). The energy recovered from these would be a primary revenue source, and with the metals being a byproduct, as they currently stand, but would be a valuable addition to the circular economy efficiencies, if they could be scaled. Conventional economic modelling for uranium extraction from seawater would not be able to take this into account, especially as these processes are still being developed, creating wide zones of uncertainty. These must be discounted from the direct comparison, but it is important to remember that the values that will be quoted are underestimates for this reason. This also applies to secondary element recovery.

In order to make an attempt at an estimate, a baseline for the amidoxime is taken from Schneider & Sachde (2012). This paper quotes the economic cost of the extraction, based on Sugo, et al. (2001) work on the best field test of recovery, and relates it to a technology base closer to currently available

techniques. Schneider and Sachde have taken into account the extensive critisms of accuracy of the findings of Sugo et al, which they have reported along with the informational estimates on the subcosts relative to the operational costs allows a mirroring of the calculations using estimated pricing of the biomasses from literature.

The referred paper quote a value of $340-$1120 per Kg U, of which 43% is due to sorbant cost. Therefore, the baseline value is $146-$481 per Kg U, adjusting for scaling: the values in the table are not adjusted however. The baseline value appear to have a disconnect as to how it relates to performance by Sugo, et al. (2001). There seems to be additional steps taken in the calculation which are not described. In order to maintain an even formulation between the bioorganics and the fibre, the quoted value for raw manufacture was used for an effective value.

In order to establish the quantity of uranium required for the capture of 1 kg of U, the best surface concentration for each of the materials used in Batch 2 were recorded in **Table 59**. This was decided because the it represented the most rigorous of the batch tests, without the interference of filter bags. The exception was garlic powder, which had a higher capture rate in the continuous flow experiment, and that value was used instead.

Since there is no formal markets for many of these materials, a search online for resources prepared to quote for the materials were made. The best price is quoted below. These are not firm guides, partly because these are not subject to any sort of competition, and partly because the price is not necessarily the materials as used. For example, the value for potato skin (£1.06 per kg) is based on a quotation for discards, which includes skin, wash starch, and offcuts, while the orange peel price came from a food fortification manufacturer and the grape skin price is for a product for home brewing fortification. These have industrial uses, and would be consequently greater than direct use, as there is a competition factor is these after preparations. That means these values are likely overestimates.

Using the measured surface concentration per gram, a total mass in tonnes required to produce 1 kg of U is calculated. Together with the price per kg of material, total cost for the 1 kg is predicted.

As can be seen from the table, this would mean that typical price per kilogram is £2 million per kilogram U, or 10 times that of the amidoxime based approach.

TABLE 59 SPECULATIVE PRICE OF URANIUM BASED ON BIOMASS NEEDED TO CAPTURE 1 KG OF URANIUM.

	U Surface Conc $mg.kg^{-1}$	Price per kg $£.kg^{-1}$	Kilotonne required for 1 kg U kt	Price per kg of Uranium M £	Source as of 31/01/24
Dried Kale (pH 5.8)	0.57	4.46	1.75	7.82	Soil Association
Garlic Powder (pH 5.2)	0.43	0.85 ($1.08)	2.33	1.98	Index Box
Orange Peel (pH 4.9)	0.47	£1.14 (120 INR)	2.13	2.43	Exporters India
Peanut shell (pH 6.1)	0.35	£0.05 (5.5 INR)	2.86	0.14	Shree Industries
Potato Skin (pH 6.1)	0.36	1.06	2.78	2.94	Soil Association
Red Grape (pH 4.3)	0.28	£9.41 ($12)	3.57	33.61	China Wholesale
Amidoxime Fibre	19800 (3300 with 6 reuses)	6900 ($8800)	0.05	0.35	(Sugo, et al., 2001; Schneider & Sachde, 2012)

Price as of 31/01/24, converted to £ by Google finance ($= £0.784 Rupee = £0.0095)

This was a rather surprising result, as the partition co-efficient (K_d) of the amidoximine doped polymers are quoted at 969.7 $g.L^{-1}$ and a capacity of 3.3 $mg.g^{-1}$, reuse of 6 times with a price of ~$8,800 per kg, per (Sugo, et al., 2001; Sugasaka, et al., 2006). Basing on the relation that if the K_d was up to 1000 times less efficient, then as long as the price was of a similar or smaller ratio lower, then there would be similar efficiencies. The samples selected had efficiencies between 2,000 and 17,000, so were expected to perform similarly. This does not resolve fully through to the results from the tests, with consequential impact that the ratio was generally an order of magnitude greater, except for peanut shell, which was 50% the cost per kilogram of U.

This can be partly atributed to three factors. Firstly, all the values for capture were conducted using relatively static tests, limiting potential maximums: even in the context of the continuous flow experiment, the reaction chambers would be flushed only every 10 hours: while the concentration was maintained, based on the ICP-MS results, this did cap the maximum potential flux, compared with

free water, such as in a open water, or even a desalination site. Furthermore, the modelling would indicate that the falling pH of the samples reduced the potential K_d, an secondary effect of the restricted oxygenation.

Secondly, the seawater used was the Irish near-shore water, as explained in Section 4.5.3, which are relatively depleted compared to those of open ocean water. Therefore the materials can be considered to be performing below their expected performance, again, limiting potential maximum.

These two together suggest that the performance is an underestimate, and a 50% improvement could be achieved simply by using general seawater concentrations (since it is 3 ppb, rather than the 2 of the tests), which was not applied to the amidoxime fibres. Another technical point is that the amidoxime fibres have a narrower window of operability, compared to the biomass: for example Wiechert, et al (2018) demonstrated that amidoxime fibres in brine (specifically the rejections from desalination processing) have only 2/3 the uptake maximum of those in seawater, an issue that does not occur in the broader spectrum sorbance of organics (Semblante, et al., 2018).

Finally, the costing is based on wholesaling price, rather than actual use: price may actually be lower if obtained directly. This is particularly true of the red grape, garlic, and kale, but is likely a factor in all other components. For example, a direct purchase of raw grapes are quoted at the same source as the skin at £6000 for a tonne, or 2/3 the price assuming that 1% of the mass is converted to skin, and the pulp is only able to be commericalised through other production techniques to match the increased processing cost.

As mentioned prior, these prices can be considered only indicative, since there is opportunity for other revenue not present with the prior technology, mitigated by other costs, but indicate that these organics are of a similar economic level to those of the high technology approach.

Considering the costings, only the peanut shell produced a more cost effective solution: it would be 50% that of the amidoxime used in 2001. This would be comparable to the performance of modern fibres, which can perform up to 6 $mg.g^{-1}$, slightly under twice that of the original fibres (Semblante, et al., 2018). Data is not available on the costings of these modern fibres. Assuming these are comparable, then the costing would be $150/kg U yellowcake, which is still greater than the current uranium price from mining, which recently (22/01/24) peaked at $105, a 10 year high, but is significantly below the current theshold of known viable terrestrial ores, which is capped at $300, and expected to be achieved in 80 years (NEA and IAEA, 2016).

A good avenue for further research is whether pre-treatment of the materials would reduce the cost: for example, amidoxime fibres are pre-treated with acids to prepare them to exchange (Cheng, et al.,

2019): no such testing occurred with the biomass. While the acid would be an addition expense, it may increase the performance, especially if, as hypothesised previously, the operational conditions of sorbance are at a slightly lower pH than their starting conditions, although that might push it towards unfavorable conditions faster, since higher acidity would limit the existing site availability, although it might open a number of new sites through fragmentation. This would be an important testing path going forward.

Future developments

One major consideration displayed from the modelling is that the particle surface area is a critical component: the size of the particles was defined by the need to carry out the work manually, and it is entirely concievable that increasing the surface area, by use of a mechanical means to reduce the volume, would increase the performance of the materials, as displayed by the modelling.

This would be greatly enhanced by successful BET measurements. The difficulties experienced attempting this element of practical work were beyond the capacity of the project focus, but it is possible to make these measurements, with some technology focus. This data would be critically informative to the modelling work, which previously relied on approximated data, rather than measured fundamental properties, and stand to validate the inputs to the models calculations.

However, using the model calculations at it's current level of development does allow some degree of testing of the impact of changes to surface area.

By modifying the surface radius to produce a similar density reading, it was possible to approximate the impact of this increase. It was found that a particle radius of 1600 nm would have comparable surface area per gram to that reported in Tavares, et al. (2021) and the consequential impact on potential site availability is listed in **Table 60**. This is a fairly crude approximation of the effect, since there are other factors involved, but can indicate the potential impact on the previously reported data.

TABLE 60 APPROXIMATIONS OF IMPACT OF DECREASING PARTICLE SIZE ON SURFACE AREA POTENTIAL

Particle radius	Log Area (m^2)	Carboxylic Site Density ($mol.g^{-1}$)	Polyphenolic Site Density ($mol.g^{-1}$)
20000	-11.8	2.62×10^{-07}	3.35×10^{-08}
10000	-14.4	5.24×10^{-07}	6.70×10^{-07}
5000	-15.0	1.05×10^{-06}	1.34×10^{-06}
1600	-16.0	3.27×10^{-06}	4.19×10^{-06}

Further to this potential change to the model, the improvements to the modelling developed over the research period have been able to grow the informative effects of altering the structure in the model: by allowing the expansion to the various multidentate interactions, we were able to display the significance to the overall sorption. The surface area model was expanded from a single input variable, to one that allows a greater range of factors to be investigated on the modelled material.

The comparison of these factors on a single structure is possible through the overlaying of outputs of the model together through an ancillary spreadsheet: however, the developments made to create the model responsitivity to carbonate concentrations would, with some further development, allow co-display natively: coupled with some work to allow the implementation of separate materials together (made possible through the surface activity variable) mean that in future, we would be able to model the combined effects and display them all both collectively, and summarily.

This would be especially valuable in the case of biomaterials, where there is substantial evidence in literature that materials maintain capacity over a range of pH, by having sites with different performance characteristics present (Parsons, et al., 2006). The majority of this work required is now implemented (with the two dominant surface structures, accounting for -90% of the total area) modeled, with only the tertary sites requiring characterisation data, and the ability to display in parallel.

Overall, the evidence gathered would be indicative that it is possible, and the potential of becoming economically viable against other forms of uranium capture from seawater exists, in the medium term, and with further research it may be possible to reduce costs further, to the point where it is

economically comparable to that of geological resources, if the quantificiation of the the secondary benefits, such as co-extractants and energy recovery proves viable.

Appendix 1 Batch 1

Batch 1 Key

Sample	Code
Potato Whole	PW
Potato skins	PS
Sweet potato Whole	SPW
Sweet potato Skin	SPS
Mange Tout	MT
Garlic Whole	GW
Coconut Butter	CN
Kale	K
Lemon	L
Sultana	S
Sultana Diced	SD
Grape Skin	GS
Grape Pulped	GP
Orange Skin	OS
Nectarine Skin	NS
Brussel Sprouts	B
Peanut Shell	PNS

Batch 1 ICP data

79167.22	45Sc	77Ar Cl	103Rh	209Bi	238U
	blank 8	10/07/2019 13:28:45			
1	1298.093	29	63042.84	44	16
2	1279.09	27	63749.74	25	10
3	1265.088	36	63031.76	42	20
x	1280.757	30.667	63274.78	37	15.333
s	16.565	4.726	411.366	10.44	5.033
%RSD	1.293	15.41	0.65	28.217	32.825
	0	10/07/2019 11:11:30			
1	1356.101	36	62649.13	26	8
2	1320.096	26	63739.67	30	6
3	1213.081	25	63455.69	23	6
x	1296.426	29	63281.5	26.333	6.667
s	74.39	6.083	565.755	3.512	1.155
%RSD	5.738	20.975	0.894	13.336	17.321
	0.1	10/07/2019 11:12:26			
1	1277.09	46	62594.76	24	7823.365
2	1298.093	27	63115.34	20	7775.324
3	1239.084	41	62247.38	23	7635.205
x	1271.422	38	62652.49	22.333	7744.631
s	29.91	9.849	436.848	2.082	97.763

%RSD		2.352	25.918	0.697	9.321	1.262
		0.3 10/07/2019 11:13:22				
	1	1344.099	32	64083.07	23	23598.59
	2	1290.092	34	62768.95	22	24073.83
	3	1209.08	29	63047.87	28	23925.44
x		1281.09	31.667	63299.97	24.333	23865.96
s		67.958	2.517	692.381	3.215	243.142
%RSD		5.305	7.947	1.094	13.21	1.019
		0.6 10/07/2019 11:14:21				
	1	1302.093	33	62267.52	32	46390.06
	2	1275.089	40	63020.68	16	46080.49
	3	1262.088	41	62387.34	19	46910.72
x		1279.757	38	62558.51	22.333	46460.43
s		20.407	4.359	404.709	8.505	419.564
%RSD		1.595	11.471	0.647	38.082	0.903
		1.0 10/07/2019 11:15:31				
	1	1325.097	40	64091.13	23	79167.22
	2	1282.09	32	62609.86	26	76750.62
	3	1224.082	36	62355.12	30	77720.82
x		1277.09	36	63018.7	26.333	77879.55
s		50.692	4	937.442	3.512	1216.09
%RSD		3.969	11.111	1.488	13.336	1.562
		2% wash 10/07/2019 11:16:49				
	1	3401.636	27	183.002	267.004	316.005
	2	3344.615	24	75	253.004	146.001
	3	3264.586	42	36	281.004	128.001
x		3336.946	31	98.001	267.004	196.669
s		68.846	9.644	76.152	14	103.739
%RSD		2.063	31.109	77.706	5.244	52.748
		PS1 SO 10/07/2019 11:18:33				
	1	2808.434	2884.458	331.006	123.001	754.031
	2	2399.317	3091.526	422.01	93	816.037
	3	2308.293	3366.623	370.008	91	762.032
x		2505.348	3114.202	374.341	102.334	777.367
s		266.397	241.881	45.656	17.926	33.727
%RSD		10.633	7.767	12.196	17.517	4.339
		PS2 SO 10/07/2019 11:19:37				
	1	3465.661	3750.774	52963.84	281.004	1108.068
	2	2670.392	3704.755	53384.29	304.005	1122.069
	3	2740.413	3522.682	53027.2	235.003	1184.077
x		2958.822	3659.404	53125.11	273.337	1138.071
s		440.329	120.619	226.679	35.134	40.453

%RSD		14.882	3.296	0.427	12.854	3.554
		GW1 SO	10/07/2019 11:20:41			
	1	9510.973	4662.195	55772.56	327.006	140.001
	2	8973.426	4464.096	55398.28	309.005	192.002
	3	8882.337	4378.054	56091.51	340.006	186.002
x		9122.245	4501.448	55754.12	325.339	172.668
s		339.714	145.707	346.983	15.568	28.449
%RSD		3.724	3.237	0.622	4.785	16.476
		GW2 SO	10/07/2019 11:22:17			
	1	8680.142	4623.175	62083.27	2000.22	18
	2	8067.578	4304.019	60355.69	1897.198	24
	3	8201.698	4252.995	60959.7	1806.179	46
x		8316.473	4393.396	61132.89	1901.199	29.333
s		322.007	200.623	876.712	97.082	14.742
%RSD		3.872	4.566	1.434	5.106	50.258
		SPS1 SO	10/07/2019 11:23:33			
	1	2977.488	5266.525	58143.34	357.007	222.003
	2	2685.397	4922.332	56278.66	298.005	274.004
	3	2658.389	5059.408	57190.33	284.004	218.003
x		2773.758	5082.755	57204.11	313.005	238.003
s		176.951	173.28	932.416	38.744	31.242
%RSD		6.379	3.409	1.63	12.378	13.127
		SPS2 SO	10/07/2019 11:24:45			
	1	2285.287	1681.155	365.007	2099.242	378.008
	2	2201.267	1554.133	286.005	2136.251	418.01
	3	2097.242	1453.116	283.004	2128.249	352.007
x		2194.599	1562.802	311.339	2121.247	382.675
s		94.2	114.267	46.503	19.472	33.248
%RSD		4.292	7.312	14.936	0.918	8.688
		SNS1 SO	10/07/2019 11:25:53			
	1	4022.89	3899.836	46943.89	311.005	1898.198
	2	3506.676	3812.799	46889.61	329.006	1940.207
	3	3345.615	3772.783	45871.44	314.005	2012.223
x		3625.061	3828.473	46568.32	318.006	1950.209
s		353.817	64.961	604.122	9.644	57.667
%RSD		9.76	1.697	1.297	3.033	2.957
		SNS2 SO	10/07/2019 11:27:09			
	1	3382.629	5691.781	58460.37	193.002	1138.071
	2	3148.545	5212.494	56897.5	216.003	1228.083
	3	2990.492	5217.497	56554.37	240.003	1152.073
x		3173.889	5373.924	57304.08	216.336	1172.742
s		197.293	275.284	1015.967	23.502	48.435

%RSD		6.216	5.123	1.773	10.864	4.13
		CN1 SO	10/07/2019 11:28:17			
	1	2411.32	5759.824	52343.26	263.004	2098.242
	2	2286.287	5466.643	52668.13	265.004	1798.178
	3	2173.26	5319.556	51786.08	262.004	1380.105
x		2290.289	5515.341	52265.82	263.337	1758.842
s		119.08	224.138	446.092	1.528	360.681
%RSD		5.199	4.064	0.854	0.58	20.507
		CN2 SO	10/07/2019 11:29:18			
	1	2374.31	5752.82	69718.31	169.002	392.008
	2	2258.28	5300.545	67560.11	160.001	368.007
	3	2196.265	5057.406	68685.5	138.001	324.006
x		2276.285	5370.257	68654.64	155.668	361.341
s		90.378	352.909	1079.432	15.948	34.488
%RSD		3.97	6.572	1.572	10.245	9.544
		0.3	10/07/2019 11:30:53			
	1	2125.248	766.032	67370.71	84	24665.42
	2	1965.212	677.025	68192.81	70	25283.11
	3	1894.197	520.015	69075.44	58	25666.18
x		1994.886	654.357	68212.99	70.667	25204.9
s		118.349	124.565	852.54	13.013	504.945
%RSD		5.933	19.036	1.25	18.414	2.003
		2% wash 1	10/07/2019 11:32:22			
	1	4350.041	396.009	294.005	491.013	236.003
	2	4278.006	351.007	242.003	398.009	178.002
	3	4199.97	335.006	246.003	518.015	232.003
x		4276.006	360.674	260.67	469.012	215.336
s		75.055	31.629	28.938	62.956	32.394
%RSD		1.755	8.77	11.101	13.423	15.044
		blank	10/07/2019 11:33:23			
	1	1849.188	228.003	10	6	0
	2	1752.169	194.002	9	6	10
	3	1696.158	184.002	7	4	2
x		1765.838	202.002	8.667	5.333	4
s		77.425	23.066	1.528	1.155	5.292
%RSD		4.385	11.419	17.625	21.651	132.288
		PS1 AS	10/07/2019 11:39:13			
	1	1702.159	1012.056	65049.9	1831.184	1126.07
	2	1588.139	1041.06	63835.34	1784.175	938.048
	3	1672.154	1083.065	62958.25	1807.18	988.054
x		1654.151	1045.393	63947.83	1807.513	1017.391
s		59.104	35.702	1050.352	23.506	97.383

%RSD		3.573	3.415	1.643	1.3	9.572
		PS2 AS	10/07/2019 11:40:22			
	1	1664.152	1268.088	65630.05	1009.056	1324.096
	2	1560.134	1244.085	66001.73	938.048	1244.085
	3	1542.131	1241.085	66472.14	1122.069	1124.07
x		1588.806	1251.086	66034.64	1023.058	1230.75
s		65.87	14.801	422.006	92.806	100.678
%RSD		4.146	1.183	0.639	9.071	8.18
		GW1 AS	10/07/2019 11:41:23			
	1	3778.785	1190.078	67672.95	1699.159	574.018
	2	3588.708	1132.071	66427.81	1633.147	562.017
	3	3554.695	1100.067	67336.46	1637.147	514.015
x		3640.729	1140.738	67145.74	1656.484	550.017
s		120.763	45.627	644.104	37.011	31.751
%RSD		3.317	4	0.959	2.234	5.773
		GW2 AS	10/07/2019 11:42:54			
	1	3477.665	1333.098	73469.68	6155.083	34
	2	3619.72	1285.091	72921.3	6165.09	34
	3	3524.683	1282.09	73049.32	6602.397	42
x		3540.69	1300.093	73146.77	6307.523	36.667
s		72.368	28.622	286.888	255.417	4.619
%RSD		2.044	2.202	0.392	4.049	12.597
		SPS1 AS	10/07/2019 11:43:57			
	1	2352.304	456.011	71360.99	1776.174	504.014
	2	2264.282	412.009	70821.8	1608.142	502.014
	3	2179.261	368.007	72385.04	1620.144	470.012
x		2265.282	412.009	71522.61	1668.153	492.013
s		86.526	44.002	794.053	93.74	19.08
%RSD		3.82	10.68	1.11	5.619	3.878
		SPS2 AS	10/07/2019 11:45:02			
	1	3198.563	4904.323	53054.36	267.004	216.003
	2	2672.393	4912.327	53468.78	236.003	298.005
	3	2613.376	4820.278	51731.77	236.003	202.002
x		2828.11	4878.976	52751.64	246.337	238.67
s		322.175	50.991	907.21	17.898	51.86
%RSD		11.392	1.045	1.72	7.266	21.729
		SNS1 AS	10/07/2019 11:46:37			
	1	2145.253	1702.159	70227.21	2851.447	1328.097
	2	2049.231	1541.131	69976.29	2706.403	1360.102
	3	2087.24	1569.135	70007.52	2652.387	1238.084
x		2093.908	1604.142	70070.34	2736.746	1308.761
s		48.357	86.033	136.748	102.941	63.265

%RSD		2.309	5.363	0.195	3.761	4.834
		SNS2 AS	10/07/2019 11:47:41			
	1	1902.199	1233.084	70455.97	1065.062	762.032
	2	1802.179	1201.079	69225.57	1087.065	790.034
	3	1737.166	1192.078	69163.1	1102.067	814.036
x		1813.848	1208.747	69614.88	1084.731	788.701
s		83.133	21.551	729.075	18.612	26.028
%RSD		4.583	1.783	1.047	1.716	3.3
		CN1 AS	10/07/2019 11:48:44			
	1	2002.22	1580.137	73064.44	2028.226	2770.422
	2	1866.191	1544.131	71087.86	1822.183	2652.387
	3	1927.204	1520.127	70834.9	2023.225	2878.456
x		1931.872	1548.132	71662.4	1957.878	2767.088
s		68.134	30.204	1220.772	117.542	113.071
%RSD		3.527	1.951	1.704	6.004	4.086
		CN2 AS	10/07/2019 11:49:45			
	1	2012.223	1668.153	71128.17	2492.342	3062.516
	2	1959.211	1636.147	71390.22	2339.301	3040.508
	3	1867.192	1559.134	70476.12	2170.259	3062.516
x		1946.209	1621.145	70998.17	2333.967	3055.18
s		73.385	56.037	470.708	161.108	12.706
%RSD		3.771	3.457	0.663	6.903	0.416
		1.0	10/07/2019 11:50:51			
	1	1859.19	458.012	72425.35	815.037	86006.93
	2	1846.187	385.008	72298.35	701.027	85914.06
	3	1850.188	322.006	72980.77	737.03	86846.86
x		1851.855	388.342	72568.16	751.031	86255.95
s		6.66	68.064	362.931	58.28	513.845
%RSD		0.36	17.527	0.5	7.76	0.596
		2% wash 2	10/07/2019 11:56:21			
	1	4078.915	99.001	807.036	615.021	1460.117
	2	4357.044	93	732.029	539.016	1142.072
	3	4297.015	98.001	500.014	567.018	992.054
x		4244.325	96.667	679.693	573.685	1198.081
s		146.36	3.215	160.062	38.439	239.005
%RSD		3.448	3.325	23.549	6.7	19.949
		blank	10/07/2019 11:57:23			
	1	1652.15	94	31	2	28
	2	1635.147	71	23	8	10
	3	1634.147	76	15	1	4
x		1640.481	80.334	23	3.667	14
s		10.118	12.097	8	3.786	12.49

%RSD		0.617	15.058	34.783	103.253	89.214
		PS1 MD	10/07/2019 11:58:32			
	1	2425.324	654.024	72833.6	2817.436	5303.547
	2	2280.286	691.026	70996.15	2862.451	5103.432
	3	2351.304	712.028	70621.24	2708.403	5101.431
x		2352.305	685.693	71483.66	2796.097	5169.47
s		72.524	29.368	1184.01	79.21	116.118
%RSD		3.083	4.283	1.656	2.833	2.246
		PS2 MD	10/07/2019 11:59:34			
	1	2092.241	481.013	84206.19	4451.089	9176.629
	2	1919.203	510.014	83912.49	4508.118	9008.461
	3	2006.221	446.011	84317.21	4387.058	8948.402
x		2005.888	479.013	84145.3	4448.755	9044.497
s		86.52	32.049	209.118	60.563	118.304
%RSD		4.313	6.691	0.249	1.361	1.308
		GW1 MD	10/07/2019 12:00:36			
	1	3725.763	732.029	68956.54	3318.606	7054.736
	2	3778.785	757.032	66959.69	3191.56	7100.772
	3	3558.696	804.036	70339.07	3476.665	7294.926
x		3687.748	764.366	68751.77	3328.943	7150.145
s		114.864	36.559	1698.968	142.833	127.479
%RSD		3.115	4.783	2.471	4.291	1.783
		GW2 MD	10/07/2019 12:02:23			
	1	3475.664	737.03	71389.21	6351.218	4859.298
	2	3310.603	743.03	70249.38	6207.118	4513.12
	3	3390.632	799.035	69996.44	6206.118	4829.282
x		3392.3	759.698	70545.01	6254.818	4733.9
s		82.543	34.198	741.955	83.486	191.789
%RSD		2.433	4.502	1.052	1.335	4.051
		MTC	10/07/2019 12:03:26			
	1	6538.35	252.003	76161.7	3823.804	358.007
	2	6718.482	208.002	75530.47	3816.801	320.006
	3	7261.899	184.002	75658.53	4021.89	264.004
x		6839.577	214.669	75783.57	3887.498	314.005
s		376.668	34.488	333.677	116.439	47.288
%RSD		5.507	16.065	0.44	2.995	15.06
		PSC	10/07/2019 12:04:25			
	1	5780.837	195.002	78462.14	103208.6	1272.089
	2	5737.81	219.003	78254.36	103213.6	1132.071
	3	5841.876	213.003	79895.55	104238.2	1196.079
x		5786.841	209.002	78870.68	103553.5	1200.079
s		52.292	12.49	893.616	593.013	70.095

%RSD		0.904	5.976	1.133	0.573	5.841
		PNS1 MD	10/07/2019 12:05:34			
	1	11588.38	774.033	56085.48	8274.764	11835.7
	2	11625.43	779.033	55529.08	7879.413	11855.73
	3	11474.24	811.036	56431.61	7988.508	12005.92
x		11562.68	788.034	56015.39	8047.562	11899.12
s		78.804	20.077	455.33	204.184	93.038
%RSD		0.682	2.548	0.813	2.537	0.782
		PNS2 MD	10/07/2019 12:06:34			
	1	15474.16	620.021	73488.84	4254.996	16420.82
	2	14918.23	596.02	73569.49	4206.973	15867.84
	3	14909.22	594.019	72845.69	4333.032	16200.42
x		15100.54	603.353	73301.34	4265	16163.03
s		323.599	14.469	396.656	63.622	278.381
%RSD		2.143	2.398	0.541	1.492	1.722
		LC	10/07/2019 12:07:36			
	1	3997.879	152.001	60879.17	8173.673	568.018
	2	4148.947	111.001	59412.51	8131.635	414.009
	3	4017.888	116.001	59360.17	8205.702	458.012
x		4054.904	126.334	59883.95	8170.337	480.013
s		82.055	22.368	862.281	37.146	79.326
%RSD		2.024	17.706	1.44	0.455	16.526
		SPW C	10/07/2019 12:08:33			
	1	4731.231	127.001	59824.2	2578.366	180.002
	2	4383.056	91	58256.06	2316.295	176.002
	3	4562.144	108.001	59609.79	2277.285	182.002
x		4558.81	108.667	59230.02	2390.649	179.335
s		174.111	18.009	850.256	163.734	3.055
%RSD		3.819	16.573	1.436	6.849	1.704
		0.3	10/07/2019 12:09:40			
	1	1894.197	84	69412.99	328.006	26326.06
	2	1866.191	66	68032.62	314.005	26733.25
	3	1636.147	94	68778.19	261.004	26602.87
x		1798.845	81.334	68741.27	301.005	26554.06
s		141.595	14.189	690.929	35.342	207.934
%RSD		7.871	17.446	1.005	11.741	0.783
		2% wash 3	10/07/2019 12:10:42			
	1	4273.004	73	784.034	597.02	970.052
	2	3995.878	86	327.006	516.015	722.029
	3	4033.895	75	262.004	594.019	420.01
x		4100.926	78	457.681	569.018	704.03
s		150.232	7	284.492	45.927	275.462

%RSD		3.663	8.974	62.159	8.071	39.127
		blank 1	10/07/2019 12:11:54			
	1	1636.147	51	12	8	2
	2	1529.129	75	15	8	6
	3	1566.135	73	23	6	8
x		1577.137	66.334	16.667	7.333	5.333
s		54.351	13.317	5.686	1.155	3.055
%RSD		3.446	20.075	34.117	15.746	57.282
		SGS1 SO	10/07/2019 12:13:05			
	1	2998.494	4512.119	67947.99	615.021	42
	2	2741.413	4762.247	69050.24	585.019	40
	3	2838.443	4984.366	70289.69	584.019	52
x		2859.45	4752.911	69095.97	594.686	44.667
s		129.822	236.262	1171.521	17.617	6.429
%RSD		4.54	4.971	1.695	2.962	14.394
		SGS2 SO	10/07/2019 12:14:15			
	1	2884.458	1127.07	83130.36	21130.53	1788.176
	2	2728.409	960.051	82687.34	21633.71	1808.18
	3	2755.418	851.04	82570.29	21451.28	1796.177
x		2789.428	979.387	82796	21405.17	1797.511
s		83.398	139.027	295.421	254.739	10.068
%RSD		2.99	14.195	0.357	1.19	0.56
		SNS1 SO	10/07/2019 12:15:17			
	1	2705.403	2000.22	66237.43	417.01	310.005
	2	2457.332	1996.219	66349.24	366.007	320.006
	3	2559.36	1892.197	66682.67	299.005	366.007
x		2574.032	1962.879	66423.11	360.674	332.006
s		124.684	61.245	231.629	59.183	29.867
%RSD		4.844	3.12	0.349	16.409	8.996
		SNS2 SO	10/07/2019 12:16:35			
	1	2654.387	1856.19	120198.4	105.001	386.008
	2	2524.35	1841.186	120858.1	133.001	360.007
	3	2499.343	1812.181	120018	109.001	366.007
x		2559.36	1836.519	120358.2	115.667	370.674
s		83.24	22.373	442.213	15.144	13.614
%RSD		3.252	1.218	0.367	13.093	3.673
		SBS1 SO	10/07/2019 12:17:37			
	1	2495.342	2096.242	65433.64	170.002	672.025
	2	2240.276	2046.23	64788.04	196.002	672.025
	3	2278.285	1995.219	64315.71	180.002	624.021
x		2337.968	2045.897	64845.8	182.002	656.024
s		137.609	50.512	561.201	13.115	27.715

%RSD		5.886	2.469	0.865	7.206	4.225
		SBS2 SO	10/07/2019 12:18:41			
	1	2247.278	2535.354	71575.66	163.001	862.041
	2	2267.283	2472.336	71553.49	151.001	898.044
	3	2278.285	2406.318	71072.74	123.001	780.033
x		2264.282	2471.336	71400.63	145.668	846.706
s		15.72	64.523	284.178	20.527	60.481
%RSD		0.694	2.611	0.398	14.091	7.143
		SWO1 SO	10/07/2019 12:19:37			
	1	2338.301	5884.904	62068.16	232.003	154.001
	2	2177.261	5532.683	62246.38	231.003	118.001
	3	2105.244	5610.731	62581.67	202.002	144.001
x		2206.935	5676.106	62298.74	221.669	138.668
s		119.329	184.987	260.725	17.04	18.583
%RSD		5.407	3.259	0.419	7.687	13.401
		SWO2 SO	10/07/2019 12:20:42			
	1	2311.294	7670.234	61331.19	185.002	3230.574
	2	2145.253	7368.985	60307.37	157.001	2410.32
	3	2189.264	7115.784	60290.26	176.002	2500.344
x		2215.27	7385.001	60642.94	172.668	2713.746
s		86.021	277.572	596.101	14.295	449.844
%RSD		3.883	3.759	0.983	8.279	16.576
		SWT1 SO	10/07/2019 12:21:41			
	1	2106.244	6076.03	63603.72	336.006	1112.068
	2	2057.233	5546.692	63082.11	266.004	1004.055
	3	1952.21	5337.566	63296.59	274.004	1128.07
x		2038.562	5653.429	63327.47	292.005	1081.398
s		78.696	380.627	262.176	38.316	67.457
%RSD		3.86	6.733	0.414	13.122	6.238
		SWT2 SO	10/07/2019 12:22:43			
	1	2188.263	6741.499	60000.35	118.001	3552.694
	2	2094.241	6216.124	60821.78	143.001	3086.524
	3	2046.23	6150.08	61033.19	127.001	2366.308
x		2109.578	6369.234	60618.44	129.334	3001.842
s		72.248	324.077	545.62	12.662	597.709
%RSD		3.425	5.088	0.9	9.79	19.911
		0.3	10/07/2019 12:23:47			
	1	2161.257	1092.066	71567.6	619.021	31099.1
	2	2080.238	752.031	72876.94	590.019	29138.62
	3	2026.226	592.019	72562.44	526.015	28759.42

x		2089.24	812.039	72335.66	578.352	29665.72
s		67.964	255.367	683.495	47.588	1255.746
%RSD		3.253	31.448	0.945	8.228	4.233
		2% wash 4	10/07/2019 12:24:57			
	1	4727.229	385.008	697.027	1127.07	896.044
	2	4470.099	350.007	488.013	980.053	630.022
	3	4425.077	367.007	473.012	958.05	638.022
x		4540.801	367.341	552.684	1021.724	721.363
s		163.013	17.503	125.229	91.893	151.331
%RSD		3.59	4.765	22.658	8.994	20.979
		blank 2	10/07/2019 12:25:56			
	1	1833.185	223.003	127.001	20	22
	2	1782.175	223.003	136.001	12	30
	3	1738.166	214.003	116.001	11	8
x		1784.508	220.003	126.334	14.333	20
s		47.552	5.196	10.017	4.933	11.136
%RSD		2.665	2.362	7.929	34.415	55.678
		SGS1 AS	10/07/2019 12:27:07			
	1	2722.408	2477.338	69573.21	12558.67	1066.063
	2	2753.417	2603.373	69840.25	12546.65	1130.07
	3	2570.363	2654.387	69585.3	12834.05	1098.066
x		2682.063	2578.366	69666.25	12646.46	1098.066
s		97.969	91.135	150.804	162.573	32.004
%RSD		3.653	3.535	0.216	1.286	2.915
		SGS2 AS	10/07/2019 12:28:01			
	1	2810.434	2617.377	52583.64	5350.574	628.022
	2	2712.405	2432.325	52021.42	5164.467	666.024
	3	2523.35	2495.342	52046.56	5207.491	596.02
x		2682.063	2515.015	52217.21	5240.844	630.022
s		145.927	94.081	317.589	97.434	35.045
%RSD		5.441	3.741	0.608	1.859	5.563
		SNS1 AS	10/07/2019 12:28:55			
	1	2912.467	587.019	75682.73	1982.216	5295.542
	2	2661.39	448.011	75505.26	1745.168	5337.566
	3	2559.36	344.007	75383.25	1812.181	5329.562
x		2711.072	459.679	75523.75	1846.521	5320.89
s		181.72	121.926	150.59	122.199	22.314
%RSD		6.703	26.524	0.199	6.618	0.419
		SNS2 AS	10/07/2019 12:29:50			
	1	4881.31	300.005	72900.13	1945.208	6840.573
	2	4864.301	325.006	73390.04	1677.155	6880.603
	3	4766.249	271.004	74285.27	1528.128	7166.824

x		4837.287	298.672	73525.15	1716.83	6962.667
s		62.105	27.026	702.386	211.352	177.935
%RSD		1.284	9.049	0.955	12.311	2.556
		SB1 AS	10/07/2019 12:31:07			
	1	2464.334	184.002	66342.19	143.001	1582.138
	2	2281.286	183.002	66294.85	118.001	1480.121
	3	2247.278	151.001	67289.11	144.001	1724.164
x		2330.966	172.668	66642.05	135.001	1595.474
s		116.745	18.771	560.872	14.731	122.567
%RSD		5.008	10.871	0.842	10.912	7.682
		SB2 AS	10/07/2019 12:32:04			
	1	2632.381	149.001	54584.38	283.004	6174.096
	2	2571.364	146.001	53945.58	230.003	5729.805
	3	2573.364	127.001	53343.04	239.003	5373.588
x		2592.37	140.668	53957.67	250.67	5759.163
s		34.665	11.931	620.756	28.362	401.061
%RSD		1.337	8.481	1.15	11.314	6.964
		SWO1 AS	10/07/2019 12:32:59			
	1	1874.193	1209.08	63336.87	6395.249	5719.799
	2	1860.19	1209.08	63045.86	6029.999	5181.476
	3	1867.192	1204.08	63228.12	5863.891	4659.194
x		1867.192	1207.414	63203.62	6096.38	5186.823
s		7.001	2.887	147.045	271.827	530.323
%RSD		0.375	0.239	0.233	4.459	10.224
		SWO2 AS	10/07/2019 12:33:55			
	1	1987.217	1750.169	75404.43	5670.768	3380.628
	2	1929.205	1745.168	74467.76	5620.737	3468.662
	3	1876.194	1646.149	74207.64	5408.608	3396.634
x		1930.872	1713.828	74693.28	5566.704	3415.308
s		55.531	58.665	629.46	139.182	46.893
%RSD		2.876	3.423	0.843	2.5	1.373
		SWT1 AS	10/07/2019 12:35:40			
	1	2117.247	1829.184	75777.51	3401.636	3046.51
	2	1497.123	1193.078	44499.65	1889.196	1974.214
	3	763.032	420.01	824.037	31	14
x		1459.134	1147.424	40367.07	1773.944	1678.242
s		677.906	705.696	37647.24	1688.271	1537.768
%RSD		46.459	61.503	93.262	95.17	91.63
		SWT2 AS	10/07/2019 12:36:37			
	1	1964.212	1445.115	72055.43	3946.857	2840.444
	2	1857.19	1506.125	70191.94	3687.748	2828.44
	3	1872.193	1518.127	72211.66	3615.719	2956.481

x		1897.865	1489.789	71486.35	3750.108	2875.121
s		57.946	39.151	1123.708	174.154	70.714
%RSD		3.053	2.628	1.572	4.644	2.46
		0.6 10/07/2019 12:37:43				
	1	2050.231	313.005	74043.31	1994.219	50956.41
	2	1929.205	333.006	74303.42	1847.188	51006.69
	3	1871.193	303.005	73489.85	1796.177	51048.93
x		1950.209	316.339	73945.53	1879.195	51004.01
s		91.349	15.276	415.508	102.827	46.317
%RSD		4.684	4.829	0.562	5.472	0.091
		2% wash 5 10/07/2019 12:38:45				
	1	4533.13	215.003	550.017	3487.669	656.024
	2	4784.259	206.002	589.019	3134.54	682.026
	3	4577.152	200.002	428.01	3179.556	564.018
x		4631.514	207.002	522.349	3267.255	634.022
s		134.1	7.55	83.995	192.206	62.004
%RSD		2.895	3.647	16.08	5.883	9.78
		blank 4 10/07/2019 12:39:42				
	1	1795.177	138.001	77	15	12
	2	1747.168	151.001	83	10	8
	3	1711.161	118.001	90	8	24
x		1751.169	135.668	83.334	11	14.667
s		42.151	16.624	6.506	3.606	8.327
%RSD		2.407	12.253	7.808	32.778	56.773
		SGS1 MD 10/07/2019 12:40:44				
	1	4893.317	414.009	62207.11	28452.46	17330.5
	2	4894.317	394.009	65657.25	29159.69	17699.21
	3	4711.22	439.011	64424.47	29181.76	18017.84
x		4832.951	415.676	64096.28	28931.3	17682.52
s		105.423	22.547	1748.326	414.841	343.971
%RSD		2.181	5.424	2.728	1.434	1.945
		SGS2 MD 10/07/2019 12:41:44				
	1	4145.945	335.006	62823.33	18407.62	16070.19
	2	4102.926	348.007	67828.1	19924.81	17346.53
	3	4167.955	341.006	66692.74	19598.1	17669.15
x		4138.942	341.34	65781.39	19310.18	17028.63
s		33.076	6.507	2623.901	798.527	845.559
%RSD		0.799	1.906	3.989	4.135	4.966
		SNS1 MD 10/07/2019 12:42:41				
	1	2716.406	2675.394	65201.99	1033.059	3108.531
	2	2555.359	2845.445	65452.78	867.041	2888.459
	3	2535.354	2971.486	65631.06	784.034	2778.425

x		2602.373	2830.775	65428.61	894.711	2925.138
s		99.261	148.59	215.554	126.797	168.082
%RSD		3.814	5.249	0.329	14.172	5.746
		SNS2 MD	10/07/2019 12:43:37			
	1	2651.387	2372.309	52872.31	280.004	1902.199
	2	2616.376	2299.291	53312.87	286.005	1864.191
	3	2443.328	2319.296	54139.73	242.003	1980.216
x		2570.364	2330.299	53441.64	269.337	1915.535
s		111.4	37.732	643.451	23.861	59.151
%RSD		4.334	1.619	1.204	8.859	3.088
		SBS1 MD	10/07/2019 12:44:39			
	1	2974.487	1465.118	56175.03	1058.062	2406.318
	2	2924.47	1342.099	55757.47	966.051	2462.333
	3	2802.432	1414.11	55353.01	1100.067	2274.284
x		2900.463	1407.109	55761.83	1041.393	2380.979
s		88.504	61.808	411.027	68.545	96.551
%RSD		3.051	4.393	0.737	6.582	4.055
		SBS2 MD	10/07/2019 12:45:51			
	1	2364.307	359.007	67296.16	746.031	348.007
	2	2341.302	281.004	66042.02	669.025	326.006
	3	2211.269	251.003	66619.21	639.022	270.004
x		2305.626	297.005	66652.46	684.693	314.672
s		82.521	55.751	627.735	55.198	40.217
%RSD		3.579	18.771	0.942	8.062	12.781
		SWO1 MD	10/07/2019 12:46:48			
	1	1916.202	1421.111	69207.43	17589	2828.44
	2	1953.21	1478.12	68044.71	17599.02	2876.455
	3	1835.185	1493.123	69777.77	17935.68	2898.462
x		1901.532	1464.118	69009.97	17707.9	2867.786
s		60.364	37.993	883.244	197.325	35.807
%RSD		3.175	2.595	1.28	1.114	1.249
		SWO2 MD	10/07/2019 12:47:48			
	1	11235.94	11251.96	52642.98	19130.11	18973.78
	2	10910.54	10624.2	52494.12	18849.52	19114.07
	3	10800.41	10286.82	52265.81	18710.23	18763.34
x		10982.3	10720.99	52467.64	18896.62	18950.4
s		226.457	489.797	189.973	213.862	176.53
%RSD		2.062	4.569	0.362	1.132	0.932
		SWT1 MD	10/07/2019 12:48:45			
	1	2132.25	3765.78	50441.55	2027.226	5069.413
	2	2092.241	3247.58	52219.55	2007.222	4739.235

	3	1999.22	2922.47	51360.68	1925.204	4861.299
x		2074.57	3311.943	51340.59	1986.551	4889.983
s		68.253	425.323	889.169	54.061	166.947
%RSD		3.29	12.842	1.732	2.721	3.414
		SWT2 MD 10/07/2019 12:49:45				
	1	2887.459	9747.223	56009.01	17119.1	16821.55
	2	2818.437	9789.268	56045.23	17334.51	16947.78
	3	2791.429	9553.017	56232.38	17515.86	16490.94
x		2832.441	9696.502	56095.54	17323.16	16753.43
s		49.523	126.028	119.884	198.621	235.915
%RSD		1.748	1.3	0.214	1.147	1.408
		SLS1 SO 10/07/2019 12:50:43				
	1	3272.589	3116.534	44093.68	425.01	474.012
	2	2804.432	2590.369	44128.85	338.006	438.011
	3	2799.431	2199.266	43152.17	325.006	400.009
x		2958.818	2635.39	43791.57	362.674	437.344
s		271.746	460.288	554.008	54.374	37.006
%RSD		9.184	17.466	1.265	14.993	8.462
		NC 10/07/2019 12:51:42				
	1	3594.711	587.019	79961.12	2038.228	132.001
	2	4104.927	436.01	75981.2	1896.198	122.001
	3	4007.883	425.01	78955.39	1855.189	92
x		3902.507	482.68	78299.24	1929.872	115.334
s		270.94	90.528	2069.501	96.054	20.817
%RSD		6.943	18.755	2.643	4.977	18.049
		KC 10/07/2019 12:52:41				
	1	2849.447	304.005	76326.07	2434.326	102.001
	2	2862.451	293.005	75027.33	2431.325	92
	3	2840.444	264.004	76451.12	2592.37	124.001
x		2850.78	287.005	75934.84	2486.007	106.001
s		11.064	20.665	788.41	92.125	16.371
%RSD		0.388	7.2	1.038	3.706	15.444
		SC 10/07/2019 12:53:48				
	1	19626.16	224.003	143959.9	14117.95	924.047
	2	18698.21	222.003	146516.3	14394.39	938.048
	3	19550	199.002	146312	14507.57	948.049
x		19291.46	215.003	145596	14339.97	936.715
s		515.177	13.893	1420.627	200.426	12.057
%RSD		2.67	6.462	0.976	1.398	1.287
		PEC 10/07/2019 12:55:36				
	1	11219.92	273.004	76485.4	6319.195	4453.09

	2	11114.79	279.004	76893.83	6335.207	4321.027
	3	10922.56	268.004	76426.91	6396.249	4473.1
x		11085.76	273.337	76602.05	6350.217	4415.739
s		150.792	5.508	254.374	40.661	82.631
%RSD		1.36	2.015	0.332	0.64	1.871
		GPC 10/07/2019 12:56:30				
	1	3239.577	157.001	73582.59	6488.315	180.002
	2	2899.462	161.001	72545.31	6047.011	152.001
	3	2995.493	137.001	75171.51	6131.067	168.002
x		3044.844	151.668	73766.47	6222.131	166.668
s		175.346	12.858	1322.724	234.322	14.048
%RSD		5.759	8.478	1.793	3.766	8.429
		PWC 10/07/2019 12:57:28				
	1	4549.138	121.001	72972.71	3388.631	44
	2	4532.129	125.001	73785.22	3368.624	48
	3	4703.216	122.001	76453.13	3285.594	42
x		4594.828	122.667	74403.69	3347.616	44.667
s		94.252	2.082	1820.774	54.637	3.055
%RSD		2.051	1.697	2.447	1.632	6.84
		OC 10/07/2019 12:58:30				
	1	6439.28	84	76278.68	12014.93	28
	2	6806.547	104.001	75731.13	12281.29	40
	3	5642.751	93	76118.34	12507.6	34
x		6296.193	93.667	76042.72	12267.94	34
s		594.946	10.017	281.5	246.603	6
%RSD		9.449	10.694	0.37	2.01	17.647
		GWC 10/07/2019 12:59:25				
	1	6607.4	129.001	71631.1	63523.16	130.001
	2	7057.739	141.001	70196.98	62691.42	156.001
	3	7194.846	146.001	72956.58	63946.11	140.001
x		6953.328	138.668	71594.88	63386.9	142.001
s		307.326	8.737	1380.156	638.349	13.115
%RSD		4.42	6.301	1.928	1.007	9.236
		SPSC 10/07/2019 13:00:23				
	1	14660.81	197.002	71168.49	25926.92	2506.345
	2	13185.56	171.002	70253.41	22707.32	2526.351
	3	12994.28	158.001	71750.03	20879.95	2462.333
x		13613.55	175.335	71057.31	23171.4	2498.343
s		911.985	19.858	754.479	2555.287	32.75
%RSD		6.699	11.326	1.062	11.028	1.311
		0.3 10/07/2019 13:01:26				
	1	2635.382	116.001	68978.7	900.045	26304

	2	2482.339	111.001	69487.56	584.019	27014.08
	3	2349.304	114.001	69782.81	457.011	26410.31
x		2489.008	113.667	69416.36	647.025	26576.13
s		143.156	2.517	406.752	228.138	382.982
%RSD		5.752	2.214	0.586	35.26	1.441
		2% wash 7	10/07/2019 13:02:26			
	1	4822.279	112.001	396.009	1963.212	496.014
	2	4598.163	102.001	230.003	2001.22	428.01
	3	4560.143	125.001	153.001	1885.195	302.005
x		4660.195	113.001	259.671	1949.876	408.676
s		141.65	11.533	124.191	59.151	98.439
%RSD		3.04	10.206	47.826	3.034	24.087
		blank 6	10/07/2019 13:03:33			
	1	2115.246	86	27	37	0
	2	2105.244	77	44	36	6
	3	2024.225	77	45	45	8
x		2081.572	80	38.667	39.333	4.667
s		49.915	5.196	10.116	4.933	4.163
%RSD		2.398	6.495	26.162	12.541	89.214
		SOS1 AS	10/07/2019 13:05:17			
	1	2602.372	79	56386.33	566.018	1340.099
	2	2440.327	93	56588.58	548.017	1238.084
	3	2521.35	90	55597.49	538.016	1270.089
x		2521.35	87.334	56190.8	550.683	1282.757
s		81.022	7.371	523.676	14.19	52.174
%RSD		3.213	8.44	0.932	2.577	4.067
		SOS2 AS	10/07/2019 13:06:16			
	1	2653.387	127.001	69511.74	507.014	338.006
	2	2520.349	121.001	69974.27	457.011	358.007
	3	2509.346	122.001	69637.7	440.011	348.007
x		2561.028	123.334	69707.9	468.012	348.007
s		80.175	3.215	239.122	34.83	10
%RSD		3.131	2.606	0.343	7.442	2.874
		SPW 1 AS	10/07/2019 13:07:18			
	1	2281.286	962.051	69778.78	1078.064	870.042
	2	2289.288	1027.058	70463.02	1125.07	894.044
	3	2305.292	1130.07	70170.78	1200.079	934.048
x		2291.956	1039.726	70137.53	1134.404	899.378
s		12.223	84.723	343.333	61.541	32.335
%RSD		0.533	8.149	0.49	5.425	3.595
		SPW2 AS	10/07/2019 13:08:32			

	1	2542.355	1351.1	70638.38	2099.242	1168.075
	2	2496.343	1409.109	70256.43	2053.232	1096.066
	3	2460.333	1334.098	69946.05	1948.209	1068.063
x		2499.677	1364.769	70280.29	2033.561	1110.735
s		41.113	39.329	346.777	77.414	51.594
%RSD		1.645	2.882	0.493	3.807	4.645

MT1 AS 10/07/2019 13:09:30

	1	3751.774	5461.64	47682.72	12015.94	4965.356
	2	3754.775	5680.774	48446.75	11812.67	4899.32
	3	3732.766	5634.746	48398.49	11771.62	5021.386
x		3746.439	5592.387	48175.99	11866.74	4962.021
s		11.935	115.545	427.86	130.827	61.102
%RSD		0.319	2.066	0.888	1.102	1.231

MT2 AS 10/07/2019 13:10:30

	1	3932.851	5695.784	63393.26	116426.8	3796.793
	2	3907.84	5667.766	63626.88	117768.9	3536.688
	3	3805.796	5642.751	64712.51	119207.5	3534.687
x		3882.162	5668.767	63910.88	117801.1	3622.722
s		67.307	26.531	703.985	1390.624	150.753
%RSD		1.734	0.468	1.102	1.18	4.161

SL1 AS 10/07/2019 13:11:45

	1	3147.545	1660.152	73173.31	13759.41	1068.063
	2	2964.483	1447.115	72281.21	12214.2	1192.078
	3	3033.506	1361.102	72284.24	11442.2	1086.065
x		3048.511	1489.456	72579.59	12471.93	1115.402
s		92.449	153.955	514.18	1179.908	67.011
%RSD		3.033	10.336	0.708	9.461	6.008

SL2 AS 10/07/2019 13:12:42

	1	3007.497	1369.103	69690.1	2171.259	1478.12
	2	2888.459	1369.103	70149.61	2324.297	1342.099
	3	2837.443	1362.102	68315.73	2417.321	1266.088
x		2911.133	1366.769	69385.15	2304.293	1362.103
s		87.265	4.042	954.218	124.245	107.422
%RSD		2.998	0.296	1.375	5.392	7.886

SK1 AS 10/07/2019 13:13:41

	1	3371.625	2458.332	63755.78	19988.95	7627.198
	2	3342.614	2499.343	62983.43	19921.8	7224.87
	3	3310.603	2486.34	63686.3	19939.84	7855.392
x		3341.614	2481.339	63475.17	19950.2	7569.154
s		30.524	20.958	427.276	34.751	319.244
%RSD		0.913	0.845	0.673	0.174	4.218

SK2 AS 10/07/2019 13:14:53

	1	3297.598	4512.119	64726.61	16401.78	2202.267
	2	3360.621	4564.145	64321.75	15777.68	2086.239
	3	3400.636	4696.213	64894.8	16272.55	2052.232
x		3352.952	4590.826	64647.72	16150.67	2113.579
s		51.945	94.902	294.558	329.419	78.665
%RSD		1.549	2.067	0.456	2.04	3.722
		PW1 AS	10/07/2019 13:15:52			
	1	2248.278	1506.125	72257.02	2193.265	378.008
	2	2149.254	1304.093	73600.74	2126.249	446.011
	3	2153.255	1256.087	72819.48	2047.23	386.008
x		2183.596	1355.435	72892.42	2122.248	403.342
s		56.052	132.69	674.82	73.099	37.168
%RSD		2.567	9.789	0.926	3.444	9.215
		PW2 AS	10/07/2019 13:17:17			
	1	2388.314	1312.095	67817.01	3709.757	666.024
	2	2302.291	1289.091	68032.62	3555.695	702.027
	3	2110.245	1340.099	67903.66	3437.65	684.026
x		2266.95	1313.762	67917.76	3567.701	684.026
s		142.363	25.545	108.491	136.45	18.001
%RSD		6.28	1.944	0.16	3.825	2.632
		SGP1 MD	10/07/2019 13:18:12			
	1	4841.289	1052.061	80913.49	84447.41	20843.87
	2	4755.243	1035.059	82229.22	85181.21	21078.41
	3	4661.195	1026.058	81947.69	83210.08	21485.36
x		4752.576	1037.726	81696.8	84279.57	21135.88
s		90.077	13.205	692.816	996.226	324.584
%RSD		1.895	1.272	0.848	1.182	1.536
		SGP2 MD	10/07/2019 13:19:21			
	1	3512.679	327.006	73822.53	8558.026	9058.511
	2	3300.599	319.006	73476.74	8300.788	9294.749
	3	3126.537	288.005	73925.36	8356.839	9244.698
x		3313.272	311.339	73741.54	8405.218	9199.319
s		193.382	20.6	235.016	135.271	124.485
%RSD		5.837	6.617	0.319	1.609	1.353
		MT1 MD	10/07/2019 13:20:24			
	1	2598.371	490.013	42805.54	5450.633	4625.176
	2	2397.316	509.014	43601.31	5441.628	4585.156
	3	2549.357	510.014	44218.28	5594.721	4587.157
x		2515.015	503.014	43541.71	5495.661	4599.163
s		104.835	11.27	708.252	85.907	22.55
%RSD		4.168	2.241	1.627	1.563	0.49
		MT2 MD	10/07/2019 13:21:41			

	1	2886.458	675.025	88773.33	13853.55	5397.602
	2	2823.438	692.026	86410.73	13602.17	5315.554
	3	2828.44	692.026	86302.71	14125.97	5273.529
x		2846.112	686.359	87162.26	13860.56	5328.895
s		35.03	9.816	1396.275	261.969	63.103
%RSD		1.231	1.43	1.602	1.89	1.184
		SPD1 MD	10/07/2019 13:22:45			
	1	5204.489	803.035	50111.74	5658.761	4955.35
	2	5777.836	842.039	50397.31	5567.704	4947.346
	3	4886.313	842.039	50516.97	5692.782	5135.45
x		5289.546	829.038	50342	5639.749	5012.715
s		451.807	22.519	208.2	64.67	106.367
%RSD		8.541	2.716	0.414	1.147	2.122
		SPD2 MD	10/07/2019 13:23:44			
	1	6178.099	1059.062	48384.42	3846.814	5417.614
	2	6046.01	1030.058	48094.89	3844.813	5479.651
	3	5993.975	1020.057	47163.02	3759.777	5299.544
x		6072.695	1036.392	47880.78	3817.135	5398.936
s		94.918	20.259	638.226	49.683	91.495
%RSD		1.563	1.955	1.333	1.302	1.695
		SL1 MD	10/07/2019 13:24:46			
	1	7817.36	723.029	64891.78	3297.598	8287.776
	2	8216.712	668.025	66349.24	3226.573	8287.776
	3	7763.313	683.026	65647.17	3239.577	7927.455
x		7932.462	691.36	65629.4	3254.583	8167.669
s		247.647	28.433	728.894	37.816	208.031
%RSD		3.122	4.113	1.111	1.162	2.547
		SL2 MD	10/07/2019 13:25:47			
	1	6486.313	583.019	51374.76	2048.231	6518.336
	2	6513.333	617.021	50457.64	1957.211	6508.329
	3	6338.209	560.017	51075.08	2029.227	6584.384
x		6445.951	586.686	50969.16	2011.556	6537.016
s		94.281	28.678	467.642	48.014	41.325
%RSD		1.463	4.888	0.917	2.387	0.632
		1	10/07/2019 13:26:52			
	1	2325.297	206.002	70798.62	148.001	83903.41
	2	2177.261	172.002	71247.1	111.001	86523.8
	3	2172.26	151.001	70610.16	96.001	85229.66
x		2224.939	176.335	70885.29	118.334	85218.96
s		86.949	27.755	327.197	26.765	1310.228
%RSD		3.908	15.74	0.462	22.618	1.537
		2% wash 9	10/07/2019 13:27:52			

	1	4609.168	106.001	532.016	739.03	1826.183
	2	4458.093	124.001	305.005	744.03	1254.086
	3	4327.029	136.001	155.001	826.038	1002.055
x		4464.764	122.001	330.674	769.699	1360.775
s		141.188	15.1	189.813	48.854	422.296
%RSD		3.162	12.377	57.402	6.347	31.033
		blank 8	10/07/2019 13:28:45			
	1	4414.071	116.001	103.001	486.013	260.004
	2	4374.052	107.001	91	475.012	264.004
	3	4262.999	110.001	95	520.015	230.003
x		4350.374	111.001	96.334	493.68	251.337
s		78.27	4.583	6.11	23.46	18.584
%RSD		1.799	4.128	6.343	4.752	7.394
		SBS1 MD 1	10/07/2019 13:29:55			
	1	3334.612	579.018	51781.05	6837.57	7603.178
	2	3366.623	584.019	52298	6914.629	7312.94
	3	3273.589	708.028	51402.92	6959.663	7501.093
x		3324.941	623.688	51827.32	6903.954	7472.404
s		47.265	73.083	449.332	61.742	147.231
%RSD		1.422	11.718	0.867	0.894	1.97
		SBS2 MD 2	10/07/2019 13:31:10			
	1	3840.811	855.04	45814.15	8774.232	8437.914
	2	3748.773	818.037	46918.76	8631.095	8175.675
	3	3532.686	829.038	48150.18	8878.333	8447.923
x		3707.423	834.038	46961.03	8761.22	8353.837
s		158.169	19.002	1168.586	124.132	154.375
%RSD		4.266	2.278	2.488	1.417	1.848
		PW1 MD 3	10/07/2019 13:32:18			
	1	7810.354	686.026	58457.35	4313.023	4627.177
	2	8485.959	670.025	63047.87	4114.931	4603.165
	3	7962.485	648.023	69690.1	4134.94	4385.057
x		8086.266	668.025	63731.77	4187.631	4538.467
s		354.403	19.08	5647.519	109.052	133.398
%RSD		4.383	2.856	8.861	2.604	2.939
		PW2 MD 4	10/07/2019 13:33:16			
	1	7787.334	614.021	59020.97	18756.33	4605.166
	2	7573.153	574.018	63318.74	18609.03	4431.08
	3	7684.246	614.021	68721.77	18923.68	4487.107
x		7681.578	600.687	63687.16	18763.01	4507.784
s		107.115	23.096	4860.882	157.431	88.866
%RSD		1.394	3.845	7.632	0.839	1.971
		SSD1 MD 5	10/07/2019 13:34:19			

	1	7406.016	879.043	42511.16	3027.504	10093.6
	2	7414.022	811.036	44741.83	2877.455	10165.68
	3	7148.81	823.037	45955.86	2722.408	9781.259
x		7322.949	837.705	44402.95	2875.789	10013.51
s		150.862	36.298	1747.174	152.555	204.341
%RSD		2.06	4.333	3.935	5.305	2.041

SSD2 MD 6 10/07/2019 13:35:14

	1	7453.054	1052.061	57886.71	1181.077	10868.49
	2	7306.935	930.048	61488.24	1088.065	10966.61
	3	7212.86	942.049	68111.2	1122.069	10522.09
x		7324.283	974.719	62495.39	1130.404	10785.73
s		121.033	67.248	5186.115	47.063	233.534
%RSD		1.652	6.899	8.298	4.163	2.165

SOS1 MD 7 10/07/2019 13:36:14

	1	4897.319	254.004	72720.7	1296.092	10049.55
	2	4682.206	219.003	78149.47	1300.093	10301.83
	3	4749.24	220.003	81636.91	1317.095	10808.42
x		4776.255	231.003	77502.36	1304.427	10386.6
s		110.072	19.925	4493.193	11.152	386.471
%RSD		2.305	8.626	5.797	0.855	3.721

SOS2 MD 8 10/07/2019 13:37:11

	1	4124.936	160.001	72735.82	510.014	6480.309
	2	3993.877	153.001	73442.47	530.015	6338.209
	3	3925.847	147.001	72361.85	533.016	6434.276
x		4014.887	153.335	72846.71	524.348	6417.598
s		101.193	6.507	548.776	12.504	72.503
%RSD		2.52	4.243	0.753	2.385	1.13

SS1 MD 10/07/2019 13:38:09

	1	7571.151	151.001	54345.96	1818.182	7132.797
	2	7493.087	170.002	54473.72	1963.212	7282.916
	3	7198.849	171.002	55115.57	2054.232	7268.905
x		7421.029	164.001	54645.08	1945.209	7228.206
s		196.333	11.27	412.432	119.051	82.923
%RSD		2.646	6.872	0.755	6.12	1.147

SS2 MD 10/07/2019 13:39:04

	1	6331.204	222.003	60756.35	1114.068	9268.723
	2	6303.184	248.003	60263.08	1103.067	8572.04
	3	6186.104	225.003	63399.3	1108.068	8574.041
x		6273.497	231.67	61472.91	1108.401	8804.934
s		76.971	14.225	1686.437	5.508	401.654
%RSD		1.227	6.14	2.743	0.497	4.562

SK2 MD 10/07/2019 13:40:06

	1	4154.949	433.01	66116.56	4265	11833.7
	2	3967.866	477.013	67227.66	4399.064	12005.92
	3	3951.859	449.011	67140.02	4349.04	11743.58
x		4024.891	453.011	66828.08	4337.701	11861.07
s		112.918	22.272	617.752	67.747	133.296
%RSD		2.805	4.916	0.924	1.562	1.124

sgp1 AS 10/07/2019 13:41:03

	1	2569.363	1648.149	63466.77	13732.36	700.027
	2	2471.336	1691.157	63517.12	13013.31	632.022
	3	2507.346	1695.158	64125.37	13011.31	582.019
x		2516.015	1678.155	63703.09	13252.33	638.023
s		49.585	26.062	366.572	415.727	59.233
%RSD		1.971	1.553	0.575	3.137	9.284

SGP2 AS 10/07/2019 13:42:05

	1	2837.443	1998.22	69984.35	7721.278	616.021
	2	2725.409	1874.193	69942.02	7492.086	618.021
	3	2732.411	1828.184	70800.63	7453.054	668.025
x		2765.087	1900.199	70242.33	7555.472	634.022
s		62.759	87.95	483.963	144.912	29.464
%RSD		2.27	4.628	0.689	1.918	4.647

SS1 AS 10/07/2019 13:43:02

	1	5563.702	695.027	9699.171	6606.4	3086.524
	2	5448.632	597.02	9446.906	6133.068	3288.595
	3	5325.559	531.016	9615.082	5661.762	3172.554
x		5445.965	607.687	9587.053	6133.743	3182.557
s		119.094	82.524	128.447	472.319	101.406
%RSD		2.187	13.58	1.34	7.7	3.186

SS2 AS 10/07/2019 13:44:01

	1	3369.624	753.031	73065.45	593.019	252.003
	2	3191.56	771.033	73224.72	636.022	194.002
	3	3186.558	781.034	75208.82	636.022	184.002
x		3249.248	768.366	73832.99	621.688	210.002
s		104.279	14.19	1194.157	24.828	36.716
%RSD		3.209	1.847	1.617	3.994	17.484

SBS2 AS 10/07/2019 13:44:58

	1	2708.403	1787.176	69268.9	8660.123	526.015
	2	2666.391	1754.169	69065.36	8563.031	534.016
	3	2664.39	1730.165	70421.71	8740.2	534.016
x		2679.728	1757.17	69585.32	8654.451	531.349
s		24.854	28.624	731.444	88.72	4.619
%RSD		0.927	1.629	1.051	1.025	0.869

ssd1 AS 10/07/2019 13:45:55

	1	4807.271	312.005	72698.52	6370.231	1036.059
	2	4603.165	280.004	72587.64	4433.081	1174.076
	3	4399.064	234.003	75017.25	3450.655	1048.06
x		4603.167	275.338	73434.47	4751.322	1086.065
s		204.103	39.21	1371.845	1485.577	76.455
%RSD		4.434	14.241	1.868	31.267	7.04
		SSD2 AS	10/07/2019 13:47:00			
	1	2892.46	299.005	84542.29	734.03	160.001
	2	2749.416	271.004	83549.17	785.034	118.001
	3	2705.403	263.004	85057.06	805.036	180.002
x		2782.426	277.671	84382.84	774.7	152.668
s		97.8	18.904	766.485	36.614	31.644
%RSD		3.515	6.808	0.908	4.726	20.728
		SGS1 AS	10/07/2019 13:48:05			
	1	3381.629	4418.073	69249.75	9046.499	582.019
	2	3289.595	4419.074	73391.05	8537.006	540.016
	3	3285.594	4347.039	73009	8709.17	518.015
x		3318.939	4394.729	71883.27	8764.225	546.683
s		54.328	41.303	2288.676	259.17	32.519
%RSD		1.637	0.94	3.184	2.957	5.948

Batch 1 Sample mass

	Seawater Batch	Container Empty (g)	Container + Mass (g)	Sample Mass (g)	% Water content	Adjusted Mass (g)	Container + Mass + Water (g)	Sample Water (g)	Total Water (g)
PW1	2	14.67	28.35	13.68	75.41%	3.36	60.37	32.02	42.34
PW2	2	14.71	27.26	12.54	75.41%	3.08	61.78	34.52	43.98
PS1	2	14.62	15.46	0.84	76.33%	0.20	60.09	44.64	45.28
PS2	2	14.71	15.41	0.70	76.33%	0.17	66.27	50.86	51.39
SPW1	2	14.66	23.24	8.58	75.98%	2.06	59.36	36.12	42.64
SPW2	2	14.59	24.14	9.55	75.98%	2.29	60.65	36.52	43.77
SPS1	2	14.58	16.00	1.42	76.33%	0.34	60.50	44.50	45.58
SPS2	2	14.71	16.02	1.31	76.33%	0.31	60.50	44.47	45.48
MT1	1	14.77	19.59	4.82	83.33%	0.80	60.23	40.64	44.66
MT2	1	14.69	20.69	6.01	83.33%	1.00	59.61	38.91	43.92
PNS1	1	14.77	16.20	1.44	6.87%	1.34	59.83	43.63	43.73
PNS2	1	14.68	15.54	0.86	6.87%	0.80	61.18	45.64	45.70
GW1	1	14.57	21.30	6.73	90.00%	0.67	61.42	40.11	46.17
GW2	1	4.69	22.13	17.44	90.00%	1.74	61.20	39.07	54.77
CN1	1	14.69	23.53	8.84	0.00%	8.84	59.84	36.31	36.31
CN2	1	14.68	21.38	6.70	0.00%	6.70	60.63	39.25	39.25
SWT1	2	14.74	14.74	0.00	0.00%	0.00	57.31	42.57	42.57
SWT2	2	14.69	14.69	0.00	0.00%	0.00	55.51	40.82	40.82
SWO1	1	14.70	14.70	0.00	0.00%	0.00	56.33	41.63	41.63
SWO2	1	14.79	14.79	0.00	0.00%	0.00	59.42	44.63	44.63
SK1	1	11.87	14.20	2.33	85.43%	0.34	42.24	28.04	30.03

SK2	1	11.83	14.77	2.94	85.43%	0.43	40.18	25.41	27.92
SL1	1	11.85	13.66	1.81	80.74%	0.35	39.06	25.40	26.86
SL2	1	11.95	13.10	1.15	80.74%	0.22	38.29	25.19	26.12
SS1	1	14.68	20.36	5.68	0.00%	5.68	45.81	25.45	25.45
SS2	1	14.71	19.72	5.01	0.00%	5.01	45.31	25.59	25.59
SSD1	1	14.69	20.17	5.48	0.00%	5.48	45.45	25.28	25.28
SSD2	1	14.75	20.23	5.48	0.00%	5.48	45.67	25.44	25.44
SGS1	1	14.63	20.07	5.44	80.49%	1.06	45.13	25.06	29.44
SGS2	1	14.69	19.54	4.85	80.49%	0.95	45.06	25.52	29.42
SGP1	1	14.71	18.51	3.80	0.00%	3.80	43.95	25.44	25.44
SGP2	1	14.71	21.51	6.80	0.00%	6.80	47.16	25.65	25.65
SOS1	1	14.59	15.17	0.58	69.45%	0.18	40.58	25.41	25.81
SOS2	1	14.50	15.42	0.92	69.45%	0.28	41.00	25.58	26.22
SNS1	1	14.63	15.53	0.90	85.30%	0.13	41.57	26.04	26.81
SNS2	1	14.86	16.27	1.41	85.30%	0.21	41.43	25.16	26.36
SBS1	1	14.66	18.34	3.68	0.00%	3.68	43.89	25.55	25.55
SBS2	1	14.57	19.34	4.77	0.00%	4.77	44.85	25.51	25.51
SB1	1	14.58	14.58	0.00	0.00%	0.00	39.44	24.86	24.86
SB2	1	14.82	14.82	0.00	0.00%	0.00	41.16	26.34	26.34

Sample	Empty (g)	Mass+ Container	Mass + Container + Water	Sample Mass	Water Content	Dry Weight	Sample Water (g)
SK1	11.87	14.2	42.24	2.33	0.85428995	0.339504	28.04
SK2	11.83	14.77	40.18	2.94	0.85428995	0.428388	25.41
SL1	11.85	13.66	39.06	1.81	0.80735719	0.348683	25.4
SL2	11.95	13.1	38.29	1.15	0.80735719	0.221539	25.19
SS1	14.68	20.36	45.81	5.68	0	5.68	25.45
SS2	14.71	19.72	45.31	5.01	0	5.01	25.59
SSD1	14.69	20.17	45.45	5.48	0	5.48	25.28
SSD2	14.75	20.23	45.67	5.48	0	5.48	25.44
SGS1	14.63	20.07	45.13	5.44	0.80492082	1.061231	25.06
SGS2	14.69	19.54	45.06	4.85	0.80492082	0.946134	25.52
SGP1	14.71	18.51	43.95	3.8	0	3.8	25.44
SGP2	14.71	21.51	47.16	6.8	0	6.8	25.65
SOS1	14.59	15.17	40.58	0.58	0.69446577	0.17721	25.41
SOS2	14.5	15.42	41	0.92	0.69446577	0.281091	25.58
SNS1	14.63	15.53	41.57	0.9	0.85301537	0.132286	26.04
SNS2	14.86	16.27	41.43	1.41	0.85301537	0.207248	25.16
SBS1	14.66	18.34	43.89	3.68	0	3.68	25.55
SBS2	14.57	19.34	44.85	4.77	0	4.77	25.51

SB1	14.58	14.58	39.44	0	0	0	24.86
SB2	14.82	14.82	41.16	0	0	0	26.34

Batch 1 Calculations

Sample	Whole Garlic 1	Whole Garlic 2	Peanut Shell 1	Peanut Shell 2
Mass (g) (dry Weight)	0.673	1.744	1.337	0.804
Seawater mass	40.11	39.07	43.63	45.64
Measured Conc of Digestate (µg/L)	0.086	0.057	0.142	0.193
Dilution of digestate	0.063	0.063	0.063	0.063
Total mass (u) µg in Biomass	0.055	0.036	0.091	0.124
Biomass Concentration (µg/g)	0.081	0.021	0.068	0.154
Biomass Concentration (µg/kg)	81.4	20.8	68.2	153.9
Average Biomass Concentration (µg/kg): RSD	51.1	59.3%	111.0	38.6%
Concentration of U in Control Mass (µg/g)	0.001	0.001	0.058	0.058
Adjusted Biomass Concentration (µg/g)	0.080	0.020	0.010	0.096
Adjusted Biomass Concentration (µg/kg)	80.271	19.655	10.397	96.125
Average Adjusted Biomass Concentration (µg/Kg)	50.0	60.7%	53.3	80.5%
Sample	Whole Garlic 1	Whole Garlic 2	Peanut Shell 1	Peanut Shell 2
Fluid Phase Solution Measured	0.007	0.000	0.012	0.015
Fluid Phase Solution Dilution	0.063	0.063	0.063	0.063
	0.004	0.000	0.009	0.011
Fluid Phase Solution Conc (microgram/L	0.105	0.007	0.195	0.236
Average fluid phase Concentration (µg/l)	0.056	87.5%	0.215	9.5%
Kd (Sorbed/Solution)	772.824	2960.595	349.930	652.976
Average Kd (Sorbed/Solution): RSD (%)	1866.710	58.6%	501.453	30.2%
Sorbed fraction of system	92.8%	99.2%	91.5%	92.0%
Average Sorbed Fraction : RSD (%)	96.0%	3.3%	91.7%	0.3%

Sample	Potato Skin 1	Potato Skin 2	Potato Whole 1	Potato Whole 2	Sweet Potato Whole 1	Sweet Potato Whole 2
Mass (g) (dry Weight)	0.199	0.165	3.364	3.084	2.061	2.293
Seawater mass	44.64	50.86	32.02	34.52	36.12	36.52
Measured Conc of Digestate (µg/L)	0.062	0.108	0.054	0.054	0.060	0.065
Dilution of digestate	0.063	0.063	0.063	0.063	0.063	0.063
Total mass (u) µg in Biomass	0.040	0.069	0.035	0.035	0.038	0.041
Biomass Concentration (µg/g)	0.199	0.419	0.010	0.011	0.019	0.018

Biomass Concentration (µg/kg)	199.4	419.5	10.3	11.2	18.6	18.0
Average Biomass Concentration (µg/kg): RSD	309.4	35.6%	10.8	4.0%	18.3	1.6%
Concentration of U in Control Mass (µg/g)	0.054	0.054	0.000	0.000	0.002	0.002
Adjusted Biomass Concentration (µg/g)	0.145	0.365	0.010	0.011	0.017	0.017
Adjusted Biomass Concentration (µg/kg)	145.132	365.197	10.013	10.875	17.118	16.522
Average Adjusted Biomass Concentration (µg/Kg)	255.2	43.1%	10.4	4.1%	16.8	1.8%
Sample	Potato Skin 1	Potato Skin 2	Potato Whole 1	Potato Whole 2	Sweet Potato Whole 1	Sweet Potato Whole 2
Fluid Phase Solution Measured	0.012	0.015	0.005	0.008	0.011	0.013
Fluid Phase Solution Dilution	0.063	0.063	0.063	0.063	0.063	0.063
	0.009	0.012	0.002	0.005	0.006	0.008
Fluid Phase Solution Conc (microgram/L	0.195	0.236	0.077	0.131	0.172	0.213
Average fluid phase Concentration (µg/l)	0.215	9.5%	0.104	25.8%	0.192	10.5%
Kd (Sorbed/Solution)	1023.389	1779.623	133.791	85.473	108.179	84.794
Average Kd (Sorbed/Solution): RSD (%)	1401.506	27.0%	109.632	22.0%	96.486	12.1%
Sorbed fraction of system	82.0%	85.3%	93.4%	88.4%	86.1%	84.2%
Average Sorbed Fraction : RSD (%)	83.6%	1.9%	90.9%	2.7%	85.1%	1.1%

Sample	Brussel Sprouts 1	Brussel Sprouts 2	Kale 2	Mange Tout 1	Mange Tout 2
Mass (g) (dry Weight)	3.680	4.770	0.428	0.804	1.002
Seawater mass	25.55	25.51	25.41	40.64	38.91
Measured Conc of Digestate (µg/L)	0.089	0.100	0.142	0.055	0.064
Dilution of digestate	0.063	0.063	0.063	0.063	0.063
Total mass (u) µg in Biomass	0.057	0.064	0.091	0.035	0.041
Biomass Concentration (µg/g)	0.016	0.013	0.212	0.044	0.041
Biomass Concentration (µg/kg)	15.6	13.4	212.1	43.8	40.8
Average Biomass Concentration (µg/kg): RSD	14.5	7.4%	212.1	42.3	3.7%

Concentration of U in Control Mass (µg/g)	0.000	0.000	0.007	0.002	0.002
Adjusted Biomass Concentration (µg/g)	0.016	0.013	0.206	0.042	0.038
Adjusted Biomass Concentration (µg/kg)	15.555	13.416	205.577	41.582	38.494
Average Adjusted Biomass Concentration (µg/Kg)	14.5	7.4%	205.6	40.0	3.9%

Sample	Brussel Sprouts 1	Brussel Sprouts 2	Kale 2	Mange Tout 1	Mange Tout 2
Fluid Phase Solution Measured	0.007	0.006	0.025	0.059	0.043
Fluid Phase Solution Dilution	0.063	0.063	0.063	0.063	0.063
	0.003	0.003	0.010	0.039	0.027
Fluid Phase Solution Conc (microgram/L	0.105	0.102	0.405	0.950	0.694
Average fluid phase Concentration (µg/l)	0.103	1.4%	0.405	0.822	15.6%
Kd (Sorbed/Solution)	148.572	131.840	523.996	46.135	58.740
Average Kd (Sorbed/Solution): RSD (%)	140.206	6.0%	523.996	52.437	12.0%
Sorbed fraction of system	95.5%	96.1%	89.8%	47.7%	60.2%
Average Sorbed Fraction : RSD (%)	95.8%	0.3%	89.8%	53.9%	11.6%

Sample	Grape Pulp 1	Grape Pulp 2	Grape Skin 1	Grape Skin 2	Sultanas Whole 1	Sultanas Whole 2	Sultanas Diced 1	Sultanas Diced 2
Mass (g) (dry Weight)	3.800	6.800	1.061	0.946	5.680	5.010	5.480	5.480
Seawater mass	25.06	25.52	25.44	25.65	25.45	25.59	25.28	25.44
Measured Conc of Digestate (µg/L)	0.253	0.110	0.212	0.204	0.087	0.105	0.120	0.129
Dilution of digestate	0.063	0.063	0.063	0.063	0.050	0.050	0.050	0.050
Total mass (u) µg in Biomass	0.162	0.070	0.135	0.130	0.069	0.084	0.096	0.103
Biomass Concentration (µg/g)	0.043	0.010	0.128	0.138	0.012	0.017	0.017	0.019
Biomass Concentration (µg/kg)	42.6	10.4	127.6	137.9	12.2	16.8	17.5	18.8
Average Biomass Concentration (µg/kg): RSD	26.5	60.9%	132.8	3.9%	14.5	16.0%	18.2	3.7%
Concentration of U in Control Mass (µg/g)	0.005	0.005	0.005	0.005	0.002	0.002	0.002	0.002
Adjusted Biomass Concentration (µg/g)	0.037	0.005	0.122	0.132	0.011	0.015	0.016	0.017
Adjusted Biomass Concentration (µg/kg)	37.122	4.877	122.155	132.388	10.603	15.247	15.915	17.265

Average Adjusted Biomass Concentration (µg/Kg)	21.0	76.8%	127.3	4.0%	12.9	18.0%	16.6	4.1%
Sample	Grape Pulp 1	Grape Pulp 2	Grape Skin 1	Grape Skin 2	Sultanas Whole 1	Sultanas Whole 2	Sultanas Diced 1	Sultanas Diced 2
Fluid Phase Solution Measured	0.008	0.008	0.013	0.008	0.038	0.003	0.013	0.002
Fluid Phase Solution Dilution	0.063	0.063	0.063	0.063	0.063	0.063	0.063	0.063
	0.003	0.003	0.005	0.003	0.016	0.001	0.005	0.001
Fluid Phase Solution Conc (microgram/L	0.122	0.121	0.210	0.121	0.610	0.040	0.208	0.029
Average fluid phase Concentration (µg/l)	0.122	0.3%	0.165	27.1%	0.325	87.6%	0.119	75.4%
Kd (Sorbed/Solution)	348.707	85.350	606.968	1142.697	19.993	418.441	84.124	644.601
Average Kd (Sorbed/Solution): RSD (%)	217.028	60.7%	874.833	30.6%	219.217	90.9%	364.363	76.9%
Sorbed fraction of system	98.1%	95.8%	96.2%	97.7%	81.7%	98.8%	94.8%	99.3%
Average Sorbed Fraction : RSD (%)	97.0%	1.2%	96.9%	0.8%	90.2%	9.5%	97.0%	2.3%

Sample	Lemon 1	Lemon 2	Nectrine Skin 1	Nectrine Skin 2	Orange Skin 1	Orange Skin 2
Mass (g) (dry Weight)	0.349	0.222	0.132	0.207	0.177	0.281
Seawater mass	25.40	25.19	26.04	25.16	25.41	25.58
Measured Conc of Digestate (µg/L)	0.098	0.078	0.035	0.023	0.124	0.077
Dilution of digestate	0.083	0.083	0.033	0.033	0.083	0.083
Total mass (u) µg in Biomass	0.047	0.038	0.042	0.028	0.060	0.037
Biomass Concentration (µg/g)	0.135	0.170	0.318	0.133	0.337	0.131
Biomass Concentration (µg/kg)	134.6	169.5	317.6	132.8	336.7	131.2
Average Biomass Concentration (µg/kg): RSD	152.1	11.5%	225.2	41.0%	234.0	43.9%
Concentration of U in Control Mass (µg/g)	0.007	0.007	0.001	0.001	0.000	0.000
Adjusted Biomass Concentration (µg/g)	0.128	0.163	0.317	0.132	0.337	0.131
Adjusted Biomass Concentration (µg/kg)	128.056	163.005	316.583	131.732	336.549	130.974
Average Adjusted Biomass Concentration (µg/Kg)	145.5	12.0%	224.2	41.2%	233.8	44.0%
Sample	Lemon 1	Lemon 2	Nectrine Skin 1	Nectrine Skin 2	Orange Skin 1	Orange Skin 2
Fluid Phase Solution Measured	0.013	0.016	0.064	0.083	0.015	0.004
Fluid Phase Solution Dilution	0.063	0.063	0.063	0.063	0.063	0.063
	0.005	0.007	0.027	0.034	0.006	0.002
Fluid Phase Solution Conc (microgram/L	0.214	0.261	1.019	1.333	0.246	0.067
Average fluid phase Concentration (µg/l)	0.237	10.0%	1.176	13.4%	0.156	57.3%
Kd (Sorbed/Solution)	630.023	649.891	311.680	99.560	1370.763	1968.151

Average Kd (Sorbed/Solution): RSD (%)	639.957	1.6%	205.620	51.6%	1669.457	17.9%
Sorbed fraction of system	89.6%	85.1%	61.3%	45.1%	90.5%	95.6%
Average Sorbed Fraction : RSD (%)	87.4%	2.6%	53.2%	15.3%	93.1%	2.7%

Appendix 2 Batch 2

Batch 2 Key

	1	LDK01	Dried Kale
	2	LGPS10	Garlic Powder
	3	LOP06	Orange Peel
	4	LPS11	Peanut shell
	5	LPSS1	Potato Skin
	6	LRG01	Red Grape
C		LSW05	Seawater (control)
	7	LVG11	Vitira Grape
	8	LWG06	White Grape

Batch 2 ICP data

	45Sc	51V	55Mn	59Co	60Ni	65Cu	95Mo	103Rh	107Ag	197Au	209Bi	238U
	ppb	ppb	ppb	ppb	ppb	ppb	ppb	ppb	ppb	ppb	ppb	ppb
	8BD 16/12/2021 18:27:26											
1	101.28%	-0.08	-0.328	2.356	-0.074	0.154	-0.027	93.06%	-0.014	0.204	91.12%	0.057
2	99.66%	-0.078	-0.33	1.62	-0.077	0.145	-0.028	90.28%	-0.011	0.205	105.52%	0.057
3	99.07%	-0.085	-0.335	1.168	-0.082	0.077	-0.034	116.67%	-0.015	0.204	103.35%	0.057
x	100.00%	-0.081	-0.331	1.715	-0.078	0.125	-0.03	100.00%	-0.013	0.205	100.00%	0.057
s	1.15%	0.003	0.003	0.6	0.004	0.042	0.004	14.50%	0.003	0	7.76%	0
%RSD	1.146	4.308	1.055	34.96	5.091	33.86	12.32	14.501	18.84	0.181	7.763	0.638
	MQ 16/12/2021 16:14:58											
1	95.95%	-0.054	-0.317	4.594	-0.063	0.39	-0.021	44.44%	-0.011	0.212	82.64%	0.057
2	93.31%	-0.077	-0.331	1.88	-0.081	0.132	-0.032	84.72%	-0.02	0.204	79.49%	0.057
3	92.02%	-0.082	-0.334	1.376	-0.084	0.088	-0.034	101.39%	-0.022	0.205	78.50%	0.057
x	93.76%	-0.071	-0.328	2.617	-0.076	0.203	-0.029	76.85%	-0.017	0.207	80.21%	0.057
s	2.01%	0.015	0.009	1.731	0.011	0.163	0.007	29.28%	0.006	0.005	2.16%	0.001
%RSD	2.139	20.89	2.885	66.15	14.55	80.13	24.01	38.095	32.97	2.21	2.698	0.906
	0ppb 16/12/2021 16:16:32											
1	97.92%	-0.067	-0.277	7.235	-0.072	-0.06	0.001	92.89%	-0.016	0.239	78.96%	0.061
2	101.04%	-0.054	-0.249	8.256	-0.057	-0.044	0	102.45%	-0.014	0.207	99.83%	0.065
3	101.04%	-0.047	-0.225	9.799	-0.046	-0.026	0.009	104.66%	-0.016	0.207	121.21%	0.067
x	100.00%	-0.056	-0.25	8.43	-0.058	-0.043	0.004	100.00%	-0.015	0.218	100.00%	0.064
s	1.80%	0.01	0.026	1.291	0.013	0.017	0.005	6.26%	0.001	0.018	21.13%	0.003
%RSD	1.799	17.68	10.4	15.31	22.65	39.27	141.6	6.256	8.369	8.415	21.13	5.169

1ppb 16/12/2021 16:17:34

1	97.61%	0.989	1.986	0.561	1.976	1.971	1.006	111.27%	0.975	1.229	53.70%	0.995
2	94.77%	0.986	2.015	1.14	1.995	2.018	0.996	108.71%	1.025	1.041	53.70%	0.997
3	91.26%	0.986	2.009	1.138	2.028	1.993	0.989	112.49%	0.989	1.082	57.91%	1.015
x	94.55%	0.987	2.003	0.946	2	1.994	0.997	110.82%	0.997	1.117	55.11%	1.002
s	3.18%	0.002	0.015	0.334	0.026	0.024	0.009	1.93%	0.026	0.099	2.43%	0.011
%RSD	3.364	0.207	0.755	35.29	1.302	1.187	0.875	1.739	2.603	8.84	4.41	1.131

2ppb 16/12/2021 16:18:37

1	87.55%	2.03	4.371	0.898	4.025	4.032	2.004	109.62%	2.008	1.936	41.75%	1.954
2	86.03%	2.018	4.268	1.072	3.98	3.888	1.984	111.63%	1.973	1.998	50.50%	1.908
3	83.11%	2.056	4.337	1.049	4.004	4.026	1.983	114.55%	2.003	1.952	52.02%	2.006
x	85.56%	2.035	4.325	1.006	4.003	3.982	1.991	111.93%	1.995	1.962	48.09%	1.956
s	2.26%	0.019	0.052	0.094	0.022	0.082	0.012	2.48%	0.019	0.033	5.54%	0.049
%RSD	2.641	0.953	1.212	9.342	0.558	2.054	0.599	2.214	0.957	1.66	11.527	2.506

5ppb 16/12/2021 16:19:39

1	79.86%	5.07	9.841	13.33	10.06	10.07	5.046	114.53%	5.058	4.439	61.61%	4.894
2	78.29%	5.085	9.927	13.9	10.01	10.01	4.914	114.97%	5.038	4.524	61.95%	4.961
3	74.76%	5.085	10.04	14.5	10.27	10.3	5.081	114.26%	5.04	4.279	65.32%	4.957
x	77.64%	5.08	9.938	13.91	10.11	10.13	5.013	114.59%	5.045	4.414	62.96%	4.937
s	2.61%	0.009	0.102	0.587	0.136	0.149	0.088	0.36%	0.011	0.124	2.05%	0.037
%RSD	3.365	0.174	1.029	4.219	1.345	1.474	1.76	0.313	0.217	2.814	3.253	0.759

10ppb 16/12/2021 16:20:47

1	73.24%	9.76	19.63	9.809	19.44	19.57	9.805	117.80%	9.758	10.48	62.29%	9.808
2	71.88%	10.06	20.24	10.25	20.22	20.26	10.1	115.04%	10.07	10.11	63.47%	10.22
3	70.46%	10.05	20.13	11.54	20.17	19.99	10.08	115.10%	10.11	10.28	62.12%	10.09
x	71.86%	9.954	20	10.53	19.94	19.94	9.996	115.98%	9.979	10.29	62.63%	10.04
s	1.39%	0.169	0.325	0.899	0.433	0.347	0.165	1.58%	0.193	0.182	0.73%	0.21
%RSD	1.936	1.694	1.624	8.537	2.17	1.741	1.654	1.358	1.931	1.771	1.172	2.091

20ppb 16/12/2021 16:21:54

1	70.14%	19.74	39.59	42.74	38.71	39.11	19.43	115.90%	19.72	17.39	52.52%	7.436
2	67.64%	19.39	38.75	45.54	38.79	38.62	19.05	118.62%	19.1	17.41	64.31%	5.845

3	67.85%	20.84	41.61	46.98	40.58	41.25	20.19	113.40%	20.48	18.41	49.66%	4.525
x	68.54%	19.99	39.98	45.09	39.36	39.66	19.56	115.97%	19.76	17.74	55.50%	5.935
s	1.38%	0.757	1.467	2.159	1.053	1.401	0.581	2.61%	0.693	0.581	7.76%	1.458
%RSD	2.019	3.788	3.67	4.788	2.676	3.531	2.969	2.251	3.506	3.278	13.988	24.56

2% acid wash 16/12/2021 16:23:14

1	63.56%	17.78	33.43	105.3	27.48	19.36	25.74	0.86%	17.86	27.52	26.09%	7.415
2	63.56%	16.67	21.38	253	16.12	15.04	36.58	0.49%	16.67	26.24	22.39%	5.863
3	62.71%	12.16	15.95	292.1	11.83	12.59	32.53	0.49%	15.57	26.57	21.55%	4.405
x	63.28%	15.54	23.59	216.8	18.48	15.66	31.62	0.61%	16.7	26.78	23.34%	5.894
s	0.49%	2.976	8.943	98.49	8.089	3.428	5.477	0.21%	1.148	0.662	2.42%	1.505
%RSD	0.781	19.16	37.92	45.43	43.78	21.89	17.32	34.298	6.874	2.472	10.359	25.54

1AS 16/12/2021 16:24:39

1	70.39%	1.246	46.67	76.89	0.16	2.052	3.571	100.74%	0.095	2.394	161.96%	0.235
2	67.09%	1.206	44.81	75.21	0.132	1.923	3.47	105.13%	0.071	1.678	157.41%	0.195
3	68.00%	1.204	44.13	70.5	0.108	1.87	3.491	106.59%	0.055	1.245	163.81%	0.164
x	68.49%	1.218	45.2	74.2	0.133	1.948	3.511	104.15%	0.074	1.772	161.06%	0.198
s	1.70%	0.024	1.317	3.311	0.026	0.094	0.053	3.05%	0.021	0.58	3.29%	0.036
%RSD	2.484	1.944	2.915	4.462	19.31	4.807	1.513	2.927	27.92	32.75	2.044	18.09

1BS 16/12/2021 16:25:41

1	68.27%	1.153	39.64	39.63	0.086	0.173	0.141	98.77%	-0.008	0.637	71.38%	0.074
2	71.91%	1.122	38.86	37.01	0.082	0.159	0.117	112.12%	-0.009	0.417	88.05%	0.074
3	69.21%	1.118	39.34	39.61	0.084	0.152	0.122	110.65%	-0.007	0.416	87.88%	0.075
x	69.80%	1.131	39.28	38.75	0.084	0.162	0.126	107.18%	-0.008	0.49	82.43%	0.074
s	1.89%	0.019	0.39	1.508	0.002	0.011	0.013	7.32%	0.001	0.127	9.58%	0
%RSD	2.705	1.72	0.993	3.891	2.64	6.552	9.909	6.832	12.13	25.98	11.615	0.516

1CS 16/12/2021 16:26:40

1	69.07%	1.124	33.54	61.53	0.041	0.606	0.075	99.15%	-0.01	0.422	75.08%	0.077
2	66.06%	1.155	34.75	60.79	0.029	0.637	0.055	94.51%	-0.011	0.343	74.07%	0.07
3	67.31%	1.138	35.24	61.2	0.03	0.641	0.065	92.67%	-0.009	0.345	71.55%	0.071
x	67.48%	1.139	34.51	61.17	0.033	0.628	0.065	95.44%	-0.01	0.37	73.57%	0.072
s	1.51%	0.016	0.877	0.367	0.007	0.019	0.01	3.34%	0.001	0.045	1.82%	0.004
%RSD	2.239	1.379	2.541	0.6	19.69	3.042	15.37	3.497	10.54	12.22	2.475	5.169

1DS 16/12/2021 16:27:40

1	68.16%	0.953	35.65	46.58	0.529	0.397	0.142	99.62%	-0.016	0.279	181.83%	0.065
2	66.18%	0.944	37.07	47.35	0.552	0.413	0.142	96.27%	-0.014	0.288	171.39%	0.066
3	64.91%	0.947	36.62	48.89	0.559	0.415	0.15	94.57%	-0.015	0.294	182.67%	0.065
x	66.42%	0.948	36.45	47.61	0.547	0.408	0.145	96.82%	-0.015	0.287	178.63%	0.065
s	1.64%	0.004	0.723	1.177	0.015	0.01	0.005	2.57%	0.001	0.008	6.28%	0
%RSD	2.471	0.445	1.985	2.473	2.805	2.468	3.151	2.657	4.64	2.637	3.518	0.502

1AA 16/12/2021 16:28:43

1	66.06%	0.051	28.43	51.26	0.031	0.323	0.101	113.42%	-0.023	0.215	219.21%	0.06
2	64.99%	-0.002	28.61	48.08	0.028	0.339	0.102	112.05%	-0.022	0.215	210.28%	0.061
3	62.21%	-0.021	28.2	48.78	0.023	0.343	0.096	110.39%	-0.02	0.214	210.12%	0.061
x	64.42%	0.009	28.41	49.38	0.027	0.335	0.1	111.95%	-0.022	0.214	213.20%	0.061
s	1.99%	0.037	0.207	1.671	0.004	0.011	0.003	1.52%	0.001	0.001	5.20%	0
%RSD	3.086	399.9	0.729	3.385	13.28	3.238	2.829	1.355	6.222	0.324	2.44	0.702

1BA 16/12/2021 16:29:51

1	65.41%	-0.034	59.98	119.9	0.17	1.076	0.191	101.92%	-0.016	0.217	228.81%	0.064
2	63.65%	-0.042	61.5	122.2	0.129	0.823	0.176	100.17%	-0.014	0.217	224.93%	0.064
3	63.78%	-0.042	62.29	123.2	0.111	0.701	0.167	98.11%	-0.014	0.216	225.78%	0.065
x	64.28%	-0.04	61.26	121.8	0.137	0.867	0.178	100.07%	-0.014	0.217	226.51%	0.064
s	0.98%	0.005	1.171	1.671	0.03	0.191	0.012	1.91%	0.001	0	2.04%	0
%RSD	1.525	12.71	1.912	1.372	22.31	22.04	6.85	1.908	6.804	0.137	0.899	0.731

1CA 16/12/2021 16:30:57

1	64.06%	-0.065	5.495	50.48	-0.001	0.331	0.095	119.20%	-0.018	0.21	216.85%	0.059
2	59.80%	-0.064	4.775	50.18	-0.013	0.322	0.09	116.72%	-0.017	0.211	215.84%	0.06
3	61.27%	-0.067	4.5	48.99	-0.013	0.312	0.089	116.23%	-0.016	0.211	220.05%	0.06
x	61.71%	-0.066	4.923	49.89	-0.009	0.322	0.091	117.39%	-0.017	0.211	217.58%	0.06
s	2.17%	0.002	0.514	0.787	0.007	0.01	0.003	1.59%	0.001	0.001	2.20%	0
%RSD	3.512	2.627	10.44	1.578	76.24	3.001	3.74	1.358	7.109	0.302	1.01	0.634

1DA 16/12/2021 16:32:04

1	63.46%	-0.075	2.444	47.1	-0.012	0.274	0.064	120.17%	-0.024	0.215	92.76%	0.059
2	62.20%	-0.079	2.294	45.65	-0.017	0.258	0.059	123.15%	-0.025	0.214	90.57%	0.059
3	61.02%	-0.078	2.286	45.69	-0.019	0.256	0.063	121.61%	-0.023	0.219	80.64%	0.059

x	62.22%	-0.077	2.342	46.15	-0.016	0.263	0.062	121.64%	-0.024	0.216	87.99%	0.059
s	1.22%	0.002	0.089	0.824	0.003	0.01	0.003	1.49%	0.001	0.002	6.46%	0
%RSD	1.958	2.448	3.808	1.786	21.77	3.727	4.04	1.223	3.093	1.031	7.342	0.311

1AD 16/12/2021 16:33:13

1	88.67%	1.144	123.9	797.4	4.022	3.845	0.51	121.19%	0	0.264	736.16%	0.164
2	84.98%	1.151	121.1	795.3	3.913	3.801	0.489	121.60%	-0.003	0.264	749.31%	0.16
3	86.10%	1.199	124.2	814.5	4.033	3.831	0.503	123.37%	0	0.264	769.53%	0.163
x	86.59%	1.165	123.1	802.4	3.989	3.826	0.501	122.05%	-0.001	0.264	751.67%	0.162
s	1.89%	0.03	1.695	10.56	0.067	0.022	0.011	1.16%	0.002	0	16.81%	0.002
%RSD	2.183	2.593	1.377	1.316	1.671	0.585	2.109	0.947	221.3	0.11	2.236	1.085

1BD 16/12/2021 16:34:18

1	96.37%	1.127	110.5	776.8	3.507	5.096	0.67	126.05%	0.271	0.236	1389.21%	0.18
2	96.96%	1.053	109	745	3.375	4.904	0.677	129.86%	0.256	0.233	1426.32%	0.174
3	93.51%	1.108	112.2	764.7	3.447	5.052	0.681	127.93%	0.281	0.237	1415.52%	0.176
x	95.61%	1.096	110.6	762.2	3.443	5.018	0.676	127.95%	0.269	0.235	1410.35%	0.177
s	1.84%	0.038	1.615	16.01	0.066	0.101	0.005	1.91%	0.013	0.002	19.08%	0.003
%RSD	1.928	3.484	1.461	2.101	1.908	2.006	0.771	1.491	4.697	0.946	1.353	1.716

1CD 16/12/2021 16:35:23

1	90.31%	0.878	55.51	569.9	2.801	3.888	0.661	131.54%	0.042	0.218	4324.35%	0.171
2	91.54%	0.923	56.64	598.4	2.868	3.956	0.678	126.91%	0.042	0.218	4240.73%	0.172
3	89.60%	0.868	54.65	577.1	2.796	3.896	0.666	129.01%	0.038	0.215	4314.53%	0.168
x	90.48%	0.89	55.6	581.8	2.822	3.913	0.668	129.15%	0.041	0.217	4293.21%	0.17
s	0.98%	0.03	0.998	14.8	0.04	0.037	0.009	2.32%	0.002	0.002	45.71%	0.002
%RSD	1.083	3.33	1.795	2.544	1.433	0.944	1.326	1.798	4.757	0.765	1.065	1.397

1DD 16/12/2021 16:36:26

1	203.74%	2.071	13.48	559.2	1.153	3.77	1.007	135.58%	0.024	0.212	1547.25%	0.234
2	194.50%	2.083	12.92	561.7	1.135	3.783	1.016	131.98%	0.026	0.211	1457.52%	0.229
3	191.13%	2.185	13.33	576.6	1.186	3.929	1.033	126.47%	0.031	0.211	1407.26%	0.234
x	196.46%	2.113	13.24	565.8	1.158	3.827	1.019	131.34%	0.027	0.211	1470.68%	0.233
s	6.53%	0.063	0.293	9.415	0.026	0.088	0.013	4.59%	0.004	0.001	70.92%	0.003
%RSD	3.325	2.976	2.21	1.664	2.266	2.295	1.311	3.493	13.3	0.253	4.822	1.233

2AS 16/12/2021 16:37:42

1	56.03%	1.085	5.878	217.7	0.248	2.373	0.238	106.79%	-0.012	0.261	343.15%	0.061
2	55.55%	1.105	6.288	225.4	0.264	2.391	0.239	104.13%	-0.01	0.27	345.17%	0.062
3	40.52%	1.069	6.142	208.6	0.248	2.251	0.226	67.00%	-0.009	0.297	210.96%	0.061
x	50.70%	1.086	6.103	217.2	0.253	2.338	0.234	92.64%	-0.01	0.276	299.76%	0.061
s	8.82%	0.018	0.208	8.407	0.009	0.076	0.007	22.24%	0.001	0.018	76.91%	0.001
%RSD	17.394	1.683	3.406	3.87	3.698	3.244	3.01	24.01	11.21	6.681	25.658	0.82

2BS 16/12/2021 16:38:48

1	51.49%	1.086	6.385	176	0.162	0.372	0.125	119.28%	-0.017	0.242	409.51%	0.06
2	50.61%	1.088	6.214	170.4	0.151	0.349	0.123	118.36%	-0.017	0.245	385.26%	0.06
3	51.06%	1.055	6.131	171	0.151	0.326	0.128	122.76%	-0.018	0.242	387.78%	0.06
x	51.05%	1.077	6.243	172.5	0.155	0.349	0.126	120.14%	-0.017	0.243	394.18%	0.06
s	0.44%	0.019	0.13	3.101	0.006	0.023	0.002	2.32%	0	0.002	13.33%	0
%RSD	0.861	1.72	2.074	1.798	4.147	6.564	1.874	1.932	1.762	0.841	3.383	0.628

2CS 16/12/2021 16:39:56

1	47.78%	1.06	6.736	157.3	1.047	0.337	0.129	114.24%	-0.017	0.232	271.41%	0.058
2	50.44%	1.048	6.645	149.6	1.056	0.329	0.141	114.88%	-0.019	0.232	242.11%	0.058
3	49.16%	1.042	6.763	160.6	1.056	0.341	0.151	113.09%	-0.017	0.234	239.42%	0.058
x	49.13%	1.05	6.715	155.8	1.053	0.336	0.14	114.07%	-0.018	0.233	250.98%	0.058
s	1.33%	0.009	0.062	5.682	0.005	0.006	0.011	0.91%	0.001	0.001	17.75%	0
%RSD	2.71	0.87	0.917	3.646	0.483	1.866	8.036	0.795	5.214	0.584	7.071	0.129

2DS 16/12/2021 16:41:07

1	52.26%	1.128	5.829	157	0.08	0.186	0.104	108.64%	-0.026	0.252	285.39%	0.057
2	49.78%	1.12	5.848	157	0.083	0.19	0.119	107.27%	-0.024	0.262	291.79%	0.057
3	50.74%	1.108	5.919	160	0.073	0.19	0.114	108.02%	-0.024	0.264	304.59%	0.057
x	50.93%	1.119	5.865	158	0.079	0.189	0.112	107.97%	-0.025	0.259	293.92%	0.057
s	1.25%	0.01	0.048	1.711	0.005	0.002	0.008	0.69%	0.001	0.006	9.78%	0
%RSD	2.459	0.921	0.816	1.083	6.099	1.173	7.01	0.635	3.498	2.496	3.326	0.23

2AA 16/12/2021 16:42:14

1	56.43%	0.102	7.621	151.5	0.132	0.746	0.277	130.25%	-0.026	0.205	460.71%	0.064
2	55.93%	0.051	7.538	151	0.13	0.751	0.277	126.80%	-0.026	0.206	445.39%	0.064
3	57.95%	0.017	7.209	149.1	0.122	0.712	0.29	131.16%	-0.026	0.202	417.93%	0.064
x	56.77%	0.056	7.456	150.6	0.128	0.736	0.282	129.40%	-0.026	0.204	441.34%	0.064
s	1.05%	0.042	0.218	1.299	0.005	0.021	0.007	2.30%	0	0.002	21.68%	0

%RSD	1.854	75.09	2.925	0.863	4.003	2.845	2.62	1.778	0.643	0.896	4.911	0.351

2BA 16/12/2021 16:43:16

1	62.14%	0.003	8.091	166.7	0.152	0.674	0.355	126.38%	-0.021	0.202	308.29%	0.067
2	60.02%	-0.002	8.24	162.8	0.153	0.662	0.378	122.84%	-0.022	0.202	303.58%	0.066
3	59.15%	-0.009	7.964	157.7	0.146	0.638	0.359	125.10%	-0.021	0.202	290.61%	0.066
x	60.44%	-0.003	8.098	162.4	0.15	0.658	0.364	124.77%	-0.021	0.202	300.83%	0.066
s	1.53%	0.006	0.138	4.49	0.004	0.018	0.012	1.79%	0.001	0	9.16%	0
%RSD	2.539	229	1.703	2.765	2.473	2.718	3.341	1.437	2.951	0.16	3.044	0.521

2CA 16/12/2021 16:44:28

1	64.70%	0.036	9.115	134.1	4.008	0.892	0.606	113.86%	-0.016	0.202	7139.92%	0.068
2	63.92%	0.036	9.216	131	4.049	0.907	0.639	110.55%	-0.013	0.203	7086.57%	0.068
3	61.82%	0.029	9.116	132.5	4.045	0.897	0.641	110.99%	-0.017	0.204	7123.61%	0.068
x	63.48%	0.033	9.149	132.5	4.034	0.899	0.629	111.80%	-0.015	0.203	7116.70%	0.068
s	1.49%	0.004	0.058	1.549	0.023	0.008	0.02	1.79%	0.002	0.001	27.34%	0
%RSD	2.353	11.73	0.636	1.169	0.56	0.873	3.143	1.605	11.67	0.537	0.384	0.406

2DA 16/12/2021 16:45:31

1	61.53%	-0.026	6.207	220	0.122	0.411	0.395	129.43%	-0.018	0.203	1151.63%	0.065
2	61.98%	-0.028	6.234	229.8	0.08	0.404	0.397	128.33%	-0.017	0.203	1081.33%	0.066
3	61.91%	-0.033	6.241	229.5	0.079	0.424	0.37	127.58%	-0.017	0.202	985.42%	0.065
x	61.81%	-0.029	6.227	226.4	0.093	0.413	0.387	128.45%	-0.017	0.202	1072.79%	0.065
s	0.24%	0.004	0.018	5.549	0.024	0.01	0.015	0.93%	0	0.001	83.44%	0
%RSD	0.393	12.12	0.285	2.451	26.16	2.527	3.816	0.722	2.428	0.365	7.777	0.283

2AD 16/12/2021 16:46:33

1	68.67%	2.709	10.51	331.7	0.474	2.545	0.795	135.41%	-0.022	0.21	229.99%	0.066
2	66.69%	2.838	10.8	337.6	0.491	2.661	0.781	132.04%	-0.022	0.209	252.55%	0.066
3	64.88%	2.727	10.43	330.2	0.457	2.598	0.741	135.80%	-0.022	0.211	264.17%	0.066
x	66.75%	2.758	10.58	333.2	0.474	2.601	0.772	134.42%	-0.022	0.21	248.90%	0.066
s	1.90%	0.07	0.193	3.89	0.017	0.058	0.028	2.07%	0	0.001	17.38%	0
%RSD	2.841	2.524	1.825	1.167	3.558	2.237	3.663	1.539	1.107	0.491	6.983	0.325

2BD 16/12/2021 16:47:40

1	64.45%	0.444	6.204	272.4	0.278	2.944	0.796	131.40%	-0.024	0.204	357.97%	0.065
2	65.32%	0.422	6.071	252.9	0.275	2.841	0.755	131.20%	-0.022	0.207	358.31%	0.064

3	61.00%	0.413	6.067	264.9	0.269	2.848	0.764	130.85%	-0.023	0.208	355.11%	0.064
x	63.59%	0.426	6.114	263.4	0.274	2.877	0.772	131.15%	-0.023	0.207	357.13%	0.064
s	2.29%	0.016	0.078	9.838	0.005	0.058	0.021	0.28%	0.001	0.002	1.76%	0
%RSD	3.599	3.765	1.276	3.735	1.716	2.003	2.751	0.211	2.77	0.914	0.492	0.759

2CD 16/12/2021 16:48:47

1	63.54%	0.775	17.24	683.6	0.876	5.439	1.447	118.40%	-0.02	0.3	229.14%	0.068
2	61.32%	0.742	16.53	665.1	0.829	5.178	1.44	122.25%	-0.02	0.295	218.70%	0.068
3	59.89%	0.743	16.59	683.7	0.835	5.285	1.432	122.67%	-0.02	0.301	220.89%	0.067
x	61.58%	0.753	16.79	677.5	0.846	5.301	1.439	121.11%	-0.02	0.299	222.91%	0.068
s	1.84%	0.019	0.392	10.71	0.026	0.131	0.007	2.35%	0	0.003	5.51%	0
%RSD	2.986	2.474	2.334	1.581	3.033	2.477	0.51	1.944	0.543	0.991	2.47	0.692

2DD 16/12/2021 16:49:53

1	56.76%	0.364	4.432	266.4	0.262	2.329	1.034	131.25%	-0.025	0.209	133.67%	0.066
2	56.15%	0.354	4.281	263.2	0.26	2.286	1	129.57%	-0.024	0.208	139.06%	0.065
3	56.79%	0.369	4.422	264.7	0.262	2.327	1.029	125.10%	-0.025	0.208	138.39%	0.066
x	56.57%	0.362	4.378	264.8	0.261	2.314	1.021	128.64%	-0.025	0.208	137.04%	0.066
s	0.36%	0.008	0.084	1.617	0.001	0.025	0.019	3.18%	0.001	0.001	2.94%	0.001
%RSD	0.643	2.21	1.922	0.611	0.473	1.059	1.847	2.472	3.004	0.29	2.142	0.864

3AS 16/12/2021 16:50:54

1	57.28%	0.843	207.5	115.8	0.085	0.542	0.444	121.41%	0.287	0.231	171.73%	0.059
2	55.84%	0.932	208.9	111.5	0.09	0.507	0.42	120.54%	0.284	0.234	181.83%	0.059
3	53.58%	0.969	204.2	102.6	0.084	0.463	0.328	122.34%	0.284	0.233	157.58%	0.059
x	55.56%	0.915	206.9	110	0.086	0.504	0.397	121.43%	0.285	0.232	170.38%	0.059
s	1.86%	0.065	2.393	6.764	0.003	0.04	0.061	0.90%	0.002	0.001	12.18%	0
%RSD	3.353	7.075	1.157	6.15	3.184	7.887	15.43	0.744	0.695	0.59	7.148	0.281

3BS 16/12/2021 16:51:55

1	55.36%	1.145	218.3	89	0.048	0.179	0.161	125.21%	0.033	0.222	65.32%	0.058
2	54.36%	1.135	217.8	83.76	0.05	0.165	0.152	125.45%	0.028	0.219	72.56%	0.058
3	54.92%	1.162	218.9	84.73	0.045	0.17	0.151	125.26%	0.024	0.218	66.33%	0.058
x	54.88%	1.148	218.3	85.83	0.048	0.171	0.155	125.31%	0.028	0.22	68.07%	0.058
s	0.50%	0.014	0.542	2.788	0.002	0.007	0.006	0.12%	0.005	0.002	3.92%	0
%RSD	0.912	1.181	0.249	3.248	5.016	4.118	3.568	0.099	16.09	0.78	5.76	0.179

3CS 16/12/2021 16:53:00

1	56.40%	1.057	183.7	71.68	0.123	0.38	0.294	137.73%	0.481	0.211	88.05%	0.058
2	55.21%	1.065	184.6	68.46	0.122	0.393	0.314	136.56%	0.499	0.216	85.69%	0.059
3	54.27%	1.099	192.1	74.72	0.136	0.405	0.308	131.54%	0.528	0.218	91.41%	0.059
x	55.29%	1.073	186.8	71.62	0.127	0.393	0.305	135.28%	0.503	0.215	88.38%	0.059
s	1.07%	0.022	4.601	3.129	0.008	0.012	0.01	3.29%	0.023	0.003	2.88%	0
%RSD	1.928	2.075	2.463	4.369	6.425	3.104	3.307	2.43	4.666	1.523	3.255	0.213

3DS 16/12/2021 16:54:09

1	51.12%	1.102	196.5	110.3	0.079	0.341	0.111	128.60%	1.579	0.216	117.34%	0.057
2	52.24%	1.081	197.5	108.7	0.073	0.323	0.112	128.79%	1.614	0.218	114.31%	0.057
3	52.81%	1.084	193.8	106.2	0.069	0.328	0.122	128.49%	1.612	0.215	102.02%	0.057
x	52.05%	1.089	195.9	108.4	0.074	0.331	0.115	128.63%	1.602	0.216	111.22%	0.057
s	0.86%	0.012	1.953	2.068	0.005	0.009	0.006	0.15%	0.019	0.001	8.11%	0
%RSD	1.649	1.07	0.997	1.908	6.454	2.865	5.288	0.115	1.206	0.585	7.295	0.083

New Rh 16/12/2021 16:55:21

1	47.77%	-0.076	0.241	-0.603	-0.085	-0.038	-0.033	1066.99%	-0.019	0.199	44.95%	0.056
2	45.55%	-0.085	-0.088	-0.662	-0.086	-0.04	-0.033	1092.14%	-0.02	0.199	36.53%	0.056
3	46.31%	-0.088	-0.224	-0.696	-0.086	-0.039	-0.034	1090.20%	-0.021	0.199	46.97%	0.056
x	46.54%	-0.083	-0.024	-0.654	-0.086	-0.039	-0.034	1083.11%	-0.02	0.199	42.82%	0.056
s	1.13%	0.006	0.239	0.047	0.001	0.001	0.001	13.99%	0.001	0	5.54%	0
%RSD	2.426	7.389	1005	7.253	0.695	1.946	2.269	1.292	6.093	0.072	12.93	0.022

3AA 16/12/2021 16:58:04

1	54.93%	0.116	255.2	102.3	1.154	2.099	0.056	118.69%	0.445	0.205	272.76%	0.06
2	52.11%	0.103	241.5	96.05	1.071	1.536	0.059	124.06%	0.421	0.203	289.26%	0.059
3	52.43%	0.107	247.6	100.2	1.109	1.386	0.073	120.24%	0.451	0.203	268.38%	0.059
x	53.16%	0.109	248.1	99.51	1.112	1.673	0.063	121.00%	0.439	0.204	276.80%	0.059
s	1.55%	0.007	6.889	3.187	0.041	0.376	0.009	2.76%	0.016	0.001	11.01%	0
%RSD	2.913	6.032	2.776	3.202	3.73	22.46	14.92	2.282	3.565	0.456	3.978	0.716

3BA 16/12/2021 16:59:04

1	50.63%	0.015	216.5	294.9	2.972	0.806	0.071	129.30%	0.12	0.203	386.10%	0.059

2	49.33%	0.007	217.8	296.3	3.018	0.796	0.07	131.21%	0.112	0.201	403.78%	0.06
3	50.26%	0.009	218.3	302.3	3.051	0.792	0.069	129.54%	0.111	0.202	382.23%	0.059
x	50.07%	0.01	217.5	297.8	3.013	0.798	0.07	130.02%	0.114	0.202	390.70%	0.06
s	0.67%	0.004	0.926	3.917	0.04	0.007	0.001	1.05%	0.005	0.001	11.49%	0
%RSD	1.346	39.03	0.426	1.315	1.319	0.91	1.617	0.804	4.454	0.288	2.942	0.415

3CA 16/12/2021 17:00:17

1	53.07%	0.047	267.8	145.8	7.321	0.845	0.214	125.74%	1.275	0.203	167.35%	0.064
2	50.29%	0.052	267.5	148.3	7.482	0.879	0.233	122.56%	1.323	0.202	167.68%	0.065
3	52.69%	0.047	261.1	143.1	7.27	0.823	0.229	129.15%	1.281	0.202	163.14%	0.065
x	52.02%	0.048	265.5	145.8	7.358	0.849	0.225	125.82%	1.293	0.203	166.06%	0.065
s	1.51%	0.003	3.749	2.59	0.111	0.028	0.01	3.30%	0.026	0.001	2.53%	0
%RSD	2.899	6.106	1.412	1.777	1.508	3.337	4.32	2.619	2.02	0.417	1.525	0.393

3DA 16/12/2021 17:01:42

1	50.49%	-0.008	230.7	82.09	0.142	0.55	0.122	129.86%	0.052	0.205	116.67%	0.058
2	48.38%	-0.023	231.4	76.93	0.083	0.569	0.108	129.32%	0.051	0.202	102.69%	0.058
3	50.12%	-0.033	230.4	79.03	0.078	0.56	0.104	129.77%	0.035	0.203	98.82%	0.058
x	49.66%	-0.021	230.8	79.35	0.101	0.56	0.111	129.65%	0.046	0.203	106.06%	0.058
s	1.13%	0.013	0.486	2.595	0.036	0.01	0.009	0.29%	0.009	0.002	9.39%	0
%RSD	2.275	58.8	0.211	3.27	35.43	1.74	8.18	0.226	20.38	0.833	8.851	0.475

3AD 16/12/2021 17:03:26

1	49.30%	0.883	421.5	487.1	4.403	11.25	0.638	140.82%	0.35	0.214	253.90%	0.106
2	49.79%	0.847	407.1	487.1	4.347	11.27	0.661	140.52%	0.351	0.215	264.17%	0.104
3	50.59%	0.878	423.4	498.4	4.525	11.66	0.672	138.30%	0.343	0.219	257.94%	0.105
x	49.89%	0.869	417.3	490.9	4.425	11.39	0.657	139.88%	0.348	0.216	258.67%	0.105
s	0.65%	0.02	8.902	6.545	0.091	0.228	0.018	1.38%	0.005	0.002	5.18%	0.001
%RSD	1.298	2.245	2.133	1.333	2.057	2.002	2.696	0.985	1.396	1.037	2.001	1.141

3BD 16/12/2021 17:04:38

1	53.08%	0.947	349.3	530.2	3.403	12.09	0.562	143.63%	1.216	0.213	101.85%	0.13
2	53.06%	0.96	362.7	545.1	3.413	12.13	0.574	140.51%	1.226	0.215	107.74%	0.126
3	51.29%	0.941	356.2	542.5	3.477	12.19	0.572	139.61%	1.2	0.222	93.77%	0.128
x	52.47%	0.95	356.1	539.3	3.431	12.14	0.569	141.25%	1.214	0.217	101.12%	0.128
s	1.03%	0.01	6.68	7.952	0.04	0.05	0.007	2.11%	0.013	0.005	7.02%	0.002
%RSD	1.961	1.018	1.876	1.475	1.166	0.414	1.173	1.493	1.103	2.113	6.938	1.327

3CD 16/12/2021 17:05:44

1	124.06%	1.583	436.9	728.1	3.846	14.71	0.899	135.39%	0.815	0.213	571.72%	0.181
2	123.42%	1.542	430.1	707.6	3.704	14.09	0.859	138.61%	0.788	0.209	576.27%	0.177
3	125.95%	1.558	428.3	703.4	3.721	14.42	0.833	137.80%	0.783	0.21	564.65%	0.177
x	124.48%	1.561	431.7	713	3.757	14.41	0.864	137.27%	0.795	0.211	570.88%	0.178
s	1.32%	0.021	4.534	13.24	0.078	0.312	0.033	1.67%	0.017	0.002	5.86%	0.002
%RSD	1.059	1.32	1.05	1.857	2.063	2.164	3.857	1.218	2.159	1.138	1.026	1.19

3DD 16/12/2021 17:06:50

1	112.35%	1.008	439.3	629.2	3.787	12.14	0.748	139.17%	0.124	0.203	261.48%	0.186
2	113.43%	0.957	437.4	635	3.748	12.13	0.739	140.54%	0.108	0.204	248.68%	0.185
3	113.21%	0.948	423.3	615.4	3.643	11.82	0.72	142.11%	0.1	0.205	247.16%	0.183
x	113.00%	0.971	433.3	626.5	3.726	12.03	0.736	140.61%	0.111	0.204	252.44%	0.185
s	0.57%	0.032	8.757	10.08	0.074	0.184	0.014	1.47%	0.012	0.001	7.86%	0.002
%RSD	0.505	3.306	2.021	1.608	1.994	1.526	1.958	1.046	11.11	0.457	3.115	0.936

4AS 16/12/2021 17:07:57

1	46.00%	1.033	10.17	152.1	0.139	0.513	0.12	115.50%	0.042	0.231	489.35%	0.064
2	43.85%	1.084	5.931	150.4	0.091	0.352	0.099	118.66%	0.04	0.23	457.01%	0.063
3	42.66%	1.084	4.099	150	0.082	0.284	0.091	119.41%	0.031	0.229	478.40%	0.062
x	44.17%	1.067	6.734	150.8	0.104	0.383	0.103	117.85%	0.038	0.23	474.92%	0.063
s	1.69%	0.03	3.115	1.104	0.031	0.117	0.015	2.07%	0.006	0.001	16.45%	0.001
%RSD	3.831	2.774	46.26	0.732	29.77	30.64	14.61	1.759	14.66	0.455	3.464	1.87

4BS 16/12/2021 17:08:59

1	47.61%	1.064	4.158	291.2	0.145	0.407	0.083	127.82%	0.17	0.215	439.66%	0.092
2	47.07%	1.029	4.228	293.4	0.147	0.409	0.079	126.91%	0.181	0.217	411.03%	0.091
3	45.49%	1.03	4.525	292.6	0.15	0.445	0.081	123.82%	0.18	0.216	405.97%	0.092
x	46.72%	1.041	4.304	292.4	0.147	0.42	0.081	126.18%	0.177	0.216	418.89%	0.091
s	1.10%	0.02	0.195	1.121	0.003	0.021	0.002	2.10%	0.006	0.001	18.17%	0.001
%RSD	2.364	1.907	4.526	0.383	1.711	5.032	2.431	1.66	3.488	0.433	4.337	0.828

4CS 16/12/2021 17:09:58

1	46.39%	0.471	1.489	223.2	0.131	0.424	0.015	208.87%	0.048	0.205	3154.76%	0.068
2	44.34%	0.448	1.409	221.5	0.132	0.415	0.014	208.76%	0.047	0.207	3129.58%	0.067
3	43.22%	0.449	1.426	227.3	0.137	0.435	0.017	202.53%	0.045	0.207	3129.75%	0.068

x	44.65%	0.456	1.441	224	0.133	0.425	0.015	206.72%	0.047	0.207	3138.03%	0.068
s	1.61%	0.013	0.043	2.947	0.003	0.01	0.001	3.63%	0.002	0.001	14.49%	0
%RSD	3.604	2.884	2.948	1.316	2.442	2.439	8.394	1.756	3.325	0.481	0.462	0.659

4DS 16/12/2021 17:11:11

1	42.14%	1.065	2.208	935	0.205	0.75	0.043	111.90%	0.504	0.21	414.06%	0.063
2	41.18%	1.038	2.192	935.7	0.21	0.761	0.051	109.13%	0.553	0.214	429.89%	0.064
3	40.18%	1.011	2.156	899.6	0.204	0.734	0.045	112.16%	0.488	0.213	402.60%	0.063
x	41.16%	1.038	2.185	923.4	0.206	0.749	0.046	111.06%	0.515	0.212	415.52%	0.064
s	0.98%	0.027	0.027	20.68	0.003	0.014	0.004	1.68%	0.034	0.002	13.70%	0
%RSD	2.381	2.612	1.224	2.239	1.545	1.827	9.394	1.513	6.569	0.984	3.297	0.384

4AA 16/12/2021 17:12:14

1	45.05%	0.419	1.55	150.4	0.114	0.853	0.123	132.16%	0.535	0.209	892.55%	0.066
2	44.35%	0.365	1.426	145.9	0.112	0.847	0.121	134.43%	0.479	0.212	847.55%	0.065
3	43.92%	0.345	1.407	141.5	0.113	0.83	0.117	134.52%	0.488	0.211	843.51%	0.065
x	44.44%	0.377	1.461	145.9	0.113	0.844	0.12	133.70%	0.501	0.211	861.20%	0.065
s	0.57%	0.038	0.078	4.447	0.001	0.012	0.003	1.33%	0.03	0.001	27.22%	0
%RSD	1.282	10.15	5.342	3.047	0.853	1.379	2.485	0.998	6.072	0.639	3.161	0.702

4BA 16/12/2021 17:13:21

1	49.00%	0.114	2.407	129.8	0.103	0.414	0.081	234.52%	0.121	0.202	207.25%	0.08
2	47.47%	0.106	2.449	131.2	0.105	0.409	0.085	233.79%	0.124	0.202	198.50%	0.08
3	47.26%	0.097	2.431	127.1	0.106	0.407	0.089	241.21%	0.12	0.202	197.32%	0.079
x	47.91%	0.106	2.429	129.4	0.105	0.41	0.085	236.51%	0.122	0.202	201.02%	0.079
s	0.95%	0.008	0.021	2.065	0.002	0.003	0.004	4.09%	0.002	0	5.43%	0.001
%RSD	1.989	7.874	0.855	1.596	1.588	0.798	5.016	1.729	2.001	0.132	2.7	0.816

4CA 16/12/2021 17:14:34

1	47.91%	0.429	3.962	450.5	0.197	1.225	0.172	128.60%	0.136	0.208	172.90%	0.095
2	46.82%	0.45	3.967	460.4	0.211	1.263	0.182	125.88%	0.141	0.208	178.46%	0.096
3	48.02%	0.449	3.882	455	0.207	1.263	0.178	128.02%	0.141	0.209	178.80%	0.096
x	47.58%	0.443	3.937	455.3	0.205	1.25	0.177	127.50%	0.139	0.208	176.72%	0.096
s	0.66%	0.012	0.048	4.963	0.007	0.022	0.005	1.43%	0.003	0	3.31%	0.001
%RSD	1.396	2.619	1.21	1.09	3.55	1.761	2.877	1.123	2.267	0.158	1.873	0.57

4DA 16/12/2021 17:15:38

1	43.37%	0.342	2.383	256	0.426	4.474	0.154	128.33%	0.649	0.205	193.78%	0.067
2	41.65%	0.33	2.338	254.8	0.418	4.498	0.142	127.25%	0.664	0.208	177.28%	0.067
3	41.63%	0.318	2.319	260.8	0.428	4.537	0.159	127.03%	0.663	0.209	183.68%	0.067
x	42.22%	0.33	2.347	257.2	0.424	4.503	0.151	127.54%	0.658	0.207	184.92%	0.067
s	1.00%	0.012	0.033	3.153	0.005	0.032	0.009	0.69%	0.008	0.002	8.32%	0
%RSD	2.372	3.543	1.409	1.226	1.239	0.702	5.761	0.544	1.25	0.835	4.499	0.515

4AD 16/12/2021 17:16:44

1	91.70%	1.722	4.729	254.9	0.672	10.76	0.84	115.74%	1.927	0.203	214.49%	0.211
2	92.24%	1.716	4.79	256.4	0.656	10.78	0.83	113.42%	1.955	0.203	190.42%	0.214
3	88.05%	1.698	4.676	247.8	0.655	10.58	0.838	113.60%	1.983	0.203	187.72%	0.216
x	90.66%	1.712	4.732	253	0.661	10.71	0.836	114.25%	1.955	0.203	197.54%	0.214
s	2.28%	0.013	0.057	4.582	0.01	0.11	0.005	1.29%	0.028	0	14.74%	0.003
%RSD	2.513	0.732	1.206	1.811	1.462	1.027	0.618	1.128	1.412	0.232	7.462	1.25

4BD 16/12/2021 17:17:50

1	186.35%	4.622	12.55	773.2	1.454	11.41	1.751	115.54%	0.092	0.202	425.01%	0.23
2	182.35%	4.599	12.38	765.4	1.445	11.18	1.745	115.46%	0.084	0.201	421.64%	0.22
3	182.88%	4.546	12.37	768.5	1.495	11.46	1.709	116.16%	0.071	0.201	429.38%	0.22
x	183.86%	4.589	12.43	769.1	1.464	11.35	1.735	115.72%	0.082	0.201	425.34%	0.224
s	2.17%	0.039	0.098	3.926	0.027	0.147	0.023	0.38%	0.011	0.001	3.89%	0.006
%RSD	1.182	0.841	0.79	0.51	1.839	1.3	1.314	0.329	13.05	0.445	0.913	2.582

4CD 16/12/2021 17:18:51

1	140.90%	2.9	9.307	473.5	1.028	7.856	1.29	117.95%	2.203	0.201	249.52%	0.182
2	135.98%	2.959	9.58	485.4	1.066	8.09	1.308	114.82%	2.217	0.203	249.86%	0.187
3	134.91%	2.936	9.298	467	1.027	8.008	1.295	116.87%	2.231	0.201	255.58%	0.187
x	137.26%	2.932	9.395	475.3	1.04	7.985	1.298	116.55%	2.217	0.202	251.65%	0.186
s	3.19%	0.03	0.16	9.371	0.022	0.119	0.009	1.59%	0.014	0.001	3.41%	0.003
%RSD	2.326	1.015	1.706	1.972	2.154	1.488	0.72	1.36	0.615	0.389	1.354	1.659

4DD 16/12/2021 17:20:06

1	110.51%	2.293	7.145	333.3	0.68	5.107	1.234	112.98%	4.063	0.203	313.85%	0.241
2	105.68%	2.353	7.193	335.2	0.721	5.28	1.244	110.92%	4.061	0.205	295.49%	0.237
3	106.63%	2.348	7.234	347.8	0.82	5.8	1.294	109.13%	4.095	0.205	312.33%	0.244
x	107.61%	2.331	7.191	338.8	0.74	5.395	1.257	111.01%	4.073	0.204	307.22%	0.241
s	2.56%	0.033	0.044	7.841	0.072	0.361	0.032	1.93%	0.019	0.001	10.19%	0.003

%RSD	2.377	1.414	0.618	2.315	9.702	6.688	2.541	1.736	0.469	0.657	3.316	1.413

c1s 16/12/2021 17:21:20

1	42.65%	1.24	0.047	102.7	0.029	1.438	0.322	113.66%	0.322	0.221	1131.91%	0.096
2	40.56%	1.276	-0.018	104	0.03	1.412	0.319	109.28%	0.269	0.217	1038.85%	0.093
3	40.38%	1.237	-0.048	102.7	0.032	1.338	0.303	111.56%	0.189	0.22	1023.17%	0.091
x	41.19%	1.251	-0.006	103.1	0.03	1.396	0.315	111.50%	0.26	0.219	1064.64%	0.093
s	1.26%	0.021	0.049	0.776	0.001	0.052	0.01	2.19%	0.067	0.002	58.78%	0.002
%RSD	3.063	1.717	786.3	0.753	4.224	3.738	3.264	1.965	25.61	0.989	5.521	2.622

C2S 16/12/2021 17:22:38

1	42.85%	1.197	-0.065	92.94	0.05	0.498	0.239	108.66%	0.033	0.209	1316.70%	0.086
2	41.83%	1.166	-0.069	93.21	0.058	0.507	0.241	106.67%	0.04	0.21	1250.94%	0.085
3	41.20%	1.194	-0.05	94.83	0.076	0.596	0.264	102.98%	0.043	0.209	1267.46%	0.085
x	41.96%	1.186	-0.061	93.66	0.061	0.533	0.248	106.10%	0.039	0.21	1278.37%	0.085
s	0.83%	0.017	0.01	1.017	0.013	0.054	0.014	2.88%	0.005	0.001	34.21%	0
%RSD	1.986	1.416	16.53	1.086	21.45	10.13	5.584	2.714	13.33	0.278	2.676	0.241

C3S 16/12/2021 17:23:41

1	41.26%	0.986	-0.202	71.27	0.003	0.496	0.169	127.05%	0.01	0.207	565.66%	0.084
2	40.65%	0.94	-0.221	67.91	-0.005	0.478	0.165	127.51%	0.012	0.208	521.52%	0.081
3	38.04%	0.931	-0.222	67.46	0.003	0.487	0.175	125.68%	0.014	0.206	543.93%	0.082
x	39.98%	0.952	-0.215	68.88	0	0.487	0.17	126.75%	0.012	0.207	543.70%	0.082
s	1.71%	0.03	0.011	2.081	0.004	0.009	0.005	0.95%	0.002	0.001	22.07%	0.001
%RSD	4.279	3.119	5.282	3.02	1753	1.847	2.955	0.749	19.73	0.414	4.059	1.708

C4S 16/12/2021 17:24:41

1	40.45%	0.966	-0.101	87.58	0.146	0.352	0.178	129.10%	0.002	0.205	997.05%	0.082
2	40.06%	0.94	-0.107	84.27	0.158	0.354	0.174	127.56%	0.003	0.206	1004.80%	0.084
3	39.64%	0.915	-0.108	89.11	0.14	0.334	0.165	128.57%	0.006	0.206	1002.78%	0.082
x	40.05%	0.94	-0.105	86.99	0.148	0.347	0.172	128.41%	0.003	0.206	1001.54%	0.082
s	0.40%	0.026	0.004	2.474	0.009	0.011	0.007	0.78%	0.002	0.001	4.02%	0.001
%RSD	1.009	2.713	3.658	2.843	6.414	3.127	4.018	0.606	61.63	0.509	0.402	1.383

C5S 16/12/2021 17:26:14

1	37.27%	1.026	-0.21	89.78	0.082	0.761	0.189	120.50%	0.031	0.209	710.38%	0.087
2	38.31%	1.071	-0.209	93.71	0.083	0.801	0.202	114.71%	0.035	0.21	690.84%	0.087

3	36.45%	1.07	-0.209	97.63	0.086	0.813	0.19	112.51%	0.032	0.209	665.06%	0.088
x	37.34%	1.056	-0.209	93.71	0.084	0.792	0.194	115.91%	0.032	0.209	688.76%	0.087
s	0.94%	0.026	0.001	3.927	0.002	0.027	0.007	4.13%	0.002	0.001	22.73%	0
%RSD	2.504	2.429	0.394	4.191	2.337	3.416	3.842	3.562	6.397	0.316	3.301	0.534

C1A 16/12/2021 17:27:26

1	35.43%	0.058	-0.149	77.86	0.003	0.368	0.111	122.69%	-0.022	0.203	207.59%	0.06
2	34.05%	0.011	-0.15	76.02	0.004	0.388	0.113	122.62%	-0.021	0.203	229.14%	0.06
3	32.94%	-0.014	-0.147	74.93	0.001	0.402	0.104	123.49%	-0.019	0.202	221.40%	0.06
x	34.14%	0.018	-0.149	76.27	0.003	0.386	0.109	122.93%	-0.02	0.203	219.38%	0.06
s	1.24%	0.036	0.002	1.483	0.001	0.017	0.005	0.49%	0.002	0.001	10.92%	0
%RSD	3.644	198.8	1.059	1.944	43.13	4.342	4.129	0.395	7.879	0.259	4.977	0.54

C2A 16/12/2021 17:28:27

1	35.77%	-0.051	-0.182	83.92	-0.009	0.252	0.121	137.46%	-0.024	0.202	129.97%	0.058
2	34.32%	-0.055	-0.186	82.23	-0.008	0.249	0.104	137.82%	-0.023	0.202	124.58%	0.058
3	34.45%	-0.055	-0.18	82.36	-0.004	0.267	0.117	132.84%	-0.023	0.201	122.90%	0.058
x	34.85%	-0.054	-0.183	82.83	-0.007	0.256	0.114	136.04%	-0.023	0.202	125.82%	0.058
s	0.80%	0.002	0.003	0.943	0.003	0.009	0.009	2.78%	0	0.001	3.69%	0
%RSD	2.301	4.631	1.832	1.138	40.01	3.565	8.034	2.042	2.148	0.325	2.936	0.215

C3A 16/12/2021 17:29:33

1	34.91%	-0.049	-0.247	45.98	0.028	0.552	0.172	109.60%	-0.022	0.202	869.29%	0.085
2	35.94%	-0.054	-0.256	41.8	0.024	0.548	0.17	110.63%	-0.021	0.201	856.65%	0.084
3	35.88%	-0.055	-0.253	46.36	0.024	0.549	0.151	108.33%	-0.02	0.203	865.08%	0.085
x	35.58%	-0.053	-0.252	44.71	0.025	0.55	0.164	109.52%	-0.021	0.202	863.67%	0.085
s	0.57%	0.003	0.005	2.532	0.002	0.002	0.011	1.15%	0.001	0.001	6.44%	0.001
%RSD	1.612	5.757	1.846	5.663	9.518	0.416	7	1.052	6.682	0.303	0.745	0.885

C4A 16/12/2021 17:30:35

1	36.19%	-0.076	-0.175	40.38	0.1	0.113	0.104	149.93%	-0.026	0.201	159.43%	0.062
2	34.25%	-0.077	-0.171	40.77	0.103	0.117	0.099	146.38%	-0.026	0.201	148.15%	0.062
3	34.81%	-0.078	-0.175	38.54	0.102	0.11	0.1	149.84%	-0.026	0.201	146.81%	0.061
x	35.08%	-0.077	-0.174	39.9	0.102	0.114	0.101	148.72%	-0.026	0.201	151.46%	0.062
s	1.00%	0.001	0.002	1.189	0.001	0.004	0.002	2.02%	0	0	6.94%	0
%RSD	2.841	1.695	1.393	2.981	1.178	3.346	2.42	1.358	0.468	0.034	4.578	0.345

C5A 16/12/2021 17:31:46

1	34.97%	-0.061	-0.089	124.1	0.251	1.064	0.27	136.75%	-0.025	0.202	441.85%	0.06
2	33.90%	-0.061	-0.086	124	0.247	1.113	0.266	134.56%	-0.026	0.202	448.08%	0.06
3	33.61%	-0.058	-0.079	129.7	0.257	1.15	0.28	129.37%	-0.025	0.201	432.75%	0.06
x	34.16%	-0.06	-0.085	125.9	0.252	1.109	0.272	133.56%	-0.025	0.202	440.89%	0.06
s	0.72%	0.002	0.005	3.302	0.005	0.043	0.007	3.79%	0	0	7.71%	0
%RSD	2.103	3.005	6.326	2.622	2.032	3.907	2.724	2.836	1.912	0.223	1.748	0.506

C1D 16/12/2021 17:32:47

1	42.86%	0.123	0.37	86.27	0.123	1.382	0.237	136.42%	0.009	0.209	########	0.077
2	42.65%	0.125	0.373	81.58	0.126	1.392	0.2	134.54%	0.009	0.209	########	0.079
3	40.94%	0.13	0.428	85.07	0.134	1.366	0.171	129.28%	0.012	0.209	########	0.077
x	42.15%	0.126	0.391	84.31	0.128	1.38	0.203	133.41%	0.01	0.209	########	0.078
s	1.06%	0.003	0.033	2.433	0.006	0.013	0.033	3.70%	0.002	0	219.99%	0.001
%RSD	2.503	2.654	8.327	2.886	4.446	0.942	16.32	2.773	17.99	0.087	1.282	0.978

C2D 16/12/2021 17:33:50

1	40.53%	0.143	0.128	88.94	0.212	0.898	0.102	123.11%	0.03	0.206	########	0.076
2	39.49%	0.138	0.123	87.81	0.206	0.928	0.1	124.35%	0.032	0.208	9985.45%	0.078
3	38.04%	0.136	0.11	90.3	0.204	0.94	0.131	127.64%	0.03	0.204	9968.90%	0.075
x	39.35%	0.139	0.12	89.02	0.207	0.922	0.111	125.03%	0.031	0.206	9996.19%	0.076
s	1.25%	0.004	0.009	1.25	0.004	0.021	0.018	2.34%	0.001	0.002	33.96%	0.001
%RSD	3.184	2.795	7.546	1.404	2.066	2.318	15.83	1.871	3.199	0.94	0.34	1.942

C3D 16/12/2021 17:34:53

1	41.34%	0.151	0.218	72.5	0.094	1.371	0.072	124.17%	0.015	0.205	########	0.074
2	40.20%	0.143	0.21	70.36	0.086	1.372	0.072	126.12%	0.012	0.204	########	0.075
3	39.57%	0.151	0.23	74.94	0.084	1.428	0.072	119.50%	0.017	0.204	########	0.075
x	40.37%	0.148	0.22	72.6	0.088	1.39	0.072	123.26%	0.015	0.204	########	0.075
s	0.90%	0.004	0.01	2.295	0.006	0.033	0	3.40%	0.002	0	73.23%	0
%RSD	2.223	2.992	4.627	3.162	6.291	2.353	0.484	2.762	14.82	0.135	0.691	0.181

C4D 16/12/2021 17:35:54

1	39.20%	0.078	0.103	67.18	0.364	1.012	0.07	125.72%	0.009	0.214	########	0.071
2	37.72%	0.072	0.093	65.75	0.351	0.946	0.067	129.90%	0.011	0.213	########	0.07
3	37.62%	0.076	0.097	67.44	0.368	0.977	0.063	128.04%	0.013	0.214	########	0.07
x	38.18%	0.075	0.098	66.79	0.361	0.978	0.067	127.89%	0.011	0.214	########	0.071

s	0.89%	0.003	0.005	0.911	0.009	0.033	0.003	2.09%	0.002	0	105.94%	0
%RSD	2.321	4.486	5.046	1.364	2.58	3.329	4.841	1.637	20.52	0.22	0.874	0.527

C5D 16/12/2021 17:36:57

1	37.02%	0.104	0.156	95.01	0.073	0.841	0.058	125.21%	0.014	0.205	9047.35%	0.072
2	36.74%	0.108	0.147	94.34	0.065	0.831	0.065	124.42%	0.02	0.205	9192.66%	0.072
3	36.30%	0.104	0.13	92.82	0.055	0.797	0.055	129.64%	0.018	0.205	9311.76%	0.072
x	36.69%	0.105	0.144	94.05	0.064	0.823	0.059	126.43%	0.017	0.205	9183.92%	0.072
s	0.36%	0.002	0.013	1.12	0.009	0.023	0.005	2.82%	0.003	0	132.42%	0
%RSD	0.98	2.181	9.035	1.191	13.87	2.771	8.161	2.227	15.72	0.084	1.442	0.49

5AS 16/12/2021 17:38:00

1	28.46%	1.069	11.85	155.3	0.036	0.354	0.011	115.94%	-0.009	0.212	142.60%	0.057
2	27.36%	1.056	12.1	155.6	0.037	0.353	0.016	116.61%	-0.009	0.21	120.88%	0.057
3	26.67%	1.026	11.74	152.9	0.034	0.35	0.014	117.78%	-0.01	0.212	103.70%	0.057
x	27.50%	1.05	11.9	154.6	0.036	0.352	0.014	116.78%	-0.009	0.211	122.39%	0.057
s	0.91%	0.022	0.184	1.484	0.002	0.002	0.002	0.93%	0.001	0.002	19.49%	0
%RSD	3.29	2.102	1.547	0.96	4.306	0.603	17.07	0.799	10.04	0.746	15.925	0.094

5BS 16/12/2021 17:39:01

1	27.86%	0.923	6.045	116.3	0.071	0.288	0.081	121.85%	-0.019	0.204	86.36%	0.057
2	26.69%	0.892	5.949	114.2	0.064	0.285	0.08	123.26%	-0.019	0.207	91.92%	0.057
3	25.77%	0.884	6.153	116.8	0.073	0.304	0.091	121.19%	-0.017	0.207	87.37%	0.057
x	26.77%	0.9	6.049	115.8	0.069	0.292	0.084	122.10%	-0.018	0.206	88.55%	0.057
s	1.05%	0.021	0.102	1.364	0.005	0.01	0.006	1.05%	0.001	0.002	2.96%	0
%RSD	3.912	2.294	1.691	1.178	6.972	3.423	7.377	0.863	6.753	0.763	3.342	0.108

5CS 16/12/2021 17:40:07

1	27.75%	0.921	8.342	118.5	0.051	0.247	0.023	124.55%	-0.019	0.205	103.03%	0.056
2	25.73%	0.894	8.459	116.4	0.047	0.263	0.019	124.24%	-0.018	0.206	107.07%	0.056
3	25.92%	0.862	8.183	116.6	0.05	0.266	0.02	126.71%	-0.019	0.206	108.25%	0.056
x	26.47%	0.892	8.328	117.2	0.049	0.259	0.021	125.17%	-0.019	0.206	106.12%	0.056
s	1.12%	0.03	0.139	1.149	0.002	0.01	0.002	1.34%	0.001	0.001	2.74%	0
%RSD	4.212	3.337	1.664	0.98	4.698	3.889	10.33	1.072	2.951	0.437	2.579	0.026

5DS 16/12/2021 17:41:16

1	29.08%	0.813	16.31	151.1	0.034	0.157	0.014	124.59%	-0.023	0.204	76.60%	0.057

2	27.61%	0.782	16.68	154	0.031	0.163	0.012	124.59%	-0.021	0.205	88.72%	0.057
3	28.37%	0.758	16.36	146.1	0.028	0.154	0.009	126.23%	-0.02	0.205	85.69%	0.057
x	28.35%	0.784	16.45	150.4	0.031	0.158	0.012	125.14%	-0.021	0.204	83.67%	0.057
s	0.74%	0.027	0.201	4.019	0.003	0.005	0.003	0.95%	0.001	0.001	6.31%	0
%RSD	2.598	3.451	1.222	2.671	10.5	3.104	22.01	0.758	5.731	0.408	7.54	0.15

5AA 16/12/2021 17:42:19

1	27.54%	0.153	12.94	257.3	18.63	0.855	0.004	122.20%	-0.023	0.202	79.97%	0.058
2	25.74%	0.099	12.75	263.9	18.6	0.863	0.006	122.80%	-0.024	0.201	81.65%	0.057
3	25.01%	0.078	12.8	262.1	18.76	0.905	0.001	121.12%	-0.023	0.202	84.01%	0.057
x	26.10%	0.11	12.83	261.1	18.66	0.875	0.004	122.04%	-0.024	0.202	81.87%	0.057
s	1.30%	0.038	0.097	3.379	0.088	0.027	0.003	0.85%	0.001	0.001	2.03%	0
%RSD	4.986	35	0.753	1.294	0.471	3.094	81	0.697	2.749	0.434	2.479	0.233

5BA 16/12/2021 17:43:28

1	28.88%	0.018	2.588	80.15	7.291	0.142	0.026	124.21%	-0.027	0.203	30.64%	0.056
2	25.59%	0.019	2.586	80.73	7.433	0.124	0.022	121.23%	-0.027	0.203	30.13%	0.056
3	26.34%	0.014	2.503	84.08	7.359	0.121	0.029	123.80%	-0.028	0.205	28.11%	0.057
x	26.94%	0.017	2.559	81.65	7.361	0.129	0.026	123.08%	-0.027	0.204	29.63%	0.056
s	1.73%	0.003	0.048	2.119	0.071	0.011	0.003	1.61%	0.001	0.001	1.34%	0
%RSD	6.403	18.14	1.882	2.595	0.971	8.736	13.16	1.312	2.025	0.686	4.51	0.16

5CA 16/12/2021 17:44:36

1	30.17%	-0.047	8.547	146.7	3.232	0.816	0.033	130.76%	-0.022	0.201	189.57%	0.058
2	29.21%	-0.049	9.052	146.2	3.231	0.856	0.033	128.77%	-0.02	0.202	187.89%	0.058
3	30.06%	-0.052	8.843	147.7	3.172	0.855	0.038	130.87%	-0.021	0.201	208.10%	0.058
x	29.81%	-0.05	8.814	146.9	3.212	0.843	0.035	130.13%	-0.021	0.201	195.19%	0.058
s	0.53%	0.002	0.254	0.765	0.035	0.023	0.003	1.18%	0.001	0.001	11.21%	0
%RSD	1.759	4.992	2.878	0.521	1.078	2.692	7.235	0.908	4.256	0.311	5.744	0.468

5DA 16/12/2021 17:45:47

1	31.68%	-0.041	17.26	192.7	5.002	1.197	0.145	125.28%	-0.017	0.2	272.25%	0.06
2	30.06%	-0.042	17.36	187.3	4.979	1.17	0.141	126.65%	-0.018	0.201	273.43%	0.06
3	30.08%	-0.042	17.46	196.1	5.103	1.209	0.14	124.37%	-0.017	0.2	282.19%	0.059
x	30.61%	-0.042	17.36	192.1	5.028	1.192	0.142	125.43%	-0.017	0.201	275.96%	0.06
s	0.93%	0.001	0.098	4.441	0.066	0.02	0.003	1.15%	0.001	0	5.43%	0
%RSD	3.048	2.068	0.567	2.313	1.313	1.651	1.823	0.916	3.946	0.213	1.967	0.208

5AD 16/12/2021 17:46:56

	1	37.05%	0.251	15.59	1345	2.972	17.39	1.324	128.33%	-0.02	0.205	1333.73%	0.171
	2	37.75%	0.245	15.31	1321	2.934	17.41	1.315	129.22%	-0.021	0.205	1353.13%	0.172
	3	36.71%	0.251	15.26	1329	2.978	17.59	1.347	127.75%	-0.02	0.207	1351.94%	0.171
x		37.17%	0.249	15.39	1332	2.961	17.46	1.329	128.43%	-0.02	0.206	1346.27%	0.171
s		0.53%	0.003	0.181	12.07	0.024	0.108	0.016	0.75%	0.001	0.002	10.87%	0
%RSD		1.433	1.325	1.175	0.907	0.811	0.618	1.211	0.58	3.316	0.736	0.808	0.234

5BD 16/12/2021 17:48:04

	1	35.22%	0.191	4.944	504.3	1.525	6.609	0.583	128.97%	-0.024	0.201	291.96%	0.155
	2	32.61%	0.183	4.784	498.5	1.529	6.621	0.565	128.59%	-0.023	0.201	283.54%	0.152
	3	33.45%	0.204	5.033	527.3	1.571	6.909	0.593	123.11%	-0.023	0.201	278.48%	0.159
x		33.76%	0.193	4.92	510.1	1.542	6.713	0.58	126.89%	-0.023	0.201	284.66%	0.155
s		1.33%	0.011	0.126	15.25	0.026	0.17	0.015	3.28%	0.001	0	6.81%	0.004
%RSD		3.951	5.466	2.557	2.989	1.676	2.526	2.5	2.583	2.675	0.205	2.391	2.254

5CD 16/12/2021 17:49:20

	1	34.89%	0.183	7.43	764.7	1.109	9.247	0.79	128.53%	-0.02	0.2	242.95%	0.168
	2	34.71%	0.191	7.583	766.7	1.15	9.334	0.829	126.30%	-0.018	0.2	264.67%	0.168
	3	35.63%	0.183	7.587	765.9	1.119	9.277	0.819	129.48%	-0.018	0.201	259.62%	0.169
x		35.08%	0.186	7.533	765.7	1.126	9.286	0.813	128.11%	-0.019	0.2	255.75%	0.169
s		0.49%	0.005	0.09	1.02	0.021	0.044	0.02	1.63%	0.001	0.001	11.37%	0
%RSD		1.382	2.493	1.191	0.133	1.876	0.476	2.515	1.273	5.3	0.303	4.445	0.243

5DD 16/12/2021 17:50:26

	1	42.95%	0.191	24.2	1681	2.052	21.02	0.79	131.87%	0.025	0.202	307.95%	0.151
	2	42.43%	0.193	24.42	1681	2.057	21.69	0.762	128.93%	0.028	0.201	337.26%	0.153
	3	42.30%	0.196	24.82	1694	2.07	21.93	0.753	128.31%	0.031	0.201	332.88%	0.154
x		42.56%	0.193	24.48	1685	2.059	21.54	0.768	129.71%	0.028	0.201	326.03%	0.153
s		0.34%	0.003	0.317	7.713	0.009	0.471	0.019	1.90%	0.003	0	15.81%	0.001
%RSD		0.797	1.409	1.294	0.458	0.444	2.189	2.535	1.466	10.29	0.245	4.848	0.798

6AS 16/12/2021 17:51:33

	1	38.19%	0.963	0.961	107.3	0.286	1.303	0.225	130.85%	-0.018	0.227	274.44%	0.078
	2	36.21%	1.004	0.911	107	0.296	1.264	0.234	125.17%	-0.018	0.232	285.05%	0.079
	3	35.57%	0.98	0.823	100.1	0.282	1.149	0.23	129.59%	-0.02	0.236	273.43%	0.077

x	36.66%	0.982	0.898	104.8	0.288	1.239	0.23	128.54%	-0.019	0.232	277.64%	0.078
s	1.37%	0.021	0.07	4.06	0.007	0.08	0.004	2.98%	0.001	0.004	6.44%	0.001
%RSD	3.734	2.126	7.788	3.873	2.407	6.481	1.908	2.319	4.74	1.796	2.318	0.756

6BS 16/12/2021 17:52:40

1	32.80%	0.747	1.552	52.3	0.14	0.358	0.085	128.17%	-0.022	0.234	163.47%	0.076
2	33.05%	0.741	1.566	52.59	0.134	0.375	0.087	125.25%	-0.021	0.246	154.89%	0.075
3	32.97%	0.738	1.576	55.34	0.143	0.381	0.085	126.72%	-0.021	0.25	153.54%	0.076
x	32.94%	0.742	1.565	53.41	0.139	0.371	0.086	126.71%	-0.022	0.243	157.30%	0.076
s	0.13%	0.005	0.012	1.68	0.004	0.012	0.001	1.46%	0.001	0.008	5.39%	0
%RSD	0.386	0.641	0.766	3.145	3.142	3.149	1.179	1.152	2.432	3.309	3.426	0.409

6CS 16/12/2021 17:53:44

1	33.81%	0.814	1.548	64.97	0.144	0.5	0.222	122.43%	-0.023	0.213	201.02%	0.072
2	32.65%	0.787	1.501	62.87	0.134	0.461	0.205	123.51%	-0.023	0.213	199.17%	0.072
3	33.43%	0.771	1.465	58.34	0.134	0.465	0.206	125.45%	-0.023	0.213	190.75%	0.073
x	33.29%	0.79	1.505	62.06	0.137	0.475	0.211	123.80%	-0.023	0.213	196.98%	0.072
s	0.59%	0.022	0.042	3.386	0.006	0.022	0.009	1.53%	0	0	5.47%	0
%RSD	1.783	2.761	2.768	5.456	4.109	4.525	4.342	1.233	1.001	0.17	2.779	0.276

6DS 16/12/2021 17:54:50

1	33.00%	0.724	0.538	59.56	0.107	0.439	0.187	129.48%	-0.023	0.214	136.37%	0.068
2	32.98%	0.696	0.536	55.51	0.097	0.432	0.191	129.22%	-0.022	0.214	138.39%	0.069
3	31.92%	0.69	0.514	58.78	0.104	0.439	0.191	128.84%	-0.021	0.216	133.17%	0.069
x	32.63%	0.704	0.529	57.95	0.102	0.437	0.19	129.18%	-0.022	0.215	135.97%	0.069
s	0.62%	0.018	0.013	2.151	0.005	0.004	0.002	0.32%	0.001	0.001	2.63%	0
%RSD	1.892	2.582	2.445	3.711	4.599	0.968	1.117	0.249	4.037	0.555	1.936	0.671

6AA 16/12/2021 17:55:54

1	39.56%	0.269	4.306	223.8	19.08	2.297	0.344	127.69%	-0.022	0.204	206.92%	0.096
2	40.58%	0.24	4.264	223.5	19.02	2.255	0.336	129.46%	-0.023	0.202	217.36%	0.096
3	38.03%	0.22	4.126	219.3	18.29	2.246	0.351	131.07%	-0.025	0.202	207.93%	0.094
x	39.39%	0.243	4.232	222.2	18.8	2.266	0.344	129.41%	-0.024	0.203	210.73%	0.096
s	1.29%	0.025	0.094	2.517	0.439	0.027	0.008	1.69%	0.002	0.001	5.76%	0.001
%RSD	3.264	10.17	2.226	1.133	2.336	1.201	2.188	1.305	6.854	0.411	2.732	1.069

6BA 16/12/2021 17:56:58

1	38.48%	0.082	2.379	129.1	8.801	1.115	0.219	176.42%	-0.015	0.201	332.21%	0.097
2	38.17%	0.08	2.431	134.1	8.986	1.134	0.229	169.34%	-0.015	0.2	328.33%	0.098
3	38.36%	0.071	2.46	129.7	8.741	1.118	0.223	173.67%	-0.015	0.2	336.75%	0.099
x	38.34%	0.078	2.423	131	8.843	1.122	0.224	173.14%	-0.015	0.2	332.43%	0.098
s	0.16%	0.006	0.041	2.711	0.128	0.01	0.005	3.57%	0	0	4.22%	0.001
%RSD	0.406	7.609	1.68	2.07	1.443	0.896	2.348	2.063	1.187	0.203	1.268	0.979

6CA 16/12/2021 17:57:57

1	37.03%	0.043	1.543	95.22	4.394	0.707	0.2	178.65%	-0.022	0.201	389.80%	0.076
2	36.41%	0.028	1.438	91.65	4.196	0.664	0.189	185.92%	-0.022	0.2	371.11%	0.074
3	37.25%	0.027	1.443	94.6	4.271	0.669	0.189	183.97%	-0.023	0.2	390.14%	0.076
x	36.90%	0.033	1.475	93.82	4.287	0.68	0.193	182.85%	-0.022	0.2	383.68%	0.075
s	0.44%	0.009	0.059	1.91	0.1	0.023	0.006	3.76%	0	0.001	10.89%	0.001
%RSD	1.183	27.27	3.989	2.035	2.331	3.411	3.335	2.057	1.222	0.344	2.839	1.348

6DA 16/12/2021 17:59:23

1	35.25%	0.016	2.628	86.07	3.542	1.476	0.251	132.66%	-0.024	0.203	314.52%	0.082
2	33.54%	0.009	2.574	83.3	3.487	1.506	0.26	133.00%	-0.023	0.201	312.67%	0.08
3	34.55%	0.008	2.619	82.37	3.504	1.497	0.252	130.98%	-0.023	0.202	331.36%	0.079
x	34.44%	0.011	2.607	83.91	3.511	1.493	0.254	132.21%	-0.023	0.202	319.52%	0.08
s	0.86%	0.004	0.029	1.922	0.028	0.015	0.005	1.08%	0.001	0.001	10.30%	0.001
%RSD	2.497	40.45	1.106	2.291	0.797	1.026	1.933	0.82	2.294	0.723	3.223	1.768

6AD 16/12/2021 18:00:44

1	42.58%	0.283	2.972	148.7	0.364	1.149	0.201	174.72%	-0.022	0.201	218.54%	0.098
2	41.75%	0.272	2.846	143.5	0.323	1.09	0.18	182.16%	-0.022	0.199	237.06%	0.1
3	43.53%	0.277	2.913	151.1	0.332	1.122	0.188	176.13%	-0.021	0.199	228.81%	0.102
x	42.62%	0.277	2.91	147.8	0.34	1.12	0.19	177.67%	-0.021	0.2	228.13%	0.1
s	0.89%	0.006	0.063	3.893	0.022	0.029	0.01	3.95%	0	0.001	9.28%	0.002
%RSD	2.092	2.022	2.176	2.634	6.487	2.632	5.5	2.223	2.122	0.556	4.068	2.054

6BD 16/12/2021 18:01:47

1	38.55%	0.375	3.293	187.5	0.51	1.044	0.29	119.04%	-0.009	0.2	364.54%	0.12
2	38.18%	0.347	3.185	171.9	0.466	0.997	0.288	124.55%	-0.009	0.201	348.20%	0.12
3	37.75%	0.364	3.242	180.5	0.485	1.021	0.294	122.75%	-0.01	0.199	358.14%	0.122
x	38.16%	0.362	3.24	180	0.487	1.021	0.29	122.11%	-0.009	0.2	356.96%	0.121
s	0.40%	0.014	0.054	7.834	0.022	0.024	0.003	2.81%	0.001	0.001	8.23%	0.001

%RSD	1.044	3.819	1.66	4.353	4.533	2.315	1.129	2.301	7.442	0.312	2.306	1.044

6CD 16/12/2021 18:02:58

1	39.43%	3.998	2.007	144.9	0.496	0.883	0.247	106.76%	-0.02	0.201	672.47%	0.129
2	38.89%	3.975	1.944	142.3	0.483	0.88	0.248	106.74%	-0.02	0.2	679.55%	0.129
3	38.25%	4.039	1.984	138.3	0.498	0.904	0.226	104.35%	-0.018	0.2	709.37%	0.129
x	38.86%	4.004	1.978	141.8	0.492	0.889	0.24	105.95%	-0.019	0.2	687.13%	0.129
s	0.59%	0.032	0.032	3.323	0.008	0.013	0.012	1.39%	0.001	0.001	19.58%	0
%RSD	1.515	0.808	1.595	2.343	1.684	1.469	5.176	1.308	7.079	0.362	2.85	0.275

6DD 16/12/2021 18:03:58

1	40.93%	0.347	2.578	146	0.281	1.039	0.199	136.91%	-0.007	0.2	7096.08%	0.118
2	40.83%	0.305	2.546	146.1	0.277	1.019	0.181	140.65%	-0.008	0.2	7382.59%	0.117
3	40.66%	0.29	2.521	144.1	0.271	1.022	0.191	139.50%	-0.007	0.199	7778.04%	0.118
x	40.81%	0.314	2.549	145.4	0.277	1.027	0.191	139.02%	-0.007	0.2	7418.90%	0.118
s	0.13%	0.029	0.028	1.1	0.005	0.011	0.009	1.92%	0.001	0	342.43%	0.001
%RSD	0.324	9.374	1.11	0.756	1.767	1.047	4.687	1.379	11.26	0.085	4.616	0.83

7AS 16/12/2021 18:04:59

1	30.07%	0.897	1.005	73.56	0.078	0.508	0.162	120.41%	-0.014	0.209	1666.35%	0.068
2	29.62%	0.903	0.981	70.45	0.075	0.495	0.139	120.14%	-0.015	0.212	1344.36%	0.066
3	28.43%	0.89	0.952	71.46	0.067	0.455	0.123	122.03%	-0.014	0.213	1030.59%	0.063
x	29.37%	0.897	0.979	71.82	0.073	0.486	0.141	120.86%	-0.015	0.211	1347.10%	0.066
s	0.85%	0.007	0.027	1.59	0.006	0.028	0.02	1.03%	0	0.002	317.89%	0.002
%RSD	2.883	0.766	2.758	2.214	8.038	5.752	14	0.849	3.013	0.849	23.598	3.257

7BS 16/12/2021 18:06:05

1	30.59%	1.132	3.609	102.6	0.17	0.528	0.798	109.73%	-0.019	0.218	328.50%	0.062
2	31.52%	1.127	3.644	107.5	0.179	0.534	0.818	107.01%	-0.016	0.221	331.53%	0.063
3	29.74%	1.109	3.688	110.5	0.189	0.569	0.806	106.50%	-0.016	0.225	322.10%	0.063
x	30.61%	1.123	3.647	106.9	0.179	0.544	0.807	107.75%	-0.017	0.221	327.38%	0.063
s	0.89%	0.012	0.04	3.946	0.01	0.022	0.01	1.74%	0.002	0.003	4.82%	0
%RSD	2.911	1.074	1.086	3.693	5.315	4.082	1.227	1.611	9.349	1.554	1.471	0.512

7CS 16/12/2021 18:07:16

1	31.11%	0.895	4.47	58.13	0.108	0.602	1.144	127.34%	-0.025	0.21	136.03%	0.057
2	30.74%	0.877	4.599	57.27	0.113	0.599	1.168	125.68%	-0.024	0.211	138.22%	0.057

3	30.12%	0.873	4.499	56.28	0.11	0.61	1.167	126.41%	-0.024	0.215	152.53%	0.057
x	30.66%	0.882	4.523	57.23	0.11	0.603	1.16	126.48%	-0.024	0.212	142.26%	0.057
s	0.51%	0.012	0.067	0.924	0.003	0.006	0.014	0.83%	0	0.003	8.96%	0
%RSD	1.646	1.324	1.492	1.615	2.328	0.932	1.192	0.658	2.017	1.197	6.3	0.136

7DS 16/12/2021 18:08:14

1	31.60%	0.702	3.044	41.68	0.084	1.359	0.423	121.63%	-0.025	0.21	115.32%	0.058
2	29.71%	0.713	3.18	41.37	0.095	1.445	0.416	115.99%	-0.024	0.213	123.57%	0.058
3	28.97%	0.683	3.073	41.32	0.082	1.396	0.391	120.63%	-0.023	0.214	114.31%	0.058
x	30.10%	0.7	3.099	41.46	0.087	1.4	0.41	119.42%	-0.024	0.212	117.73%	0.058
s	1.35%	0.015	0.072	0.195	0.007	0.043	0.017	3.01%	0.001	0.002	5.08%	0
%RSD	4.499	2.184	2.311	0.47	7.927	3.061	4.084	2.519	3.187	0.929	4.315	0.15

7AA 16/12/2021 18:09:16

1	27.35%	0.043	1.269	47.12	0.081	0.612	0.181	132.80%	-0.028	0.203	254.40%	0.06
2	26.98%	-0.004	1.186	45.31	0.081	0.601	0.167	135.18%	-0.027	0.204	258.44%	0.059
3	26.48%	-0.021	1.187	46.81	0.081	0.644	0.181	133.95%	-0.027	0.202	250.87%	0.059
x	26.94%	0.006	1.214	46.41	0.081	0.619	0.177	133.98%	-0.027	0.203	254.57%	0.059
s	0.44%	0.033	0.047	0.971	0	0.022	0.008	1.19%	0.001	0.001	3.79%	0
%RSD	1.616	533.1	3.904	2.092	0.504	3.61	4.593	0.886	2.26	0.451	1.489	0.495

7BA 16/12/2021 18:10:27

1	32.46%	-0.03	2.952	40.84	0.085	0.417	0.731	117.11%	-0.029	0.204	100.67%	0.057
2	29.64%	-0.037	3.048	39.04	0.088	0.423	0.737	115.54%	-0.029	0.203	99.66%	0.057
3	30.19%	-0.036	3.129	40.43	0.09	0.422	0.733	112.96%	-0.028	0.203	95.29%	0.057
x	30.76%	-0.034	3.043	40.11	0.088	0.421	0.734	115.20%	-0.029	0.203	98.54%	0.057
s	1.49%	0.004	0.089	0.944	0.003	0.004	0.003	2.09%	0	0.001	2.86%	0
%RSD	4.853	10.54	2.911	2.354	2.96	0.84	0.405	1.816	1.299	0.366	2.906	0.076

7CA 16/12/2021 18:11:26

1	34.59%	-0.037	3.376	27.23	0.001	0.2	1.117	143.96%	-0.03	0.202	101.18%	0.056
2	32.38%	-0.037	3.351	28.15	0.002	0.2	1.072	144.36%	-0.03	0.201	103.70%	0.056
3	31.96%	-0.037	3.316	25.92	0.005	0.209	1.053	146.99%	-0.03	0.202	106.73%	0.057
x	32.98%	-0.037	3.348	27.1	0.003	0.203	1.08	145.10%	-0.03	0.202	103.87%	0.056
s	1.42%	0	0.03	1.123	0.002	0.005	0.033	1.65%	0	0.001	2.78%	0
%RSD	4.292	1.099	0.901	4.142	74.11	2.581	3.053	1.134	0.602	0.267	2.678	0.224

7DA 16/12/2021 18:12:29

1	32.24%	-0.055	0.749	33.45	0.097	0.221	0.637	129.22%	-0.026	0.262	83.84%	0.056
2	31.20%	-0.059	0.71	34.21	0.093	0.211	0.648	130.65%	-0.027	0.265	86.19%	0.056
3	31.73%	-0.059	0.674	30.66	0.092	0.218	0.618	130.85%	-0.026	0.262	84.51%	0.056
x	31.72%	-0.058	0.711	32.77	0.094	0.217	0.634	130.24%	-0.026	0.263	84.85%	0.056
s	0.52%	0.002	0.037	1.87	0.003	0.005	0.016	0.89%	0	0.001	1.21%	0
%RSD	1.648	3.776	5.236	5.705	2.685	2.274	2.465	0.68	1.755	0.524	1.431	0.034

7Ad 16/12/2021 18:13:30

1	32.94%	0.131	0.505	57.57	0.242	0.925	1.327	118.04%	-0.023	0.211	406.82%	0.124
2	32.65%	0.139	0.513	61.16	0.25	0.959	1.29	116.96%	-0.023	0.212	433.26%	0.128
3	31.65%	0.136	0.506	63.42	0.252	0.947	1.277	118.22%	-0.024	0.213	446.06%	0.125
x	32.41%	0.135	0.508	60.72	0.248	0.943	1.298	117.74%	-0.023	0.212	428.71%	0.126
s	0.68%	0.004	0.004	2.954	0.005	0.017	0.026	0.68%	0	0.001	20.01%	0.002
%RSD	2.093	3.099	0.862	4.865	2.159	1.838	2.028	0.578	1.253	0.303	4.668	1.926

7BD 16/12/2021 18:14:34

1	33.14%	0.047	0.896	155.6	0.684	2.062	2.174	129.32%	-0.026	0.211	321.60%	0.113
2	32.50%	0.049	0.892	161.3	0.697	2.056	2.174	129.59%	-0.026	0.208	321.09%	0.114
3	31.35%	0.049	0.926	175.2	0.855	2.261	2.197	128.46%	-0.026	0.208	320.58%	0.113
x	32.33%	0.048	0.905	164	0.745	2.126	2.182	129.12%	-0.026	0.209	321.09%	0.113
s	0.91%	0.001	0.019	10.11	0.095	0.117	0.014	0.59%	0	0.002	0.51%	0.001
%RSD	2.811	2.448	2.06	6.161	12.73	5.495	0.623	0.457	1.275	0.929	0.157	0.503

7CD 16/12/2021 18:15:32

1	35.83%	0.113	7.547	197.6	0.503	8.865	2.505	113.55%	0.023	0.208	237.90%	0.169
2	34.72%	0.105	7.457	191.9	0.485	8.754	2.57	112.18%	0.023	0.206	231.16%	0.159
3	36.98%	0.095	7.535	191.2	0.504	8.793	2.515	113.58%	0.023	0.208	229.31%	0.16
x	35.84%	0.104	7.513	193.6	0.497	8.804	2.53	113.10%	0.023	0.207	232.79%	0.163
s	1.13%	0.009	0.048	3.539	0.011	0.057	0.035	0.80%	0	0.001	4.52%	0.005
%RSD	3.149	8.936	0.645	1.828	2.159	0.644	1.387	0.708	1.496	0.39	1.941	3.299

7DD 16/12/2021 18:16:39

1	37.43%	0.061	2.318	72.97	0.118	7.366	2.297	167.00%	-0.024	0.205	543.59%	0.116
2	35.82%	0.064	2.348	75.33	0.119	7.486	2.252	161.87%	-0.023	0.204	530.79%	0.115
3	34.46%	0.065	2.355	74.55	0.129	7.56	2.212	161.63%	-0.024	0.207	546.46%	0.116
x	35.90%	0.063	2.34	74.28	0.122	7.471	2.254	163.50%	-0.023	0.205	540.28%	0.115

s	1.49%	0.002	0.019	1.202	0.006	0.098	0.043	3.03%	0.001	0.001	8.34%	0.001
%RSD	4.141	3.572	0.826	1.618	5.221	1.308	1.907	1.855	2.298	0.619	1.544	0.564

8AS 16/12/2021 18:17:48

1	34.38%	0.89	12.45	208.8	0.26	0.988	0.445	112.23%	0.031	0.207	300.71%	0.064
2	32.89%	0.946	13.05	208.7	0.278	0.924	0.423	108.86%	0.029	0.207	274.44%	0.064
3	34.05%	0.952	12.88	212.7	0.281	0.824	0.358	108.09%	0.029	0.206	275.28%	0.063
x	33.77%	0.929	12.8	210	0.273	0.912	0.409	109.73%	0.029	0.207	283.48%	0.064
s	0.78%	0.034	0.31	2.268	0.011	0.083	0.045	2.20%	0.001	0.001	14.93%	0.001
%RSD	2.307	3.688	2.419	1.08	4.215	9.08	11.02	2.009	3.494	0.422	5.267	1.219

8BS 16/12/2021 18:18:49

1	33.14%	0.863	10.86	180.2	0.253	0.425	0.108	111.06%	-0.011	0.206	201.53%	0.059
2	33.17%	0.868	11.03	183.9	0.261	0.427	0.113	109.46%	-0.013	0.206	209.11%	0.06
3	32.65%	0.873	11.01	178.3	0.259	0.422	0.118	108.07%	-0.01	0.205	217.69%	0.059
x	32.99%	0.868	10.97	180.8	0.258	0.425	0.113	109.53%	-0.012	0.206	209.44%	0.059
s	0.30%	0.005	0.09	2.852	0.004	0.002	0.005	1.50%	0.001	0	8.09%	0
%RSD	0.895	0.579	0.82	1.577	1.635	0.503	4.542	1.367	11.63	0.123	3.862	0.318

8CS 16/12/2021 18:19:50

1	36.16%	0.873	12.18	192.9	0.288	0.673	0.069	130.39%	-0.018	0.202	194.12%	0.06
2	34.02%	0.884	12.53	205.2	0.301	0.702	0.087	124.92%	-0.018	0.203	179.98%	0.06
3	34.74%	0.851	12.17	205.7	0.289	0.681	0.084	130.61%	-0.016	0.203	178.97%	0.06
x	34.97%	0.87	12.29	201.3	0.293	0.686	0.08	128.64%	-0.017	0.203	184.35%	0.06
s	1.09%	0.017	0.202	7.222	0.007	0.015	0.01	3.23%	0.001	0.001	8.47%	0
%RSD	3.113	1.949	1.641	3.589	2.486	2.14	11.9	2.508	7.33	0.261	4.596	0.679

8DS 16/12/2021 18:20:52

1	34.30%	0.815	9.221	163.7	0.251	0.176	0.046	122.71%	-0.024	0.202	114.98%	0.058
2	34.32%	0.794	10.27	162.4	0.246	0.168	0.047	122.00%	-0.023	0.2	114.48%	0.058
3	32.51%	0.799	9.056	164.8	0.245	0.176	0.044	122.07%	-0.024	0.203	107.24%	0.058
x	33.71%	0.802	9.515	163.6	0.247	0.173	0.046	122.26%	-0.024	0.202	112.23%	0.058
s	1.04%	0.011	0.657	1.176	0.003	0.005	0.001	0.39%	0	0.001	4.33%	0
%RSD	3.072	1.382	6.91	0.719	1.119	2.775	2.634	0.32	1.037	0.611	3.861	0.388

8AA 16/12/2021 18:21:53

1	27.50%	0.024	12.7	160	0.212	0.892	0.016	129.90%	-0.03	0.204	259.29%	0.058

2	27.91%	-0.017	12.63	167	0.205	0.939	0.016	129.10%	-0.029	0.205	263.50%	0.058
3	27.50%	-0.038	12.6	157.2	0.208	0.957	0.015	129.08%	-0.028	0.204	266.02%	0.058
x	27.64%	-0.01	12.64	161.4	0.209	0.929	0.016	129.36%	-0.029	0.204	262.93%	0.058
s	0.23%	0.032	0.048	5.049	0.004	0.034	0.001	0.47%	0.001	0.001	3.40%	0
%RSD	0.844	304	0.381	3.128	1.703	3.627	3.144	0.363	2.021	0.286	1.294	0.14

8BA 16/12/2021 18:22:57

1	28.27%	-0.058	14.04	198.4	0.346	0.856	0.033	115.90%	-0.025	0.201	364.71%	0.058
2	28.24%	-0.063	13.93	187	0.343	0.843	0.025	117.40%	-0.025	0.2	353.59%	0.058
3	28.32%	-0.065	13.8	185.8	0.342	0.801	0.029	119.24%	-0.026	0.2	382.90%	0.058
x	28.28%	-0.062	13.92	190.4	0.344	0.833	0.029	117.51%	-0.025	0.2	367.07%	0.058
s	0.04%	0.004	0.118	6.979	0.002	0.029	0.004	1.67%	0.001	0	14.79%	0
%RSD	0.148	6.477	0.848	3.666	0.612	3.428	14.68	1.424	2.61	0.201	4.03	0.397

8CA 16/12/2021 18:23:57

1	27.57%	-0.075	16.31	230.6	0.36	0.703	0.032	107.63%	-0.025	0.23	293.13%	0.058
2	27.45%	-0.076	16.51	239.1	0.368	0.706	0.028	105.81%	-0.025	0.231	299.87%	0.058
3	26.91%	-0.078	16.79	235.4	0.355	0.717	0.027	105.12%	-0.024	0.236	307.79%	0.058
x	27.31%	-0.076	16.54	235	0.361	0.709	0.029	106.19%	-0.025	0.232	300.26%	0.058
s	0.36%	0.002	0.242	4.267	0.006	0.007	0.003	1.30%	0	0.003	7.33%	0
%RSD	1.299	2.194	1.461	1.816	1.727	1.013	9.312	1.225	1.775	1.4	2.442	0.136

8Da 16/12/2021 18:25:22

1	25.87%	-0.085	11.29	181.9	0.28	0.499	0.018	135.36%	-0.029	0.202	265.52%	0.059
2	25.99%	-0.085	11.15	178.8	0.267	0.479	0.023	135.72%	-0.027	0.201	263.66%	0.059
3	27.17%	-0.087	10.8	172.5	0.262	0.469	0.025	143.12%	-0.029	0.201	256.42%	0.058
x	26.35%	-0.086	11.08	177.8	0.27	0.482	0.022	138.07%	-0.028	0.201	261.87%	0.059
s	0.72%	0.001	0.25	4.774	0.009	0.015	0.003	4.38%	0.001	0.001	4.81%	0
%RSD	2.716	1.615	2.256	2.686	3.456	3.142	15.9	3.171	3.367	0.483	1.835	0.263

8AD 16/12/2021 18:26:25

1	153.24%	1.924	14.17	613.1	1.224	3.757	0.984	136.23%	0.009	0.207	1339.30%	0.224
2	150.84%	2.07	15.09	655.5	1.304	3.907	1.037	129.96%	0.012	0.206	1350.93%	0.238
3	147.58%	1.977	14.47	629.3	1.239	3.83	1.015	132.69%	0.017	0.206	1257.01%	0.233
x	150.55%	1.99	14.58	632.6	1.256	3.831	1.012	132.96%	0.013	0.206	1315.75%	0.231
s	2.84%	0.074	0.472	21.41	0.042	0.075	0.026	3.15%	0.004	0.001	51.20%	0.007
%RSD	1.889	3.715	3.24	3.384	3.37	1.949	2.608	2.368	31.38	0.508	3.891	3.156

8BD 16/12/2021 18:27:26

1	66.31%	1.305	124.9	879.7	4.334	6.232	0.85	118.20%	0.061	0.215	1922.32%	0.204
2	66.75%	1.327	130.2	924.2	4.57	6.492	0.864	117.00%	0.072	0.216	2012.10%	0.208
3	65.80%	1.278	127.2	883.3	4.452	6.299	0.86	121.23%	0.071	0.214	1966.70%	0.206
x	66.28%	1.303	127.4	895.7	4.452	6.341	0.858	118.81%	0.068	0.215	1967.04%	0.206
s	0.48%	0.024	2.647	24.73	0.118	0.135	0.007	2.18%	0.006	0.001	44.89%	0.002
%RSD	0.718	1.875	2.078	2.761	2.65	2.128	0.852	1.836	8.798	0.627	2.282	0.896

8CD 16/12/2021 18:28:28

1	145.27%	2.507	13.94	670.6	1.662	3.045	0.922	127.45%	0.001	0.21	1056.21%	0.229
2	145.96%	2.479	12.43	673.6	1.606	2.999	0.891	129.96%	0	0.212	1152.47%	0.23
3	145.20%	2.406	11.9	643	1.549	2.938	0.887	130.87%	-0.003	0.21	1131.91%	0.223
x	145.47%	2.464	12.76	662.4	1.606	2.994	0.9	129.43%	-0.001	0.21	1113.53%	0.227
s	0.42%	0.052	1.057	16.86	0.056	0.054	0.019	1.77%	0.002	0.001	50.69%	0.004
%RSD	0.289	2.123	8.285	2.546	3.513	1.802	2.106	1.365	331.2	0.46	4.552	1.714

8dd 16/12/2021 18:29:30

1	65.80%	2.233	4.807	526.5	1.314	2.144	0.817	121.87%	-0.022	0.203	228.64%	0.206
2	65.05%	2.207	4.544	510.1	1.257	2.053	0.786	124.53%	-0.021	0.202	239.42%	0.204
3	62.87%	2.164	4.302	496.9	1.228	2.002	0.78	128.53%	-0.021	0.202	197.99%	0.194
x	64.57%	2.201	4.551	511.2	1.266	2.066	0.794	124.98%	-0.021	0.202	222.02%	0.201
s	1.52%	0.035	0.253	14.84	0.044	0.072	0.02	3.35%	0.001	0.001	21.49%	0.006
%RSD	2.352	1.58	5.559	2.903	3.484	3.491	2.457	2.683	2.474	0.28	9.68	3.086

sTANDARD 16/12/2021 18:30:40

1	20.72%	4.944	9.96	27.66	9.634	9.651	5.028	123.64%	4.658	3.646	68.35%	4.853
2	22.39%	5	10.02	27.01	9.661	9.889	4.981	125.26%	4.672	3.378	69.70%	4.954
3	20.99%	4.946	9.855	21.04	9.484	9.566	4.826	128.35%	4.632	3.466	57.91%	4.885
x	21.37%	4.963	9.944	25.24	9.593	9.702	4.945	125.75%	4.654	3.497	65.32%	4.897
s	0.90%	0.032	0.082	3.651	0.096	0.168	0.106	2.39%	0.02	0.137	6.45%	0.052
%RSD	4.204	0.639	0.824	14.47	0.998	1.729	2.146	1.902	0.437	3.907	9.875	1.052

WASH 16/12/2021 18:31:54

1	18.99%	2.133	4.981	252.9	3.985	5.108	3.148	3.43%	2.385	4.036	9.43%	1.477
2	18.61%	0.884	1.799	331.2	1.201	3.794	2.665	3.03%	1.033	5.372	15.32%	0.676

3	18.08%	0.832	1.583	255.3	0.884	3.662	2.51	2.61%	0.994	5.148	15.15%	0.596
x	18.56%	1.283	2.787	279.8	2.023	4.188	2.774	3.02%	1.47	4.852	13.30%	0.916
s	0.45%	0.737	1.903	44.51	1.706	0.799	0.333	0.41%	0.792	0.715	3.35%	0.488
%RSD	2.442	57.45	68.26	15.91	84.34	19.08	12.01	13.583	53.87	14.74	25.222	53.22

Batch 2 Sample Mass

Sample	Empty (g)	Mass+ Container	Mass + Container + Water	Sample Mass	Water Content	Dry Weight
LSWC1	14.6623	14.6623	65.913	0	1	0
LSWC2	14.6996	14.6996	66.146	0	1	0
LPSS1	14.692	15.3901	64.6779	0.6981	1	0.6981
LPSS2	14.5108	14.8988	65.3943	0.388	1	0.388
LPSS3	14.6795	15.2683	65.118	0.5888	1	0.5888
LPSS4	14.6563	15.2253	64.2631	0.569	1	0.569
LPSS5	14.452	14.9057	65.3939	0.4537	1	0.4537
LGPS6	14.7181	16.2281	66.6936	1.51	1	1.51
LGPS7	14.6158	16.2342	67.4021	1.6184	1	1.6184
LGPS8	14.6784	16.67	65.0752	1.9916	1	1.9916
LGPS9	14.7183	16.4711	65.8578	1.7528	1	1.7528
LGPS10	14.72	15.8748	66.8885	1.1548	1	1.1548
LSWC3	0	0	65.7998	0	1	0
LSWC4	0	0	66.8457	0	1	0
LSW05	14.5381	14.5381	65.2026	0	1	0
LSW06	14.65556	14.65556	65.6806	0	1	0
LSW07	14.6941	14.6941	65.2504	0	1	0
LSW08	14.4616	14.4616	65.7328	0	1	0
LSW09	14.6919	14.6919	65.3823	0	1	0
LSW10	14.6781	14.6781	65.5578	0	1	0
LSW11	14.5343	14.5343	67.4976	0	1	0
LSW12	14.6467	14.6467	64.9649	0	1	0
LSW13	14.6987	14.6987	55.2556	0	1	0
LSW14	14.5125	14.5125	54.9546	0	1	0
LRG01	14.6209	15.2121	52.0207	0.5912	1	0.5912
LRG02	14.6809	14.9638	50.6822	0.2829	1	0.2829
LRG03	14.6211	14.9197	51.0158	0.2986	1	0.2986
LRG04	14.581	14.8434	51.0761	0.2624	1	0.2624
LRG05	14.5025	14.7483	50.5272	0.2458	1	0.2458
LSW15	14.594	14.594	56.225	0	1	0
LWG06	14.6487	15.2735	50.8862	0.6248	1	0.6248
LWG07	14.5741	15.3101	52.4334	0.736	1	0.736
LWG08	14.7101	14.9057	50.8668	0.1956	1	0.1956
LWG09	14.5839	15.1745	50.3276	0.5906	1	0.5906
LWG10	14.6343	15.0553	51.2621	0.421	1	0.421

LSW16	14.6748	14.6748	55.5605	0	1	0
LVG11	14.6929	15.0686	50.3391	0.3757	1	0.3757
LVG12	14.4974	15.1806	51.4337	0.6832	1	0.6832
LVG13	14.5523	15.1457	50.6615	0.5934	1	0.5934
LVG14	14.7037	15.2884	50.1796	0.5847	1	0.5847
LVG15	14.7001	15.2161	50.9471	0.516	1	0.516
LSW17	14.5372	14.5372	60.1457	0	1	0
LSW18	14.7188	14.7188	60.6342	0	1	0
LSW19	14.7194	14.7194	60.467	0	1	0
LSW20	14.6609	14.6609	62.5185	0	1	0
LDK01	14.4988	14.7124	61.084	0.2136	1	0.2136
LDK02	14.5372	14.7438	60.7746	0.2066	1	0.2066
LDK03	14.5104	14.669	60.5572	0.1586	1	0.1586
LDK04	14.702	14.8815	62.0978	0.1795	1	0.1795
LDK05	14.6676	14.815	60.8328	0.1474	1	0.1474
LSW21	14.6163	14.6163	60.0479	0	1	0
LOP06	14.5335	14.7285	60.4433	0.195	1	0.195
LOP07	14.6731	14.9479	63.0392	0.2748	1	0.2748
LOP08	14.6122	14.9106	61.1177	0.2984	1	0.2984
LOP09	14.641	14.8391	60.0256	0.1981	1	0.1981
LOP10	14.9119	15.1302	59.8235	0.2183	1	0.2183
LSW22	14.62	14.62	60.9661	0	1	0
LPS11	14.7318	14.9954	58.6484	0.2636	1	0.2636
LPS12	14.9081	15.1605	59.6368	0.2524	1	0.2524
LPS13	14.7056	15.062	60.8864	0.3564	1	0.3564
LPS14	14.5523	14.9117	57.6953	0.3594	1	0.3594
LPS15	14.5465	14.9398	59.3801	0.3933	1	0.3933
LSW23	14.5091	14.5091	61.6232	0	1	0
LSW24	14.6114	14.6114	59.9685	0	1	0

Appendix 3 Batch 3 and Continuous flow

Batch 3 Key

1	White Birch	6.20
2	Kale	5.90
3	Tea Bag	5.40
4	Peanut Shell	5.90
5	Coffee frounds	5.80
6	Garlic	5.60
7	Spring Greens	5.00
8	Blackberry Tea Bag	4.30

Batch 3 ICP Data

Run	45Sc ppb	51V ppb	55Mn ppb	59Co ppb	60Ni ppb	65Cu ppb	95Mo ppb	103Rh ppb	107Ag ppb	197Au ppb	209Bi ppb	238U ppb
	8BD 16/12/2021 18:27:26											
1	101.28%	-0.08	0.328	2.356	0.074	0.154	0.027	93.06%	0.014	0.204	91.12%	0.057
2	99.66%	0.078	-0.33	1.62	0.077	0.145	0.028	90.28%	0.011	0.205	105.52%	0.057
3	99.07%	0.085	0.335	1.168	0.082	0.077	0.034	116.67%	0.015	0.204	103.35%	0.057
x	100.00%	0.081	0.331	1.715	0.078	0.125	-0.03	100.00%	0.013	0.205	100.00%	0.057
s	1.15%	0.003	0.003	0.6	0.004	0.042	0.004	14.50%	0.003	0	7.76%	0
%RSD	1.146	4.308	1.055	34.96	5.091	33.86	12.32	14.501	18.84	0.181	7.763	0.638
	MQ 16/12/2021 16:14:58											
1	95.95%	0.054	0.317	4.594	0.063	0.39	0.021	44.44%	0.011	0.212	82.64%	0.057
2	93.31%	0.077	0.331	1.88	0.081	0.132	0.032	84.72%	-0.02	0.204	79.49%	0.057
3	92.02%	0.082	0.334	1.376	0.084	0.088	0.034	101.39%	0.022	0.205	78.50%	0.057
x	93.76%	0.071	0.328	2.617	0.076	0.203	0.029	76.85%	0.017	0.207	80.21%	0.057
s	2.01%	0.015	0.009	1.731	0.011	0.163	0.007	29.28%	0.006	0.005	2.16%	0.001
%RSD	2.139	20.89	2.885	66.15	14.55	80.13	24.01	38.095	32.97	2.21	2.698	0.906
	0ppb 16/12/2021 16:16:32											
1	97.92%	0.067	0.277	7.235	0.072	-0.06	0.001	92.89%	0.016	0.239	78.96%	0.061
2	101.04%	0.054	0.249	8.256	0.057	0.044	0	102.45%	0.014	0.207	99.83%	0.065
3	101.04%	0.047	0.225	9.799	0.046	0.026	0.009	104.66%	0.016	0.207	121.21%	0.067
x	100.00%	0.056	-0.25	8.43	0.058	0.043	0.004	100.00%	0.015	0.218	100.00%	0.064
s	1.80%	0.01	0.026	1.291	0.013	0.017	0.005	6.26%	0.001	0.018	21.13%	0.003
%RSD	1.799	17.68	10.4	15.31	22.65	39.27	141.6	6.256	8.369	8.415	21.13	5.169
	1ppb 16/12/2021 16:17:34											
1	97.61%	0.989	1.986	0.561	1.976	1.971	1.006	111.27%	0.975	1.229	53.70%	0.995
2	94.77%	0.986	2.015	1.14	1.995	2.018	0.996	108.71%	1.025	1.041	53.70%	0.997
3	91.26%	0.986	2.009	1.138	2.028	1.993	0.989	112.49%	0.989	1.082	57.91%	1.015

x	94.55%	0.987	2.003	0.946	2	1.994	0.997	110.82%	0.997	1.117	55.11%	1.002
s	3.18%	0.002	0.015	0.334	0.026	0.024	0.009	1.93%	0.026	0.099	2.43%	0.011
%RSD	3.364	0.207	0.755	35.29	1.302	1.187	0.875	1.739	2.603	8.84	4.41	1.131
	2ppb 16/12/2021 16:18:37											
1	87.55%	2.03	4.371	0.898	4.025	4.032	2.004	109.62%	2.008	1.936	41.75%	1.954
2	86.03%	2.018	4.268	1.072	3.98	3.888	1.984	111.63%	1.973	1.998	50.50%	1.908
3	83.11%	2.056	4.337	1.049	4.004	4.026	1.983	114.55%	2.003	1.952	52.02%	2.006
x	85.56%	2.035	4.325	1.006	4.003	3.982	1.991	111.93%	1.995	1.962	48.09%	1.956
s	2.26%	0.019	0.052	0.094	0.022	0.082	0.012	2.48%	0.019	0.033	5.54%	0.049
%RSD	2.641	0.953	1.212	9.342	0.558	2.054	0.599	2.214	0.957	1.66	11.527	2.506
	5ppb 16/12/2021 16:19:39											
1	79.86%	5.07	9.841	13.33	10.06	10.07	5.046	114.53%	5.058	4.439	61.61%	4.894
2	78.29%	5.085	9.927	13.9	10.01	10.01	4.914	114.97%	5.038	4.524	61.95%	4.961
3	74.76%	5.085	10.04	14.5	10.27	10.3	5.081	114.26%	5.04	4.279	65.32%	4.957
x	77.64%	5.08	9.938	13.91	10.11	10.13	5.013	114.59%	5.045	4.414	62.96%	4.937
s	2.61%	0.009	0.102	0.587	0.136	0.149	0.088	0.36%	0.011	0.124	2.05%	0.037
%RSD	3.365	0.174	1.029	4.219	1.345	1.474	1.76	0.313	0.217	2.814	3.253	0.759
	10ppb 16/12/2021 16:20:47											
1	73.24%	9.76	19.63	9.809	19.44	19.57	9.805	117.80%	9.758	10.48	62.29%	9.808
2	71.88%	10.06	20.24	10.25	20.22	20.26	10.1	115.04%	10.07	10.11	63.47%	10.22
3	70.46%	10.05	20.13	11.54	20.17	19.99	10.08	115.10%	10.11	10.28	62.12%	10.09
x	71.86%	9.954	20	10.53	19.94	19.94	9.996	115.98%	9.979	10.29	62.63%	10.04
s	1.39%	0.169	0.325	0.899	0.433	0.347	0.165	1.58%	0.193	0.182	0.73%	0.21
%RSD	1.936	1.694	1.624	8.537	2.17	1.741	1.654	1.358	1.931	1.771	1.172	2.091
	20ppb 16/12/2021 16:21:54											
1	70.14%	19.74	39.59	42.74	38.71	39.11	19.43	115.90%	19.72	17.39	52.52%	7.436
2	67.64%	19.39	38.75	45.54	38.79	38.62	19.05	118.62%	19.1	17.41	64.31%	5.845
3	67.85%	20.84	41.61	46.98	40.58	41.25	20.19	113.40%	20.48	18.41	49.66%	4.525
x	68.54%	19.99	39.98	45.09	39.36	39.66	19.56	115.97%	19.76	17.74	55.50%	5.935
s	1.38%	0.757	1.467	2.159	1.053	1.401	0.581	2.61%	0.693	0.581	7.76%	1.458
%RSD	2.019	3.788	3.67	4.788	2.676	3.531	2.969	2.251	3.506	3.278	13.988	24.56
	2% acid wash 16/12/2021 16:23:14											
1	63.56%	17.78	33.43	105.3	27.48	19.36	25.74	0.86%	17.86	27.52	26.09%	7.415
2	63.56%	16.67	21.38	253	16.12	15.04	36.58	0.49%	16.67	26.24	22.39%	5.863
3	62.71%	12.16	15.95	292.1	11.83	12.59	32.53	0.49%	15.57	26.57	21.55%	4.405
x	63.28%	15.54	23.59	216.8	18.48	15.66	31.62	0.61%	16.7	26.78	23.34%	5.894
s	0.49%	2.976	8.943	98.49	8.089	3.428	5.477	0.21%	1.148	0.662	2.42%	1.505
%RSD	0.781	19.16	37.92	45.43	43.78	21.89	17.32	34.298	6.874	2.472	10.359	25.54
	1AS 16/12/2021 16:24:39											
1	70.39%	1.246	46.67	76.89	0.16	2.052	3.571	100.74%	0.095	2.394	161.96%	0.235
2	67.09%	1.206	44.81	75.21	0.132	1.923	3.47	105.13%	0.071	1.678	157.41%	0.195

3	68.00%	1.204	44.13	70.5	0.108	1.87	3.491	106.59%	0.055	1.245	163.81%	0.164
x	68.49%	1.218	45.2	74.2	0.133	1.948	3.511	104.15%	0.074	1.772	161.06%	0.198
s	1.70%	0.024	1.317	3.311	0.026	0.094	0.053	3.05%	0.021	0.58	3.29%	0.036
%RSD	2.484	1.944	2.915	4.462	19.31	4.807	1.513	2.927	27.92	32.75	2.044	18.09
	1BS 16/12/2021 16:25:41											
1	68.27%	1.153	39.64	39.63	0.086	0.173	0.141	98.77%	-0.008	0.637	71.38%	0.074
2	71.91%	1.122	38.86	37.01	0.082	0.159	0.117	112.12%	-0.009	0.417	88.05%	0.074
3	69.21%	1.118	39.34	39.61	0.084	0.152	0.122	110.65%	-0.007	0.416	87.88%	0.075
x	69.80%	1.131	39.28	38.75	0.084	0.162	0.126	107.18%	-0.008	0.49	82.43%	0.074
s	1.89%	0.019	0.39	1.508	0.002	0.011	0.013	7.32%	0.001	0.127	9.58%	0
%RSD	2.705	1.72	0.993	3.891	2.64	6.552	9.909	6.832	12.13	25.98	11.615	0.516
	1CS 16/12/2021 16:26:40											
1	69.07%	1.124	33.54	61.53	0.041	0.606	0.075	99.15%	-0.01	0.422	75.08%	0.077
2	66.06%	1.155	34.75	60.79	0.029	0.637	0.055	94.51%	-0.011	0.343	74.07%	0.07
3	67.31%	1.138	35.24	61.2	0.03	0.641	0.065	92.67%	-0.009	0.345	71.55%	0.071
x	67.48%	1.139	34.51	61.17	0.033	0.628	0.065	95.44%	-0.01	0.37	73.57%	0.072
s	1.51%	0.016	0.877	0.367	0.007	0.019	0.01	3.34%	0.001	0.045	1.82%	0.004
%RSD	2.239	1.379	2.541	0.6	19.69	3.042	15.37	3.497	10.54	12.22	2.475	5.169
	1DS 16/12/2021 16:27:40											
1	68.16%	0.953	35.65	46.58	0.529	0.397	0.142	99.62%	-0.016	0.279	181.83%	0.065
2	66.18%	0.944	37.07	47.35	0.552	0.413	0.142	96.27%	-0.014	0.288	171.39%	0.066
3	64.91%	0.947	36.62	48.89	0.559	0.415	0.15	94.57%	-0.015	0.294	182.67%	0.065
x	66.42%	0.948	36.45	47.61	0.547	0.408	0.145	96.82%	-0.015	0.287	178.63%	0.065
s	1.64%	0.004	0.723	1.177	0.015	0.01	0.005	2.57%	0.001	0.008	6.28%	0
%RSD	2.471	0.445	1.985	2.473	2.805	2.468	3.151	2.657	4.64	2.637	3.518	0.502
	1AA 16/12/2021 16:28:43											
1	66.06%	0.051	28.43	51.26	0.031	0.323	0.101	113.42%	-0.023	0.215	219.21%	0.06
2	64.99%	-0.002	28.61	48.08	0.028	0.339	0.102	112.05%	-0.022	0.215	210.28%	0.061
3	62.21%	-0.021	28.2	48.78	0.023	0.343	0.096	110.39%	-0.02	0.214	210.12%	0.061
x	64.42%	0.009	28.41	49.38	0.027	0.335	0.1	111.95%	-0.022	0.214	213.20%	0.061
s	1.99%	0.037	0.207	1.671	0.004	0.011	0.003	1.52%	0.001	0.001	5.20%	0
%RSD	3.086	399.9	0.729	3.385	13.28	3.238	2.829	1.355	6.222	0.324	2.44	0.702
	1BA 16/12/2021 16:29:51											
1	65.41%	-0.034	59.98	119.9	0.17	1.076	0.191	101.92%	-0.016	0.217	228.81%	0.064
2	63.65%	-0.042	61.5	122.2	0.129	0.823	0.176	100.17%	-0.014	0.217	224.93%	0.064
3	63.78%	-0.042	62.29	123.2	0.111	0.701	0.167	98.11%	-0.014	0.216	225.78%	0.065
x	64.28%	-0.04	61.26	121.8	0.137	0.867	0.178	100.07%	-0.014	0.217	226.51%	0.064

s	0.98%	0.005	1.171	1.671	0.03	0.191	0.012	1.91%	0.001	0	2.04%	0
%RSD	1.525	12.71	1.912	1.372	22.31	22.04	6.85	1.908	6.804	0.137	0.899	0.731

1CA 16/12/2021 16:30:57

1	64.06%	-0.065	5.495	50.48	-0.001	0.331	0.095	119.20%	-0.018	0.21	216.85%	0.059
2	59.80%	-0.064	4.775	50.18	-0.013	0.322	0.09	116.72%	-0.017	0.211	215.84%	0.06
3	61.27%	-0.067	4.5	48.99	-0.013	0.312	0.089	116.23%	-0.016	0.211	220.05%	0.06
x	61.71%	-0.066	4.923	49.89	-0.009	0.322	0.091	117.39%	-0.017	0.211	217.58%	0.06
s	2.17%	0.002	0.514	0.787	0.007	0.01	0.003	1.59%	0.001	0.001	2.20%	0
%RSD	3.512	2.627	10.44	1.578	76.24	3.001	3.74	1.358	7.109	0.302	1.01	0.634

1DA 16/12/2021 16:32:04

1	63.46%	-0.075	2.444	47.1	-0.012	0.274	0.064	120.17%	-0.024	0.215	92.76%	0.059
2	62.20%	-0.079	2.294	45.65	-0.017	0.258	0.059	123.15%	-0.025	0.214	90.57%	0.059
3	61.02%	-0.078	2.286	45.69	-0.019	0.256	0.063	121.61%	-0.023	0.219	80.64%	0.059
x	62.22%	-0.077	2.342	46.15	-0.016	0.263	0.062	121.64%	-0.024	0.216	87.99%	0.059
s	1.22%	0.002	0.089	0.824	0.003	0.01	0.003	1.49%	0.001	0.002	6.46%	0
%RSD	1.958	2.448	3.808	1.786	21.77	3.727	4.04	1.223	3.093	1.031	7.342	0.311

1AD 16/12/2021 16:33:13

1	88.67%	1.144	123.9	797.4	4.022	3.845	0.51	121.19%	0	0.264	736.16%	0.164
2	84.98%	1.151	121.1	795.3	3.913	3.801	0.489	121.60%	-0.003	0.264	749.31%	0.16
3	86.10%	1.199	124.2	814.5	4.033	3.831	0.503	123.37%	0	0.264	769.53%	0.163
x	86.59%	1.165	123.1	802.4	3.989	3.826	0.501	122.05%	-0.001	0.264	751.67%	0.162
s	1.89%	0.03	1.695	10.56	0.067	0.022	0.011	1.16%	0.002	0	16.81%	0.002
%RSD	2.183	2.593	1.377	1.316	1.671	0.585	2.109	0.947	221.3	0.11	2.236	1.085

1BD 16/12/2021 16:34:18

1	96.37%	1.127	110.5	776.8	3.507	5.096	0.67	126.05%	0.271	0.236	1389.21%	0.18
2	96.96%	1.053	109	745	3.375	4.904	0.677	129.86%	0.256	0.233	1426.32%	0.174
3	93.51%	1.108	112.2	764.7	3.447	5.052	0.681	127.93%	0.281	0.237	1415.52%	0.176
x	95.61%	1.096	110.6	762.2	3.443	5.018	0.676	127.95%	0.269	0.235	1410.35%	0.177
s	1.84%	0.038	1.615	16.01	0.066	0.101	0.005	1.91%	0.013	0.002	19.08%	0.003
%RSD	1.928	3.484	1.461	2.101	1.908	2.006	0.771	1.491	4.697	0.946	1.353	1.716

1CD 16/12/2021 16:35:23

1	90.31%	0.878	55.51	569.9	2.801	3.888	0.661	131.54%	0.042	0.218	4324.35%	0.171
2	91.54%	0.923	56.64	598.4	2.868	3.956	0.678	126.91%	0.042	0.218	4240.73%	0.172
3	89.60%	0.868	54.65	577.1	2.796	3.896	0.666	129.01%	0.038	0.215	4314.53%	0.168
x	90.48%	0.89	55.6	581.8	2.822	3.913	0.668	129.15%	0.041	0.217	4293.21%	0.17
s	0.98%	0.03	0.998	14.8	0.04	0.037	0.009	2.32%	0.002	0.002	45.71%	0.002
%RSD	1.083	3.33	1.795	2.544	1.433	0.944	1.326	1.798	4.757	0.765	1.065	1.397

1DD 16/12/2021 16:36:26

1	203.74%	2.071	13.48	559.2	1.153	3.77	1.007	135.58%	0.024	0.212	1547.25%	0.234
2	194.50%	2.083	12.92	561.7	1.135	3.783	1.016	131.98%	0.026	0.211	1457.52%	0.229
3	191.13%	2.185	13.33	576.6	1.186	3.929	1.033	126.47%	0.031	0.211	1407.26%	0.234
x	196.46%	2.113	13.24	565.8	1.158	3.827	1.019	131.34%	0.027	0.211	1470.68%	0.233
s	6.53%	0.063	0.293	9.415	0.026	0.088	0.013	4.59%	0.004	0.001	70.92%	0.003
%RSD	3.325	2.976	2.21	1.664	2.266	2.295	1.311	3.493	13.3	0.253	4.822	1.233

2AS 16/12/2021 16:37:42

1	56.03%	1.085	5.878	217.7	0.248	2.373	0.238	106.79%	-0.012	0.261	343.15%	0.061
2	55.55%	1.105	6.288	225.4	0.264	2.391	0.239	104.13%	-0.01	0.27	345.17%	0.062
3	40.52%	1.069	6.142	208.6	0.248	2.251	0.226	67.00%	-0.009	0.297	210.96%	0.061
x	50.70%	1.086	6.103	217.2	0.253	2.338	0.234	92.64%	-0.01	0.276	299.76%	0.061
s	8.82%	0.018	0.208	8.407	0.009	0.076	0.007	22.24%	0.001	0.018	76.91%	0.001
%RSD	17.394	1.683	3.406	3.87	3.698	3.244	3.01	24.01	11.21	6.681	25.658	0.82

2BS 16/12/2021 16:38:48

1	51.49%	1.086	6.385	176	0.162	0.372	0.125	119.28%	-0.017	0.242	409.51%	0.06
2	50.61%	1.088	6.214	170.4	0.151	0.349	0.123	118.36%	-0.017	0.245	385.26%	0.06
3	51.06%	1.055	6.131	171	0.151	0.326	0.128	122.76%	-0.018	0.242	387.78%	0.06
x	51.05%	1.077	6.243	172.5	0.155	0.349	0.126	120.14%	-0.017	0.243	394.18%	0.06
s	0.44%	0.019	0.13	3.101	0.006	0.023	0.002	2.32%	0	0.002	13.33%	0
%RSD	0.861	1.72	2.074	1.798	4.147	6.564	1.874	1.932	1.762	0.841	3.383	0.628

2CS 16/12/2021 16:39:56

1	47.78%	1.06	6.736	157.3	1.047	0.337	0.129	114.24%	-0.017	0.232	271.41%	0.058
2	50.44%	1.048	6.645	149.6	1.056	0.329	0.141	114.88%	-0.019	0.232	242.11%	0.058
3	49.16%	1.042	6.763	160.6	1.056	0.341	0.151	113.09%	-0.017	0.234	239.42%	0.058
x	49.13%	1.05	6.715	155.8	1.053	0.336	0.14	114.07%	-0.018	0.233	250.98%	0.058
s	1.33%	0.009	0.062	5.682	0.005	0.006	0.011	0.91%	0.001	0.001	17.75%	0
%RSD	2.71	0.87	0.917	3.646	0.483	1.866	8.036	0.795	5.214	0.584	7.071	0.129

2DS 16/12/2021 16:41:07

1	52.26%	1.128	5.829	157	0.08	0.186	0.104	108.64%	-0.026	0.252	285.39%	0.057
2	49.78%	1.12	5.848	157	0.083	0.19	0.119	107.27%	-0.024	0.262	291.79%	0.057
3	50.74%	1.108	5.919	160	0.073	0.19	0.114	108.02%	-0.024	0.264	304.59%	0.057
x	50.93%	1.119	5.865	158	0.079	0.189	0.112	107.97%	-0.025	0.259	293.92%	0.057
s	1.25%	0.01	0.048	1.711	0.005	0.002	0.008	0.69%	0.001	0.006	9.78%	0
%RSD	2.459	0.921	0.816	1.083	6.099	1.173	7.01	0.635	3.498	2.496	3.326	0.23

2AA 16/12/2021 16:42:14

1	56.43%	0.102	7.621	151.5	0.132	0.746	0.277	130.25%	-0.026	0.205	460.71%	0.064
2	55.93%	0.051	7.538	151	0.13	0.751	0.277	126.80%	-0.026	0.206	445.39%	0.064

3	57.95%	0.017	7.209	149.1	0.122	0.712	0.29	131.16%	-0.026	0.202	417.93%	0.064
x	56.77%	0.056	7.456	150.6	0.128	0.736	0.282	129.40%	-0.026	0.204	441.34%	0.064
s	1.05%	0.042	0.218	1.299	0.005	0.021	0.007	2.30%	0	0.002	21.68%	0
%RSD	1.854	75.09	2.925	0.863	4.003	2.845	2.62	1.778	0.643	0.896	4.911	0.351

2BA 16/12/2021 16:43:16

1	62.14%	0.003	8.091	166.7	0.152	0.674	0.355	126.38%	-0.021	0.202	308.29%	0.067
2	60.02%	-0.002	8.24	162.8	0.153	0.662	0.378	122.84%	-0.022	0.202	303.58%	0.066
3	59.15%	-0.009	7.964	157.7	0.146	0.638	0.359	125.10%	-0.021	0.202	290.61%	0.066
x	60.44%	-0.003	8.098	162.4	0.15	0.658	0.364	124.77%	-0.021	0.202	300.83%	0.066
s	1.53%	0.006	0.138	4.49	0.004	0.018	0.012	1.79%	0.001	0	9.16%	0
%RSD	2.539	229	1.703	2.765	2.473	2.718	3.341	1.437	2.951	0.16	3.044	0.521

2CA 16/12/2021 16:44:28

1	64.70%	0.036	9.115	134.1	4.008	0.892	0.606	113.86%	-0.016	0.202	7139.92%	0.068
2	63.92%	0.036	9.216	131	4.049	0.907	0.639	110.55%	-0.013	0.203	7086.57%	0.068
3	61.82%	0.029	9.116	132.5	4.045	0.897	0.641	110.99%	-0.017	0.204	7123.61%	0.068
x	63.48%	0.033	9.149	132.5	4.034	0.899	0.629	111.80%	-0.015	0.203	7116.70%	0.068
s	1.49%	0.004	0.058	1.549	0.023	0.008	0.02	1.79%	0.002	0.001	27.34%	0
%RSD	2.353	11.73	0.636	1.169	0.56	0.873	3.143	1.605	11.67	0.537	0.384	0.406

2DA 16/12/2021 16:45:31

1	61.53%	-0.026	6.207	220	0.122	0.411	0.395	129.43%	-0.018	0.203	1151.63%	0.065
2	61.98%	-0.028	6.234	229.8	0.08	0.404	0.397	128.33%	-0.017	0.203	1081.33%	0.066
3	61.91%	-0.033	6.241	229.5	0.079	0.424	0.37	127.58%	-0.017	0.202	985.42%	0.065
x	61.81%	-0.029	6.227	226.4	0.093	0.413	0.387	128.45%	-0.017	0.202	1072.79%	0.065
s	0.24%	0.004	0.018	5.549	0.024	0.01	0.015	0.93%	0	0.001	83.44%	0
%RSD	0.393	12.12	0.285	2.451	26.16	2.527	3.816	0.722	2.428	0.365	7.777	0.283

2AD 16/12/2021 16:46:33

1	68.67%	2.709	10.51	331.7	0.474	2.545	0.795	135.41%	-0.022	0.21	229.99%	0.066
2	66.69%	2.838	10.8	337.6	0.491	2.661	0.781	132.04%	-0.022	0.209	252.55%	0.066
3	64.88%	2.727	10.43	330.2	0.457	2.598	0.741	135.80%	-0.022	0.211	264.17%	0.066
x	66.75%	2.758	10.58	333.2	0.474	2.601	0.772	134.42%	-0.022	0.21	248.90%	0.066
s	1.90%	0.07	0.193	3.89	0.017	0.058	0.028	2.07%	0	0.001	17.38%	0
%RSD	2.841	2.524	1.825	1.167	3.558	2.237	3.663	1.539	1.107	0.491	6.983	0.325

2BD 16/12/2021 16:47:40

1	64.45%	0.444	6.204	272.4	0.278	2.944	0.796	131.40%	-0.024	0.204	357.97%	0.065
2	65.32%	0.422	6.071	252.9	0.275	2.841	0.755	131.20%	-0.022	0.207	358.31%	0.064

3	61.00%	0.413	6.067	264.9	0.269	2.848	0.764	130.85%	-0.023	0.208	355.11%	0.064
x	63.59%	0.426	6.114	263.4	0.274	2.877	0.772	131.15%	-0.023	0.207	357.13%	0.064
s	2.29%	0.016	0.078	9.838	0.005	0.058	0.021	0.28%	0.001	0.002	1.76%	0
%RSD	3.599	3.765	1.276	3.735	1.716	2.003	2.751	0.211	2.77	0.914	0.492	0.759

2CD 16/12/2021 16:48:47

1	63.54%	0.775	17.24	683.6	0.876	5.439	1.447	118.40%	-0.02	0.3	229.14%	0.068
2	61.32%	0.742	16.53	665.1	0.829	5.178	1.44	122.25%	-0.02	0.295	218.70%	0.068
3	59.89%	0.743	16.59	683.7	0.835	5.285	1.432	122.67%	-0.02	0.301	220.89%	0.067
x	61.58%	0.753	16.79	677.5	0.846	5.301	1.439	121.11%	-0.02	0.299	222.91%	0.068
s	1.84%	0.019	0.392	10.71	0.026	0.131	0.007	2.35%	0	0.003	5.51%	0
%RSD	2.986	2.474	2.334	1.581	3.033	2.477	0.51	1.944	0.543	0.991	2.47	0.692

2DD 16/12/2021 16:49:53

1	56.76%	0.364	4.432	266.4	0.262	2.329	1.034	131.25%	-0.025	0.209	133.67%	0.066
2	56.15%	0.354	4.281	263.2	0.26	2.286	1	129.57%	-0.024	0.208	139.06%	0.065
3	56.79%	0.369	4.422	264.7	0.262	2.327	1.029	125.10%	-0.025	0.208	138.39%	0.066
x	56.57%	0.362	4.378	264.8	0.261	2.314	1.021	128.64%	-0.025	0.208	137.04%	0.066
s	0.36%	0.008	0.084	1.617	0.001	0.025	0.019	3.18%	0.001	0.001	2.94%	0.001
%RSD	0.643	2.21	1.922	0.611	0.473	1.059	1.847	2.472	3.004	0.29	2.142	0.864

3AS 16/12/2021 16:50:54

1	57.28%	0.843	207.5	115.8	0.085	0.542	0.444	121.41%	0.287	0.231	171.73%	0.059
2	55.84%	0.932	208.9	111.5	0.09	0.507	0.42	120.54%	0.284	0.234	181.83%	0.059
3	53.58%	0.969	204.2	102.6	0.084	0.463	0.328	122.34%	0.284	0.233	157.58%	0.059
x	55.56%	0.915	206.9	110	0.086	0.504	0.397	121.43%	0.285	0.232	170.38%	0.059
s	1.86%	0.065	2.393	6.764	0.003	0.04	0.061	0.90%	0.002	0.001	12.18%	0
%RSD	3.353	7.075	1.157	6.15	3.184	7.887	15.43	0.744	0.695	0.59	7.148	0.281

3BS 16/12/2021 16:51:55

1	55.36%	1.145	218.3	89	0.048	0.179	0.161	125.21%	0.033	0.222	65.32%	0.058
2	54.36%	1.135	217.8	83.76	0.05	0.165	0.152	125.45%	0.028	0.219	72.56%	0.058
3	54.92%	1.162	218.9	84.73	0.045	0.17	0.151	125.26%	0.024	0.218	66.33%	0.058
x	54.88%	1.148	218.3	85.83	0.048	0.171	0.155	125.31%	0.028	0.22	68.07%	0.058
s	0.50%	0.014	0.542	2.788	0.002	0.007	0.006	0.12%	0.005	0.002	3.92%	0
%RSD	0.912	1.181	0.249	3.248	5.016	4.118	3.568	0.099	16.09	0.78	5.76	0.179

3CS 16/12/2021 16:53:00

1	56.40%	1.057	183.7	71.68	0.123	0.38	0.294	137.73%	0.481	0.211	88.05%	0.058
2	55.21%	1.065	184.6	68.46	0.122	0.393	0.314	136.56%	0.499	0.216	85.69%	0.059
3	54.27%	1.099	192.1	74.72	0.136	0.405	0.308	131.54%	0.528	0.218	91.41%	0.059
x	55.29%	1.073	186.8	71.62	0.127	0.393	0.305	135.28%	0.503	0.215	88.38%	0.059
s	1.07%	0.022	4.601	3.129	0.008	0.012	0.01	3.29%	0.023	0.003	2.88%	0
%RSD	1.928	2.075	2.463	4.369	6.425	3.104	3.307	2.43	4.666	1.523	3.255	0.213

3DS 16/12/2021 16:54:09

1	51.12%	1.102	196.5	110.3	0.079	0.341	0.111	128.60%	1.579	0.216	117.34%	0.057
2	52.24%	1.081	197.5	108.7	0.073	0.323	0.112	128.79%	1.614	0.218	114.31%	0.057
3	52.81%	1.084	193.8	106.2	0.069	0.328	0.122	128.49%	1.612	0.215	102.02%	0.057
x	52.05%	1.089	195.9	108.4	0.074	0.331	0.115	128.63%	1.602	0.216	111.22%	0.057
s	0.86%	0.012	1.953	2.068	0.005	0.009	0.006	0.15%	0.019	0.001	8.11%	0
%RSD	1.649	1.07	0.997	1.908	6.454	2.865	5.288	0.115	1.206	0.585	7.295	0.083

New Rh 16/12/2021 16:55:21

1	47.77%	-0.076	-0.241	-0.603	-0.085	-0.038	-0.033	1066.99%	-0.019	0.199	44.95%	0.056
2	45.55%	-0.085	-0.088	-0.662	-0.086	-0.04	-0.033	1092.14%	-0.02	0.199	36.53%	0.056
3	46.31%	-0.088	-0.224	-0.696	-0.086	-0.039	-0.034	1090.20%	-0.021	0.199	46.97%	0.056
x	46.54%	-0.083	-0.024	-0.654	-0.086	-0.039	-0.034	1083.11%	-0.02	0.199	42.82%	0.056
s	1.13%	0.006	0.239	0.047	0.001	0.001	0.001	13.99%	0.001	0	5.54%	0
%RSD	2.426	7.389	1005	7.253	0.695	1.946	2.269	1.292	6.093	0.072	12.93	0.022

3AA 16/12/2021 16:58:04

1	54.93%	0.116	255.2	102.3	1.154	2.099	0.056	118.69%	0.445	0.205	272.76%	0.06
2	52.11%	0.103	241.5	96.05	1.071	1.536	0.059	124.06%	0.421	0.203	289.26%	0.059
3	52.43%	0.107	247.6	100.2	1.109	1.386	0.073	120.24%	0.451	0.203	268.38%	0.059
x	53.16%	0.109	248.1	99.51	1.112	1.673	0.063	121.00%	0.439	0.204	276.80%	0.059
s	1.55%	0.007	6.889	3.187	0.041	0.376	0.009	2.76%	0.016	0.001	11.01%	0
%RSD	2.913	6.032	2.776	3.202	3.73	22.46	14.92	2.282	3.565	0.456	3.978	0.716

3BA 16/12/2021 16:59:04

1	50.63%	0.015	216.5	294.9	2.972	0.806	0.071	129.30%	0.12	0.203	386.10%	0.059
2	49.33%	0.007	217.8	296.3	3.018	0.796	0.07	131.21%	0.112	0.201	403.78%	0.06
3	50.26%	0.009	218.3	302.3	3.051	0.792	0.069	129.54%	0.111	0.202	382.23%	0.059
x	50.07%	0.01	217.5	297.8	3.013	0.798	0.07	130.02%	0.114	0.202	390.70%	0.06
s	0.67%	0.004	0.926	3.917	0.04	0.007	0.001	1.05%	0.005	0.001	11.49%	0
%RSD	1.346	39.03	0.426	1.315	1.319	0.91	1.617	0.804	4.454	0.288	2.942	0.415

3CA 16/12/2021 17:00:17

1	53.07%	0.047	267.8	145.8	7.321	0.845	0.214	125.74%	1.275	0.203	167.35%	0.064
2	50.29%	0.052	267.5	148.3	7.482	0.879	0.233	122.56%	1.323	0.202	167.68%	0.065
3	52.69%	0.047	261.1	143.1	7.27	0.823	0.229	129.15%	1.281	0.202	163.14%	0.065
x	52.02%	0.048	265.5	145.8	7.358	0.849	0.225	125.82%	1.293	0.203	166.06%	0.065
s	1.51%	0.003	3.749	2.59	0.111	0.028	0.01	3.30%	0.026	0.001	2.53%	0
%RSD	2.899	6.106	1.412	1.777	1.508	3.337	4.32	2.619	2.02	0.417	1.525	0.393

3DA 16/12/2021 17:01:42

1	50.49%	-0.008	230.7	82.09	0.142	0.55	0.122	129.86%	0.052	0.205	116.67%	0.058
2	48.38%	-0.023	231.4	76.93	0.083	0.569	0.108	129.32%	0.051	0.202	102.69%	0.058
3	50.12%	-0.033	230.4	79.03	0.078	0.56	0.104	129.77%	0.035	0.203	98.82%	0.058
x	49.66%	-0.021	230.8	79.35	0.101	0.56	0.111	129.65%	0.046	0.203	106.06%	0.058
s	1.13%	0.013	0.486	2.595	0.036	0.01	0.009	0.29%	0.009	0.002	9.39%	0

%RSD	2.275	58.8	0.211	3.27	35.43	1.74	8.18	0.226	20.38	0.833	8.851	0.475
	3AD 16/12/2021 17:03:26											
1	49.30%	0.883	421.5	487.1	4.403	11.25	0.638	140.82%	0.35	0.214	253.90%	0.106
2	49.79%	0.847	407.1	487.1	4.347	11.27	0.661	140.52%	0.351	0.215	264.17%	0.104
3	50.59%	0.878	423.4	498.4	4.525	11.66	0.672	138.30%	0.343	0.219	257.94%	0.105
x	49.89%	0.869	417.3	490.9	4.425	11.39	0.657	139.88%	0.348	0.216	258.67%	0.105
s	0.65%	0.02	8.902	6.545	0.091	0.228	0.018	1.38%	0.005	0.002	5.18%	0.001
%RSD	1.298	2.245	2.133	1.333	2.057	2.002	2.696	0.985	1.396	1.037	2.001	1.141
	3BD 16/12/2021 17:04:38											
1	53.08%	0.947	349.3	530.2	3.403	12.09	0.562	143.63%	1.216	0.213	101.85%	0.13
2	53.06%	0.96	362.7	545.1	3.413	12.13	0.574	140.51%	1.226	0.215	107.74%	0.126
3	51.29%	0.941	356.2	542.5	3.477	12.19	0.572	139.61%	1.2	0.222	93.77%	0.128
x	52.47%	0.95	356.1	539.3	3.431	12.14	0.569	141.25%	1.214	0.217	101.12%	0.128
s	1.03%	0.01	6.68	7.952	0.04	0.05	0.007	2.11%	0.013	0.005	7.02%	0.002
%RSD	1.961	1.018	1.876	1.475	1.166	0.414	1.173	1.493	1.103	2.113	6.938	1.327
	3CD 16/12/2021 17:05:44											
1	124.06%	1.583	436.9	728.1	3.846	14.71	0.899	135.39%	0.815	0.213	571.72%	0.181
2	123.42%	1.542	430.1	707.6	3.704	14.09	0.859	138.61%	0.788	0.209	576.27%	0.177
3	125.95%	1.558	428.3	703.4	3.721	14.42	0.833	137.80%	0.783	0.21	564.65%	0.177
x	124.48%	1.561	431.7	713	3.757	14.41	0.864	137.27%	0.795	0.211	570.88%	0.178
s	1.32%	0.021	4.534	13.24	0.078	0.312	0.033	1.67%	0.017	0.002	5.86%	0.002
%RSD	1.059	1.32	1.05	1.857	2.063	2.164	3.857	1.218	2.159	1.138	1.026	1.19
	3DD 16/12/2021 17:06:50											
1	112.35%	1.008	439.3	629.2	3.787	12.14	0.748	139.17%	0.124	0.203	261.48%	0.186
2	113.43%	0.957	437.4	635	3.748	12.13	0.739	140.54%	0.108	0.204	248.68%	0.185
3	113.21%	0.948	423.3	615.4	3.643	11.82	0.72	142.11%	0.1	0.205	247.16%	0.183
x	113.00%	0.971	433.3	626.5	3.726	12.03	0.736	140.61%	0.111	0.204	252.44%	0.185
s	0.57%	0.032	8.757	10.08	0.074	0.184	0.014	1.47%	0.012	0.001	7.86%	0.002
%RSD	0.505	3.306	2.021	1.608	1.994	1.526	1.958	1.046	11.11	0.457	3.115	0.936
	4AS 16/12/2021 17:07:57											
1	46.00%	1.033	10.17	152.1	0.139	0.513	0.12	115.50%	0.042	0.231	489.35%	0.064
2	43.85%	1.084	5.931	150.4	0.091	0.352	0.099	118.66%	0.04	0.23	457.01%	0.063
3	42.66%	1.084	4.099	150	0.082	0.284	0.091	119.41%	0.031	0.229	478.40%	0.062
x	44.17%	1.067	6.734	150.8	0.104	0.383	0.103	117.85%	0.038	0.23	474.92%	0.063
s	1.69%	0.03	3.115	1.104	0.031	0.117	0.015	2.07%	0.006	0.001	16.45%	0.001
%RSD	3.831	2.774	46.26	0.732	29.77	30.64	14.61	1.759	14.66	0.455	3.464	1.87
	4BS 16/12/2021 17:08:59											
1	47.61%	1.064	4.158	291.2	0.145	0.407	0.083	127.82%	0.17	0.215	439.66%	0.092
2	47.07%	1.029	4.228	293.4	0.147	0.409	0.079	126.91%	0.181	0.217	411.03%	0.091
3	45.49%	1.03	4.525	292.6	0.15	0.445	0.081	123.82%	0.18	0.216	405.97%	0.092
x	46.72%	1.041	4.304	292.4	0.147	0.42	0.081	126.18%	0.177	0.216	418.89%	0.091
s	1.10%	0.02	0.195	1.121	0.003	0.021	0.002	2.10%	0.006	0.001	18.17%	0.001

%RSD	2.364	1.907	4.526	0.383	1.711	5.032	2.431	1.66	3.488	0.433	4.337	0.828
	4CS 16/12/2021 17:09:58											
1	46.39%	0.471	1.489	223.2	0.131	0.424	0.015	208.87%	0.048	0.205	3154.76%	0.068
2	44.34%	0.448	1.409	221.5	0.132	0.415	0.014	208.76%	0.047	0.207	3129.58%	0.067
3	43.22%	0.449	1.426	227.3	0.137	0.435	0.017	202.53%	0.045	0.207	3129.75%	0.068
x	44.65%	0.456	1.441	224	0.133	0.425	0.015	206.72%	0.047	0.207	3138.03%	0.068
s	1.61%	0.013	0.043	2.947	0.003	0.01	0.001	3.63%	0.002	0.001	14.49%	0
%RSD	3.604	2.884	2.948	1.316	2.442	2.439	8.394	1.756	3.325	0.481	0.462	0.659
	4DS 16/12/2021 17:11:11											
1	42.14%	1.065	2.208	935	0.205	0.75	0.043	111.90%	0.504	0.21	414.06%	0.063
2	41.18%	1.038	2.192	935.7	0.21	0.761	0.051	109.13%	0.553	0.214	429.89%	0.064
3	40.18%	1.011	2.156	899.6	0.204	0.734	0.045	112.16%	0.488	0.213	402.60%	0.063
x	41.16%	1.038	2.185	923.4	0.206	0.749	0.046	111.06%	0.515	0.212	415.52%	0.064
s	0.98%	0.027	0.027	20.68	0.003	0.014	0.004	1.68%	0.034	0.002	13.70%	0
%RSD	2.381	2.612	1.224	2.239	1.545	1.827	9.394	1.513	6.569	0.984	3.297	0.384
	4AA 16/12/2021 17:12:14											
1	45.05%	0.419	1.55	150.4	0.114	0.853	0.123	132.16%	0.535	0.209	892.55%	0.066
2	44.35%	0.365	1.426	145.9	0.112	0.847	0.121	134.43%	0.479	0.212	847.55%	0.065
3	43.92%	0.345	1.407	141.5	0.113	0.83	0.117	134.52%	0.488	0.211	843.51%	0.065
x	44.44%	0.377	1.461	145.9	0.113	0.844	0.12	133.70%	0.501	0.211	861.20%	0.065
s	0.57%	0.038	0.078	4.447	0.001	0.012	0.003	1.33%	0.03	0.001	27.22%	0
%RSD	1.282	10.15	5.342	3.047	0.853	1.379	2.485	0.998	6.072	0.639	3.161	0.702
	4BA 16/12/2021 17:13:21											
1	49.00%	0.114	2.407	129.8	0.103	0.414	0.081	234.52%	0.121	0.202	207.25%	0.08
2	47.47%	0.106	2.449	131.2	0.105	0.409	0.085	233.79%	0.124	0.202	198.50%	0.08
3	47.26%	0.097	2.431	127.1	0.106	0.407	0.089	241.21%	0.12	0.202	197.32%	0.079
x	47.91%	0.106	2.429	129.4	0.105	0.41	0.085	236.51%	0.122	0.202	201.02%	0.079
s	0.95%	0.008	0.021	2.065	0.002	0.003	0.004	4.09%	0.002	0	5.43%	0.001
%RSD	1.989	7.874	0.855	1.596	1.588	0.798	5.016	1.729	2.001	0.132	2.7	0.816
	4CA 16/12/2021 17:14:34											
1	47.91%	0.429	3.962	450.5	0.197	1.225	0.172	128.60%	0.136	0.208	172.90%	0.095
2	46.82%	0.45	3.967	460.4	0.211	1.263	0.182	125.88%	0.141	0.208	178.46%	0.096
3	48.02%	0.449	3.882	455	0.207	1.263	0.178	128.02%	0.141	0.209	178.80%	0.096
x	47.58%	0.443	3.937	455.3	0.205	1.25	0.177	127.50%	0.139	0.208	176.72%	0.096
s	0.66%	0.012	0.048	4.963	0.007	0.022	0.005	1.43%	0.003	0	3.31%	0.001
%RSD	1.396	2.619	1.21	1.09	3.55	1.761	2.877	1.123	2.267	0.158	1.873	0.57
	4DA 16/12/2021 17:15:38											
1	43.37%	0.342	2.383	256	0.426	4.474	0.154	128.33%	0.649	0.205	193.78%	0.067
2	41.65%	0.33	2.338	254.8	0.418	4.498	0.142	127.25%	0.664	0.208	177.28%	0.067
3	41.63%	0.318	2.319	260.8	0.428	4.537	0.159	127.03%	0.663	0.209	183.68%	0.067
x	42.22%	0.33	2.347	257.2	0.424	4.503	0.151	127.54%	0.658	0.207	184.92%	0.067
s	1.00%	0.012	0.033	3.153	0.005	0.032	0.009	0.69%	0.008	0.002	8.32%	0

%RSD	2.372	3.543	1.409	1.226	1.239	0.702	5.761	0.544	1.25	0.835	4.499	0.515
	4AD 16/12/2021 17:16:44											
1	91.70%	1.722	4.729	254.9	0.672	10.76	0.84	115.74%	1.927	0.203	214.49%	0.211
2	92.24%	1.716	4.79	256.4	0.656	10.78	0.83	113.42%	1.955	0.203	190.42%	0.214
3	88.05%	1.698	4.676	247.8	0.655	10.58	0.838	113.60%	1.983	0.203	187.72%	0.216
x	90.66%	1.712	4.732	253	0.661	10.71	0.836	114.25%	1.955	0.203	197.54%	0.214
s	2.28%	0.013	0.057	4.582	0.01	0.11	0.005	1.29%	0.028	0	14.74%	0.003
%RSD	2.513	0.732	1.206	1.811	1.462	1.027	0.618	1.128	1.412	0.232	7.462	1.25
	4BD 16/12/2021 17:17:50											
1	186.35%	4.622	12.55	773.2	1.454	11.41	1.751	115.54%	0.092	0.202	425.01%	0.23
2	182.35%	4.599	12.38	765.4	1.445	11.18	1.745	115.46%	0.084	0.201	421.64%	0.22
3	182.88%	4.546	12.37	768.5	1.495	11.46	1.709	116.16%	0.071	0.201	429.38%	0.22
x	183.86%	4.589	12.43	769.1	1.464	11.35	1.735	115.72%	0.082	0.201	425.34%	0.224
s	2.17%	0.039	0.098	3.926	0.027	0.147	0.023	0.38%	0.011	0.001	3.89%	0.006
%RSD	1.182	0.841	0.79	0.51	1.839	1.3	1.314	0.329	13.05	0.445	0.913	2.582
	4CD 16/12/2021 17:18:51											
1	140.90%	2.9	9.307	473.5	1.028	7.856	1.29	117.95%	2.203	0.201	249.52%	0.182
2	135.98%	2.959	9.58	485.4	1.066	8.09	1.308	114.82%	2.217	0.203	249.86%	0.187
3	134.91%	2.936	9.298	467	1.027	8.008	1.295	116.87%	2.231	0.201	255.58%	0.187
x	137.26%	2.932	9.395	475.3	1.04	7.985	1.298	116.55%	2.217	0.202	251.65%	0.186
s	3.19%	0.03	0.16	9.371	0.022	0.119	0.009	1.59%	0.014	0.001	3.41%	0.003
%RSD	2.326	1.015	1.706	1.972	2.154	1.488	0.72	1.36	0.615	0.389	1.354	1.659
	4DD 16/12/2021 17:20:06											
1	110.51%	2.293	7.145	333.3	0.68	5.107	1.234	112.98%	4.063	0.203	313.85%	0.241
2	105.68%	2.353	7.193	335.2	0.721	5.28	1.244	110.92%	4.061	0.205	295.49%	0.237
3	106.63%	2.348	7.234	347.8	0.82	5.8	1.294	109.13%	4.095	0.205	312.33%	0.244
x	107.61%	2.331	7.191	338.8	0.74	5.395	1.257	111.01%	4.073	0.204	307.22%	0.241
s	2.56%	0.033	0.044	7.841	0.072	0.361	0.032	1.93%	0.019	0.001	10.19%	0.003
%RSD	2.377	1.414	0.618	2.315	9.702	6.688	2.541	1.736	0.469	0.657	3.316	1.413
	c1s 16/12/2021 17:21:20											
1	42.65%	1.24	0.047	102.7	0.029	1.438	0.322	113.66%	0.322	0.221	1131.91%	0.096
2	40.56%	1.276	-0.018	104	0.03	1.412	0.319	109.28%	0.269	0.217	1038.85%	0.093
3	40.38%	1.237	-0.048	102.7	0.032	1.338	0.303	111.56%	0.189	0.22	1023.17%	0.091
x	41.19%	1.251	-0.006	103.1	0.03	1.396	0.315	111.50%	0.26	0.219	1064.64%	0.093
s	1.26%	0.021	0.049	0.776	0.001	0.052	0.01	2.19%	0.067	0.002	58.78%	0.002
%RSD	3.063	1.717	786.3	0.753	4.224	3.738	3.264	1.965	25.61	0.989	5.521	2.622
	C2S 16/12/2021 17:22:38											
1	42.85%	1.197	-0.065	92.94	0.05	0.498	0.239	108.66%	0.033	0.209	1316.70%	0.086
2	41.83%	1.166	-0.069	93.21	0.058	0.507	0.241	106.67%	0.04	0.21	1250.94%	0.085
3	41.20%	1.194	-0.05	94.83	0.076	0.596	0.264	102.98%	0.043	0.209	1267.46%	0.085

x	41.96%	1.186	-0.061	93.66	0.061	0.533	0.248	106.10%	0.039	0.21	1278.37%	0.085
s	0.83%	0.017	0.01	1.017	0.013	0.054	0.014	2.88%	0.005	0.001	34.21%	0
%RSD	1.986	1.416	16.53	1.086	21.45	10.13	5.584	2.714	13.33	0.278	2.676	0.241

C3S 16/12/2021 17:23:41

1	41.26%	0.986	-0.202	71.27	0.003	0.496	0.169	127.05%	0.01	0.207	565.66%	0.084
2	40.65%	0.94	-0.221	67.91	-0.005	0.478	0.165	127.51%	0.012	0.208	521.52%	0.081
3	38.04%	0.931	-0.222	67.46	0.003	0.487	0.175	125.68%	0.014	0.206	543.93%	0.082
x	39.98%	0.952	-0.215	68.88	0	0.487	0.17	126.75%	0.012	0.207	543.70%	0.082
s	1.71%	0.03	0.011	2.081	0.004	0.009	0.005	0.95%	0.002	0.001	22.07%	0.001
%RSD	4.279	3.119	5.282	3.02	1753	1.847	2.955	0.749	19.73	0.414	4.059	1.708

C4S 16/12/2021 17:24:41

1	40.45%	0.966	-0.101	87.58	0.146	0.352	0.178	129.10%	0.002	0.205	997.05%	0.082
2	40.06%	0.94	-0.107	84.27	0.158	0.354	0.174	127.56%	0.003	0.206	1004.80%	0.084
3	39.64%	0.915	-0.108	89.11	0.14	0.334	0.165	128.57%	0.006	0.206	1002.78%	0.082
x	40.05%	0.94	-0.105	86.99	0.148	0.347	0.172	128.41%	0.003	0.206	1001.54%	0.082
s	0.40%	0.026	0.004	2.474	0.009	0.011	0.007	0.78%	0.002	0.001	4.02%	0.001
%RSD	1.009	2.713	3.658	2.843	6.414	3.127	4.018	0.606	61.63	0.509	0.402	1.383

C5S 16/12/2021 17:26:14

1	37.27%	1.026	-0.21	89.78	0.082	0.761	0.189	120.50%	0.031	0.209	710.38%	0.087
2	38.31%	1.071	-0.209	93.71	0.083	0.801	0.202	114.71%	0.035	0.21	690.84%	0.087
3	36.45%	1.07	-0.209	97.63	0.086	0.813	0.19	112.51%	0.032	0.209	665.06%	0.088
x	37.34%	1.056	-0.209	93.71	0.084	0.792	0.194	115.91%	0.032	0.209	688.76%	0.087
s	0.94%	0.026	0.001	3.927	0.002	0.027	0.007	4.13%	0.002	0.001	22.73%	0
%RSD	2.504	2.429	0.394	4.191	2.337	3.416	3.842	3.562	6.397	0.316	3.301	0.534

C1A 16/12/2021 17:27:26

1	35.43%	0.058	-0.149	77.86	0.003	0.368	0.111	122.69%	-0.022	0.203	207.59%	0.06
2	34.05%	0.011	-0.15	76.02	0.004	0.388	0.113	122.62%	-0.021	0.203	229.14%	0.06
3	32.94%	-0.014	-0.147	74.93	0.001	0.402	0.104	123.49%	-0.019	0.202	221.40%	0.06
x	34.14%	0.018	-0.149	76.27	0.003	0.386	0.109	122.93%	-0.02	0.203	219.38%	0.06
s	1.24%	0.036	0.002	1.483	0.001	0.017	0.005	0.49%	0.002	0.001	10.92%	0
%RSD	3.644	198.8	1.059	1.944	43.13	4.342	4.129	0.395	7.879	0.259	4.977	0.54

C2A 16/12/2021 17:28:27

1	35.77%	-0.051	-0.182	83.92	-0.009	0.252	0.121	137.46%	-0.024	0.202	129.97%	0.058
2	34.32%	-0.055	-0.186	82.23	-0.008	0.249	0.104	137.82%	-0.023	0.202	124.58%	0.058
3	34.45%	-0.055	-0.18	82.36	-0.004	0.267	0.117	132.84%	-0.023	0.201	122.90%	0.058
x	34.85%	-0.054	-0.183	82.83	-0.007	0.256	0.114	136.04%	-0.023	0.202	125.82%	0.058

s	0.80%	0.002	0.003	0.943	0.003	0.009	0.009	2.78%	0	0.001	3.69%	0
%RSD	2.301	4.631	1.832	1.138	40.01	3.565	8.034	2.042	2.148	0.325	2.936	0.215
	C3A 16/12/2021 17:29:33											
1	34.91%	-0.049	-0.247	45.98	0.028	0.552	0.172	109.60%	-0.022	0.202	869.29%	0.085
2	35.94%	-0.054	-0.256	41.8	0.024	0.548	0.17	110.63%	-0.021	0.201	856.65%	0.084
3	35.88%	-0.055	-0.253	46.36	0.024	0.549	0.151	108.33%	-0.02	0.203	865.08%	0.085
x	35.58%	-0.053	-0.252	44.71	0.025	0.55	0.164	109.52%	-0.021	0.202	863.67%	0.085
s	0.57%	0.003	0.005	2.532	0.002	0.002	0.011	1.15%	0.001	0.001	6.44%	0.001
%RSD	1.612	5.757	1.846	5.663	9.518	0.416	7	1.052	6.682	0.303	0.745	0.885
	C4A 16/12/2021 17:30:35											
1	36.19%	-0.076	-0.175	40.38	0.1	0.113	0.104	149.93%	-0.026	0.201	159.43%	0.062
2	34.25%	-0.077	-0.171	40.77	0.103	0.117	0.099	146.38%	-0.026	0.201	148.15%	0.062
3	34.81%	-0.078	-0.175	38.54	0.102	0.11	0.1	149.84%	-0.026	0.201	146.81%	0.061
x	35.08%	-0.077	-0.174	39.9	0.102	0.114	0.101	148.72%	-0.026	0.201	151.46%	0.062
s	1.00%	0.001	0.002	1.189	0.001	0.004	0.002	2.02%	0	0	6.94%	0
%RSD	2.841	1.695	1.393	2.981	1.178	3.346	2.42	1.358	0.468	0.034	4.578	0.345
	C5A 16/12/2021 17:31:46											
1	34.97%	-0.061	-0.089	124.1	0.251	1.064	0.27	136.75%	-0.025	0.202	441.85%	0.06
2	33.90%	-0.061	-0.086	124	0.247	1.113	0.266	134.56%	-0.026	0.202	448.08%	0.06
3	33.61%	-0.058	-0.079	129.7	0.257	1.15	0.28	129.37%	-0.025	0.201	432.75%	0.06
x	34.16%	-0.06	-0.085	125.9	0.252	1.109	0.272	133.56%	-0.025	0.202	440.89%	0.06
s	0.72%	0.002	0.005	3.302	0.005	0.043	0.007	3.79%	0	0	7.71%	0
%RSD	2.103	3.005	6.326	2.622	2.032	3.907	2.724	2.836	1.912	0.223	1.748	0.506
	C1D 16/12/2021 17:32:47											
1	42.86%	0.123	0.37	86.27	0.123	1.382	0.237	136.42%	0.009	0.209	17213.38%	0.077
2	42.65%	0.125	0.373	81.58	0.126	1.392	0.2	134.54%	0.009	0.209	17353.18%	0.079
3	40.94%	0.13	0.428	85.07	0.134	1.366	0.171	129.28%	0.012	0.209	16921.99%	0.077
x	42.15%	0.126	0.391	84.31	0.128	1.38	0.203	133.41%	0.01	0.209	17162.85%	0.078
s	1.06%	0.003	0.033	2.433	0.006	0.013	0.033	3.70%	0.002	0	219.99%	0.001
%RSD	2.503	2.654	8.327	2.886	4.446	0.942	16.32	2.773	17.99	0.087	1.282	0.978
	C2D 16/12/2021 17:33:50											
1	40.53%	0.143	0.128	88.94	0.212	0.898	0.102	123.11%	0.03	0.206	10034.22%	0.076
2	39.49%	0.138	0.123	87.81	0.206	0.928	0.1	124.35%	0.032	0.208	9985.45%	0.078
3	38.04%	0.136	0.11	90.3	0.204	0.94	0.131	127.64%	0.03	0.204	9968.90%	0.075
x	39.35%	0.139	0.12	89.02	0.207	0.922	0.111	125.03%	0.031	0.206	9996.19%	0.076
s	1.25%	0.004	0.009	1.25	0.004	0.021	0.018	2.34%	0.001	0.002	33.96%	0.001
%RSD	3.184	2.795	7.546	1.404	2.066	2.318	15.83	1.871	3.199	0.94	0.34	1.942
	C3D 16/12/2021 17:34:53											

1	41.34%	0.151	0.218	72.5	0.094	1.371	0.072	124.17%	0.015	0.205	10672.53%	0.074
2	40.20%	0.143	0.21	70.36	0.086	1.372	0.072	126.12%	0.012	0.204	10533.59%	0.075
3	39.57%	0.151	0.23	74.94	0.084	1.428	0.072	119.50%	0.017	0.204	10562.95%	0.075
x	40.37%	0.148	0.22	72.6	0.088	1.39	0.072	123.26%	0.015	0.204	10589.69%	0.075
s	0.90%	0.004	0.01	2.295	0.006	0.033	0	3.40%	0.002	0	73.23%	0
%RSD	2.223	2.992	4.627	3.162	6.291	2.353	0.484	2.762	14.82	0.135	0.691	0.181

C4D 16/12/2021 17:35:54

1	39.20%	0.078	0.103	67.18	0.364	1.012	0.07	125.72%	0.009	0.214	12202.45%	0.071
2	37.72%	0.072	0.093	65.75	0.351	0.946	0.067	129.90%	0.011	0.213	12146.18%	0.07
3	37.62%	0.076	0.097	67.44	0.368	0.977	0.063	128.04%	0.013	0.214	11997.41%	0.07
x	38.18%	0.075	0.098	66.79	0.361	0.978	0.067	127.89%	0.011	0.214	12115.34%	0.071
s	0.89%	0.003	0.005	0.911	0.009	0.033	0.003	2.09%	0.002	0	105.94%	0
%RSD	2.321	4.486	5.046	1.364	2.58	3.329	4.841	1.637	20.52	0.22	0.874	0.527

C5D 16/12/2021 17:36:57

1	37.02%	0.104	0.156	95.01	0.073	0.841	0.058	125.21%	0.014	0.205	9047.35%	0.072
2	36.74%	0.108	0.147	94.34	0.065	0.831	0.065	124.42%	0.02	0.205	9192.66%	0.072
3	36.30%	0.104	0.13	92.82	0.055	0.797	0.055	129.64%	0.018	0.205	9311.76%	0.072
x	36.69%	0.105	0.144	94.05	0.064	0.823	0.059	126.43%	0.017	0.205	9183.92%	0.072
s	0.36%	0.002	0.013	1.12	0.009	0.023	0.005	2.82%	0.003	0	132.42%	0
%RSD	0.98	2.181	9.035	1.191	13.87	2.771	8.161	2.227	15.72	0.084	1.442	0.49

5AS 16/12/2021 17:38:00

1	28.46%	1.069	11.85	155.3	0.036	0.354	0.011	115.94%	-0.009	0.212	142.60%	0.057
2	27.36%	1.056	12.1	155.6	0.037	0.353	0.016	116.61%	-0.009	0.21	120.88%	0.057
3	26.67%	1.026	11.74	152.9	0.034	0.35	0.014	117.78%	-0.01	0.212	103.70%	0.057
x	27.50%	1.05	11.9	154.6	0.036	0.352	0.014	116.78%	-0.009	0.211	122.39%	0.057
s	0.91%	0.022	0.184	1.484	0.002	0.002	0.002	0.93%	0.001	0.002	19.49%	0
%RSD	3.29	2.102	1.547	0.96	4.306	0.603	17.07	0.799	10.04	0.746	15.925	0.094

5BS 16/12/2021 17:39:01

1	27.86%	0.923	6.045	116.3	0.071	0.288	0.081	121.85%	-0.019	0.204	86.36%	0.057
2	26.69%	0.892	5.949	114.2	0.064	0.285	0.08	123.26%	-0.019	0.207	91.92%	0.057
3	25.77%	0.884	6.153	116.8	0.073	0.304	0.091	121.19%	-0.017	0.207	87.37%	0.057
x	26.77%	0.9	6.049	115.8	0.069	0.292	0.084	122.10%	-0.018	0.206	88.55%	0.057
s	1.05%	0.021	0.102	1.364	0.005	0.01	0.006	1.05%	0.001	0.002	2.96%	0
%RSD	3.912	2.294	1.691	1.178	6.972	3.423	7.377	0.863	6.753	0.763	3.342	0.108

5CS 16/12/2021 17:40:07

1	27.75%	0.921	8.342	118.5	0.051	0.247	0.023	124.55%	-0.019	0.205	103.03%	0.056
2	25.73%	0.894	8.459	116.4	0.047	0.263	0.019	124.24%	-0.018	0.206	107.07%	0.056
3	25.92%	0.862	8.183	116.6	0.05	0.266	0.02	126.71%	-0.019	0.206	108.25%	0.056
x	26.47%	0.892	8.328	117.2	0.049	0.259	0.021	125.17%	-0.019	0.206	106.12%	0.056

s	1.12%	0.03	0.139	1.149	0.002	0.01	0.002	1.34%	0.001	0.001	2.74%	0
%RSD	4.212	3.337	1.664	0.98	4.698	3.889	10.33	1.072	2.951	0.437	2.579	0.026
	5DS 16/12/2021 17:41:16											
1	29.08%	0.813	16.31	151.1	0.034	0.157	0.014	124.59%	-0.023	0.204	76.60%	0.057
2	27.61%	0.782	16.68	154	0.031	0.163	0.012	124.59%	-0.021	0.205	88.72%	0.057
3	28.37%	0.758	16.36	146.1	0.028	0.154	0.009	126.23%	-0.02	0.205	85.69%	0.057
x	28.35%	0.784	16.45	150.4	0.031	0.158	0.012	125.14%	-0.021	0.204	83.67%	0.057
s	0.74%	0.027	0.201	4.019	0.003	0.005	0.003	0.95%	0.001	0.001	6.31%	0
%RSD	2.598	3.451	1.222	2.671	10.5	3.104	22.01	0.758	5.731	0.408	7.54	0.15
	5AA 16/12/2021 17:42:19											
1	27.54%	0.153	12.94	257.3	18.63	0.855	0.004	122.20%	-0.023	0.202	79.97%	0.058
2	25.74%	0.099	12.75	263.9	18.6	0.863	0.006	122.80%	-0.024	0.201	81.65%	0.057
3	25.01%	0.078	12.8	262.1	18.76	0.905	0.001	121.12%	-0.023	0.202	84.01%	0.057
x	26.10%	0.11	12.83	261.1	18.66	0.875	0.004	122.04%	-0.024	0.202	81.87%	0.057
s	1.30%	0.038	0.097	3.379	0.088	0.027	0.003	0.85%	0.001	0.001	2.03%	0
%RSD	4.986	35	0.753	1.294	0.471	3.094	81	0.697	2.749	0.434	2.479	0.233
	5BA 16/12/2021 17:43:28											
1	28.88%	0.018	2.588	80.15	7.291	0.142	0.026	124.21%	-0.027	0.203	30.64%	0.056
2	25.59%	0.019	2.586	80.73	7.433	0.124	0.022	121.23%	-0.027	0.203	30.13%	0.056
3	26.34%	0.014	2.503	84.08	7.359	0.121	0.029	123.80%	-0.028	0.205	28.11%	0.057
x	26.94%	0.017	2.559	81.65	7.361	0.129	0.026	123.08%	-0.027	0.204	29.63%	0.056
s	1.73%	0.003	0.048	2.119	0.071	0.011	0.003	1.61%	0.001	0.001	1.34%	0
%RSD	6.403	18.14	1.882	2.595	0.971	8.736	13.16	1.312	2.025	0.686	4.51	0.16
	5CA 16/12/2021 17:44:36											
1	30.17%	-0.047	8.547	146.7	3.232	0.816	0.033	130.76%	-0.022	0.201	189.57%	0.058
2	29.21%	-0.049	9.052	146.2	3.231	0.856	0.033	128.77%	-0.02	0.202	187.89%	0.058
3	30.06%	-0.052	8.843	147.7	3.172	0.855	0.038	130.87%	-0.021	0.201	208.10%	0.058
x	29.81%	-0.05	8.814	146.9	3.212	0.843	0.035	130.13%	-0.021	0.201	195.19%	0.058
s	0.53%	0.002	0.254	0.765	0.035	0.023	0.003	1.18%	0.001	0.001	11.21%	0
%RSD	1.759	4.992	2.878	0.521	1.078	2.692	7.235	0.908	4.256	0.311	5.744	0.468
	5DA 16/12/2021 17:45:47											
1	31.68%	-0.041	17.26	192.7	5.002	1.197	0.145	125.28%	-0.017	0.2	272.25%	0.06
2	30.06%	-0.042	17.36	187.3	4.979	1.17	0.141	126.65%	-0.018	0.201	273.43%	0.06
3	30.08%	-0.042	17.46	196.1	5.103	1.209	0.14	124.37%	-0.017	0.2	282.19%	0.059
x	30.61%	-0.042	17.36	192.1	5.028	1.192	0.142	125.43%	-0.017	0.201	275.96%	0.06
s	0.93%	0.001	0.098	4.441	0.066	0.02	0.003	1.15%	0.001	0	5.43%	0

%RSD	3.048	2.068	0.567	2.313	1.313	1.651	1.823	0.916	3.946	0.213	1.967	0.208
	5AD 16/12/2021 17:46:56											
1	37.05%	0.251	15.59	1345	2.972	17.39	1.324	128.33%	-0.02	0.205	1333.73%	0.171
2	37.75%	0.245	15.31	1321	2.934	17.41	1.315	129.22%	-0.021	0.205	1353.13%	0.172
3	36.71%	0.251	15.26	1329	2.978	17.59	1.347	127.75%	-0.02	0.207	1351.94%	0.171
x	37.17%	0.249	15.39	1332	2.961	17.46	1.329	128.43%	-0.02	0.206	1346.27%	0.171
s	0.53%	0.003	0.181	12.07	0.024	0.108	0.016	0.75%	0.001	0.002	10.87%	0
%RSD	1.433	1.325	1.175	0.907	0.811	0.618	1.211	0.58	3.316	0.736	0.808	0.234
	5BD 16/12/2021 17:48:04											
1	35.22%	0.191	4.944	504.3	1.525	6.609	0.583	128.97%	-0.024	0.201	291.96%	0.155
2	32.61%	0.183	4.784	498.5	1.529	6.621	0.565	128.59%	-0.023	0.201	283.54%	0.152
3	33.45%	0.204	5.033	527.3	1.571	6.909	0.593	123.11%	-0.023	0.201	278.48%	0.159
x	33.76%	0.193	4.92	510.1	1.542	6.713	0.58	126.89%	-0.023	0.201	284.66%	0.155
s	1.33%	0.011	0.126	15.25	0.026	0.17	0.015	3.28%	0.001	0	6.81%	0.004
%RSD	3.951	5.466	2.557	2.989	1.676	2.526	2.5	2.583	2.675	0.205	2.391	2.254
	5CD 16/12/2021 17:49:20											
1	34.89%	0.183	7.43	764.7	1.109	9.247	0.79	128.53%	-0.02	0.2	242.95%	0.168
2	34.71%	0.191	7.583	766.7	1.15	9.334	0.829	126.30%	-0.018	0.2	264.67%	0.168
3	35.63%	0.183	7.587	765.9	1.119	9.277	0.819	129.48%	-0.018	0.201	259.62%	0.169
x	35.08%	0.186	7.533	765.7	1.126	9.286	0.813	128.11%	-0.019	0.2	255.75%	0.169
s	0.49%	0.005	0.09	1.02	0.021	0.044	0.02	1.63%	0.001	0.001	11.37%	0
%RSD	1.382	2.493	1.191	0.133	1.876	0.476	2.515	1.273	5.3	0.303	4.445	0.243
	5DD 16/12/2021 17:50:26											
1	42.95%	0.191	24.2	1681	2.052	21.02	0.79	131.87%	0.025	0.202	307.95%	0.151
2	42.43%	0.193	24.42	1681	2.057	21.69	0.762	128.93%	0.028	0.201	337.26%	0.153
3	42.30%	0.196	24.82	1694	2.07	21.93	0.753	128.31%	0.031	0.201	332.88%	0.154
x	42.56%	0.193	24.48	1685	2.059	21.54	0.768	129.71%	0.028	0.201	326.03%	0.153
s	0.34%	0.003	0.317	7.713	0.009	0.471	0.019	1.90%	0.003	0	15.81%	0.001
%RSD	0.797	1.409	1.294	0.458	0.444	2.189	2.535	1.466	10.29	0.245	4.848	0.798
	6AS 16/12/2021 17:51:33											
1	38.19%	0.963	0.961	107.3	0.286	1.303	0.225	130.85%	-0.018	0.227	274.44%	0.078
2	36.21%	1.004	0.911	107	0.296	1.264	0.234	125.17%	-0.018	0.232	285.05%	0.079
3	35.57%	0.98	0.823	100.1	0.282	1.149	0.23	129.59%	-0.02	0.236	273.43%	0.077
x	36.66%	0.982	0.898	104.8	0.288	1.239	0.23	128.54%	-0.019	0.232	277.64%	0.078
s	1.37%	0.021	0.07	4.06	0.007	0.08	0.004	2.98%	0.001	0.004	6.44%	0.001
%RSD	3.734	2.126	7.788	3.873	2.407	6.481	1.908	2.319	4.74	1.796	2.318	0.756
	6BS 16/12/2021 17:52:40											
1	32.80%	0.747	1.552	52.3	0.14	0.358	0.085	128.17%	-0.022	0.234	163.47%	0.076

2	33.05%	0.741	1.566	52.59	0.134	0.375	0.087	125.25%	-0.021	0.246	154.89%	0.075
3	32.97%	0.738	1.576	55.34	0.143	0.381	0.085	126.72%	-0.021	0.25	153.54%	0.076
x	32.94%	0.742	1.565	53.41	0.139	0.371	0.086	126.71%	-0.022	0.243	157.30%	0.076
s	0.13%	0.005	0.012	1.68	0.004	0.012	0.001	1.46%	0.001	0.008	5.39%	0
%RSD	0.386	0.641	0.766	3.145	3.142	3.149	1.179	1.152	2.432	3.309	3.426	0.409
	6CS 16/12/2021 17:53:44											
1	33.81%	0.814	1.548	64.97	0.144	0.5	0.222	122.43%	-0.023	0.213	201.02%	0.072
2	32.65%	0.787	1.501	62.87	0.134	0.461	0.205	123.51%	-0.023	0.213	199.17%	0.072
3	33.43%	0.771	1.465	58.34	0.134	0.465	0.206	125.45%	-0.023	0.213	190.75%	0.073
x	33.29%	0.79	1.505	62.06	0.137	0.475	0.211	123.80%	-0.023	0.213	196.98%	0.072
s	0.59%	0.022	0.042	3.386	0.006	0.022	0.009	1.53%	0	0	5.47%	0
%RSD	1.783	2.761	2.768	5.456	4.109	4.525	4.342	1.233	1.001	0.17	2.779	0.276
	6DS 16/12/2021 17:54:50											
1	33.00%	0.724	0.538	59.56	0.107	0.439	0.187	129.48%	-0.023	0.214	136.37%	0.068
2	32.98%	0.696	0.536	55.51	0.097	0.432	0.191	129.22%	-0.022	0.214	138.39%	0.069
3	31.92%	0.69	0.514	58.78	0.104	0.439	0.191	128.84%	-0.021	0.216	133.17%	0.069
x	32.63%	0.704	0.529	57.95	0.102	0.437	0.19	129.18%	-0.022	0.215	135.97%	0.069
s	0.62%	0.018	0.013	2.151	0.005	0.004	0.002	0.32%	0.001	0.001	2.63%	0
%RSD	1.892	2.582	2.445	3.711	4.599	0.968	1.117	0.249	4.037	0.555	1.936	0.671
	6AA 16/12/2021 17:55:54											
1	39.56%	0.269	4.306	223.8	19.08	2.297	0.344	127.69%	-0.022	0.204	206.92%	0.096
2	40.58%	0.24	4.264	223.5	19.02	2.255	0.336	129.46%	-0.023	0.202	217.36%	0.096
3	38.03%	0.22	4.126	219.3	18.29	2.246	0.351	131.07%	-0.025	0.202	207.93%	0.094
x	39.39%	0.243	4.232	222.2	18.8	2.266	0.344	129.41%	-0.024	0.203	210.73%	0.096
s	1.29%	0.025	0.094	2.517	0.439	0.027	0.008	1.69%	0.002	0.001	5.76%	0.001
%RSD	3.264	10.17	2.226	1.133	2.336	1.201	2.188	1.305	6.854	0.411	2.732	1.069
	6BA 16/12/2021 17:56:58											
1	38.48%	0.082	2.379	129.1	8.801	1.115	0.219	176.42%	-0.015	0.201	332.21%	0.097
2	38.17%	0.08	2.431	134.1	8.986	1.134	0.229	169.34%	-0.015	0.2	328.33%	0.098
3	38.36%	0.071	2.46	129.7	8.741	1.118	0.223	173.67%	-0.015	0.2	336.75%	0.099
x	38.34%	0.078	2.423	131	8.843	1.122	0.224	173.14%	-0.015	0.2	332.43%	0.098
s	0.16%	0.006	0.041	2.711	0.128	0.01	0.005	3.57%	0	0	4.22%	0.001
%RSD	0.406	7.609	1.68	2.07	1.443	0.896	2.348	2.063	1.187	0.203	1.268	0.979
	6CA 16/12/2021 17:57:57											
1	37.03%	0.043	1.543	95.22	4.394	0.707	0.2	178.65%	-0.022	0.201	389.80%	0.076

2	36.41%	0.028	1.438	91.65	4.196	0.664	0.189	185.92%	-0.022	0.2	371.11%	0.074
3	37.25%	0.027	1.443	94.6	4.271	0.669	0.189	183.97%	-0.023	0.2	390.14%	0.076
x	36.90%	0.033	1.475	93.82	4.287	0.68	0.193	182.85%	-0.022	0.2	383.68%	0.075
s	0.44%	0.009	0.059	1.91	0.1	0.023	0.006	3.76%	0	0.001	10.89%	0.001
%RSD	1.183	27.27	3.989	2.035	2.331	3.411	3.335	2.057	1.222	0.344	2.839	1.348
	6DA 16/12/2021 17:59:23											
1	35.25%	0.016	2.628	86.07	3.542	1.476	0.251	132.66%	-0.024	0.203	314.52%	0.082
2	33.54%	0.009	2.574	83.3	3.487	1.506	0.26	133.00%	-0.023	0.201	312.67%	0.08
3	34.55%	0.008	2.619	82.37	3.504	1.497	0.252	130.98%	-0.023	0.202	331.36%	0.079
x	34.44%	0.011	2.607	83.91	3.511	1.493	0.254	132.21%	-0.023	0.202	319.52%	0.08
s	0.86%	0.004	0.029	1.922	0.028	0.015	0.005	1.08%	0.001	0.001	10.30%	0.001
%RSD	2.497	40.45	1.106	2.291	0.797	1.026	1.933	0.82	2.294	0.723	3.223	1.768
	6AD 16/12/2021 18:00:44											
1	42.58%	0.283	2.972	148.7	0.364	1.149	0.201	174.72%	-0.022	0.201	218.54%	0.098
2	41.75%	0.272	2.846	143.5	0.323	1.09	0.18	182.16%	-0.022	0.199	237.06%	0.1
3	43.53%	0.277	2.913	151.1	0.332	1.122	0.188	176.13%	-0.021	0.199	228.81%	0.102
x	42.62%	0.277	2.91	147.8	0.34	1.12	0.19	177.67%	-0.021	0.2	228.13%	0.1
s	0.89%	0.006	0.063	3.893	0.022	0.029	0.01	3.95%	0	0.001	9.28%	0.002
%RSD	2.092	2.022	2.176	2.634	6.487	2.632	5.5	2.223	2.122	0.556	4.068	2.054
	6BD 16/12/2021 18:01:47											
1	38.55%	0.375	3.293	187.5	0.51	1.044	0.29	119.04%	-0.009	0.2	364.54%	0.12
2	38.18%	0.347	3.185	171.9	0.466	0.997	0.288	124.55%	-0.009	0.201	348.20%	0.12
3	37.75%	0.364	3.242	180.5	0.485	1.021	0.294	122.75%	-0.01	0.199	358.14%	0.122
x	38.16%	0.362	3.24	180	0.487	1.021	0.29	122.11%	-0.009	0.2	356.96%	0.121
s	0.40%	0.014	0.054	7.834	0.022	0.024	0.003	2.81%	0.001	0.001	8.23%	0.001
%RSD	1.044	3.819	1.66	4.353	4.533	2.315	1.129	2.301	7.442	0.312	2.306	1.044
	6CD 16/12/2021 18:02:58											
1	39.43%	3.998	2.007	144.9	0.496	0.883	0.247	106.76%	-0.02	0.201	672.47%	0.129
2	38.89%	3.975	1.944	142.3	0.483	0.88	0.248	106.74%	-0.02	0.2	679.55%	0.129
3	38.25%	4.039	1.984	138.3	0.498	0.904	0.226	104.35%	-0.018	0.2	709.37%	0.129
x	38.86%	4.004	1.978	141.8	0.492	0.889	0.24	105.95%	-0.019	0.2	687.13%	0.129
s	0.59%	0.032	0.032	3.323	0.008	0.013	0.012	1.39%	0.001	0.001	19.58%	0
%RSD	1.515	0.808	1.595	2.343	1.684	1.469	5.176	1.308	7.079	0.362	2.85	0.275
	6DD 16/12/2021 18:03:58											
1	40.93%	0.347	2.578	146	0.281	1.039	0.199	136.91%	-0.007	0.2	7096.08%	0.118
2	40.83%	0.305	2.546	146.1	0.277	1.019	0.181	140.65%	-0.008	0.2	7382.59%	0.117

3	40.66%	0.29	2.521	144.1	0.271	1.022	0.191	139.50%	-0.007	0.199	7778.04%	0.118
x	40.81%	0.314	2.549	145.4	0.277	1.027	0.191	139.02%	-0.007	0.2	7418.90%	0.118
s	0.13%	0.029	0.028	1.1	0.005	0.011	0.009	1.92%	0.001	0	342.43%	0.001
%RSD	0.324	9.374	1.11	0.756	1.767	1.047	4.687	1.379	11.26	0.085	4.616	0.83

7AS 16/12/2021 18:04:59

1	30.07%	0.897	1.005	73.56	0.078	0.508	0.162	120.41%	-0.014	0.209	1666.35%	0.068
2	29.62%	0.903	0.981	70.45	0.075	0.495	0.139	120.14%	-0.015	0.212	1344.36%	0.066
3	28.43%	0.89	0.952	71.46	0.067	0.455	0.123	122.03%	-0.014	0.213	1030.59%	0.063
x	29.37%	0.897	0.979	71.82	0.073	0.486	0.141	120.86%	-0.015	0.211	1347.10%	0.066
s	0.85%	0.007	0.027	1.59	0.006	0.028	0.02	1.03%	0	0.002	317.89%	0.002
%RSD	2.883	0.766	2.758	2.214	8.038	5.752	14	0.849	3.013	0.849	23.598	3.257

7BS 16/12/2021 18:06:05

1	30.59%	1.132	3.609	102.6	0.17	0.528	0.798	109.73%	-0.019	0.218	328.50%	0.062
2	31.52%	1.127	3.644	107.5	0.179	0.534	0.818	107.01%	-0.016	0.221	331.53%	0.063
3	29.74%	1.109	3.688	110.5	0.189	0.569	0.806	106.50%	-0.016	0.225	322.10%	0.063
x	30.61%	1.123	3.647	106.9	0.179	0.544	0.807	107.75%	-0.017	0.221	327.38%	0.063
s	0.89%	0.012	0.04	3.946	0.01	0.022	0.01	1.74%	0.002	0.003	4.82%	0
%RSD	2.911	1.074	1.086	3.693	5.315	4.082	1.227	1.611	9.349	1.554	1.471	0.512

7CS 16/12/2021 18:07:16

1	31.11%	0.895	4.47	58.13	0.108	0.602	1.144	127.34%	-0.025	0.21	136.03%	0.057
2	30.74%	0.877	4.599	57.27	0.113	0.599	1.168	125.68%	-0.024	0.211	138.22%	0.057
3	30.12%	0.873	4.499	56.28	0.11	0.61	1.167	126.41%	-0.024	0.215	152.53%	0.057
x	30.66%	0.882	4.523	57.23	0.11	0.603	1.16	126.48%	-0.024	0.212	142.26%	0.057
s	0.51%	0.012	0.067	0.924	0.003	0.006	0.014	0.83%	0	0.003	8.96%	0
%RSD	1.646	1.324	1.492	1.615	2.328	0.932	1.192	0.658	2.017	1.197	6.3	0.136

7DS 16/12/2021 18:08:14

1	31.60%	0.702	3.044	41.68	0.084	1.359	0.423	121.63%	-0.025	0.21	115.32%	0.058
2	29.71%	0.713	3.18	41.37	0.095	1.445	0.416	115.99%	-0.024	0.213	123.57%	0.058
3	28.97%	0.683	3.073	41.32	0.082	1.396	0.391	120.63%	-0.023	0.214	114.31%	0.058
x	30.10%	0.7	3.099	41.46	0.087	1.4	0.41	119.42%	-0.024	0.212	117.73%	0.058
s	1.35%	0.015	0.072	0.195	0.007	0.043	0.017	3.01%	0.001	0.002	5.08%	0
%RSD	4.499	2.184	2.311	0.47	7.927	3.061	4.084	2.519	3.187	0.929	4.315	0.15

7AA 16/12/2021 18:09:16

1	27.35%	0.043	1.269	47.12	0.081	0.612	0.181	132.80%	-0.028	0.203	254.40%	0.06
2	26.98%	-0.004	1.186	45.31	0.081	0.601	0.167	135.18%	-0.027	0.204	258.44%	0.059

3	26.48%	-0.021	1.187	46.81	0.081	0.644	0.181	133.95%	-0.027	0.202	250.87%	0.059
x	26.94%	0.006	1.214	46.41	0.081	0.619	0.177	133.98%	-0.027	0.203	254.57%	0.059
s	0.44%	0.033	0.047	0.971	0	0.022	0.008	1.19%	0.001	0.001	3.79%	0
%RSD	1.616	533.1	3.904	2.092	0.504	3.61	4.593	0.886	2.26	0.451	1.489	0.495

7BA 16/12/2021 18:10:27

1	32.46%	-0.03	2.952	40.84	0.085	0.417	0.731	117.11%	-0.029	0.204	100.67%	0.057
2	29.64%	-0.037	3.048	39.04	0.088	0.423	0.737	115.54%	-0.029	0.203	99.66%	0.057
3	30.19%	-0.036	3.129	40.43	0.09	0.422	0.733	112.96%	-0.028	0.203	95.29%	0.057
x	30.76%	-0.034	3.043	40.11	0.088	0.421	0.734	115.20%	-0.029	0.203	98.54%	0.057
s	1.49%	0.004	0.089	0.944	0.003	0.004	0.003	2.09%	0	0.001	2.86%	0
%RSD	4.853	10.54	2.911	2.354	2.96	0.84	0.405	1.816	1.299	0.366	2.906	0.076

7CA 16/12/2021 18:11:26

1	34.59%	-0.037	3.376	27.23	0.001	0.2	1.117	143.96%	-0.03	0.202	101.18%	0.056
2	32.38%	-0.037	3.351	28.15	0.002	0.2	1.072	144.36%	-0.03	0.201	103.70%	0.056
3	31.96%	-0.037	3.316	25.92	0.005	0.209	1.053	146.99%	-0.03	0.202	106.73%	0.057
x	32.98%	-0.037	3.348	27.1	0.003	0.203	1.08	145.10%	-0.03	0.202	103.87%	0.056
s	1.42%	0	0.03	1.123	0.002	0.005	0.033	1.65%	0	0.001	2.78%	0
%RSD	4.292	1.099	0.901	4.142	74.11	2.581	3.053	1.134	0.602	0.267	2.678	0.224

7DA 16/12/2021 18:12:29

1	32.24%	-0.055	0.749	33.45	0.097	0.221	0.637	129.22%	-0.026	0.262	83.84%	0.056
2	31.20%	-0.059	0.71	34.21	0.093	0.211	0.648	130.65%	-0.027	0.265	86.19%	0.056
3	31.73%	-0.059	0.674	30.66	0.092	0.218	0.618	130.85%	-0.026	0.262	84.51%	0.056
x	31.72%	-0.058	0.711	32.77	0.094	0.217	0.634	130.24%	-0.026	0.263	84.85%	0.056
s	0.52%	0.002	0.037	1.87	0.003	0.005	0.016	0.89%	0	0.001	1.21%	0
%RSD	1.648	3.776	5.236	5.705	2.685	2.274	2.465	0.68	1.755	0.524	1.431	0.034

7Ad 16/12/2021 18:13:30

1	32.94%	0.131	0.505	57.57	0.242	0.925	1.327	118.04%	-0.023	0.211	406.82%	0.124
2	32.65%	0.139	0.513	61.16	0.25	0.959	1.29	116.96%	-0.023	0.212	433.26%	0.128
3	31.65%	0.136	0.506	63.42	0.252	0.947	1.277	118.22%	-0.024	0.213	446.06%	0.125
x	32.41%	0.135	0.508	60.72	0.248	0.943	1.298	117.74%	-0.023	0.212	428.71%	0.126
s	0.68%	0.004	0.004	2.954	0.005	0.017	0.026	0.68%	0	0.001	20.01%	0.002
%RSD	2.093	3.099	0.862	4.865	2.159	1.838	2.028	0.578	1.253	0.303	4.668	1.926

7BD 16/12/2021 18:14:34

1	33.14%	0.047	0.896	155.6	0.684	2.062	2.174	129.32%	-0.026	0.211	321.60%	0.113
2	32.50%	0.049	0.892	161.3	0.697	2.056	2.174	129.59%	-0.026	0.208	321.09%	0.114

3	31.35%	0.049	0.926	175.2	0.855	2.261	2.197	128.46%	-0.026	0.208	320.58%	0.113
x	32.33%	0.048	0.905	164	0.745	2.126	2.182	129.12%	-0.026	0.209	321.09%	0.113
s	0.91%	0.001	0.019	10.11	0.095	0.117	0.014	0.59%	0	0.002	0.51%	0.001
%RSD	2.811	2.448	2.06	6.161	12.73	5.495	0.623	0.457	1.275	0.929	0.157	0.503
	7CD 16/12/2021 18:15:32											
1	35.83%	0.113	7.547	197.6	0.503	8.865	2.505	113.55%	0.023	0.208	237.90%	0.169
2	34.72%	0.105	7.457	191.9	0.485	8.754	2.57	112.18%	0.023	0.206	231.16%	0.159
3	36.98%	0.095	7.535	191.2	0.504	8.793	2.515	113.58%	0.023	0.208	229.31%	0.16
x	35.84%	0.104	7.513	193.6	0.497	8.804	2.53	113.10%	0.023	0.207	232.79%	0.163
s	1.13%	0.009	0.048	3.539	0.011	0.057	0.035	0.80%	0	0.001	4.52%	0.005
%RSD	3.149	8.936	0.645	1.828	2.159	0.644	1.387	0.708	1.496	0.39	1.941	3.299
	7DD 16/12/2021 18:16:39											
1	37.43%	0.061	2.318	72.97	0.118	7.366	2.297	167.00%	-0.024	0.205	543.59%	0.116
2	35.82%	0.064	2.348	75.33	0.119	7.486	2.252	161.87%	-0.023	0.204	530.79%	0.115
3	34.46%	0.065	2.355	74.55	0.129	7.56	2.212	161.63%	-0.024	0.207	546.46%	0.116
x	35.90%	0.063	2.34	74.28	0.122	7.471	2.254	163.50%	-0.023	0.205	540.28%	0.115
s	1.49%	0.002	0.019	1.202	0.006	0.098	0.043	3.03%	0.001	0.001	8.34%	0.001
%RSD	4.141	3.572	0.826	1.618	5.221	1.308	1.907	1.855	2.298	0.619	1.544	0.564
	8AS 16/12/2021 18:17:48											
1	34.38%	0.89	12.45	208.8	0.26	0.988	0.445	112.23%	0.031	0.207	300.71%	0.064
2	32.89%	0.946	13.05	208.7	0.278	0.924	0.423	108.86%	0.029	0.207	274.44%	0.064
3	34.05%	0.952	12.88	212.7	0.281	0.824	0.358	108.09%	0.029	0.206	275.28%	0.063
x	33.77%	0.929	12.8	210	0.273	0.912	0.409	109.73%	0.029	0.207	283.48%	0.064
s	0.78%	0.034	0.31	2.268	0.011	0.083	0.045	2.20%	0.001	0.001	14.93%	0.001
%RSD	2.307	3.688	2.419	1.08	4.215	9.08	11.02	2.009	3.494	0.422	5.267	1.219
	8BS 16/12/2021 18:18:49											
1	33.14%	0.863	10.86	180.2	0.253	0.425	0.108	111.06%	-0.011	0.206	201.53%	0.059
2	33.17%	0.868	11.03	183.9	0.261	0.427	0.113	109.46%	-0.013	0.206	209.11%	0.06
3	32.65%	0.873	11.01	178.3	0.259	0.422	0.118	108.07%	-0.01	0.205	217.69%	0.059
x	32.99%	0.868	10.97	180.8	0.258	0.425	0.113	109.53%	-0.012	0.206	209.44%	0.059
s	0.30%	0.005	0.09	2.852	0.004	0.002	0.005	1.50%	0.001	0	8.09%	0
%RSD	0.895	0.579	0.82	1.577	1.635	0.503	4.542	1.367	11.63	0.123	3.862	0.318
	8CS 16/12/2021 18:19:50											
1	36.16%	0.873	12.18	192.9	0.288	0.673	0.069	130.39%	-0.018	0.202	194.12%	0.06
2	34.02%	0.884	12.53	205.2	0.301	0.702	0.087	124.92%	-0.018	0.203	179.98%	0.06
3	34.74%	0.851	12.17	205.7	0.289	0.681	0.084	130.61%	-0.016	0.203	178.97%	0.06
x	34.97%	0.87	12.29	201.3	0.293	0.686	0.08	128.64%	-0.017	0.203	184.35%	0.06
s	1.09%	0.017	0.202	7.222	0.007	0.015	0.01	3.23%	0.001	0.001	8.47%	0

%RSD	3.113	1.949	1.641	3.589	2.486	2.14	11.9	2.508	7.33	0.261	4.596	0.679
	8DS 16/12/2021 18:20:52											
1	34.30%	0.815	9.221	163.7	0.251	0.176	0.046	122.71%	-0.024	0.202	114.98%	0.058
2	34.32%	0.794	10.27	162.4	0.246	0.168	0.047	122.00%	-0.023	0.2	114.48%	0.058
3	32.51%	0.799	9.056	164.8	0.245	0.176	0.044	122.07%	-0.024	0.203	107.24%	0.058
x	33.71%	0.802	9.515	163.6	0.247	0.173	0.046	122.26%	-0.024	0.202	112.23%	0.058
s	1.04%	0.011	0.657	1.176	0.003	0.005	0.001	0.39%	0	0.001	4.33%	0
%RSD	3.072	1.382	6.91	0.719	1.119	2.775	2.634	0.32	1.037	0.611	3.861	0.388
	8AA 16/12/2021 18:21:53											
1	27.50%	0.024	12.7	160	0.212	0.892	0.016	129.90%	-0.03	0.204	259.29%	0.058
2	27.91%	-0.017	12.63	167	0.205	0.939	0.016	129.10%	-0.029	0.205	263.50%	0.058
3	27.50%	-0.038	12.6	157.2	0.208	0.957	0.015	129.08%	-0.028	0.204	266.02%	0.058
x	27.64%	-0.01	12.64	161.4	0.209	0.929	0.016	129.36%	-0.029	0.204	262.93%	0.058
s	0.23%	0.032	0.048	5.049	0.004	0.034	0.001	0.47%	0.001	0.001	3.40%	0
%RSD	0.844	304	0.381	3.128	1.703	3.627	3.144	0.363	2.021	0.286	1.294	0.14
	8BA 16/12/2021 18:22:57											
1	28.27%	-0.058	14.04	198.4	0.346	0.856	0.033	115.90%	-0.025	0.201	364.71%	0.058
2	28.24%	-0.063	13.93	187	0.343	0.843	0.025	117.40%	-0.025	0.2	353.59%	0.058
3	28.32%	-0.065	13.8	185.8	0.342	0.801	0.029	119.24%	-0.026	0.2	382.90%	0.058
x	28.28%	-0.062	13.92	190.4	0.344	0.833	0.029	117.51%	-0.025	0.2	367.07%	0.058
s	0.04%	0.004	0.118	6.979	0.002	0.029	0.004	1.67%	0.001	0	14.79%	0
%RSD	0.148	6.477	0.848	3.666	0.612	3.428	14.68	1.424	2.61	0.201	4.03	0.397
	8CA 16/12/2021 18:23:57											
1	27.57%	-0.075	16.31	230.6	0.36	0.703	0.032	107.63%	-0.025	0.23	293.13%	0.058
2	27.45%	-0.076	16.51	239.1	0.368	0.706	0.028	105.81%	-0.025	0.231	299.87%	0.058
3	26.91%	-0.078	16.79	235.4	0.355	0.717	0.027	105.12%	-0.024	0.236	307.79%	0.058
x	27.31%	-0.076	16.54	235	0.361	0.709	0.029	106.19%	-0.025	0.232	300.26%	0.058
s	0.36%	0.002	0.242	4.267	0.006	0.007	0.003	1.30%	0	0.003	7.33%	0
%RSD	1.299	2.194	1.461	1.816	1.727	1.013	9.312	1.225	1.775	1.4	2.442	0.136
	8Da 16/12/2021 18:25:22											
1	25.87%	-0.085	11.29	181.9	0.28	0.499	0.018	135.36%	-0.029	0.202	265.52%	0.059
2	25.99%	-0.085	11.15	178.8	0.267	0.479	0.023	135.72%	-0.027	0.201	263.66%	0.059
3	27.17%	-0.087	10.8	172.5	0.262	0.469	0.025	143.12%	-0.029	0.201	256.42%	0.058
x	26.35%	-0.086	11.08	177.8	0.27	0.482	0.022	138.07%	-0.028	0.201	261.87%	0.059
s	0.72%	0.001	0.25	4.774	0.009	0.015	0.003	4.38%	0.001	0.001	4.81%	0
%RSD	2.716	1.615	2.256	2.686	3.456	3.142	15.9	3.171	3.367	0.483	1.835	0.263

	8AD 16/12/2021 18:26:25											
1	153.24%	1.924	14.17	613.1	1.224	3.757	0.984	136.23%	0.009	0.207	1339.30%	0.224
2	150.84%	2.07	15.09	655.5	1.304	3.907	1.037	129.96%	0.012	0.206	1350.93%	0.238
3	147.58%	1.977	14.47	629.3	1.239	3.83	1.015	132.69%	0.017	0.206	1257.01%	0.233
x	150.55%	1.99	14.58	632.6	1.256	3.831	1.012	132.96%	0.013	0.206	1315.75%	0.231
s	2.84%	0.074	0.472	21.41	0.042	0.075	0.026	3.15%	0.004	0.001	51.20%	0.007
%RSD	1.889	3.715	3.24	3.384	3.37	1.949	2.608	2.368	31.38	0.508	3.891	3.156
	8BD 16/12/2021 18:27:26											
1	66.31%	1.305	124.9	879.7	4.334	6.232	0.85	118.20%	0.061	0.215	1922.32%	0.204
2	66.75%	1.327	130.2	924.2	4.57	6.492	0.864	117.00%	0.072	0.216	2012.10%	0.208
3	65.80%	1.278	127.2	883.3	4.452	6.299	0.86	121.23%	0.071	0.214	1966.70%	0.206
x	66.28%	1.303	127.4	895.7	4.452	6.341	0.858	118.81%	0.068	0.215	1967.04%	0.206
s	0.48%	0.024	2.647	24.73	0.118	0.135	0.007	2.18%	0.006	0.001	44.89%	0.002
%RSD	0.718	1.875	2.078	2.761	2.65	2.128	0.852	1.836	8.798	0.627	2.282	0.896
	8CD 16/12/2021 18:28:28											
1	145.27%	2.507	13.94	670.6	1.662	3.045	0.922	127.45%	0.001	0.21	1056.21%	0.229
2	145.96%	2.479	12.43	673.6	1.606	2.999	0.891	129.96%	0	0.212	1152.47%	0.23
3	145.20%	2.406	11.9	643	1.549	2.938	0.887	130.87%	-0.003	0.21	1131.91%	0.223
x	145.47%	2.464	12.76	662.4	1.606	2.994	0.9	129.43%	-0.001	0.21	1113.53%	0.227
s	0.42%	0.052	1.057	16.86	0.056	0.054	0.019	1.77%	0.002	0.001	50.69%	0.004
%RSD	0.289	2.123	8.285	2.546	3.513	1.802	2.106	1.365	331.2	0.46	4.552	1.714
	8dd 16/12/2021 18:29:30											
1	65.80%	2.233	4.807	526.5	1.314	2.144	0.817	121.87%	-0.022	0.203	228.64%	0.206
2	65.05%	2.207	4.544	510.1	1.257	2.053	0.786	124.53%	-0.021	0.202	239.42%	0.204
3	62.87%	2.164	4.302	496.9	1.228	2.002	0.78	128.53%	-0.021	0.202	197.99%	0.194
x	64.57%	2.201	4.551	511.2	1.266	2.066	0.794	124.98%	-0.021	0.202	222.02%	0.201
s	1.52%	0.035	0.253	14.84	0.044	0.072	0.02	3.35%	0.001	0.001	21.49%	0.006
%RSD	2.352	1.58	5.559	2.903	3.484	3.491	2.457	2.683	2.474	0.28	9.68	3.086
	sTANDARD 16/12/2021 18:30:40											
1	20.72%	4.944	9.96	27.66	9.634	9.651	5.028	123.64%	4.658	3.646	68.35%	4.853
2	22.39%	5	10.02	27.01	9.661	9.889	4.981	125.26%	4.672	3.378	69.70%	4.954
3	20.99%	4.946	9.855	21.04	9.484	9.566	4.826	128.35%	4.632	3.466	57.91%	4.885
x	21.37%	4.963	9.944	25.24	9.593	9.702	4.945	125.75%	4.654	3.497	65.32%	4.897
s	0.90%	0.032	0.082	3.651	0.096	0.168	0.106	2.39%	0.02	0.137	6.45%	0.052
%RSD	4.204	0.639	0.824	14.47	0.998	1.729	2.146	1.902	0.437	3.907	9.875	1.052
	WASH 16/12/2021 18:31:54											
1	18.99%	2.133	4.981	252.9	3.985	5.108	3.148	3.43%	2.385	4.036	9.43%	1.477
2	18.61%	0.884	1.799	331.2	1.201	3.794	2.665	3.03%	1.033	5.372	15.32%	0.676
3	18.08%	0.832	1.583	255.3	0.884	3.662	2.51	2.61%	0.994	5.148	15.15%	0.596

x	18.56%	1.283	2.787	279.8	2.023	4.188	2.774	3.02%	1.47	4.852	13.30%	0.916
s	0.45%	0.737	1.903	44.51	1.706	0.799	0.333	0.41%	0.792	0.715	3.35%	0.488
%RSD	2.442	57.45	68.26	15.91	84.34	19.08	12.01	13.583	53.87	14.74	25.222	53.22

Batch 3 Sample Mass

Sample	Empty (g)	Bag	sample + bag	sample + Container bag + Water	Sample Mass	Water Content	Dry Weight	Sample Water (g)	Post contact weight	mass change %
1										
1A	14.66	0.37	1.69	59.4486	1.318	1	1.318	43.0986	2.0028	1.519575114
1B	14.59	0.35	1.6	58.5306	1.25	1	1.25	42.3406	1.8866	1.50928
1C	14.71	0.38	1.21	55.9846	0.835	1	0.835	40.0646	1.4015	1.678443114
1D	14.61	0.37	1.55	58.9436	1.178	1	1.178	42.7836	1.9121	1.623174873
1E	14.56	0.35	1.71	57.5295	1.358	1	1.358	41.2595		
2								0		1.582618275
2A	14.62	0.39	1.44	56.8975	1.052	1	1.052	40.8375		0
2B	14.66	0.38	1.42	56.2265	1.043	1	1.043	40.1465		0
2C	14.51	0.37	1.63	56.3907	1.257	1	1.257	40.2507		0
2D	14.59	0.37	1.175	57.5003	0.802	1	0.802	41.7353		0
2E	14.5	0.38	1.435	56.069	1.06	1	1.06	40.134		
3								0		0
3A	14.71		2.66	57.349	2.66	1	2.66	39.979	2.9245	1.09943609
3B	14.54		2.66	57.4818	2.66	1	2.66	40.2818	2.8142	1.057969925
3C	14.7		2.62	57.5681	2.62	1	2.62	40.2481	2.7958	1.067099237
3D	14.59		2.69	57.7797	2.69	1	2.69	40.4997	2.847	1.058364312
3E	14.7		2.72	57.8153	2.72	1	2.72	40.3953		
4								0		1.070717391
4A	14.67	0.39	0.87	55.7286	0.48	1	0.48	40.1886	1.0506	2.18875
4B	14.65	0.38	1.89	56.6458	1.51	1	1.51	40.1058	2.0855	1.381125828
4C	14.67	0.37	1.53	56.5452	1.16	1	1.16	40.3452	1.7263	1.488189655
4D	14.66	0.37	1.08	55.8268	0.71	1	0.71	40.0868	1.2086	1.702253521
4E	14.56	0.4	1.23	56.6567	0.83	1	0.83	40.8667		
5								0		1.690079751
5A	14.63	0.38	2.57	57.7242	2.19	1	2.19	40.5242	2.6855	1.226255708
5B	14.43	0.37	1.41	56.1832	1.04	1	1.04	40.3432	1.5282	1.469423077
5C	14.52	0.38	1.74	56.5485	1.36	1	1.36	40.2885	1.8269	1.343308824
5D	14.69	0.38	3.35	54.2192	2.97	1	2.97	36.1792	3.4474	1.160740741
5E	14.59	0.38	2.1	57.2956	1.72	1	1.72	40.6056		
6								0		1.299932087
6A	14.55	0.38	3.16	58.042	2.78	1	2.78	40.332	1.171	0.421223022
6B	14.91	0.37	2.5	58.5105	2.13	1	2.13	41.1005	1.0193	0.478544601
6C	14.61	0.38	2	56.8501	1.62	1	1.62	40.2401	0.858	0.52962963
6D	14.7	0.39	2.25	57.9627	1.86	1	1.86	41.0127	0.9989	0.537043011
6E	14.6	0.38	2.65	59.6146	2.27	1	2.27	42.3646		
7								0		0.491610066
7A	14.9	0.38	0.6525	56.0059	0.2745	1	0.2745	40.4534	0.6193	2.256102004
7B	14.66	0.38	1.145	56.7913	0.765	1	0.765	40.9863	1.0987	1.43620915
7C	14.68	0.38	1.498	56.6945	1.119	1	1.119	40.5165	1.3712	1.225379803
7D	14.65	0.38	1.258	56.3628	0.88	1	0.88	40.4548	1.1107	1.262159091
7E	14.61	0.38	1.158	56.3955	0.779	1	0.779	40.6275		
8								0		1.544962512
8A	14.56		1.128	55.7164	1.128	1	1.128	40.0284	1.3723	1.216578014
8B	14.44		1.05	55.4994	1.05	1	1.05	40.0094	1.2781	1.217238095
8C	14.44		1.197	55.7817	1.197	1	1.197	40.1447	1.2559	1.049206349
8D	14.44		1.086	56.0046	1.086	1	1.086	40.4786	1.1342	1.044383057
8E	14.67		1.173	55.6223	1.173	1	1.173	39.7793		
										1.131851379

6.0 References

Aguiar, J., Estevinho, B. & Santos, L., 2016. Microencapsulation of Natural Antioxidants for Food Application – The Specific Case of Coffee Antioxidants – A Review. *Trends in Food Science & Technology,* Volume 58, pp. 21-39.

Ahmad, M. et al., 2012. Effects of pyrolysis temperature on soybean stover- and peanut shell-derived biochar properties and TCE adsorption in water. *Bioresource Technology,* Volume 118, pp. 536-544.

Aihara, T. et al., 1992. Rate of adsorption of uranium from seawater with a calix(6)arene adsorbent. *Sep. Sci. Technol.,* Volume 27, p. 1655–1667.

Akyol, H. et al., 2016. Phenolic Compounds in the Potato and Its Byproducts: An Overview. *Int. J. Mol. Sci.,* Volume 17, p. 835.

Aly, Z. & Luca, V., 2013. Uranium extraction from aqueous solution using dried. *J Radioanal Nucl Chem,* Volume 295, p. 889–900.

Ao, J. et al., 2019. Trace Zinc-Preload for Enhancement of Uranium Adsorption Performance and Antifouling Property of AO-Functionalized UHMWPE Fiber. *Ind. Eng. Chem. Res.,* Volume 58, p. 8026−8034.

Araújo, L. C. A. d. & Oliveira, M. B. M. d., 2020. Effect of Heavy Metals on the Biofilm Formed by Microorganisms from Impacted Aquatic Environments. In: S. Dincer, M. S. Özdenefe & A. Arkut, eds. *Bacterial Biofilms.* s.l.:s.n.

Assinder, D. J., 1999. A review of the occurrence and behaviour of neptunium in the Irish Sea. *J. Environm. Radioactivity,* Volume 44, pp. 335-347.

Atomic Energy Agency (IAEA), 2009. *Establishment of Uranium Mining and Processing Operations in the Context of Sustainable Development,* s.l.: International Atomic Energy Agency (IAEA).

Bampaiti, A. et al., 2016. Investigation of uranium biosorption from aqueous solutions by Dictyopteris polypodioides brown algae. *Radioanal. Nucl. Chem.,* Volume 307, p. 1335–1343.

Beazley, M. et al., 2007. Uranium biomineralization as a result of bacterial phosphatase activity: insights from bacterial isolates from a contaminated subsurface.. *Environ. Sci. Technol.,* Volume 41, pp. 5701-5707.

Bhatti, H. & Hamid, S., 2014. Removal of uranium(VI) from aqueous solutions using Eucalyptus citriodora distillation sludge. *nt J Environ Sci Technol,* Volume qq, p. 813–22.

Birol, F., 2019. *Nuclear Power in a clean energy system,* May: IEA.

BLOXHAM, M. J., 1994. THE DETERMINATION OF TRACE METALS IN SEA WATER USING ICP-MS. *04 University of Plymouth Research Theses*.

Bogolitsyn, K. et al., 2023. Sorption of uranium and thorium by cellulose complexes of Arctic brown algae. *Journal of Applied Phycology,* pp. 1813-1819.

Boudet, A., 2000. Lignins and lignification: Selected issues. *Plant Physiology and Biochem.,* Volume 38, pp. 81-96.

Carbonaro, R., Atalay, Y. & Toro, D. D., 2011. Linear free energy relationships for metal-ligand complexation: bidentate binding to negatively-charged oxygen donor atoms. *Geochim Cosmochim. Acta,* Volume 75, pp. 2499-2511.

Carboni, M., Abney, C. W., Liu, S. & Lin, W., 2013. Highly porous and stable metal–organic frameworks for uranium extraction. *Chemical Science,* Issue 6.

Carvalho, F. P., 2017. Mining industry and sustainable development: time for change. *Food and Energy Security,* 6(2), pp. 61-77.

Chekki, R., Snoussi, A., Hamrouni, I. & N, N. B., 2014. Chemical composition, antibacterial and antioxidant activities of Tunisian garlic (Allium sativum) essential oil and ethanol extract. *Mediterranean J. Chem.,* Volume 3, pp. 947-956.

Cheng, Y. et al., 2019. Polyamine and amidoxime groups modified bifunctional polyacrylonitrile-based ion exchange fibers for highly efficient extraction of U(VI) from real uranium mine water. *Chemical Engineering Journal,* Issue 367, pp. 198-207.

Cieslik, E., Greda, A. & Adamus, W., 2006. Contents of polyphenols in fruit and vegetables. *Food Chem.,* Volume 94, pp. 135-142.

Cipolletta, G. et al., 2021. Brine treatment technologies towards minimum/zero liquid discharge and resource recovery: State of the art and techno-economic assessment. *Journal of Environmental Management,* Volume 300, p. 113681.

Crozier, A., Ashihara, H. & Tomas-Barberan, F. A., 2011. *Teas, Cocoa and Coffee Plant Secondary Metabolites and Health..* Chichester, West Sussex ; Hoboken, NJ: Wiley-Blackwell.

Das, A. K. et al., 2020. Review on tannins: Extraction processes, applications and possibilities. *South African Journal of Botany,* Volume 135, pp. 57-70.

Das, S. et al., 2008. Chemical aspects of uranium recovery from seawater by amidoximated electron-beam-grafted polypropylene membranes. *Desalination,* Issue 232, pp. 243-253.

Degueldre, C. A., Dawson, R. J. & Najdanovic-Visaka, V., 2019. Nuclear fuel cycle, with a liquid ore and fuel: toward renewable energy. *Sustainable Energy & Fuels.*

Degueldre, C., Bilewicz, A., Hummel, W. & LLoizeau, J., 2001. Sorption behaviour of Am on marl groundwater colloids. *Journal of Environmental Radioactivity,* 55(3), pp. 241-255.

Degueldre, C. & McGowan, S., 2020. Simulating uranium sorption onto inorganic model substrates: effect of redox potential.. *J. Environmental Radioactivity,* Volume 225, p. 11.

Degueldre, C. et al., 1996. Colloid properties in granitic groundwater systems. I: Sampling and characterisation. *Appl. Geochem.,,* Volume 11, pp. 677-695.

Degueldre, C., Ulrich, H. J. & Silby, H., 1994. Sorption of241 Am onto Montmorillonite, Illite and Hematite Colloids. *Radiochimica Acta,* Volume 65, pp. 173-179.

Diallo, M. S., Kotte, M. R. & Cho, M., 2015. Mining Critical Metals and Elements from Seawater: Opportunities and Challenges. *Environ. Sci. Technol.,* 49(16), p. 9390–9399.

Djogic, R. & Branica, M., 1993. Uranyl mixed-ligand complex formation in. *Chemical Speciation & Bioavailability,* 5(3), pp. 101-105.

Djogic, R., Sipos, L. & Branica, M., 1986. Characterization of uranium(VI) in seawater. *Limnol. Oceanography,* Volume 31, pp. 1122-1131.

Dotto, G. et al., 2013. reatment of chitin effluents by coagulation–flocculation with chitin and aluminum sulfate. *J Environ Chem Eng,* 1(1-2), p. 50–55.

Drysdale, J. A. & Buesseler, K. O., 2020. Uranium adsorption behaviour of amidoximated fibers under coastal ocean conditions. *Progress in Nuclear Energy,* Volume 119, p. 103170.

Eksi, G., Kurbanoglu, S. & Ozkan, S., 2019. Chapt. 12.2.2 Organo-Sulfur Compounds, in Engineering Tools in the Beverage Industry. In: *Fortification of Functional and Medicinal Beverages With Botanical Products and Their Analysis.* s.l.:s.n.

El-aal, H. A. & Halaweish, F., 2010. Food preservative activity of phenolic compounds in orange peel extracts (Citrus Sinensis L.). *Lucrări Ştiinţifice,* Volume 53, pp. 457-464.

El-Sheikh, E., 2016. Application of waste frying oil as an extractant for uranium from sulfate leach liquor. *J. Radiation Res. Appl. Sci.,* Issue 9, pp. 155-163.

Ewing, R. C., 2004. Environmental impact of the nuclear fuel cycle. *Geological Society, London, Special Publications,,* Volume 236, pp. 7-23.

Ganguly, P., Sengupta, S., Das, P. & Bhowal, A., 2020. Valorization of food waste: Extraction of cellulose, lignin and their application in energy use and water treatment. *Fuel,* Volume 280, p. 118581.

Gardner., D., 1973. *Marine Pollution: Diagnosis and therapy.* s.l.:Springer.

Gil, M., Tomás-Barberán, F., Hess-Pierce, B. & Kader, A., 2002. Antioxidant Capacities, Phenolic Compounds, Carotenoids, and Vitamin C Contents of Nectarine, Peach, and Plum Cultivars from California. *J. Agric. Food Chem.,* Volume 50, p. 4976−4982.

Goldberg, E. D. et al., 1989. Some comparative marine chemistries of platinum and iridium.. *Appl. Geochem.,* Volume 1, pp. 227-232.

Gondhalekar, S. & Shukla, S., 2014. Equilibrium and kinetics study of uranium(VI) from aqueous solution by Citrus limetta peels. *J Radioanal Nucl Chem,* Issue 302, pp. 451-7.

Gregorič, A., Kotnik, J., Horvat, M. & Pirrone, N., 2008. Dissolved radon and gaseous mercury in the Mediterranean seawater. *J. Environm. Radioactivity,* Volume 99, pp. 1068-1074.

Grenthe, I. et al., 2006. Uranium, in:. In: *The chemistry of the actinide and transactinide elements.* s.l.:Springer.

Groenenberg, J. E. et al., 2012. Evaluation of the performance and limitations of empirical partition-relations and process based multisurface models to predict trace element solubility in soils. *Environmental Pollution,* Volume 166, pp. 98-107.

Jones, K., 1991. *A comparison of the distribution of heterotrophic nitrogen fixing bacteria in coastal waters of Morecambe Bay, UK, the Ligurian Sea, France, the Bay of Naples, Italy and the Pacific Ocean, Hawaii, USA; in Estuaries and Coasts: Spatial and Temporal interc.* Ducrotoy, ESCA19, Symposium, Olsen & Olsen.

Jones, R. E. & Templeton, D. H., 1958. The crystal structure of acetic acid. *Acta Cryst,* Volume 11, pp. 484-487.

Ju, P. et al., 2019. Hyperbranched topological swollen-layer constructs of multi-active sites polyacrylonitrile (PAN) adsorbent for uranium(VI) extraction from seawater.. *Chemical Engineering Journal,* Volume 374, pp. 1204-1213.

Kim, S., Lee, Y., Park, M. & Hoon Young Jeong, 2024. Immobilization of hexavalent uranium U(VI) by hydroxyapatite under oxic conditions. *Journal of Nuclear Materials,* Volume 595, p. 155059.

Krestou, A. & Panias, D., 2004. Uranium (VI) speciation diagrams in the UO2(2+)/CO3(2-)/H2O system at 25 deg C.. *European Journal of Mineral Processing and Environmental Protection,,* 4(2), p. 113–129..

Laane, R. et al., 1996. Changes and causes of variability in salinity and dissolved inorganic phosphate in the Irish Sea, English Channel, and Dutch coastal zone.. *ICES J. Marine Sci.,* Volume 53, p. 933–944.

Lambert, F., Danten, Y., Gatti, C. & Frayret, C., 2020. A tool for deciphering the redox potential ranking of organic compounds: a case study of biomass-extracted quinones for sustainable energy. *Phys. Chem. Chem. Phys,* Volume 22, pp. 20212-20226.

Langmuir, D., 1978. Uranium solution–mineral equilibria at low temperatures with applications to sedimentary ore. *Geochim Cosmochim Acta,* Volume 42, pp. 547-569.

Lanzmann-Petithory, D., 2002. *La diététique de la longévité.* Paris: Ed. Odile Jacob.

Lashley, M. A. ,. M. N. et al., 2016. Amidoximes as ligand functionalities for braided polymeric materials for the recovery of uranium from seawater. *Polyhedron,* Volume 109, pp. 81-91.

Linde, M., Öborn, I. & Gustafsson, J. P., 2007. Effects of Changed Soil Conditions on the Mobility of Trace Metals in Moderately Contaminated Urban Soils. *Water, Air and Soil Pollution,* 183(1-4), pp. 69-83.

Li, Y. H., 1981. Ultimate removal mechanisms of elements from the ocean. *Geochim. Cosmochim. Acta,* Volume 45, pp. 1659-1664.

Loganathan, P., Naidu, G. & Vigneswaran, S., 2017. Mining valuable minerals from seawater: a critical review. *Environ. Sci.: Water Res. Technol.,* Volume 3, pp. 37-53.

Loiseau, T., Mihalcea, I., Henry, N. & Volkringer, C., 2014. The crystal chemistry of uranium carboxylates. *Coordination Chemistry Reviews,* Volume 266–267, pp. 69-109.

Lucks, C. et al., 2012. Aqueous uranium(VI) complexes with acetic and succinic acid: Speciation and Structure Revisited. *Inorganic Chemistry,,* Volume 51, pp. 12288-12300.

Matharu, A. S., Melo, E. M. d. & Houghton, J. A., 2016. Opportunity for high value-added chemicals from food supply chain wastes. *Bioresource Technology,* Volume 215, pp. 123-130.

McGowan, S., Zhang, H. & Degueldre, C., 2022. Testing sorption of uranium from seawater on waste biomass: A feasibility study. *Fuel,* Volume 315, p. 123224.

McKee, B. & Todd., J., 1993. Uranium behavior in a permanently anoxic Fjord: Microbial control?. *Limnology and Oceanography,* Volume 38, pp. 408-414.

Millero, F., 2013. *Chemical oceanography.* s.l.:CRC press.

MOHAGHEGHI, A., 1985. The role of aqueous sulfide- andsulfate-reducing bacteria in the kinetics and mecha-nisms of the reduction of uranyl ion.. *Ph.D. thesis,Colorado School of Mines,* Volume T-3029.

MOHAGHEGHI, A., UPDEGRAFF, D. M. & GOLDHABER, M. B., 1985. The role of sulfate-reducing bacteria in the deposition of sedimentary uranium ores. *Geomicrobiol. J,* Volume 4, pp. 153-173.

Monforte, M. T. et al., 2018. Evaluation of antioxidant, antiinflammatory, and gastroprotective properties of Rubus fruticosus L. fruit juice. *Phytotherapy Research,* 32(7), pp. 1404-414.

Möser, C., Kautenburger, R. & Beck, H. P., 2012. Complexation of europium and uranium by humic acids analyzed by capillary electrophoresis-inductively coupled plasma mass spectrometry. *ELECTROPHORESIS,* may, 33(9-10), pp. 1482-1487.

Nakajima, A., Horikoshi, T. & Sakaguchi, T., 1982. Recovery of uranium by immobilized microorganisms. *Eur. J. Appl. Microbiol. Biotechnol.,* Volume 16, pp. 88-91.

Nakajima, A. & Sakaguchi, T., 1989. Adsorption of Uranium by Vegetable Crude Drugs.. *Agricultural and Biological Chem.,* Volume 53, p. 2853–9.

Nalladiyil, A., Prakash, P. & Babu, G. S., 2023. Garbage enzyme-mediated treatment of landfill leachate: A sustainable approach. *Bioresource Technology,* Volume 385, p. 129361.

National Minerals Information Center, U., 2023. *Mineral commodity summaries 2023,* Washington: USGS.

NEA and IAEA, 2016. Uranium 2016 – resource, production and demand. *OECD publishing,* p. 548.

NEA, 2004. *Chemical thermodynamics of uranium, Data bank Radioactive waste management,* s.l.: OECD/NEA.

Nile, S. H., Kim, S. H., Ko, E. Y. & Park, S. W., 2013. Polyphenolic Contents and Antioxidant Properties of Different Grape (V. vinifera, V. labrusca, and V. hybrid) Cultivars. *BioMed. Research International,* pp. 1-5.

Park, J. et al., 2016. Effect of Biofouling on the Performance of Amidoxime-Based Polymeric Uranium Adsorbents. *Industrial & Engineering Chemistry Research,* 55(15), pp. 4328-4338.

Parsons, J. G., Tiemann, K. J., Peralta-Videa, J. R. & Gardea-Torresdey, J. L., 2006. Sorption of Uranyl Cations onto Inactivated Cells of Alfalfa Biomass Investigated Using Chemical Modification, ICP-OES, and XAS. *Environ. Sci. Technol.,* 40(13), pp. 4181-4188.

Pastrana-Bonilla, C. C. A., Sellappan, S. & Krewer, G., 2003. Phenolic Content and Antioxidant Capacity of Muscadine Grapes. *J. Agric. Food Chem.,* Volume 51, pp. 5497-5503.

Pathak, P. D., Mandavgane1, S. A. & Kulkarni, B. D., 2017. Fruit peel waste: characterization and its potential uses. *CURRENT SCIENCE,* 113(3), pp. 444-454.

Pathak, P., Mandavgane, S. & K. B., 2015. Fruit peel waste as a novel low-cost bio adsorbent. *Rev Chem Eng,* Volume ;31:, p. 361–81.

Perea-Moreno, M.-A., Manzano-Agugliaro, F., Hernandez-Escobedo, Q. & Perea-Moreno, A.-J., 2018. Peanut Shell for Energy: Properties and Its Potential to Respect the Environment. *Sustainability,* 10(9), p. 3254.

Pigford, T. H., 1976. Environmental aspects of nuclear energy production. *Annual Rev. Energy,* Volume 1, pp. 515-559.

Qiu, J. et al., 2012. Screening natural antioxidants in peanut shell using DPPH–HPLC–DAD–TOF/MS methods.. *Food Chemistry,* Volume 135, pp. 2366-2371.

Ramamoorthy, S., Raghavan, A. & Santappa, M., 1969. Complexes of uranyl ion with butyric. *Inorg Nucl Chem,* Issue 31, p. 1765–9.

Rérolle, V. et al., 2012. Seawater-pH measurements for ocean-acidification observations, TrAC. *TrAC Trends in Analytical Chemistry,* Volume 40, pp. 146-157.

Ritchie, J. D. & Perdue, E. M., 2003. Proton-binding study of standard and reference fulvic acids, humic acids, and natural. *Geochimica et Cosmochimica Acta,* 67(1).

Rosales-Martínez, P. et al., 2014. Comparison Between Antioxidant Activities of Phenolic Extracts from Mexican Peanuts, Peanuts Skins, Nuts and Pistachios. *J. Mex. Chem. Soc.,* 58(2), pp. 185-193.

Safdar, M. et al., 2017. Extraction and quantification of polyphenols from kinnow (Citrus reticulate L.) peel using ultrasound and maceration techniques. *J. Food Drug Anal.,* Volume 25, pp. 488-500.

Sakaguchi, T., Horikoshi, T. & Nakajima, A., 1981. Adsorption of Uranium by Chitin Phosphate. *Agricultural and Biological Chem. ,* Issue 10, p. 2191–5.

Sakaguchi, T., Nakajima, A. & Horikoshi, T., 1979. Adsorption of uranium from sea water by biological substances. Studies on the accumulation of heavy metal elements in biological systems. *Nippon Nogei kagaku Kaisi,* Issue 53, pp. 149-156.

Satari, B. & Karimi, K., 2018. Citrus processing wastes: Environmental impacts, recent advances, and future perspectives in total valorization. *Resour Conserv Recycl,* Issue 129, p. 153–67.

Schenk, H. J., Astheimer, L., Witte, E. G. & Schwochau, K., 1982. Development of Sorbers for the Recovery of Uranium from Seawater. 1. Assessment of Key Parameters and Screening Studies of Sorber Materials. *Separation Science and Technology,* 17(11), pp. 1293-1308.

Schneider, E. & Sachde, D., 2012. The Cost of Recovering Uranium from Seawater by a Braided Polymer Adsorbent System. *Sci. Global Security,* Volume 21, pp. 134-163.

Sekiguchi, K., Saito, K., Konishi, S. & Furusaki, S., 1994. Effect of Seawater Temperature on Uranium Recovery from Seawater. *Ind. Eng. Chem. Res.,* Volume 33, pp. 662-666.

Sekiguchi, K. et al., 1994. Effect of seawater temperature on uranium recovery from seawater using amidoxime adsorbents. *nd. Eng. Chem. Res.,* pp. 662-666.

Semblante, G. U. et al., 2018. Brine pre-treatment technologies for zero liquid discharge systems. *Desalination,* Volume 441, pp. 96-111.

Senko, J., Istok, J., Suflita, J. & Krumholzan, L. R., 2002. In-Situ Evidence for Uranium Immobilization and Remobilization. *Environ. Sci. Technol.,* Issue 36, p. 1491–1496.

Sharp, J. et al., 2017. Spectrophotometric Determination of Carbonate Ion Concentrations: Elimination of Instrument-Dependent Offsets and Calculation of In Situ Saturation States. *Environ. Sci. Technol.,* p. 9127–9136.

Sikora, E. & Bodziarczyk, I., 2012. Composition and Antioxidant Activity of Kale (Brassica Oleracea L. Var. Acephala) Raw and Cooked.. *Acta Sci. Pol. Technol. Aliment Actions,* Volume 11, pp. 239-248.

Smith, R. M. & Martell, A. E., 1990. *Critical Stability Constants V 2-6.* 2nd ed. New York: Plenum Press.

Strandberg, G., W., S. S. I. & Parrott, J., 1981. Microbial cells as biosorbants for heavymetals: Accumulation of uranium by Succharolnycescerevisiae and Pseudomonas aeruginosa.. *Appl. En-viron. Microbial. 41: 237-245.,* Volume 41, pp. 237-245.

Sugasaka, K. et al., 2006. Recovery of Uranium from Seawater. *Separation Science and Technology,* pp. 971-985.

Sugo, T. et al., 2001. Recovery System for Uranium from Seawater with Fibrous Adsorbent and Its Preliminary Cost Estimation. *J. Atom. Energy Soc. Japan,* Volume 43, pp. 1010-1016.

Su, S. et al., 2018. High efficiency extraction of U(VI) from seawater by incorporation of polyethyleneimine, polyacrylic acid hydrogel and Luffa cylindrical fibers,. *Chem. Engin. J.,* Volume 345, pp. 526-535.

Szabo, G. et al., 2006. Investigation of complexation of thorium by humic acid using chemically immobilized humic acid on silica gel. *Radiochimica Acta,* Volume 94, pp. 553-557.

Tang, G. et al., 2013. Bioreduction with Emulsified Vegetable Oil as the Electron Donor – Model Application to a Field Test. *Environm. Sci. Technology,* Issue 47, p. 3218–25.

Tavares, L., Pelayo, C. & Noreña, Z., 2021. Characterization of the physicochemical, structural and thermodynamic properties of encapsulated garlic extract in multilayer wall materials,. *Powder Technology,* 378(A), pp. 388-399.

Tomoko, V., 2019. *Direct analysis of environmental samples using ICP-MS with argon gas dilution,* s.l.: Thermoscientific.

Turekian, K. K., 1978. *Oceans, Foundations of Earth Science Series.* Englewood, Cliffs: Prentice-Hall.

Turetta, C., Cozzi, G., Varga, A. & Cescon, P., 2003. Platinum group elements determination in seawater by ICP-SFMS: initial results. *J. de Physique,* Volume 107, pp. 1-4.

Van Loon, A. J. et al., 2013. Diffusion of U(VI) in Opalinus Clay: Influence of temperature and humic acid. *Geochim. Cosmochim. Acta,* Volume 109, pp. 74-89.

Van Loon, L. & Kopajtic, Z., (Part 1) 1991. The adsorption of radionuclides on bitumen, Part I strontium. *Radiochim. Acta,* Volume 55, pp. 83-89.

Van Loon, L. & Kopajtic, Z., (Part 2) 1991. The adsorption of radionuclides on bitumen Part II nickel. *Radiochim. Acta,* Volume 55, pp. 91-94.

Varanasi, S., Low, Z.-X. & Batchelor, W., 2015. Cellulose nanofibre composite membranes – Biodegradable and recyclable UF membranes. *Chemical Engineering Journal,* Volume 265, pp. 138-146.

Walker, M. & Rose, K., 1989. *The radioactivity of the sea,* Harwell,: UKAEA, .

Wang, Z. et al., 2013. Biological and Environmental Transformations of Copper-Based Nanomaterials. *ACS Nano.,* 7(10), p. 8715–8727.

Whitehead, D., 2000. *Nutrient Elements in Grassland : Soil-plant-animal Relationships.* s.l.:CABI.

Wiechert, A. I. et al., 2018. Uranium Resource Recovery from Desalination Plant Feed and Reject Water using Amidoxime Functionalized Adsorbent. *Industrial & Engineering Chemistry Research,* 57(50), p. 17237–17244.

Wiechert, A. I. et al., 2018. Uranium Resource Recovery from Desalination Plant Feed and Reject Water Using Amidoxime Functionalized Adsorbent. *Ind. Eng. Chem. Res.,* 50(57), p. 17237–17244.

Wongjaikham, W. et al., 2018. Enhancement of uranium recovery from seawater using amidoximated polymer gel synthesized from radiation-polymerization and crosslinking of acrylonitrile and methacrylic acid monomers. *J. Environmental Chemical Engineering,* Volume 6, pp. 2768-2777.

Wooles, A. J. et al., 2018. Uranium(III)-carbon multiple bonding supported by arene δ-bonding in mixed-valence hexauranium nanometre-scale rings. *Nat Commun,* Volume 9, p. 2097.

Xu, X. et al., 2019. 3D hierarchical porous amidoxime fibers speed up uranium extraction from seawater. *Energy Environ. Sci.,* Volume 12, pp. 1979-1988.

Yamashita, H., Ozawa, Y., Nakajima, F. & Murata, T., 1980. The collection of uranium from seawater with hydrous metal oxide. III. The effects of diverse ions in seawater on uranium adsorption by hydrous titanium(IV). *Bull. Chem. Soc. Jpn.,* Volume 53, p. 1331 – 1334.

Yu, H. et al., 2015. Recovery of uranium ions from simulated seawater with palygorskite/amidoxime polyacrylonitrile composite. *Applied Clay Science,* Volume 111, pp. 67-75.

Yu, J. et al., 2022. Hydrous titanium oxide and bayberry tannin co-immobilized nano collagen fibrils for uranium extraction from seawater and recovery from nuclear wastewater. *Chemosphere,* Volume 286, p. 131626.

Zhang, A., Uchiyama, G. & Asakura, T., 2005. pH Effect on the uranium adsorption from seawater by a macroporous fibrous polymeric material containing amidoxime chelating functional group. *React. Funct. Polym.,* Volume 63, pp. 143-153.

Zhang, H. & Davison, W., 1995. Performance characteristics of diffusion gradients in thin films for the in situ measurement of trace metals in aqueous solution. *Anal. Chem.,* Volume 67, pp. 3391-3400.

Zhang, L. et al., 2016. Polyphenol–Aluminium Complex Formation: Implications for Aluminium Tolerance in Plants. *Agric. Food Chem,* Volume 64, pp. 3025-3033.

Zhang, S., Zhang, C., Zhang, X. & Ma, E., 2023. A mechanochemical method for one-step leaching of metals from spent LIBs. *Waste Management,* Volume 161, pp. 245-253.

Zhang, X., Zhao, W., Zhang, Y. & Jegatheesan, V., 2021. A review of resource recovery from seawater desalination brine. *Rev Environ Sci Biotechnol,* Volume 20, pp. 333-361.

Zhang, Y. et al., 2018. Adsorption and desorption of uranium(VI) onto humic acids derived from uranium-enriched lignites. *Water Sci Technol.,* Volume 77, pp. 920-930.